

**Applications of the Moment Method to Optical
Communications Systems :
Amplifier Noise and Timing Jitter**

by

Jayanthi Santhanam

Submitted in Partial Fulfillment

of the

Requirements for the Degree

Doctor of Philosophy

Supervised by

Professor Govind P. Agrawal

Department of Physics and Astronomy

The College

Arts and Sciences

University of Rochester

Rochester, New York

2004

To Bhagwan Sri Satya Sai Baba – with all my Pranams.

To my husband, Nazim – with all my love.

Curriculum Vitae

Jayanthi Santhanam was born in Madras, India on 18th August, 1976. She received the Bachelor of Science (Hons.) degree in Physics with distinction and honors from Sri Satya Sai Institute of Higher Learning, Anantapur, Andhra Pradesh, India in 1997. In the summer of 1998, she worked on creating Computer Generated Holograms at the Raman Research Institute, Bangalore, India under the supervision of Dr. Hema Ramachandran. In 1999, she studied various “Back-action evading techniques”, suggested by V. B. Braginsky that can be applied to “Quantum non-demolition measurements” under the supervision of Dr. M. V. Satyanarayana as partial fulfillment to the completion of the Master of Science degree in Physics from the Indian Institute of Technology, Madras, India, which she received in July 1999. Jayanthi began her graduate studies at the University of Rochester in the Fall of 1999 when she joined the Department of Physics and Astronomy. She pursued her research in the field of optical fiber communications under the supervision of Professor Colin J. McKinstrie in the summer of 2000. She continued her research in optical fiber communications under Professor Govind P. Agrawal from January 2001. She received the Master of Arts degree from the University of Rochester in May 2001.

Acknowledgments

I thank my advisor, Professor Govind Agrawal, for his guidance, his inspiration, and the many useful skills which he has taught me, including technical writing and critical thinking. His support and consideration during the tough times are especially appreciated.

I thank Dr. Colin McKinstrie for helping me start my work in this topic in 2000. I thank our graduate secretary Barbara Warren for all her help.

Among my colleagues, I thank in particular Qiang Lin for his generous help with Matlab and many useful discussions. He has also patiently answered many questions which I raised. I thank Fatih Yaman for his discussions and help with our work on loss induced timing jitter. Especially his help in understanding how amplifier gain and noise are estimated and his help with figuring out the n_{sp} factor are appreciated. I thank Ekaterina Poutrina for her help with the Fortran codes. I thank Nick Usechak for his help with problems with my computer.

Most importantly, I thank my family for all their help and support through these years. I am grateful to baba for his affection, advice, support and encouragement. Most of all, I thank my husband for his love, care, support and encouragement.

Publications

1. "Effects of pre-compensation and post-compensation on timing jitter in dispersion-managed systems", J. Santhanam, C. J. McKinstrie, T. I. Lakoba and G. P. Agrawal, *Optics Letters*, **26**, 1131-1133 (2001).
2. "Gordon-Haus timing jitter in dispersion-managed systems with lumped amplification: an analytical approach", C. J. McKinstrie, J. Santhanam and G. P. Agrawal, *J. Opt. Soc. Am. B* **19** 640-649 (2002).
3. "Raman-induced timing jitter in dispersion-managed communication systems", J. Santhanam and G. P. Agrawal, *IEEE J. Sel. Topics Quant. Electron.* **8** 632-639 (2002).
4. "Reduced timing jitter in dispersion-managed Lightwave system through Parametric Amplification", J. Santhanam and G. P. Agrawal, *J. Opt. Soc. Am. B* **20** 284-291 (2003).
5. "Raman-induced Spectral Shifts in Optical fibers: General theory based on the Moment Method", J. Santhanam and G. P. Agrawal, *Opt. Commun.* **222** 413-420 (2003).

Conference Presentations

1. "Effects of pre-compensation and post-compensation in dispersion-managed systems", at the Annual Meeting of Optical Society of America, Long Beach, California (16th October 2001).
2. "Effect of fiber losses on timing jitter in dispersion-managed communication systems", at the Optical Fiber Communications conference, Atlanta (25th March 2003).
3. "Parametric amplification for controlling timing jitter in dispersion-managed systems", a poster presentation at the Optical Fiber Communications conference, Atlanta (24th March 2003).

Abstract

Optical pulse propagation through a fiber is governed by the nonlinear Schrödinger equation. In most cases when the system is not dissipative, using the variational method can help reduce this partial differential equation that governs the pulse propagation into many ordinary differential equations. This reduction makes it easier to study the changes in pulse parameters and hence easier to study the pulse propagation through the fiber. However for dissipative system this method cannot be used. In a communication systems with high bit rates (> 40 Gb/s) when ultrashort solitons are used as optical bits of information, the communication system becomes dissipative due to intra pulse Raman scattering in the fiber. In such a case, the system becomes non Hamiltonian and variational method cannot be used for such systems. We show that the moment method remains valid for both dissipative and non-dissipative systems and hence can be used to study the pulse propagation in both high and low bit rate systems. In particular we apply this method to study the effect of amplifier noise on the pulse parameters and analytically calculate the timing jitter due to the amplifiers that are used periodically to compensate the fiber losses.

Amplifiers used in soliton communications systems restore the soliton energy, but also add *amplified spontaneous emission* noise. This noise affects the soliton evolution along the fiber link limiting the total transmission distance by reducing the signal to noise ratio of the system. The amplifier induced noise also fluctuate the amplitude, frequency and position of the pulse thus causing timing jitter in the system that lead to increased bit error. We use the moment method to calculate the timing jitter at the end of the system and show using this method that several different techniques can help reduce the timing jitter at the end of the system.

For systems using bit rates < 40 Gb/s the timing jitter is mainly due to Gordon–Haus effect which has its origin in amplified spontaneous emission-induced frequency fluctuations. By apply-

ing the moment method to such systems we show that dispersion compensation techniques can reduce timing jitter. However, at higher bit rates for which the pulse width becomes shorter than 5 ps, the Raman jitter induced by intra pulse Raman scattering in the fiber is likely to become the most limiting factor. For such a system we show that using parametric amplifiers instead of fiber amplifiers can reduce timing jitter. We apply the moment method not only to soliton systems but also to non-soliton systems and show that these techniques work for both the systems.

Contents

Curriculum Vitae	ii
Acknowledgments	iii
Publications	iv
1 Introduction	1
1.1 Historic Overview of Optical communications Systems	1
1.2 Group Velocity Dispersion	2
1.3 Fiber Nonlinearity	2
1.4 Dispersion-Managed Solitons	3
1.5 Goal of the Thesis	4
1.6 Outline of the Thesis	5
2 Nonlinear Schrödinger Equation	7
2.1 Solutions of the nonlinear Schrödinger equation	14
2.1.1 Standard Soliton pulse	15
2.1.2 Chirped Gaussian Pulse	17
2.2 Numerical Methods	19
2.2.1 Split-Step Fourier Method	19
2.2.2 Finite-Difference Methods	20
2.3 Chapter Summary	21
3 Variational Method and its limitations	22
3.1 Variational analysis of pulse propagation in non-dissipative systems	23
3.1.1 Fundamental Soliton	24

<i>CONTENTS</i>	viii
3.1.2 Gaussian pulse	27
3.2 Intrapulse Raman Scattering	30
3.3 Chapter Summary	33
4 The Moment Method	35
4.1 Definition of the Moments	35
4.1.1 Energy Evolution	36
4.1.2 Evolution of Pulse Position	38
4.1.3 Evolution of Frequency Shift	40
4.1.4 Evolution of chirp parameter	43
4.1.5 Evolution of the RMS width	46
4.2 Fundamental Soliton	49
4.3 Gaussian Pulse	54
4.4 Raman-induced Frequency shift	58
4.4.1 Fundamental Soliton	59
4.4.2 Chirped Gaussian Pulses	62
4.5 Chapter Summary	65
5 Amplifier Noise and Bit Error Rate	66
5.1 Bit Error Rate	67
5.2 Q-factor	69
5.2.1 Energy Fluctuations	70
5.2.2 Q-factor Estimation	73
5.3 Chapter Summary	75
6 Timing Jitter in Lightwave Systems	76
6.1 Gordon-Haus Timing Jitter	78
6.2 Single Amplifier per Map Period	78
6.2.1 Solitons Systems	83
6.2.2 Non-soliton Systems	88
6.3 Multiple Amplifiers per Map Period	91

<i>CONTENTS</i>	ix
6.3.1 Soliton Systems	92
6.3.2 Non-soliton Systems	99
6.4 Chapter Summary	102
7 Timing Jitter induced by Intrapulse Raman Scattering	104
7.1 Solitons Systems	106
7.1.1 Fundamental solitons in DDFs	106
7.1.2 Dispersion-Managed Solitons	114
7.2 Non-soliton Systems	120
7.3 Numerical Results	125
7.4 Chapter Summary	127
8 Control of Timing Jitter	129
8.1 Compensation Techniques	130
8.1.1 Soliton Systems	130
8.1.2 Non-soliton Systems	135
8.2 Parametric amplifiers	140
8.2.1 Soliton Systems	143
8.2.2 Non-soliton Systems	151
8.3 Chapter Summary	155
9 Conclusions	158
10 Bibliography	164
A Acronyms	170

List of Figures

4.1	RIFS in the case of fundamental soliton in anomalous dispersion	61
4.2	RIFS in the case of fundamental soliton in normal dispersion	62
4.3	RIFS in the case of Gaussian in anomalous dispersion	63
4.4	RIFS in the case of Gaussian pulses in normal dispersion	64
5.1	Bit Error probabilities.	67
5.2	Bit Error rate versus Q factor.	70
6.1	Increased BER due to timing jitter.	77
6.2	Origin of timing jitter.	78
6.3	Timing jitter as a function of distance for a 10 Gb/s DM soliton system with smaller map strength	95
6.4	Timing jitter as a function of distance for a 10 Gb/s DM soliton system with larger map strength	96
6.5	Timing jitter as a function of distance for a 10 Gb/s fundamental soliton in DDF system	97
6.6	Reduction in timing jitter when several amplifiers are placed at equal distances in each map period.	98
6.7	Timing jitter as a function of distance for a 10 Gb/s non-soliton system	102
7.1	Timing jitter as a function of distance for a 160 Gb/s fundamental soliton in DDF system with large average dispersion	113
7.2	Timing jitter as a function of distance for a 160 Gb/s fundamental soliton in DDF system with small average dispersion	114

7.3 Timing jitter as a function of distance for a 160 Gb/s DM soliton system. 120

7.4 Timing jitter as a function of distance for a 160 Gb/s non-soliton system. 124

7.5 Numerical verification of timing jitter for a 160 Gb/s DM soliton systems. 125

7.6 Numerical verification of timing jitter for a 160 Gb/s non-soliton system. 126

8.1 Effect of post-compensation for fundamental solitons in DDF systems. 132

8.2 Effect of post-compensation for fundamental solitons in DDF systems when 2 amplifiers are used per map period. 133

8.3 Effect of post-compensation for DM soliton systems. 134

8.4 Effect of post-compensation for DM soliton systems with larger map strength. . . . 135

8.5 Effect of pre- and post-compensation for non-soliton systems. 140

8.6 Reduced jitter in fundamental soliton systems using parametric amplifiers. 146

8.7 Reduced jitter in DM systems using parametric amplifiers. 150

8.8 Numerical verification of reduced Gordon-Haus jitter when using parametric amplifiers. 151

8.9 Reduced jitter in non-soliton systems using parametric amplifiers. 155

List of Tables

3.1	Integration table to find the Lagrangian given by Eq. (3.14)	26
3.2	Integration table to find the Lagrangian given by Eq. (3.30)	28
4.1	Integration table to get the evolution of pulse parameters of fundamental soliton . .	50
4.2	Evolution of the pulse parameters for the Fundamental soliton obtained using the moment method	53
4.3	Integration table to get the evolution of pulse parameters of a Gaussian pulse	54
4.4	Evolution of pulse parameters for Gaussian pulse obtained using the moment method	58

Chapter 1

Introduction

Optical communications systems use near-infrared lightwave pulses in optical fibers as carrier of information from one place to another. The basic components of an optical communications systems are an optical transmitter which converts electrical signal into optical signal and launches it into the optical fiber, an optical fiber cable and a receiver that converts the optical signal received into an electrical signal [1]. In order to compensate for fiber losses for long distance transmission, optical amplifiers are used periodically after every 80–100 km along the fiber link. These amplifiers compensate for fiber losses by amplifying the signal, thus enabling the signal to be transmitted over long distances. The system performance is characterized by bit-error rate (BER) which is the average probability of incorrect bit identification. In order to have a low BER, which means a better system performance, it is essential that the optical signals are carried over long distances with minimum distortions.

1.1 Historic Overview of Optical communications Systems

The idea of optical waves for communications was faced with two main problems in the early 1960s. The first problem was the availability of a suitable source of such waves. Secondly, the need for a suitable medium of transmission delayed the progress. In 1970 the availability of GaAs semiconductor lasers and low loss silica fibers that can guide the optical waves over long distances solved both the problems. An optical communication system based on a single mode fiber transmitted 2 Gb/s over 40 km in 1981 [2]. Since then, the communication technology has shown rapid

progress. In just 20 years the bit rates have increased to 40 Gb/s and more. Moreover the use of wavelength-division-multiplexing (WDM) technique has revolutionized and increased the capacity of modern optical communication systems to beyond 1 Tb/s.

1.2 Group Velocity Dispersion

In a single-mode fiber, the group velocity associated with the fundamental mode is frequency dependent. Hence, different spectral components of an optical pulse travel at slightly different group velocities, a phenomenon known as the group-velocity dispersion (GVD). When the optical pulse is transmitted through a single mode fiber, different spectral components of the pulse disperse during propagation and do not arrive simultaneously at the output, causing the pulse to broaden. The extent of this broadening is governed by the GVD coefficient, β_2 , related to the dispersion parameter of the fiber D as $D = -(2\pi c/\lambda^2)\beta_2$, where c is the speed of light and λ is the wavelength of the lightwave. The time delay ΔT due to GVD should be less than the bit slot $T_B = 1/B$, where B is the bit rate, which means $B\Delta T < 1$. For a single-mode fiber of length L , the time delay is given by $\Delta T = LD\Delta\lambda$ [1], where $\Delta\lambda$ is the range of wavelengths emitted by the optical source. As a result, $BL|D|\Delta\lambda < 1$ gives the limitation on the bit rate due to GVD in the fiber. Also while using amplifiers at regular intervals, GVD can also cause increased timing jitter in the system, thus leading to system degradation. To increase the bit rate, the pulse spread due to GVD should be kept small. The pulse spread due to GVD can be avoided when the fiber dispersion is close to zero. However, if the dispersion is close to zero, four-wave mixing (FWM) interactions can cause severe distortion to the signal when amplifiers are used.

1.3 Fiber Nonlinearity

The refractive index of silica is power dependent, and the nonlinear contribution become important at high power levels. The effect of such nonlinear refraction is to produce a nonlinear phase shift that is dependent on the input power of the optical pulse. The time dependence of the input power of the pulse causes the nonlinear phase shift to vary with time, resulting in frequency chirping, which means that the carrier frequency of the input pulse changes with time. The time dependence

of the carrier frequency of the pulse in turn affects the pulse shape through GVD. Hence the power dependence of the refractive index can be a limiting factor for the optical communication systems. Since the nonlinear phase shift responsible for the effects is induced by the optical field itself, the nonlinear phenomenon responsible for this limitation is referred to as self-phase modulation (SPM). SPM can lead to considerable spectral broadening of pulses propagating inside an optical fiber.

1.4 Dispersion-Managed Solitons

In 1972, Zakharov and Shabat [3] and later Hasegawa and Tappert [4] showed that a wave envelope propagating in an ideal optical fiber with GVD and nonlinearity has a solitary wave solution, called the ‘soliton’ when dispersion in the fiber is anomalous ($\beta_2 < 0$). An optical soliton is produced by the balance between nonlinear SPM effect and the GVD effect and thus suffers no distortion due to GVD or SPM and maintains its shape along the fiber. However in the presence of fiber losses, the pulse starts losing energy and the pulse width increases. In such a case one needs to use optical amplifiers to reshape the pulse and restore its energy. An important issue for such periodically amplified systems is the amplifier spacing L_A between the amplifiers. In order to keep the cost minimum, the amplifier spacing should be as large as possible. Typically for a non-soliton system it is 80-100 km. In the case of soliton system the spacing should be smaller than the dispersion length $L_D = T_0^2/\beta_2$ where T_0 is the pulse width. This is because, when the amplifier amplifies the soliton energy to the input level, the soliton is perturbed and adjusts its width in the fiber section following the amplifier by shedding a part of its energy as dispersive waves.

In order to reduce the dispersive waves, one has to reduce the amplifier spacing so that the soliton is not perturbed much. For systems that use bit rates more than 10 Gb/s, it becomes difficult to realize the condition $L_A \ll L_D$ in practice. The solution to this problem is dispersion-management. One such dispersion management scheme that helps relax this condition is achieved by using dispersion-decreasing fibers (DDFs) [5]. DDFs are designed such that the GVD decreases along the fiber and counteracts the decreased nonlinearity experienced by the soliton affected by fiber losses. This can solve the problem of achieving the amplifier spacing condition. But the average GVD of the entire link is often relatively large. For reducing timing jitter, a low average

dispersion is desirable. Dispersion maps that consist of alternating GVD fibers can help reduce the average GVD of the entire fiber link while keeping the GVD in each section large to avoid the FWM effects. This approach can also help in achieving an amplifier spacing of 80 to 100 km. In such a system the pulse width and shape of optical pulses evolve periodically. The pulse thus gets back its original shape and width after each map period and is called the dispersion-managed soliton (DMS).

1.5 Goal of the Thesis

Optical amplifiers are used to solve the problem of fiber losses, and GVD can be reduced on average by using dispersion management. However another factor that can limit the communications system is the SPM phenomenon. The effects of SPM cannot be treated alone as the GVD and the SPM effects act on the optical pulse simultaneously. In order to give a mathematical description of both the effects, one needs to use the nonlinear Schrödinger (NLS) equation which governs the propagation of optical pulses through a fiber in the presence of fiber losses, dispersion and nonlinearity. The NLS equation is a nonlinear partial differential equation. In the case of constant dispersion fibers, Zakharov and Shabat succeeded in solving the NLS equation by using the inverse scattering method [6] and demonstrated that the solution to the equation is a solitary wave, called soliton, when the dispersion is anomalous [3].

When the dispersion changes sign periodically like in the dispersion management case, the NLS equation has to be solved numerically. The variational approach can be used to give approximate analytical results that agree well with numerical simulations [7]– [10]. The variational approach is based on the observation that in the absence of nonlinearity in the fiber, a chirped Gaussian pulse maintains its shape during propagation although its amplitude, width and chirp changes. In the case of dispersion-managed soliton, the nonlinear effects are weak locally in each fiber section compared to the dispersive effects. Hence a Gaussian shaped pulse launched into such a fiber will maintain its shape while its amplitude, width, chirp and the phase all vary along the fiber. For such a system, variations in the pulse parameters can be studied using the variational approach, thus enabling a better system design. With all the improvements provided by the dispersion-management technique, the bit rates have now increased to 40 Gb/s or more, leading to the use of ultrashort

solitons. For such a system, higher-order dispersion effects and intrapulse Raman scattering (IRS) cannot be neglected. Even though dispersion effects can be handled using a variational approach, this method cannot be used to account for intrapulse Raman scattering because the Lagrangian density needed for it does not exist due to the dissipative nature of the Raman effect. Thus the variational approach fails if the system becomes non-Hamiltonian.

It becomes necessary to use a different method that will work for both dissipative and non-dissipative systems. The moment method first introduced by Vlasov [11] can be used for this purpose. The goal of this thesis is to use the moment method for studying dispersion-managed lightwave systems. We use this method in particular to study the effects of amplifier noise in the system, to calculate the timing jitter induced by the amplifier noise at the end of the system, and to study the extent of system degradation caused by the timing jitter. We apply this method to both soliton and non-soliton systems. We also describe the techniques that can help reduce timing jitter, and using the moment method we show that these techniques are effective for both soliton and non-soliton systems.

1.6 Outline of the Thesis

Chapter 2 gives an introduction of the basic mathematical description of light propagation in optical fibers. It shows how starting from Maxwell's equations, the nonlinear Schrödinger (NLS) equation that governs the propagation of optical pulses through an optical fiber can be derived. The later part of the chapter gives the solution of the NLS equation and describes various numerical techniques that can be used to solve this equation.

Chapter 3 describes the variational approach and its application to a non-dissipative system (operating at a bit rate < 40 Gb/s). For two different pulse shapes we derive the variational equations that describe the evolution of the pulse parameters along the fiber. The later part of the chapter provides a detailed description of intrapulse Raman scattering (IRS) and shows why a variational approach cannot be used to describe this effect.

Chapter 4 describes the moment method and shows how the moment method can be used to study the pulse evolution along the fiber in the presence of IRS. The results shown are general and can be used for any given pulse shape. The application of this method for two different pulse

shapes is discussed in the final part of this chapter.

Chapter 5 gives details on amplifier noise and shows the results obtained using the moment method to calculate the bit error rate (BER) of a system using amplifiers at regular intervals. The BER of the system is related to the the signal to noise ratio (SNR) of the system and hence describes the system performance.

Chapter 6 gives the analytical results obtained using the moment method to calculate the Gordon-Haus timing jitter in both soliton and non soliton systems. In the later part of this chapter we consider the Gordon-Haus timing jitter in systems when two or more amplifiers are used within one map period.

Chapter 7 considers the effects of IRS and third order dispersion on timing jitter. Using the moment method we calculate the total timing jitter including Raman jitter and Gordon-Haus jitter for both soliton and nonsoliton systems. We show that timing jitter in this case is mainly due to Raman jitter and it limits the system to lengths below 500 km. We also include the numerical simulations conducted to verify the results obtained by the moment method and show that they agree very well.

Chapter 8 discusses various techniques that can be used to reduce timing jitter in a system. First we consider dispersion compensation and show using the moment method that this technique works for soliton and non-soliton systems and we also show that there is an optimum compensation for which the system works better. Secondly, we consider using parametric amplifiers instead of erbium doped fiber amplifiers (EDFAs). In this case we show that both Gordon-Haus jitter and Raman jitter are reduced for both soliton and nonsoliton systems. Finally we show using numerical simulations that by replacing EDFAs with parametric amplifiers indeed reduces both Raman and Gordon-Haus timing jitters. The results obtained by numerical simulation agrees well with the results obtained using the moment method.

Chapter 9 summarizes the main results of this thesis and should be useful for a quick review of the results.

Chapter 2

Nonlinear Schrödinger Equation

Optical communication systems use the phenomenon of total internal reflection for guiding optical pulses in optical fibers. The propagation of light through such a dielectric waveguide can be described using Maxwell's equations for electromagnetic waves. The propagation of electromagnetic fields in any medium whose electric and magnetic field vectors are given by E and H and their corresponding flux densities are given by D and B , respectively, is governed by the following four Maxwell's equations:

$$\nabla \times E = -\frac{\partial B}{\partial t}, \quad (2.1)$$

$$\nabla \times H = J + \frac{\partial D}{\partial t}, \quad (2.2)$$

$$\nabla \cdot D = \rho_f, \quad (2.3)$$

$$\nabla \cdot B = 0. \quad (2.4)$$

where the volume density for free current, J and the volume density for free charge ρ_f represent the sources for the electromagnetic field. The flux densities are related to the field vectors by

$$D = \epsilon_0 E + P, \quad (2.5)$$

$$B = \mu_0 H + M, \quad (2.6)$$

where ϵ_0 is the vacuum permittivity, μ_0 is the vacuum permeability, P is the induced electric polarization vector and M is the induced magnetic polarization vector. Once the total electric and magnetic response of the medium is known, all electromagnetic phenomena can be explained

using Maxwell's equations (2.1)–(2.4) together with the constitutive relations (2.5) and (2.6). Since fibers are source free and nonmagnetic, $\rho_f = 0$, $J = 0$ and $M = 0$. Hence Eqs. (2.1)–(2.6) reduces to

$$\nabla \times E = -\frac{\partial B}{\partial t}, \quad (2.7)$$

$$\nabla \times H = \frac{\partial D}{\partial t}, \quad (2.8)$$

$$\nabla \bullet D = 0, \quad (2.9)$$

$$\nabla \bullet B = 0, \quad (2.10)$$

$$D = \epsilon_0 E + P, \quad (2.11)$$

$$B = \mu_0 H. \quad (2.12)$$

Taking the curl of Eq. (2.7) and using Eq. (2.12) we get

$$\nabla \times \nabla \times E = -\mu_0 \frac{\partial}{\partial t} (\nabla \times H). \quad (2.13)$$

Using Eqs. (2.8) and (2.11) in Eq. (2.13) we find

$$\nabla \times \nabla \times E = -\frac{1}{c^2} \frac{\partial^2 E}{\partial t^2} - \mu_0 \frac{\partial^2 P}{\partial t^2}, \quad (2.14)$$

where c is the speed of light in vacuum and is given by $1/c^2 = \mu_0 \epsilon_0$. Using $\nabla \times \nabla \times E = \nabla(\nabla \bullet E) - \nabla^2 E$ and $\nabla \bullet D = \epsilon \nabla \bullet E = 0$, we can write Eq. (2.14) as

$$\nabla^2 E - \frac{1}{c^2} \frac{\partial^2 E}{\partial t^2} = \mu_0 \frac{\partial^2 P}{\partial t^2}, \quad (2.15)$$

The induced polarization $P(\mathbf{r}, t)$ can be written as

$$P(\mathbf{r}, t) = P_L(\mathbf{r}, t) + P_{NL}(\mathbf{r}, t) \quad (2.16)$$

where P_L is the linear part and is related to the electric field E as

$$P_L(\mathbf{r}, t) = \epsilon_0 \int_{-\infty}^{\infty} \chi^{(1)}(t-t') E(\mathbf{r}, t') dt', \quad (2.17)$$

and P_{NL} is the nonlinear part and is related to the electric field E as

$$P_{NL}(\mathbf{r}, t) = \epsilon_0 \int \int \int_{-\infty}^{\infty} \chi^{(3)}(t-t_1, t-t_2, t-t_3) \dot{\cdot} \times E(\mathbf{r}, t_1) E(\mathbf{r}, t_2) E(\mathbf{r}, t_3) dt_1 dt_2 dt_3, \quad (2.18)$$

where $\chi^{(1)}$ and $\chi^{(3)}$ are the first and third order susceptibilities. The second order susceptibility is not considered because it vanishes due the molecular symmetry of silica glass. Hence Eq. (2.15) becomes

$$\nabla^2 E - \frac{1}{c^2} \frac{\partial^2 E}{\partial t^2} = \mu_0 \frac{\partial^2 P_L}{\partial t^2} + \mu_0 \frac{\partial^2 P_{NL}}{\partial t^2}. \quad (2.19)$$

In order solve Eq. (2.19) first we assume that the nonlinear induced polarization P_{NL} is a small perturbation to P_L , secondly, the optical field maintains its polarization along the fiber length and finally the optical field is quasi-monochromatic, i.e., the pulse spectrum, centered at ω_0 , has a spectral width $\Delta\omega$ such that $\Delta\omega/\omega_0 \ll 1$. Using the slowly varying envelope approximation, the electric field can be written as

$$E = \frac{1}{2} \hat{x} [E(\mathbf{r}, t) \exp(-i\omega_0 t) + c.c], \quad (2.20)$$

where \hat{x} is the polarization unit vector, and $E(\mathbf{r}, t)$ is a slowly varying function of time. The polarization P_L and P_{NL} can also be expressed similarly as

$$P_L = \frac{1}{2} \hat{x} [P_L(\mathbf{r}, t) \exp(-i\omega_0 t) + c.c], \quad (2.21)$$

$$P_{NL} = \frac{1}{2} \hat{x} [P_{NL}(\mathbf{r}, t) \exp(-i\omega_0 t) + c.c], \quad (2.22)$$

Substituting Eqs. (2.20) and (2.21) into Eq. (2.17) we can find that the amplitude of the linear part of induced polarization given by

$$\begin{aligned} P_L(\mathbf{r}, t) &= \epsilon_0 \int_{-\infty}^{\infty} \chi_{xx}^{(1)}(t-t') E(\mathbf{r}, t') \exp[-i\omega_0(t-t')] dt', \\ &= \frac{\epsilon_0}{2\pi} \int_{-\infty}^{\infty} \tilde{\chi}_{xx}^{(1)}(\omega) \tilde{E}(\mathbf{r}, \omega - \omega_0) \exp[-i(\omega - \omega_0)t] d\omega, \end{aligned} \quad (2.23)$$

where $\tilde{E}(\mathbf{r}, \omega)$ is the Fourier transform of $E(\mathbf{r}, t)$ and is defined as

$$\tilde{E}(\mathbf{r}, \omega) = \int_{-\infty}^{\infty} E(\mathbf{r}, t) \exp[i\omega t] dt \quad (2.24)$$

Similarly the amplitude of the nonlinear part of the induced polarization can be found from Eq. (2.18) to be

$$P_{NL}(\mathbf{r}, t) = \epsilon_0 \int \int \int_{-\infty}^{\infty} \chi^{(3)}(t-t_1, t-t_2, t-t_3) \dot{\times} E(\mathbf{r}, t_1) E(\mathbf{r}, t_2) E(\mathbf{r}, t_3) dt_1 dt_2 dt_3, \quad (2.25)$$

where the $\dot{\times}$ show that the multiplication between the E and $\chi^{(3)}$ is for the respective time coordinates.

Assuming that the nonlinear response in the fiber is instantaneous, the Eq. (2.25) can be simplified by using $\chi^{(3)}(t-t_1, t-t_2, t-t_3) = \chi^{(3)}\delta(t-t_1)\delta(t-t_2)\delta(t-t_3)$ to give

$$P_{NL} = \epsilon_0 \chi^{(3)} : \times E(\mathbf{r}, t)E(\mathbf{r}, t)E(\mathbf{r}, t). \quad (2.26)$$

This assumption will not be valid when pulse width is smaller than 1 ps due to the contribution of molecular vibrations (the Raman effect) to $\chi^{(3)}$. This contribution and its effect will be considered at the end of the next chapter when intrapulse Raman scattering is discussed. This condition is valid for pulse widths > 1 ps because for silica fibers the Raman response occurs on a time scale of 60 – 70 fs. Substituting Eqs. (2.20) and (2.22) into Eq. (2.26) we get two terms, one oscillating at ω_0 and another term oscillating at $3\omega_0$. The term oscillating at $3\omega_0$ requires phase matching and is generally negligible in optical fibers. Hence the P_{NL} can be written as

$$\begin{aligned} P_{NL} &= \frac{3}{4} \epsilon_0 \chi_{xxxx}^{(3)} E(\mathbf{r}, t) |E(\mathbf{r}, t)|^2 \\ &= \epsilon_0 \epsilon_{NL} E(\mathbf{r}, t), \end{aligned} \quad (2.27)$$

where $\epsilon_{NL} = (3/4) \chi_{xxxx}^{(3)} |E(\mathbf{r}, t)|^2$. Due to the presence of the intensity in the term P_{NL} ($\epsilon_{NL} \propto |E(\mathbf{r}, t)|^2$), Eq. (2.19) is nonlinear and is difficult to solve. Hence we treat ϵ_{NL} as a constant by treating P_{NL} as a perturbation. It is then easier to work in the Fourier domain in order to obtain a wave equation for $E(\mathbf{r}, t)$.

Using Eqs. (2.24), (2.23) and (2.27) we can write Eqs. (2.20)–(2.22) as

$$E = \frac{\hat{x}}{4\pi} \int_{-\infty}^{\infty} [\tilde{E}(\mathbf{r}, \omega - \omega_0) \exp(-i\omega t) + c.c.] d\omega, \quad (2.28)$$

$$P_L = \frac{\hat{x}}{4\pi} \epsilon_0 \int_{-\infty}^{\infty} [\tilde{\chi}_{xx}^{(1)}(\omega) \tilde{E}(\mathbf{r}, \omega - \omega_0) \exp(-i\omega t) + c.c.] d\omega, \quad (2.29)$$

$$P_{NL} = \frac{\hat{x}}{4\pi} \epsilon_0 \epsilon_{NL} \int_{-\infty}^{\infty} [\tilde{E}(\mathbf{r}, \omega - \omega_0) \exp(-i\omega t) + c.c.] d\omega, \quad (2.30)$$

From Eq. (2.28)

$$\nabla^2 E = \frac{\hat{x}}{4\pi} \int_{-\infty}^{\infty} [\nabla^2 \tilde{E}(\mathbf{r}, \omega - \omega_0) \exp(-i\omega t) + c.c.] d\omega, \quad (2.31)$$

$$\frac{\partial^2 E}{\partial t^2} = -\frac{\hat{x}}{4\pi} \int_{-\infty}^{\infty} \omega^2 [\tilde{E}(\mathbf{r}, \omega - \omega_0) \exp(-i\omega t) + c.c.] d\omega. \quad (2.32)$$

Differentiating Eq. (2.29) twice w.r.t t we get

$$\frac{\partial^2 P_L}{\partial t^2} = -\frac{\hat{x}}{4\pi} \epsilon_0 \int_{-\infty}^{\infty} \omega^2 [\tilde{\chi}_{xx}^{(1)}(\omega) \tilde{E}(\mathbf{r}, \omega - \omega_0) \exp(-i\omega t) + c.c.] d\omega. \quad (2.33)$$

Similarly from Eq. (2.30) we get

$$\frac{\partial^2 P_{NL}}{\partial t^2} = -\frac{\hat{x}}{4\pi} \epsilon_0 \epsilon_{NL} \int_{-\infty}^{\infty} \omega^2 [\tilde{E}(\mathbf{r}, \omega - \omega_0) \exp(-i\omega t) + c.c.] d\omega, \quad (2.34)$$

Substituting Eqs. (2.31)–(2.34) in Eq. (2.19) we can show that $E(\mathbf{r}, t)$ satisfies the Helmholtz equation

$$\nabla^2 \tilde{E} + k_0^2 \epsilon(\omega) \tilde{E} = 0, \quad (2.35)$$

where $\epsilon(\omega) = 1 + \tilde{\chi}_{xx}^{(1)}(\omega) + \epsilon_{NL}$ is the dielectric constant, $k_0 = \omega/c$ and the relation $\mu_0 \epsilon_0 = 1/c^2$ was used. The refractive index and absorption coefficient are related to the dielectric constant and can be written in the form

$$\tilde{n} = n + n_2 |E|^2 \quad \tilde{\alpha} = \alpha + \alpha_2 |E|^2, \quad (2.36)$$

respectively. Using the relations, $(\tilde{n} + i\tilde{\alpha}/2k_0)^2 = \epsilon(\omega) = 1 + \tilde{\chi}_{xx}^{(1)}(\omega) + \epsilon_{NL}$ and $\epsilon_{NL} = (3/4)\chi_{xxxx}^{(3)} |E(\mathbf{r}, t)|^2$ we get

$$\begin{aligned} \tilde{n} - \tilde{\alpha}^2/(4k_0^2) + i\tilde{n}\tilde{\alpha}/k_0 = 1 + \tilde{\chi}_{xx}^{(1)}(\omega) + (3/4)\chi_{xxxx}^{(3)} |E|^2 \\ (n + \frac{i\alpha}{2k_0})^2 + [2nn_2 - \frac{\alpha\alpha_2}{2k_0^2} + i(n_2 \frac{\alpha}{k_0} + n \frac{\alpha_2}{k_0})] |E|^2 = 1 + \tilde{\chi}_{xx}^{(1)}(\omega) + (3/4)\chi_{xxxx}^{(3)} |E|^2 \end{aligned} \quad (2.37)$$

From Eq. (2.37) we can write

$$n(\omega) = 1 + \frac{1}{2} \text{Re}[\tilde{\chi}^{(1)}(\omega)] \quad \alpha(\omega) = \frac{k_0}{n} \text{Im}[\tilde{\chi}^{(1)}(\omega)], \quad (2.38)$$

$$n_2(\omega) = \frac{3}{8n} \text{Re}[\chi^{(3)}(\omega)] \quad \alpha_2(\omega) = \frac{3k_0}{4n} \text{Im}[\chi^{(3)}(\omega)]. \quad (2.39)$$

Eq. (2.35) can be solved using the method of separation of variables where we assume a solution of the form

$$\tilde{E}(\mathbf{r}, \omega - \omega_0) = F(x, y) \tilde{A}(z, \omega - \omega_0) \exp(i\beta_0 z) \quad (2.40)$$

where $\tilde{A}(z, \omega)$ is a slowly varying function of z and β_0 is the wave number to be determined. Substituting this solution into Eq. (2.35) and rearranging we get the following two equation for $F(x, y)$ and $\tilde{A}(z, \omega)$:

$$\frac{\partial^2 F}{\partial x^2} + \frac{\partial^2 F}{\partial y^2} + [\epsilon(\omega)k_0^2 - \tilde{\beta}^2]F = 0 \quad (2.41)$$

$$2i\beta_0 \frac{\partial \tilde{A}}{\partial z} + (\tilde{\beta}^2 - \beta_0^2)\tilde{A} = 0 \quad (2.42)$$

Since $\tilde{A}(z, \omega)$ is a slowly varying function of z we have neglected the second derivative with respect to z in the above equation.

It is easier to solve Eq. (2.41) in the cylindrical co-ordinates. So using the relations

$$F(x, y) = f(\rho) \exp(-im\phi)$$

$$\frac{\partial^2 F}{\partial x^2} + \frac{\partial^2 F}{\partial y^2} = \frac{\partial^2 F}{\partial \rho^2} + \frac{1}{\rho^2} \frac{\partial F}{\partial \rho} + \frac{1}{\rho^2} \frac{\partial^2 F}{\partial \phi^2},$$

we can write Eq. (2.41) in cylindrical co-ordinates as

$$\frac{d^2 f}{d\rho^2} + \frac{1}{\rho} \frac{df}{d\rho} + \left(\varepsilon(\omega) k_0^2 - \tilde{\beta}^2 - \frac{m^2}{\rho^2} \right) f = 0. \quad (2.43)$$

The dielectric constant $\varepsilon(\omega)$ can be approximated as $\varepsilon(\omega) = (n + \Delta n)^2 \approx n^2 + 2n\Delta n$ in Eq. (2.43), where $\Delta n = n_2 |E|^2 + i\tilde{\alpha}/2k_0$ is a small perturbation. Hence Eq. (2.43) can be written as

$$\frac{d^2 f}{d\rho^2} + \frac{1}{\rho} \frac{df}{d\rho} + \left(n^2 k_0^2 - \tilde{\beta}^2 - \frac{m^2}{\rho} + 2n\Delta n k_0^2 \right) f = 0. \quad (2.44)$$

This equation can be solved using perturbation method. When $\Delta n = 0$, Eq. (2.44) reduces to the well-known differential equations for Bessel functions. For a fiber of core radius a that has a refractive index $n = n_1$ but takes the value $n = n_2'$ outside the core ($\rho > a$), the general solution for Eq. (2.44) inside the core can be written as

$$f(\rho) = C_1 J_m(\kappa\rho) + C_2 N_m(\kappa\rho), \quad (2.45)$$

where J_m is the Bessel function, N_m is the Neumann function, and

$$\kappa = (n_1^2 k_0^2 - \tilde{\beta}^2)^{1/2}. \quad (2.46)$$

The constants C_1 and C_2 can be found using the appropriate boundary conditions. N_m has a singularity at $\rho = 0$ and hence for a physical solution $C_2 = 0$. Thus $F(\rho, \phi) = J_m(\kappa\rho) \exp(-im\phi)$, for $\rho < a$ and in the cladding region ($\rho > a$), the solution $F(\rho, \phi) = K_m(\gamma\rho) \exp(-im\phi)$ where K_m is modified Bessel function and $\gamma = (\tilde{\beta}^2 - n_2'^2 k_0^2)^{1/2}$. Using the same method, the magnetic component \tilde{H}_z can be found. The boundary condition that the tangential components of $\tilde{E}(\mathbf{r}, t)$ and $\tilde{H}(\mathbf{r}, t)$ be continuous at $\rho = a$ can be used to find $\tilde{\beta}$.

We now include the effect of Δn in Eq. (2.44). In the first-order perturbation theory, Δn does not affect $F(\rho, \phi)$. However $\tilde{\beta}$ becomes

$$\tilde{\beta}' = \tilde{\beta} + \Delta\beta, \quad (2.47)$$

where

$$\Delta\beta = \frac{k_0 \int \int \rho \Delta n |F(\rho, \phi)|^2 d\rho d\phi}{\int \int \rho |F(\rho, \phi)|^2 d\rho d\phi}. \quad (2.48)$$

This completes the formal solution of Eq. (2.41) to the first-order in perturbation Δn . Next in order to complete the calculation of the electric field $E(\mathbf{r}, t)$, we need to solve Eq. (2.42) for the slowly varying pulse envelope. Using Eq. (2.47) we can approximate $\tilde{\beta}'^2 - \beta_0^2$ in Eq. (2.42) by $2\beta_0(\tilde{\beta}' - \beta_0)$. Eq. (2.42) can then be written as

$$\frac{\partial \tilde{A}}{\partial z} = i[\tilde{\beta}(\omega) + \Delta\beta - \beta_0]\tilde{A}. \quad (2.49)$$

This equation shows that as the pulse propagates along the fiber each spectral component within the pulse envelope acquires a phase shift whose magnitude is both frequency and intensity dependent. Expanding $\tilde{\beta}(\omega)$ in a Fourier series about the carrier frequency ω_0 we get

$$\tilde{\beta}(\omega) = \beta_0 + (\omega - \omega_0)\beta_1 + \frac{1}{2}(\omega - \omega_0)^2\beta_2 + \frac{1}{6}(\omega - \omega_0)^3\beta_3 + \dots, \quad (2.50)$$

where

$$\beta_m = \left(\frac{d^m \tilde{\beta}}{d\omega^m} \right)_{\omega=\omega_0} \quad (m = 1, 2, \dots). \quad (2.51)$$

The cubic and higher order terms in the expansion in Eq. (2.50) are negligible if the spectral width $\Delta\omega \ll \omega_0$. Substituting Eq. (2.50) in Eq. (2.49) and taking the inverse Fourier transform by using

$$A(z, t) = \frac{1}{2\pi} \int_{-\infty}^{\infty} \tilde{A}(z, \omega - \omega_0) \exp[-i(\omega - \omega_0)t] d\omega, \quad (2.52)$$

Eq. (2.49) can be written as

$$\frac{\partial A}{\partial z} = -\beta_1 \frac{\partial A}{\partial t} - \frac{i\beta_2}{2} \frac{\partial^2 A}{\partial t^2} + i\Delta\beta A. \quad (2.53)$$

The term with $\Delta\beta$ includes the effect of fiber loss and nonlinearity. Using $\Delta n = n_2 |E|^2 + i\tilde{\alpha}/2k_0$ in Eq. (2.48) and substituting for $\Delta\beta$ in Eq. (2.53) we get

$$\frac{\partial A}{\partial z} + \beta_1 \frac{\partial A}{\partial t} + \frac{i\beta_2}{2} \frac{\partial^2 A}{\partial t^2} + \frac{\alpha}{2} A = i\gamma |A|^2 A, \quad (2.54)$$

where the nonlinearity parameter γ is defined as

$$\gamma = \frac{n_2 \omega_0}{c A_{eff}}. \quad (2.55)$$

The parameter A_{eff} is known as the effective core area and is defined as

$$A_{eff} = \frac{(\int \int \rho \Delta n |F(\rho, \phi)|^2 d\rho d\phi)^2}{\int \int \rho |F(\rho, \phi)|^4 d\rho d\phi}. \quad (2.56)$$

The parameter A_{eff} depends on the fiber parameters such as the core radius and core-cladding index difference and its evaluation requires the use of the function $F(\rho, \phi)$. Using a transformation, $t' = t - \beta_1 z$, into Eq. (2.54) we get

$$\frac{\partial A}{\partial z} + \frac{i\beta_2}{2} \frac{\partial^2 A}{\partial t'^2} + \frac{\alpha}{2} A = i\gamma |A|^2 A. \quad (2.57)$$

The above equation describes the propagation of picoseconds optical pulse in single-mode fibers. It is often referred to as the *nonlinear Schrödinger equation*. It includes the effects of fiber losses through α , GVD through β_2 and fiber nonlinearity through γ . The GVD parameter β_2 can be positive or negative. In the anomalous dispersion regime $\beta_2 < 0$ and the fiber can support optical solitons.

2.1 Solutions of the nonlinear Schrödinger equation

The mathematical description of solitons employs the NLS equation satisfied by the pulse envelope $A(z, t)$ in the presence of GVD and SPM. In order to discuss the solution to this equation in a simple way consider that the fiber is lossless ($\alpha = 0$). Hence normalizing Eq. (2.57) using

$$\tau = \frac{t'}{T_0}, \quad \zeta = \frac{z}{L_D}, \quad U = \frac{A}{\sqrt{P_0}}, \quad (2.58)$$

where T_0 is a measure of the pulse width, P_0 is the peak power of the pulse and $L_D = T_0^2/\beta_2$ is the dispersion length, it takes the form

$$i \frac{\partial U}{\partial \zeta} - \frac{s}{2} \frac{\partial^2 U}{\partial \tau^2} + N^2 |U|^2 U = 0, \quad (2.59)$$

where $s = \text{sgn}(\beta_2) = +1$ or -1 , depending on whether β_2 is positive (normal GVD) or negative (anomalous GVD). The parameter N is then defined as

$$N^2 = \gamma P_0 L_D = \gamma P_0 T_0^2 / |\beta_2|. \quad (2.60)$$

It is useful to introduce another length scale called the nonlinear length, $L_{NL} = 1/\gamma P_0$. The dispersion length L_D and the nonlinear length L_{NL} provide the length scales over which the dispersive

or nonlinear effects become important for pulse evolution along the fiber length L . When the fiber length L is such that $L \ll L_{NL}$ and $L \ll L_D$, neither dispersive nor nonlinear effects play a significant role during pulse propagation. When the fiber length L is such that $L \ll L_{NL}$ and $L \geq L_D$, the pulse evolution is governed by GVD and nonlinear effects play a minor role. This can happen for short pulses or pulses with peak power $P_0 \ll 1$ W. When the fiber length L is such that $L \ll L_D$ and $L \geq L_{NL}$, the pulse evolution is governed by SPM and dispersive effects play a minor role. This can happen for relatively wide pulses with a peak power $P_0 \geq 1$ W. When the fiber length is comparable to L_D and L_{NL} , dispersion and nonlinearity act together as the pulse propagates along the fiber.

2.1.1 Standard Soliton pulse

The NLS equation is a nonlinear partial differential equation that cannot be solved analytically except for some specific cases in which the inverse scattering method [3] can be used to solve the NLS equation. Numerical approach is often employed for understanding the nonlinear effects in optical fibers. The details of the inverse scattering method are discussed in many books devoted to solitons [12]– [15]. The main result can be summarized as follows. When an input pulse having an amplitude

$$U(0, t) = N \operatorname{sech}(t), \quad (2.61)$$

is launched into a fiber that has anomalous GVD, its shape remains unchanged during propagation when $N = 1$ but follows a periodic pattern for integer values of $N > 1$ such that the input shape is recovered at $\zeta = m\pi/2$, where m is an integer. An optical soliton whose pulse parameters satisfy the condition $N = 1$ is called the *fundamental soliton*. Pulses corresponding to other integer values of N are called *higher-order solitons* and the parameter N represents the order of the soliton. Only a fundamental soliton maintains its shape during propagation inside the optical fibers.

The solution of the NLS that corresponds to the fundamental soliton can be obtained by solving Eq. (2.59) directly, without recourse to inverse scattering method. Using the fact that $N = 1$ for fundamental solitons and that in the anomalous dispersion regime β_2 is negative, Eq. (2.59) can be written as

$$i \frac{\partial U}{\partial \zeta} + \frac{1}{2} \frac{\partial^2 U}{\partial \tau^2} + |U|^2 U = 0, \quad (2.62)$$

The approach consists of assuming that there exists a solution of the form

$$U(\zeta, \tau) = V(\tau) \exp[i\phi(\zeta)], \quad (2.63)$$

to Eq. (2.62), where V must be independent of ζ to represent fundamental soliton that maintains its shape during propagation. The phase ϕ depends on ζ but is assumed to be independent of time. Substituting Eq. (2.63) into Eq. (2.62) and rearranging we obtain

$$\frac{d\phi}{d\zeta} = \frac{1}{V} \left(\frac{1}{2} \frac{\partial^2 V}{\partial \tau^2} + V^3 \right) = K, \quad (2.64)$$

where K is a constant. From Eq. (2.64) we can write the phase $\phi = K\zeta$. The function $V(\tau)$ is then found to satisfy the nonlinear differential equation

$$\frac{d^2 V}{d\tau^2} = 2V(K - V^2). \quad (2.65)$$

Multiplying Eq. (2.65) by $2(dV/d\tau)$ and integrating over τ ,

$$(dV/d\tau)^2 = 2KV^2 - V^4 + C, \quad (2.66)$$

where C is a constant of integration. Using the boundary condition that both V and $dV/d\tau$ should vanish as $|\tau| \rightarrow \infty$ for pulses, C is found to be 0. The constant K is found to be $1/2$ using the condition that at the soliton peak $\tau = 0$, $V = 1$ and $dV/d\tau = 0$. Using these values for the constants and integrating Eq. (2.66) we obtain $V(\tau) = \text{sech}(\tau)$. Using this in Eq. (2.63) we can write

$$U(\zeta, \tau) = \text{sech}(\tau) \exp(i\zeta/2), \quad (2.67)$$

Eq. (2.67) represents the well-known ‘‘sech’’ solution for the fundamental soliton. It shows that the input pulse acquires a phase shift of $\zeta/2$ as it propagates inside the fiber, but its amplitude remains unchanged. In essence, the effects of fiber dispersion are exactly compensated for by the fiber nonlinearity when the input pulse has a ‘‘sech’’ shape and its width and peak power are related as given by Eq. (2.60) with $N = 1$. This is true only if the fiber losses are negligible. In the presence of loss and/or amplification, the soliton may be perturbed and using the variational or perturbation method the approximate soliton solution is given by

$$U(z, t) = a \text{sech} \left(\frac{t - T}{\tau} \right) \exp[i\phi - i\Omega(t - T) - iC(t - T)^2/2\tau^2], \quad (2.68)$$

where the amplitude a , phase ϕ , frequency Ω , time delay T , chirp C and width τ all are functions of z .

2.1.2 Chirped Gaussian Pulse

When nonlinear effects play a minor role, and the pulse propagation is governed mainly by GVD, the last term in Eq. (2.62) can be neglected. However we cannot use the dimensionless parameters ζ and τ in Eq. (2.62) because the pulse width and the shape in general can vary along the fiber length. Hence Eq. (2.62) is written in physical units as

$$i \frac{\partial U}{\partial z} = \frac{\beta_2}{2} \frac{\partial^2 U}{\partial t^2}. \quad (2.69)$$

Eq. (2.69) has the same form as a free particle equation and can be solved by using the Fourier method. If $\tilde{U}(z, \omega)$ is the Fourier transform of $U(z, t)$ such that

$$\tilde{U}(z, \omega) = \int_{-\infty}^{\infty} U(z, t) \exp[i\omega t] dt, \quad (2.70)$$

then it satisfies an ordinary differential equation

$$i \frac{\partial \tilde{U}}{\partial z} = -\frac{\beta_2}{2} \omega^2 \tilde{U}, \quad (2.71)$$

whose solution is given by

$$\tilde{U}(z, \omega) = \tilde{U}(0, \omega) \exp\left(\frac{i}{2} \beta_2 \omega^2 z\right). \quad (2.72)$$

Taking the inverse Fourier transform we obtain

$$U(z, t) = \frac{1}{2\pi} \int_{-\infty}^{\infty} \tilde{U}(0, \omega) \exp\left[\frac{i}{2} \beta_2 \omega^2 z - i\omega t\right] dt, \quad (2.73)$$

Eq. (2.73) shows that GVD changes the phase of each spectral component of the pulse by an amount that depends on the frequency and the propagated distance. Even though such a phase change does not affect the pulse spectrum, it can modify the pulse shape.

Consider that the pulse shape $U(0, t)$ is given by a chirped Gaussian pulse of form

$$U(0, t) = \exp\left[-\frac{(1+iC)t^2}{2\tau_0^2}\right], \quad (2.74)$$

where C is the chirp parameter and τ_0 is the initial pulse width. Using Eq. (2.74) in Eq. (2.70) we get

$$\tilde{U}(0, \omega) = \left[\frac{2\pi\tau_0^2}{1+iC}\right]^{1/2} \exp\left[-\frac{\omega^2\tau_0^2}{2(1+iC)}\right]. \quad (2.75)$$

Substituting $\tilde{U}(0, \omega)$ from Eq. (2.75) in Eq. (2.73) and carrying out the integration we get

$$U(z, t) = \frac{\tau_0}{[\tau_0^2 - i\beta_2 z(1 + iC)]^{1/2}} \exp \left[-\frac{(1 + iC)t^2}{2[\tau_0^2 - i\beta_2 z(1 + iC)]} \right]. \quad (2.76)$$

Thus a chirped Gaussian pulse maintains its shape during propagation, however its width changes due to GVD. The width of such a pulse after propagating a distance z is related to the initial width τ_0 by

$$\frac{\tau}{\tau_0} = \left[\left(1 + \frac{C\beta_2 z}{\tau_0^2} \right)^2 + \left(\frac{\beta_2 z}{\tau_0^2} \right)^2 \right]^{1/2}. \quad (2.77)$$

The above equation shows that the broadening depends on relative signs of the GVD parameter β_2 and the chirp parameter C . When $\beta_2 C > 0$ the pulse broadens monotonically while when $\beta_2 C < 0$, it goes through an initial narrowing stage and then increases with distance. When the pulse is initially chirped and the condition $\beta_2 C < 0$ is satisfied, the dispersion induced chirp is in the opposite direction leading to an initial pulse narrowing. The minimum pulse width occurs at

$$z_{min} = \frac{C}{1 + C^2} L_D \quad (2.78)$$

and has the value

$$\tau_{min} = \frac{\tau_0}{(1 + C^2)^{1/2}}. \quad (2.79)$$

Chirped Gaussian pulses are used in describing dispersion managed solitons in dispersion maps that consist of the alternating GVD fibers [9]. The use of such maps lowers the average GVD of the entire link while keeping the GVD of each section large enough that the FWM and TOD effects remain negligible. In such a system, the GVD parameter takes values β_{2a} and β_{2n} in the anomalous and normal sections of lengths l_a and l_n . The map period L_m is then given by $l_a + l_n$. The properties of DM solitons will depend on several map parameters. If the map period is a fraction of the nonlinear length, the nonlinear effects are relatively small, and the pulse evolves in a linear fashion over one map period. On a longer length scale, solitons can still form if the SPM effects are balanced by the average dispersion. As a result solitons can survive even though not only peak power but also the width and shape of such solitons oscillate periodically. For such a case the nonlinear term can no longer be neglected. Hence the pulse propagation is governed by

$$i \frac{\partial U}{\partial z} - \frac{\beta_2(z)}{2} \frac{\partial^2 U}{\partial t^2} + \gamma(z) |U|^2 U = 0, \quad (2.80)$$

Eq. (2.80) cannot be solved easily since both β_2 and γ vary with z and the nonlinear effects are non zero. Often numerical techniques are used to solve such an equation. Numerical simulations show that a nearly periodic solution can often be found by adjusting input pulse parameters such as the pulse width, chirp and peak power. The pulse shape of DM soliton can then in general be represented by a chirped Gaussian of the form

$$U(z, t) = a \exp[i\phi - i\Omega(t - T) - (1 + iC)(t - T)^2 / 2\tau^2]. \quad (2.81)$$

Several approximate analytical approaches can be used to get further physical insights. A common approach makes use of the variational method [7]–[10]. Another approach expands the solution to Eq. (2.80) in terms of a complete set of Hermite-Gauss functions that are solutions of the linear problem [16]. A third approach solves an integral equation derived in the spectral domain using perturbation theory [17]–[19]. We focus on the variational method in the next chapter.

2.2 Numerical Methods

The numerical techniques used to study pulse propagation in optical fibers can be classified into two broad categories known as the finite difference methods and the pseudo spectral methods. One example of the pseudo spectral methods is the split-step fourier method [20]–[22]. A numerical approach is often necessary to understand the nonlinear effects in optical fibers. Hence understanding these numerical methods becomes essential [23].

2.2.1 Split-Step Fourier Method

The propagation equation Eq. (2.80) describes the effects of the dispersion in a linear medium and the nonlinear effects that arise due to fiber nonlinearities. Hence rewriting Eq. (2.80) in terms of the linear and nonlinear operators,

$$\frac{\partial A}{\partial z} = (\hat{D} + \hat{N})A, \quad (2.82)$$

where \hat{D} is the differential operator that describes the effects of dispersion and \hat{N} accounts for fiber nonlinearity. These operators are given by

$$\hat{D} = -\frac{i\beta_2}{2} \frac{\partial^2}{\partial t^2} + \frac{\beta_3}{6} \frac{\partial^3}{\partial t^3} \quad (2.83)$$

$$\hat{N} = i\gamma|A|^2 \quad (2.84)$$

In general, dispersion and nonlinearity act together along the length of the fiber. The split-step Fourier method obtains an approximate solution by assuming that in propagating through the optical fiber over a small distance h , the dispersive and nonlinear effects can be considered to act independently. More specifically, propagation from z to $z+h$ is carried out in two steps. In the first step, the nonlinearity acts alone, and $\hat{D} = 0$ in Eq. (2.82). In the second step, dispersion acts alone and $\hat{N} = 0$ in Eq. (2.82). The effect of dispersion is then found by taking the Fourier transform of the equation. The accuracy of the split-step Fourier method can be improved by keeping the step size h small.

2.2.2 Finite-Difference Methods

An inherent fundamental approximation in the derivation of the NLS equation is the slowly varying envelope approximation. In order to relax this approximation finite-difference methods are used in place of the split-step Fourier method. Another approximation used in deriving the NLS equation is that there is no backward propagating waves. Such problems require the simultaneous considering of both forward and backward propagating waves. Also in order to consider the birefringence effects of the fiber one needs to consider the vector nature of the electromagnetic fields. For the case of linear medium the algorithms that solve the Maxwell equations Eqs. (2.7)–(2.10) directly in the time domain by using finite-difference methods have been developed for many years [24]–[28]. However in 1992, such algorithms were extended to the case of nonlinear media [29]–[33]. In particular this method was used to study pulse propagation in optical fibers in [29]–[31]. Conceptually, the main difference between the finite-difference time-domain method and split-step Fourier method is that the former deals with all electromagnetic components. The finite-difference time-domain method is certainly more accurate since it solves the Maxwell equations directly with a minimum number of approximations. However it is more time consuming than the split-step Fourier method. It may be necessary to use this method for ultrashort pulses whose width is less than 10 fs. However in most applications of nonlinear fiber optics, pulses are much wider than 10 fs and using the split-step Fourier method provides reasonably accurate solution in such cases.

2.3 Chapter Summary

Pulse propagation in optical fibers is governed by the NLS equation. In this chapter we have derived the NLS equation that governs the propagation of optical pulses in optical fibers from the Maxwell's equations. We gave the analytical solutions to this equation for two specific cases and discussed the properties of these solutions. We showed that standard solitons can maintain their pulse shape and width during propagation in the optical fibers if their pulse energy is chosen appropriately. When nonlinear effects can be neglected, we showed that the solution to the NLS equation is given by a chirped Gaussian function. We also showed that such a solution does not maintain its pulse width during propagation. However the evolution of their pulse width and chirp can be found analytically. We also presented various numerical methods that can be used to study the propagation of pulses through optical fibers.

Chapter 3

Variational Method and its limitations

As discussed in Chapter 2, pulse propagation in a nonlinear dispersive medium such as silica fibers is governed by the NLS equation. In the case of single-mode fibers that allow the propagation of a single electromagnetic-wave mode, the NLS equation can be written as [1]

$$i\frac{\partial A}{\partial z} - \frac{\beta_2}{2}\frac{\partial^2 A}{\partial t^2} + \gamma|A|^2A = -\frac{i\alpha}{2}A, \quad (3.1)$$

where $A(z, t)$ is the slowly varying amplitude of the pulse envelope, α accounts for fiber losses, β_2 is the GVD coefficient, and γ is the nonlinear parameter responsible for SPM. In a constant dispersion fiber, the GVD coefficient β_2 , γ and α are all constant throughout the fiber. The NLS equation can be solved in that case by the inverse scattering method if $\alpha = 0$ [3] and the solution to the NLS equation in the case of anomalous dispersion can be found to be of the form shown in Eq. (2.67). Such a solution is called the fundamental soliton and maintains its pulse shape and width as it propagates along the fiber. However, in the presence of fiber losses the pulse begins to spread due to GVD.

In the absence of nonlinearity, the accumulated dispersion over the length of the fiber can be compensated at the receiver end. This is not the case in the presence of nonlinear effects. Also when amplifiers are used to compensate for fiber losses the GVD can lead to increased timing jitter in the system. A simple solution is provided by dispersion-management. Dispersion maps that consists of alternating GVD fibers can help reduce the average GVD. However β_2 , γ and α are now periodic functions of z because of their different values in two or more fiber sections used to form a dispersion map. Solving the NLS then becomes complicated. Analytical calculations for

such a case is possible using a variational approach. In this approach, one assumes that the pulse propagates with a self-similar shape. With this assumption, the optical system is described by the averaged Lagrangian density which is the *action functional*. The corresponding Euler-Lagrange equations that describe the evolution of pulse parameters can be then derived by equating the variational derivative of the action functional to zero. The variational approach hence offers a simple approximate analytical method of solving the NLS equation. The variational method can be used to study a variety of problems in DM systems and the results agree reasonably well with numerical simulations [7]– [10]. The variational method can be used for conservative systems even when the coefficients are explicitly coordinate dependent. However, the variational approach cannot be used for dissipative systems.

3.1 Variational analysis of pulse propagation in non-dissipative systems

It is useful to eliminate the last term in Eq. (3.1) with the transformation

$$A(z, t) = B(z, t) \exp \left[-\frac{1}{2} \int_0^z \alpha(z) dz \right]. \quad (3.2)$$

Eq. (3.1) then takes the form

$$i \frac{\partial B}{\partial z} - \frac{\beta_2}{2} \frac{\partial^2 B}{\partial t^2} + \bar{\gamma} |B|^2 B = 0, \quad (3.3)$$

where the power variations along the DM fiber link are included through a periodically varying nonlinear parameter $\bar{\gamma} = \gamma \exp[-\int_0^z \alpha(z) dz]$. In general Eq. (3.3) is solved numerically to study the performance of DM systems. However considerable insights into the design of DM systems can be gained using the variational method. One can posit a Lagrangian density of the form

$$K = \frac{i}{2} \left(B^* \frac{\partial B}{\partial z} - B \frac{\partial B^*}{\partial z} \right) + \frac{1}{2} \left(\beta_2 \left| \frac{\partial B}{\partial t} \right|^2 + \bar{\gamma} |B|^4 \right). \quad (3.4)$$

and using the Euler-Lagrange equations

$$\frac{\partial}{\partial t} \left(\frac{\partial K}{\partial q_t} \right) + \frac{\partial}{\partial z} \left(\frac{\partial K}{\partial q_z} \right) - \frac{\partial K}{\partial q} = 0, \quad (3.5)$$

where the generalized coordinate q is B^* , q_t is $\frac{\partial B^*}{\partial t}$ and q_z is $\frac{\partial B^*}{\partial z}$, one can reproduce Eq. (3.3). The averaged Lagrangian density L is defined as $L = \int_{-\infty}^{\infty} K(t, q(z)) dt$. Then the reduced Euler-lagrangian density can be written as

$$\frac{d}{dz} \left(\frac{\partial L}{\partial q_z} \right) - \frac{\partial L}{\partial q} = 0, \quad (3.6)$$

where q are the pulse parameters that depend on z . For further calculations one needs to use a pulse shape.

3.1.1 Fundamental Soliton

A well-known solution to the NLS equation in a lossless, anomalous-dispersion, fiber is the fundamental soliton. But in the presence of loss and/or amplification, the fundamental soliton is perturbed. Hence we first consider a perturbed fundamental soliton for the pulse shape. The pulse shape is then given by

$$B(z, t) = a \operatorname{sech} \left(\frac{t-T}{\tau} \right) \exp[i\phi - i\Omega(t-T) - iC(t-T)^2/2\tau^2], \quad (3.7)$$

where the amplitude a , phase ϕ , frequency Ω , time delay T , chirp C and width τ all are functions of z . Normally, soliton pulses are unchirped. As an extension, we allow for a chirp on the input pulse that is small enough that the soliton shape does not change even though its width can change.

Using Eq. (3.7) in Eq. (3.4) we can find the Lagrangian density. In order to calculate the first term in the Lagrangian density we take the derivative of the pulse shape from Eq. (3.7) with respect to z and we get

$$\begin{aligned} \frac{\partial B}{\partial z} &= a \operatorname{sech} \left(\frac{t-T}{\tau} \right) \exp[i\phi - i\Omega(t-T) - iC(t-T)^2/2\tau^2] \\ &\quad \left[i \frac{\partial \phi}{\partial z} - i(t-T) \frac{\partial \Omega}{\partial z} + i\Omega \frac{\partial T}{\partial z} + i \frac{C(t-T)}{\tau^2} \frac{\partial T}{\partial z} - i \frac{(t-T)^2}{2\tau^2} \frac{\partial C}{\partial z} + iC \frac{(t-T)^2}{\tau^3} \frac{\partial \tau}{\partial z} \right] \\ &\quad + \frac{a}{\tau} \frac{\partial T}{\partial z} \operatorname{sech} \left(\frac{t-T}{\tau} \right) \tanh \left(\frac{t-T}{\tau} \right), \end{aligned} \quad (3.8)$$

and from Eq. (3.7)

$$\begin{aligned} B^* \frac{\partial B}{\partial z} &= \left[i \frac{\partial \phi}{\partial z} - i(t-T) \frac{\partial \Omega}{\partial z} + i\Omega \frac{\partial T}{\partial z} + i \frac{C(t-T)}{\tau^2} \frac{\partial T}{\partial z} - i \frac{(t-T)^2}{2\tau^2} \frac{\partial C}{\partial z} + iC \frac{(t-T)^2}{\tau^3} \frac{\partial \tau}{\partial z} \right] \\ &\quad a^2 \operatorname{sech}^2 \left(\frac{t-T}{\tau} \right) + \frac{a^2}{\tau} \frac{\partial T}{\partial z} \operatorname{sech}^2 \left(\frac{t-T}{\tau} \right) \tanh \left(\frac{t-T}{\tau} \right). \end{aligned} \quad (3.9)$$

Subtracting the complex conjugate of Eq. (3.9) from Eq. (3.9) we can write the first term in the Lagrangian density as

$$\frac{i}{2} \left(B^* \frac{\partial B}{\partial z} - B \frac{\partial B^*}{\partial z} \right) = \left[-\frac{\partial \phi}{\partial z} + (t-T) \frac{\partial \Omega}{\partial z} - \Omega \frac{\partial T}{\partial z} - \frac{C(t-T)}{\tau^2} \frac{\partial T}{\partial z} + \frac{(t-T)^2}{2\tau^2} \frac{\partial C}{\partial z} - C \frac{(t-T)^2}{\tau^3} \frac{\partial \tau}{\partial z} \right] \times a^2 \operatorname{sech}^2 \left(\frac{t-T}{\tau} \right). \quad (3.10)$$

Now to find the second term in the Lagrangian density, we take the derivative of Eq. (3.7) with respect to t to find that

$$\frac{\partial B}{\partial t} = - \left[\frac{a}{\tau} \operatorname{sech} \left(\frac{t-T}{\tau} \right) \tanh \left(\frac{t-T}{\tau} \right) + a \operatorname{sech} \left(\frac{t-T}{\tau} \right) (-i\Omega - iC(t-T)/\tau^2) \right] \exp[i\phi - i\Omega(t-T) - iC(t-T)^2/2\tau^2]. \quad (3.11)$$

Hence the second term of the lagrangian density can now be written from Eqs. (3.11) and (3.7) as

$$\frac{1}{2} \left(\beta_2 \left| \frac{\partial B}{\partial t} \right|^2 + \bar{\gamma} |B|^4 \right) = \left[\frac{\beta_2}{\tau^2} \tanh^2 \left(\frac{t-T}{\tau} \right) + \beta_2 \left(\Omega + C \frac{(t-T)}{\tau^2} \right)^2 + \bar{\gamma} a^2 \operatorname{sech}^2 \left(\frac{t-T}{\tau} \right) \right] \frac{a^2}{2} \operatorname{sech}^2 \left(\frac{t-T}{\tau} \right). \quad (3.12)$$

From Eqs. (3.10) and (3.12) the total Lagrangian density is given by

$$K = a^2 \operatorname{sech}^2 \left(\frac{t-T}{\tau} \right) \left[-\frac{\partial \phi}{\partial z} + (t-T) \frac{\partial \Omega}{\partial z} - \Omega \frac{\partial T}{\partial z} - \frac{C(t-T)}{\tau^2} \frac{\partial T}{\partial z} + \frac{(t-T)^2}{2\tau^2} \frac{\partial C}{\partial z} - C \frac{(t-T)^2}{\tau^3} \frac{\partial \tau}{\partial z} \right] + \frac{a^2}{2} \operatorname{sech}^2 \left(\frac{t-T}{\tau} \right) \left[\frac{\beta_2}{\tau^2} \tanh^2 \left(\frac{t-T}{\tau} \right) + \beta_2 \left(\Omega + C \frac{(t-T)}{\tau^2} \right)^2 + \bar{\gamma} a^2 \operatorname{sech}^2 \left(\frac{t-T}{\tau} \right) \right]. \quad (3.13)$$

Integrating the Lagrangian density K in Eq. (3.13) over t from $-\infty$ to ∞ , we can find the averaged Lagrangian density. All integrals can be evaluated analytically with the help of Table 3.1.1. The final result is

$$L = E \left[-\frac{d\phi}{dz} - \Omega \frac{dT}{dz} + \frac{\pi^2}{12} \left(\frac{1}{2} \frac{dC}{dz} - \frac{C}{\tau} \frac{d\tau}{dz} \right) \right] + \frac{\beta_2 E}{2} \left[\frac{1}{3\tau^2} \left(1 + \frac{\pi^2}{4} C^2 \right) + \Omega^2 \right] + \frac{\bar{\gamma} E^2}{6\tau}, \quad (3.14)$$

where $E = \int_{-\infty}^{\infty} a^2 \operatorname{sech}^2 \left(\frac{t-T}{\tau} \right) dt = 2a^2\tau$ is the energy of the pulse.

The evolution of various pulse parameters along the fiber can be found by applying Eq. (3.6) to Eq. (3.14). The resulting equations are called the variational equations. When $q = \phi$ we get the variational equation for the pulse energy E as

$$\frac{dE}{dz} = 0. \quad (3.15)$$

$f(x)$	1	x	x^2	$\tanh^2(x)$	$\operatorname{sech}^2(x)$
$\int_{-\infty}^{\infty} f(x) \operatorname{sech}^2(x) dx$	2	0	$\pi^2/6$	2/3	4/3

Table 3.1: Integration table to find the Lagrangian given by Eq. (3.14)

If $q = \Omega$ we get the equation for time delay T

$$\frac{dT}{dz} = \beta_2 \Omega, \quad (3.16)$$

if $q = T$ we get frequency equation

$$\frac{d\Omega}{dz} = 0, \quad (3.17)$$

when $q = C$ we get the equation for pulse width

$$\frac{d\tau}{dz} = \frac{\beta_2 C}{\tau}, \quad (3.18)$$

when $q = \tau$ we get the equation for variation in chirp

$$\frac{dC}{dz} = \frac{\beta_2}{\tau^2} \left(\frac{4}{\pi^2} + C^2 \right) + \beta_2 \Omega^2 + \frac{2\bar{\gamma}E}{\pi^2 \tau}. \quad (3.19)$$

The evolution of phase of the pulse can be found by using $q = E$ in Eq. (3.6) to be

$$\frac{d\phi}{dz} = \frac{\beta_2}{3\tau^2} + \frac{5\bar{\gamma}E}{12\tau}, \quad (3.20)$$

These variational equations show how the pulse parameters change over the fiber length and hence give insight into the pulse propagation along the fiber. The energy equation can be easily integrated over the fiber length. If the initial pulse has zero frequency shift, $\Omega(0) = 0$, then it will remain zero in the absence of amplifier noise. Since the temporal position, depends only on the frequency shift, the temporal position also remains constant in the absence of amplifier noise. The phase equation can be ignored as it is not coupled to the other parameters. Thus one needs to solve coupled equation that describe the pulse width and chirp which reduces to

$$\frac{d\tau}{dz} = \frac{\beta_2 C}{\tau}, \quad (3.21)$$

$$\frac{dC}{dz} = \frac{\beta_2}{\tau^2} \left(\frac{4}{\pi^2} + C^2 \right) + \frac{2\bar{\gamma}E}{\pi^2 \tau}. \quad (3.22)$$

For a fundamental soliton that is unchirped ($C = 0$), in the absence of effective fiber losses due to distributed amplification, we find from the variational equations that the energy E and pulse width τ remain constant along the fiber. Also, E and τ are not independent but related to each other by the soliton condition given in Eq. (2.60). The peak power of the solitons is related to the soliton energy $E = 2P_0\tau$. Using this relation, in Eq. (2.60) we find that $E = 2|\beta_2|/\gamma\tau$ for fundamental solitons. Eqs. (3.21) and (3.22) show that initially unchirped soliton maintains both its chirp and pulse width while propagating in an anomalous GVD fiber as expected.

3.1.2 Gaussian pulse

Next consider the case of a DM soliton that can be represented by a chirped-Gaussian shape pulse of the form

$$B(z, t) = a \exp[i\phi - i\Omega(t - T) - (1 + iC)(t - T)^2/2\tau^2]. \quad (3.23)$$

Using such a pulse shape in Eq. (3.4), the Lagrangian density can be found in the case of Gaussian pulses. In order to find the first term of the Lagrangian density, we take the derivative of Eq. (3.23) with respect to z and get

$$\begin{aligned} \frac{\partial B}{\partial z} = a \exp[i\phi - i\Omega(t - T) - (1 + iC)(t - T)^2/2\tau^2] & \left[i \frac{\partial \phi}{\partial z} - i(t - T) \frac{\partial \Omega}{\partial z} + i\Omega \frac{\partial T}{\partial z} \right. \\ & \left. + (1 + iC) \frac{(t - T)}{\tau^2} \frac{\partial T}{\partial z} - i \frac{(t - T)^2}{2\tau^2} \frac{\partial C}{\partial z} + (1 + iC) \frac{(t - T)^2}{\tau^3} \frac{\partial \tau}{\partial z} \right]. \end{aligned} \quad (3.24)$$

Using Eqs. (3.23) and (3.24) we find

$$\begin{aligned} B^* \frac{\partial B}{\partial z} = a \exp[-(t - T)^2/\tau^2] & \left[i \frac{\partial \phi}{\partial z} - i(t - T) \frac{\partial \Omega}{\partial z} + \left(i\Omega + (1 + iC) \frac{(t - T)}{\tau^2} \right) \frac{\partial T}{\partial z} \right. \\ & \left. - i \frac{(t - T)^2}{2\tau^2} \frac{\partial C}{\partial z} + (1 + iC) \frac{(t - T)^2}{\tau^3} \frac{\partial \tau}{\partial z} \right]. \end{aligned} \quad (3.25)$$

Subtracting the complex conjugate of Eq. (3.24) from Eq. (3.25) we get the first term of the Lagrangian density to be

$$\begin{aligned} \frac{i}{2} \left(B^* \frac{\partial B}{\partial z} - B \frac{\partial B^*}{\partial z} \right) = & \left[-\frac{\partial \phi}{\partial z} + (t - T) \frac{\partial \Omega}{\partial z} - \left(\Omega + C \frac{(t - T)}{\tau^2} \right) \frac{\partial T}{\partial z} + i \frac{(t - T)^2}{2\tau^2} \frac{\partial C}{\partial z} \right. \\ & \left. + (1 - iC) \frac{(t - T)^2}{\tau^3} \frac{\partial \tau}{\partial z} \right] a^2 \exp[-(t - T)^2/\tau^2]. \end{aligned} \quad (3.26)$$

$f(x)$	1	x	x^2	$\exp(-x^2)$
$\int_{-\infty}^{\infty} f(x) \exp(-x^2) dx$	$\sqrt{\pi}$	0	$\sqrt{\pi}/2$	$\sqrt{\pi/2}$

Table 3.2: Integration table to find the Lagrangian given by Eq. (3.30)

Now to calculate the second term of the Lagrangian density we take the derivative of Eq. (3.23) with respect to t and find

$$\frac{\partial B}{\partial t} = a \exp[i\phi - i\Omega(t-T) - (1+iC)(t-T)^2/2\tau^2] (-i\Omega - (1+iC)(t-T)/\tau^2), \quad (3.27)$$

Using Eqs. (3.23) and (3.27) we can write the second term of the Lagrangian density as

$$\begin{aligned} \frac{1}{2} \left(\beta_2 \left| \frac{\partial B}{\partial t} \right|^2 + \bar{\gamma} |B|^4 \right) &= \frac{\beta_2 a^2}{2} \exp\left[-\frac{(t-T)^2}{\tau^2}\right] \left[\frac{(t-T)^2}{\tau^4} + \left(\Omega + C \frac{(t-T)}{\tau^2} \right)^2 \right] \\ &\quad + \frac{\bar{\gamma}}{2} a^4 \exp\left[-\frac{2(t-T)^2}{\tau^2}\right]. \end{aligned} \quad (3.28)$$

From Eqs (3.26) and (3.28) the total Lagrangian density can be written as

$$\begin{aligned} K &= a^2 \exp[-(t-T)^2/\tau^2] \left[-\frac{\partial \phi}{\partial z} + (t-T) \frac{\partial \Omega}{\partial z} - \left(\Omega + C \frac{(t-T)}{\tau^2} \right) \frac{\partial T}{\partial z} + \frac{(t-T)^2}{2\tau^2} \frac{\partial C}{\partial z} - C \frac{(t-T)^2}{\tau^3} \frac{\partial \tau}{\partial z} \right] \\ &\quad + \frac{a^2}{2} \exp[-(t-T)^2/\tau^2] \left[\beta_2 \left(\frac{(t-T)^2}{\tau^4} + \left(\Omega + C \frac{(t-T)}{\tau^2} \right)^2 \right) + \bar{\gamma} a^2 \exp\left[-\frac{(t-T)^2}{\tau^2}\right] \right]. \end{aligned} \quad (3.29)$$

Integrating Eq (3.32) over t from $-\infty$ to ∞ we find the averaged Lagrangian density. The integral can again be performed analytically with the help of Table 3.1.2. The final result is

$$L = E \left[-\frac{d\phi}{dz} - \Omega \frac{dT}{dz} + \left(\frac{1}{4} \frac{dC}{dz} - \frac{C}{2\tau} \frac{d\tau}{dz} \right) \right] + \frac{\beta_2 E}{4\tau^2} (1 + C^2) + \beta_2 E \Omega^2 / 2 + \frac{\bar{\gamma} E^2}{(8\pi)^{1/2} \tau}, \quad (3.30)$$

where the pulse energy in this case is given by $E = \int_{-\infty}^{\infty} a^2 \exp\left[-\frac{(t-T)^2}{\tau^2}\right] dt = \sqrt{\pi} a^2 \tau$.

Applying Eq. (3.6) to Eq. (3.30) we can find the evolution of various pulse parameters. First the equation for energy can be found by using $q = \phi$ in Eq. (3.6) and can be written as

$$\frac{dE}{dz} = 0. \quad (3.31)$$

When $q = \Omega$ we get the equation for time delay T

$$\frac{dT}{dz} = \beta_2 \Omega, \quad (3.32)$$

if $q = T$ we get frequency equation

$$\frac{d\Omega}{dz} = 0, \quad (3.33)$$

when $q = C$ we get the equation for pulse width

$$\frac{d\tau}{dz} = \frac{\beta_2 C}{\tau}, \quad (3.34)$$

and when $q = \tau$ we get the equation for variation in chirp

$$\frac{dC}{dz} = \frac{\beta_2}{\tau^2}(1 + C^2) + \beta_2 \Omega^2 + \frac{2\bar{\gamma}E}{\sqrt{8\pi\tau}}, \quad (3.35)$$

and the phase evolution can then be found again by using $q = E$ in Eq. (3.6) to be

$$\frac{d\phi}{dz} = \frac{\beta_2}{2\tau^2} + \frac{5\bar{\gamma}E}{2^{5/2}\pi^{1/2}\tau}, \quad (3.36)$$

Similar to the fundamental soliton case, we can ignore the energy and phase equations. In the absence of Raman Scattering, the frequency remains constant and hence the temporal position equation is integrable and the coupled equations for τ and C can be written as

$$\frac{d\tau}{dz} = \frac{\beta_2 C}{\tau}, \quad (3.37)$$

$$\frac{dC}{dz} = \frac{\beta_2}{\tau^2}(1 + C^2) + \frac{2\bar{\gamma}E}{\sqrt{8\pi\tau}}. \quad (3.38)$$

In the absence of nonlinearity, the ratio $(1 + C^2)/\tau^2$ is related to the spectral width of the pulse which remains constant in a linear medium. For such a case the Eqs. (3.37) and (3.38) can now be solved analytically and have the following general solution:

$$\tau^2(z) = \tau^2(0) + 2 \int_0^z \beta_2(z)C(z)dz, \quad C(z) = C(0) + \frac{1 + C^2(0)}{\tau^2(0)} \int_0^z \beta_2(z)dz. \quad (3.39)$$

Integrating over two sections of the dispersion map, the value of pulse width and chirp at the end of the first map period L_m are given by

$$\tau(L_m) = \tau(0)[(1 + C(0)d)^2 + d^2]^{1/2}, \quad C(L_m) = C(0) + (1 + C^2(0))d, \quad (3.40)$$

where $d = \beta_{av}L_m/\tau^2(0)$ and β_{av} is the average GVD value. When $\bar{\beta}_2 = 0$, both the pulse width and chirp return to the input values at the end of each map period. If the average dispersion is non-zero, then the pulse does not evolve periodically. If the input peak power is so large that the nonlinearity cannot be neglected, the pulse parameters do not return to their input values even for perfect

GVD compensation. However one can find periodic solutions of these equations numerically by imposing the periodic boundary conditions $\tau(L_m) = \tau(0)$ and $C(L_m) = C(0)$ which ensure that the pulse recovers its initial shape at the end of each map period. Such pulses propagate through the dispersion managed link in a periodic fashion and are called dispersion-managed solitons.

Thus a combination of the variational method with direct numerical simulations can form an efficient approach to many problems in fiber communications. However the use of the variational method is limited to systems that conserve energy. However in the presence of higher-order nonlinear effects such as intrapulse Raman scattering which can cause dissipation in the system and so writing a Lagrangian for such systems is not possible. Thus the variational method cannot be used to study such systems and one has to revert to other approximate methods.

3.2 Intrapulse Raman Scattering

It was discovered in 1985 numerically [34] that the spectrum of an ultra short optical pulse can shift toward longer wavelengths (a “red” shift) when the pulse propagates in the anomalous-dispersion regime of an optical fiber. Such a spectral shift was observed in a 1986 experiment [35] by using a stabilized, mode-locked laser capable of emitting pulses shorter than 1 ps. It was called the soliton self-frequency shift (SSFS) because pulses whose spectrum was red-shifted were propagating as solitons inside the optical fiber used in the experiment. In fact, Gordon used a perturbation theory of solitons for predicting the magnitude of the spectral shift and its dependence on the pulse and fiber parameters [36]. Physically, the spectral shift is attributed to the intrapulse Raman scattering (IRS), a phenomenon in which high-frequency components of an optical pulse pump the low-frequency components of the same pulse, thereby transferring energy to the red side through stimulated Raman scattering [37]– [40].

In order to understand the phenomenon of IRS better we have to go to the derivation of the NLS equation in chapter 2. Eq. (2.57) should be modified for ultrashort optical pulses whose width is ≤ 5 ps. The spectral width of such pulses becomes comparable to the carrier frequency and several approximations made in the derivation of Eq. (2.57) become questionable. Furthermore, the spectrum of such short pulses is wide enough that the Raman gain in the fiber can amplify their low-frequency components by transferring energy from high-frequency components of the

same pulse, leading to the IRS that causes the pulse spectrum to shift toward the red side as the pulse propagates inside the fiber. The physical origin of this effect is related to the retarded nature of nonlinear response. While deriving Eq. (2.57) from Eq. (2.19), we made the assumption that the nonlinear response of the fiber is instantaneous. Using this we modified Eq. (2.26) to give Eq. (2.27), by using $\chi^{(3)}(t-t_1, t-t_2, t-t_3) = \delta(t-t_1)\delta(t-t_2)\delta(t-t_3)$. This approximation is no longer valid.

Delayed nonlinear effects can be included by assuming the following functional form for the third-order susceptibility,

$$\chi^{(3)}(t-t_1, t-t_2, t-t_3) = \chi^{(3)}R(t-t_1)\delta(t-t_2)\delta(t-t_3) \quad (3.41)$$

where $R(t-t_1)$ is the nonlinear response function normalized similar to the delta function as $\int_{-\infty}^{\infty} R(t)dt = 1$. Substituting this form for $\chi^{(3)}$ in Eq. (2.25) and carrying out the two integrals over the delta functions, we can write the nonlinear polarization as

$$P_{NL} = \epsilon_0 \chi^{(3)} E(\mathbf{r}, t) \int_{-\infty}^t R(t-t_1) |E(\mathbf{r}, t_1)|^2 dt_1, \quad (3.42)$$

where it is assumed that the electric field and the induced polarization vectors point along the same direction. The upper limit of integration extends only up to t because the response function $R(t-t_1)$ must be zero for $t_1 > t$ to ensure causality. Now using Eqs. (3.42), (2.28) and (2.29) we can rewrite Eq. (2.35) as

$$\begin{aligned} \nabla^2 \tilde{E} + n^2(\omega) k_0^2 \tilde{E} &= -ik_0 \alpha + \chi^{(3)} k_0^2 \int \int_{-\infty}^{\infty} \tilde{R}(\omega - \omega_1) \\ &\times \tilde{E}(\omega_1, z) \tilde{E}(\omega_2, z) \tilde{E}(\omega_1 + \omega_2 - \omega, z) d\omega_1 d\omega_2, \end{aligned} \quad (3.43)$$

where $\tilde{R}(\omega)$ is the Fourier transform of $R(t)$. As before, we can treat the terms on the right hand side of Eq. (3.43) as a small perturbation and obtain the modal distribution by the same method used in chapter 2. Using the slowly varying amplitude $A(z, t)$ as in Eq. (2.40) we can get the following equation for ultrashort pulses inside the fiber [52]:

$$\begin{aligned} \frac{\partial A}{\partial z} + \frac{\alpha}{2} A + \beta_1 \frac{\partial A}{\partial t} + \frac{i\beta_2}{2} \frac{\partial^2 A}{\partial t^2} - \frac{\beta_3}{6} \frac{\partial^3 A}{\partial t^3} \\ = i\gamma \left(1 + \frac{i}{\omega_0} \frac{\partial}{\partial t} \right) \left(A(z, t) \int_{-\infty}^{\infty} R(t') |A(z, t-t')|^2 dt' \right), \end{aligned} \quad (3.44)$$

where γ is the nonlinear parameter defined in Eq. (2.55) and ω_0 is the center frequency of the pulse spectrum. The time derivative appearing on the right hand side of Eq. (3.44) includes the self steepening effect, shock formation at the pulse edge and IRS.

The response function $R(t)$ should include both the electronic and vibrational (Raman) contributions. Assuming that the electronic contribution is nearly instantaneous, the functional form of $R(t)$ can be written as [41]–[45]

$$R(t) = (1 - f_R)\delta(t) + f_R h_R(t), \quad (3.45)$$

where f_R represents the fractional contribution of the delayed Raman response to the nonlinear polarization. The Raman response function $h_R(t)$ is responsible for the Raman gain. For pulses shorter than 5 ps we can use the Taylor-series expansion to $|A(z, t - t')|^2$ such that

$$|A(z, t - t')|^2 \approx |A(z, t)|^2 - t' \frac{\partial}{\partial t} |A(z, t)|^2. \quad (3.46)$$

This approximation is valid if the pulse envelope evolves slowly along the fiber. Defining the first moment of the nonlinear response function as

$$T_R = \int_{-\infty}^{\infty} t h_R(t) dt, \quad (3.47)$$

and using that $\int_{-\infty}^{\infty} R(t) dt = 1$ along with Eq. (3.46) in Eq. (3.44) we get

$$\frac{\partial A}{\partial z} + \frac{\alpha}{2} A + \beta_1 \frac{\partial A}{\partial t} + \frac{i\beta_2}{2} \frac{\partial^2 A}{\partial t^2} - \frac{\beta_3}{6} \frac{\partial^3 A}{\partial t^3} = i\gamma \left(|A|^2 A + \frac{i}{\omega_0} \frac{\partial}{\partial t} (|A|^2 A) - T_R A \frac{\partial |A|^2}{\partial t} \right). \quad (3.48)$$

Once again using the transformation $t' = t - \beta_1 z$, we can write Eq. (3.48) as

$$\frac{\partial A}{\partial z} + \frac{\alpha}{2} A + \frac{i\beta_2}{2} \frac{\partial^2 A}{\partial t'^2} - \frac{\beta_3}{6} \frac{\partial^3 A}{\partial t'^3} = i\gamma \left(|A|^2 A + \frac{i}{\omega_0} \frac{\partial}{\partial t'} (|A|^2 A) - T_R A \frac{\partial |A|^2}{\partial t'} \right). \quad (3.49)$$

Now using the transformation in Eq. (3.2) we can eliminate the loss term and for the sake of simplicity dropping the prime on t we can write Eq. (3.49) as

$$\frac{\partial B}{\partial z} + \frac{i\beta_2}{2} \frac{\partial^2 B}{\partial t^2} - \frac{\beta_3}{6} \frac{\partial^3 B}{\partial t^3} = \bar{\gamma} |B|^2 B - \frac{\bar{\gamma}}{\omega_0} \frac{\partial}{\partial t} (|B|^2 B) - i\bar{\gamma} T_R B \frac{\partial |B|^2}{\partial t}. \quad (3.50)$$

The term proportional to β_3 governs the effects of third-order dispersion and becomes important for ultra short pulses. The term proportional to ω_0^{-1} is responsible for self-steepening and shock formation and is important for pulses shorter than a few fs. The last term proportional to T_R is

responsible for intrapulse Raman scattering and is related to the slope of the Raman gain spectrum of the material of the fiber and takes a value of 3 fs for a pulse propagating at $1.55\mu\text{m}$ in standard silica fiber. All three parameters are negligible for pulses whose width, $\tau \gg 1$ ps but they become appreciable for femtosecond pulses. As an example consider a 30 fs (full width at half maximum of 50 fs) propagating at $\lambda = 1.55 \mu\text{m}$, whose carrier frequency ω_0 is given by $2\pi c/\lambda$. For such a system the self steepening coefficient, $\omega_0^{-1} = 0.8$ fs while Raman scattering coefficient T_R is 3 fs. Hence the self-steepening term can be neglected for pulses whose width is larger than 30 fs but the term responsible for intrapulse Raman scattering is still important.

3.3 Chapter Summary

As seen before the IRS can lead to a shift in the soliton frequency. This Raman-induced frequency shift (RIFS) is negligible for pulse width larger than 10 ps but becomes of considerable importance for short solitons ($\tau(0) < 1\text{ps}$). The RIFS leads to considerable changes in the evolution of solitons as it modifies the gain and dispersion experienced by solitons. When the spectral shift becomes large that it cannot be compensated, the soliton moves out of the gain window of the amplifiers thus losing all its energy. For ultrashort solitons, including the IRS and third-order dispersion, the NLS equation given in Eq. (3.49) can be written as

$$\frac{\partial A}{\partial z} + \frac{\alpha}{2}A + \frac{i\beta_2}{2} \frac{\partial^2 A}{\partial t^2} - \frac{\beta_3}{6} \frac{\partial^3 A}{\partial t^3} = i\gamma|A|^2A + -i\gamma T_R A \frac{\partial |A|^2}{\partial t}. \quad (3.51)$$

In the presence of IRS, the system becomes dissipative and writing a Lagrangian density for such a system is not possible. Hence the variational method cannot be used to study the effects of IRS on pulse propagation in a fiber. To study the IRS in solitons, soliton perturbation theory can be used. However for ultrashort pulses, the IRS is no longer small enough to be treated as a perturbation. Also from a physical standpoint, it is hard to see why the spectral red shift of ultrashort pulses should require the formation of solitons. The IRS phenomenon should occur for any optical pulse, irrespective of whether it propagates in the normal- or anomalous-dispersion regime of an optical fiber. It should also be affected by the frequency chirp, if the input pulse is chirped. In effect, although the variational approach works well for conservative systems, it fails in the presence of Raman scattering in the fiber. Hence a more generalized theory that will work for both dissipative

and non-dissipative systems has to be used in order to study the pulse propagation in the case of systems using ultrashort pulses. In the next chapter we use the moment method to develop a general theory to study the pulse propagation in optical fibers.

Chapter 4

The Moment Method

The Moment method was developed as early as 1971 [11] and has been used to calculate timing jitter in DM systems [56]. This method provides simple analytic theory for studying the evolution of the pulse parameters thus helping to gain insights into pulse propagation. Since this method does not require a Lagrangian, this method can be used for both dissipative and non dissipative systems.

4.1 Definition of the Moments

The basic idea of the Moment method is to treat the optical pulse like a particle [11] whose energy E , position T , and the frequency Ω are defined as

$$E = \int_{-\infty}^{\infty} |B|^2 dt, \quad (4.1)$$

$$T = \frac{1}{E} \int_{-\infty}^{\infty} t |B|^2 dt, \quad (4.2)$$

$$\Omega = \frac{i}{2E} \int_{-\infty}^{\infty} \left(B^* \frac{\partial B}{\partial t} - B \frac{\partial B^*}{\partial t} \right) dt, \quad (4.3)$$

where B is related to the envelope of the pulse, A launched into the fiber by the transformation shown in Eq. (3.2). The root mean square (RMS) width of such a pulse is defined as

$$\sigma^2 = \frac{1}{E} \int_{-\infty}^{\infty} (t - T)^2 |B|^2 dt. \quad (4.4)$$

The actual pulse width is related to the RMS width by a constant factor that depends on the pulse shape. We introduce one more moment related to the chirp of the pulse by the same constant factor

using the definition

$$\tilde{C} = \frac{i}{2E} \int_{-\infty}^{\infty} (t - T) \left(B^* \frac{\partial B}{\partial t} - B \frac{\partial B^*}{\partial t} \right) dt. \quad (4.5)$$

Evidently, the evolution of these pulse parameters depend on the evolution of the pulse itself in the fiber which is governed by the NLS equation Eq. (3.50) in the case of ultra short pulses. To find the evolution of these pulse parameters we use Eqs. (4.1)– (4.5) along with Eq. (3.50).

4.1.1 Energy Evolution

First consider the evolution of the pulse energy. To find that we differentiate Eq. (4.1) with respect to z and get

$$\frac{dE}{dz} = \int_{-\infty}^{\infty} \left(B^* \frac{\partial B}{\partial z} + B \frac{\partial B^*}{\partial z} \right) dt. \quad (4.6)$$

Using Eq. (3.48) we find that

$$\frac{\partial B}{\partial z} = -i \frac{\beta_2}{2} \frac{\partial^2 B}{\partial t^2} + \frac{\beta_3}{6} \frac{\partial^3 B}{\partial t^3} - \frac{\bar{\gamma}}{\omega_0} \frac{\partial}{\partial t} (|B|^2 B) - i \bar{\gamma} T_R B \frac{\partial |B|^2}{\partial t} + i \bar{\gamma} |B|^2 B. \quad (4.7)$$

Hence we can write

$$B^* \frac{\partial B}{\partial z} = -i \frac{\beta_2}{2} B^* \frac{\partial^2 B}{\partial t^2} + \frac{\beta_3}{6} B^* \frac{\partial^3 B}{\partial t^3} - B^* \frac{\bar{\gamma}}{\omega_0} \frac{\partial}{\partial t} (|B|^2 B) - i \bar{\gamma} T_R |B|^2 \frac{\partial |B|^2}{\partial t} + i \bar{\gamma} |B|^4, \quad (4.8)$$

$$B \frac{\partial B^*}{\partial z} = i \frac{\beta_2}{2} B \frac{\partial^2 B^*}{\partial t^2} + \frac{\beta_3}{6} B \frac{\partial^3 B^*}{\partial t^3} - B \frac{\bar{\gamma}}{\omega_0} \frac{\partial}{\partial t} (|B|^2 B^*) + i \bar{\gamma} T_R |B|^2 \frac{\partial |B|^2}{\partial t} - i \bar{\gamma} |B|^4. \quad (4.9)$$

Adding Eqs. (4.8) and (4.9) and substituting in Eq. (4.6) we get

$$\begin{aligned} \frac{dE}{dz} &= \int_{-\infty}^{\infty} i \frac{\beta_2}{2} \left(B \frac{\partial^2 B^*}{\partial t^2} - B^* \frac{\partial^2 B}{\partial t^2} \right) dt + \int_{-\infty}^{\infty} \frac{\beta_3}{6} \left(B^* \frac{\partial^3 B}{\partial t^3} + B \frac{\partial^3 B^*}{\partial t^3} \right) dt \\ &\quad - \frac{\bar{\gamma}}{\omega_0} \int_{-\infty}^{\infty} \left(B^* \frac{\partial}{\partial t} (|B|^2 B) + B \frac{\partial}{\partial t} (|B|^2 B^*) \right) dt. \end{aligned} \quad (4.10)$$

Consider the first integral in Eq. (4.10). Leaving out the coefficients it is given by

$$\int_{-\infty}^{\infty} \left(B \frac{\partial^2 B^*}{\partial t^2} - B^* \frac{\partial^2 B}{\partial t^2} \right) dt = \int_{-\infty}^{\infty} B \frac{\partial^2 B^*}{\partial t^2} dt - \int_{-\infty}^{\infty} B^* \frac{\partial^2 B}{\partial t^2} dt. \quad (4.11)$$

Integrating by parts we find that

$$\int_{-\infty}^{\infty} \left(B \frac{\partial^2 B^*}{\partial t^2} - B^* \frac{\partial^2 B}{\partial t^2} \right) dt = B \frac{\partial B^*}{\partial t} \Big|_{-\infty}^{\infty} - \int_{-\infty}^{\infty} \left| \frac{\partial B}{\partial t} \right|^2 dt - B^* \frac{\partial B}{\partial t} \Big|_{-\infty}^{\infty} + \int_{-\infty}^{\infty} \left| \frac{\partial B}{\partial t} \right|^2 dt. \quad (4.12)$$

The second and the fourth term in Eq. (4.12) cancel each other and since $B(z, t)$ is the pulse envelope and hence at $t \rightarrow \infty$ the field must vanish which means as $t \rightarrow \infty$, $B(z, t)$ and $\frac{\partial B}{\partial t}$ exponentially tend to zero. Using these conditions in Eq. (4.12) we get

$$\int_{-\infty}^{\infty} \left(B \frac{\partial^2 B^*}{\partial t^2} - B^* \frac{\partial^2 B}{\partial t^2} \right) dt = 0. \quad (4.13)$$

Now considering the second integral in Eq. (4.10) given by

$$\int_{-\infty}^{\infty} \left(B^* \frac{\partial^3 B}{\partial t^3} + B \frac{\partial^3 B^*}{\partial t^3} \right) dt = \int_{-\infty}^{\infty} B^* \frac{\partial^3 B}{\partial t^3} dt + \int_{-\infty}^{\infty} B \frac{\partial^3 B^*}{\partial t^3} dt. \quad (4.14)$$

Performing the integration by parts we get

$$\int_{-\infty}^{\infty} \left(B^* \frac{\partial^3 B}{\partial t^3} + B \frac{\partial^3 B^*}{\partial t^3} \right) dt = B^* \frac{\partial^2 B}{\partial t^2} \Big|_{-\infty}^{\infty} - \int_{-\infty}^{\infty} \frac{\partial B}{\partial t} \frac{\partial^2 B^*}{\partial t^2} dt + B \frac{\partial^2 B^*}{\partial t^2} \Big|_{-\infty}^{\infty} - \int_{-\infty}^{\infty} \frac{\partial B^*}{\partial t} \frac{\partial^2 B}{\partial t^2} dt. \quad (4.15)$$

The first and the third terms equal 0 since B and B^* vanish at the limits. Hence we have

$$\int_{-\infty}^{\infty} \left(B^* \frac{\partial^3 B}{\partial t^3} + B \frac{\partial^3 B^*}{\partial t^3} \right) dt = - \int_{-\infty}^{\infty} \left(\frac{\partial B}{\partial t} \frac{\partial^2 B^*}{\partial t^2} + \frac{\partial B^*}{\partial t} \frac{\partial^2 B}{\partial t^2} \right) dt. \quad (4.16)$$

Integrating again by parts

$$\begin{aligned} \int_{-\infty}^{\infty} \left(B^* \frac{\partial^3 B}{\partial t^3} + B \frac{\partial^3 B^*}{\partial t^3} \right) dt &= - \int_{-\infty}^{\infty} \left(\frac{\partial B}{\partial t} \frac{\partial^2 B^*}{\partial t^2} + \frac{\partial B^*}{\partial t} \frac{\partial^2 B}{\partial t^2} \right) dt, \\ &= - \left| \frac{\partial B}{\partial t} \right|^2 + \int_{-\infty}^{\infty} \frac{\partial B^*}{\partial t} \frac{\partial^2 B}{\partial t^2} dt - \left| \frac{\partial B}{\partial t} \right|^2 + \int_{-\infty}^{\infty} \frac{\partial B}{\partial t} \frac{\partial^2 B^*}{\partial t^2} dt, \\ &= \int_{-\infty}^{\infty} \left(\frac{\partial B}{\partial t} \frac{\partial^2 B^*}{\partial t^2} + \frac{\partial B^*}{\partial t} \frac{\partial^2 B}{\partial t^2} \right) dt. \end{aligned} \quad (4.17)$$

From Eqs. (4.16) and (4.17) we can conclude

$$\int_{-\infty}^{\infty} \left(B^* \frac{\partial^3 B}{\partial t^3} + B \frac{\partial^3 B^*}{\partial t^3} \right) dt = 0. \quad (4.18)$$

Expanding the final integral in Eq. (4.10) we get

$$\begin{aligned} \int_{-\infty}^{\infty} \left(B^* \frac{\partial}{\partial t} (|B|^2 B) + B \frac{\partial}{\partial t} (|B|^2 B^*) \right) dt &= \int_{-\infty}^{\infty} \left(|B|^2 \frac{\partial |B|^2}{\partial t} + B^* |B|^2 \frac{\partial B}{\partial t} + |B|^2 \frac{\partial |B|^2}{\partial t} + B |B|^2 \frac{\partial B^*}{\partial t} \right) dt, \\ &= 3 \int_{-\infty}^{\infty} |B|^2 \frac{\partial |B|^2}{\partial t} dt. \end{aligned} \quad (4.19)$$

Integrating Eq. (4.19) by parts we get

$$\int_{-\infty}^{\infty} |B|^2 \frac{\partial |B|^2}{\partial t} dt = |B|^4 \Big|_{-\infty}^{\infty} - \int_{-\infty}^{\infty} |B|^2 \frac{\partial |B|^2}{\partial t} dt. \quad (4.20)$$

The first term in Eq. (4.20) goes to zero at the limits. Hence we can write

$$\int_{-\infty}^{\infty} |B|^2 \frac{\partial |B|^2}{\partial t} dt = - \int_{-\infty}^{\infty} |B|^2 \frac{\partial |B|^2}{\partial t} dt = 0. \quad (4.21)$$

Substituting Eqs. (4.13), (4.18) and (4.21) in Eq. (4.10) we find the evolution of pulse energy along the fiber is given by

$$\frac{dE}{dz} = 0. \quad (4.22)$$

Eq. (4.22) shows that the pulse energy remains constant when the pulse propagates along the fiber just as in a losses fiber. This is because the power losses are included in the nonlinear parameter $\bar{\gamma}$, while making the transformation in Eq. (3.2).

4.1.2 Evolution of Pulse Position

Next we find the evolution of the pulse position along the fiber. Differentiating Eq. (4.2) with respect to z we get

$$\frac{dT}{dz} = \frac{1}{E} \int_{-\infty}^{\infty} t \left(B^* \frac{\partial B}{\partial z} + B \frac{\partial B^*}{\partial z} \right) dt. \quad (4.23)$$

Adding Eqs. (4.8) and (4.9) and substituting in Eq. (4.23) we get

$$\begin{aligned} \frac{dT}{dz} = & \frac{i\beta_2}{2E} \int_{-\infty}^{\infty} t \left(B \frac{\partial^2 B^*}{\partial t^2} - B^* \frac{\partial^2 B}{\partial t^2} \right) dt + \frac{\beta_3}{6E} \int_{-\infty}^{\infty} t \left(B^* \frac{\partial^3 B}{\partial t^3} + B \frac{\partial^3 B^*}{\partial t^3} \right) dt \\ & - \frac{\bar{\gamma}}{\omega_0 E} \int_{-\infty}^{\infty} t \left(B^* \frac{\partial}{\partial t} (B|B|^2) + B \frac{\partial}{\partial t} (B^*|B|^2) \right) dt. \end{aligned} \quad (4.24)$$

Considering the first integral we can do the integration by parts and get

$$\int_{-\infty}^{\infty} t \left(B \frac{\partial^2 B^*}{\partial t^2} - B^* \frac{\partial^2 B}{\partial t^2} \right) dt = tB \frac{\partial B^*}{\partial t} \Big|_{-\infty}^{\infty} - \int_{-\infty}^{\infty} \frac{\partial B^*}{\partial t} \frac{\partial (tB)}{\partial t} dt - tB^* \frac{\partial B}{\partial t} \Big|_{-\infty}^{\infty} + \int_{-\infty}^{\infty} \frac{\partial B}{\partial t} \frac{\partial (tB^*)}{\partial t} dt. \quad (4.25)$$

The first and third terms vanish at the limits and hence we have

$$\begin{aligned} \int_{-\infty}^{\infty} t \left(B \frac{\partial^2 B^*}{\partial t^2} - B^* \frac{\partial^2 B}{\partial t^2} \right) dt &= \int_{-\infty}^{\infty} \left(\frac{\partial B}{\partial t} \frac{\partial (tB^*)}{\partial t} - \frac{\partial B^*}{\partial t} \frac{\partial (tB)}{\partial t} \right) dt, \\ &= \int_{-\infty}^{\infty} \left(t \left| \frac{\partial B}{\partial t} \right|^2 + B^* \frac{\partial B}{\partial t} - t \left| \frac{\partial B}{\partial t} \right|^2 - B \frac{\partial B^*}{\partial t} \right) dt, \\ &= \int_{-\infty}^{\infty} \left(B^* \frac{\partial B}{\partial t} - B \frac{\partial B^*}{\partial t} \right) dt. \end{aligned} \quad (4.26)$$

From the definition of frequency in Eq (4.3) we can write Eq. (4.26) as

$$\int_{-\infty}^{\infty} t \left(B \frac{\partial^2 B^*}{\partial t^2} - B^* \frac{\partial^2 B}{\partial t^2} \right) dt = -2iE\Omega. \quad (4.27)$$

Now consider the second term in Eq. (4.24) given by

$$\int_{-\infty}^{\infty} t \left(B^* \frac{\partial^3 B}{\partial t^3} + B \frac{\partial^3 B^*}{\partial t^3} \right) dt = t B^* \frac{\partial^2 B}{\partial t^2} \Big|_{-\infty}^{\infty} - \int_{-\infty}^{\infty} \frac{\partial^2 B}{\partial t^2} \frac{\partial(tB^*)}{\partial t} dt + t B \frac{\partial^2 B^*}{\partial t^2} \Big|_{-\infty}^{\infty} - \int_{-\infty}^{\infty} \frac{\partial^2 B^*}{\partial t^2} \frac{\partial(tB)}{\partial t} dt. \quad (4.28)$$

The first and third terms vanish at the limits. Hence Eq. (4.28) can be written as

$$\begin{aligned} \int_{-\infty}^{\infty} t \left(B^* \frac{\partial^3 B}{\partial t^3} + B \frac{\partial^3 B^*}{\partial t^3} \right) dt &= - \int_{-\infty}^{\infty} \left(t \frac{\partial^2 B}{\partial t^2} \frac{\partial B^*}{\partial t} + B^* \frac{\partial^2 B}{\partial t^2} + t \frac{\partial^2 B^*}{\partial t^2} \frac{\partial B}{\partial t} + B \frac{\partial^2 B^*}{\partial t^2} \right) dt. \\ &= - \int_{-\infty}^{\infty} t \left(\frac{\partial^2 B}{\partial t^2} \frac{\partial B^*}{\partial t} + \frac{\partial^2 B^*}{\partial t^2} \frac{\partial B}{\partial t} \right) dt - \int_{-\infty}^{\infty} \left(B^* \frac{\partial^2 B}{\partial t^2} + B \frac{\partial^2 B^*}{\partial t^2} \right) dt. \end{aligned} \quad (4.29)$$

Now consider the first term on the right hand side of Eq. (4.29).

$$\begin{aligned} - \int_{-\infty}^{\infty} t \left(\frac{\partial^2 B}{\partial t^2} \frac{\partial B^*}{\partial t} + \frac{\partial^2 B^*}{\partial t^2} \frac{\partial B}{\partial t} \right) dt &= -t \left| \frac{\partial B}{\partial t} \right|^2 \Big|_{-\infty}^{\infty} + \int_{-\infty}^{\infty} \frac{\partial B}{\partial t} \left[\frac{\partial B^*}{\partial t} + t \frac{\partial^2 B^*}{\partial t^2} \right] dt \\ &\quad - t \left| \frac{\partial B}{\partial t} \right|^2 \Big|_{-\infty}^{\infty} + \int_{-\infty}^{\infty} \frac{\partial B^*}{\partial t} \left[\frac{\partial B}{\partial t} + t \frac{\partial^2 B}{\partial t^2} \right] dt. \end{aligned} \quad (4.30)$$

The first and third terms go to zero at the limits. Rearranging the remaining terms we get

$$\begin{aligned} -2 \int_{-\infty}^{\infty} t \left(\frac{\partial B}{\partial t} \frac{\partial^2 B^*}{\partial t^2} + \frac{\partial B^*}{\partial t} \frac{\partial^2 B}{\partial t^2} \right) dt &= 2 \int_{-\infty}^{\infty} \left| \frac{\partial B}{\partial t} \right|^2 dt, \\ \int_{-\infty}^{\infty} t \left(\frac{\partial B}{\partial t} \frac{\partial^2 B^*}{\partial t^2} + \frac{\partial B^*}{\partial t} \frac{\partial^2 B}{\partial t^2} \right) dt &= - \int_{-\infty}^{\infty} \left| \frac{\partial B}{\partial t} \right|^2 dt. \end{aligned} \quad (4.31)$$

Next consider the second term on the right hand side of Eq. (4.29).

$$\begin{aligned} - \int_{-\infty}^{\infty} \left(B^* \frac{\partial^2 B}{\partial t^2} + B \frac{\partial^2 B^*}{\partial t^2} \right) dt &= -B^* \frac{\partial B}{\partial t} \Big|_{-\infty}^{\infty} + \int_{-\infty}^{\infty} \left| \frac{\partial B}{\partial t} \right|^2 - B \frac{\partial B^*}{\partial t} \Big|_{-\infty}^{\infty} + \int_{-\infty}^{\infty} \left| \frac{\partial B}{\partial t} \right|^2 dt, \\ &= 2 \int_{-\infty}^{\infty} \left| \frac{\partial B}{\partial t} \right|^2 dt. \end{aligned} \quad (4.32)$$

Substituting Eqs (4.31) and (4.32) into Eq. (4.29) we get

$$\int_{-\infty}^{\infty} t \left(B^* \frac{\partial^3 B}{\partial t^3} + B \frac{\partial^3 B^*}{\partial t^3} \right) dt = 3 \int_{-\infty}^{\infty} \left| \frac{\partial B}{\partial t} \right|^2 dt. \quad (4.33)$$

Now consider the final integral in Eq. (4.24). From Eq. (4.19) we can write

$$\int_{-\infty}^{\infty} t \left(B^* \frac{\partial}{\partial t} (B|B|^2) + B \frac{\partial}{\partial t} (B^*|B|^2) \right) dt = 3 \int_{-\infty}^{\infty} t |B|^2 \frac{\partial |B|^2}{\partial t} dt. \quad (4.34)$$

Integrating Eq. (4.34) by parts we get

$$\begin{aligned} \int_{-\infty}^{\infty} t|B|^2 \frac{\partial |B|^2}{\partial t} dt &= t|B|^4 \Big|_{-\infty}^{\infty} - \int_{-\infty}^{\infty} |B|^2 \left(t \frac{\partial |B|^2}{\partial t} + |B|^2 \right) dt, \\ \int_{-\infty}^{\infty} t|B|^2 \frac{\partial |B|^2}{\partial t} dt &= -1/2 \int_{-\infty}^{\infty} |B|^4 dt. \end{aligned} \quad (4.35)$$

Substituting Eqs (4.27), (4.33), (4.34) and Eq. (4.35) into Eq. (4.24) we can find that the evolution of pulse position along the fiber is given by

$$\frac{dT}{dz} = \beta_2 \Omega + \frac{\beta_3}{2E} \int_{-\infty}^{\infty} \left| \frac{\partial B}{\partial t} \right|^2 dt + \frac{3\bar{\gamma}}{2\omega_0 E} \int_{-\infty}^{\infty} |B|^4 dt. \quad (4.36)$$

Eq.(4.36) shows that the pulse position is affected by any frequency shift due to GVD and also because of TOD. In the absence of amplifiers, this shift in the position is deterministic.

4.1.3 Evolution of Frequency Shift

Next we find the evolution of frequency, Ω along the fiber. Differentiating Eq. (4.3) with respect to z we get

$$\frac{d\Omega}{dz} = \frac{i}{2E} \int_{-\infty}^{\infty} \left[\frac{\partial}{\partial z} \left(B^* \frac{\partial B}{\partial t} \right) - \frac{\partial}{\partial z} \left(B \frac{\partial B^*}{\partial t} \right) \right] dt. \quad (4.37)$$

Now consider

$$\frac{\partial}{\partial z} \left(B^* \frac{\partial B}{\partial t} \right) = B^* \frac{\partial^2 B}{\partial z \partial t} + \frac{\partial B^*}{\partial z} \frac{\partial B}{\partial t}. \quad (4.38)$$

From Eq. (4.7) we can write

$$\begin{aligned} \frac{\partial^2 B}{\partial z \partial t} &= -i \frac{\beta_2}{2} \frac{\partial^3 B}{\partial t^3} + \frac{\beta_3}{6} \frac{\partial^4 B}{\partial t^4} - i\bar{\gamma} T_R \frac{\partial B}{\partial t} \frac{\partial |B|^2}{\partial t} - i\bar{\gamma} T_R B \frac{\partial^2 |B|^2}{\partial t^2} \\ &\quad - \frac{\bar{\gamma}}{\omega_0} \frac{\partial}{\partial t^2} (|B|^2 B) + i\bar{\gamma} B \frac{\partial |B|^2}{\partial t} + i\bar{\gamma} |B|^2 \frac{\partial B}{\partial t}, \end{aligned} \quad (4.39)$$

$$\begin{aligned} B^* \frac{\partial^2 B}{\partial z \partial t} &= -i \frac{\beta_2}{2} B^* \frac{\partial^3 B}{\partial t^3} + \frac{\beta_3}{6} B^* \frac{\partial^4 B}{\partial t^4} - i\bar{\gamma} T_R B^* \frac{\partial B}{\partial t} \frac{\partial |B|^2}{\partial t} - i\bar{\gamma} T_R |B|^2 \frac{\partial^2 |B|^2}{\partial t^2} \\ &\quad - \frac{\bar{\gamma}}{\omega_0} B^* \frac{\partial^2}{\partial t^2} (|B|^2 B) + i\bar{\gamma} |B|^2 \frac{\partial |B|^2}{\partial t} + i\bar{\gamma} |B|^2 B^* \frac{\partial B}{\partial t}, \end{aligned} \quad (4.40)$$

$$\begin{aligned} \frac{\partial B^*}{\partial z} \frac{\partial B}{\partial t} &= i \frac{\beta_2}{2} \frac{\partial^2 B^*}{\partial t^2} \frac{\partial B}{\partial t} + \frac{\beta_3}{6} \frac{\partial^3 B^*}{\partial t^3} \frac{\partial B}{\partial t} + i\bar{\gamma} T_R B^* \frac{\partial |B|^2}{\partial t} \frac{\partial B}{\partial t} - i\bar{\gamma} |B|^2 B^* \frac{\partial B}{\partial t} \\ &\quad - \frac{\bar{\gamma}}{\omega_0} \frac{\partial}{\partial t} (|B|^2 B^*) \frac{\partial B}{\partial t}. \end{aligned} \quad (4.41)$$

Adding Eqs. (4.40) and (4.41) and substituting into Eq. (4.38) we find

$$\begin{aligned} \frac{\partial}{\partial z} \left(B^* \frac{\partial B}{\partial t} \right) &= i \frac{\beta_2}{2} \left(\frac{\partial^2 B^*}{\partial t^2} \frac{\partial B}{\partial t} - B^* \frac{\partial^3 B}{\partial t^3} \right) + \frac{\beta_3}{6} \left(B^* \frac{\partial^4 B}{\partial t^4} + \frac{\partial^3 B^*}{\partial t^3} \frac{\partial B}{\partial t} \right) - i \bar{\gamma} T_R |B|^2 \frac{\partial^2 |B|^2}{\partial t^2} \\ &\quad + i \bar{\gamma} |B|^2 \frac{\partial |B|^2}{\partial t} - \frac{\bar{\gamma}}{\omega_0} \left(B^* \frac{\partial^2}{\partial t^2} (|B|^2 B) + \frac{\partial}{\partial t} (|B|^2 B^*) \frac{\partial B}{\partial t} \right). \end{aligned} \quad (4.42)$$

Hence we can write

$$\begin{aligned} \frac{\partial}{\partial z} \left(B \frac{\partial B^*}{\partial t} \right) &= -i \frac{\beta_2}{2} \left(\frac{\partial^2 B}{\partial t^2} \frac{\partial B^*}{\partial t} - B \frac{\partial^3 B^*}{\partial t^3} \right) + \frac{\beta_3}{6} \left(B \frac{\partial^4 B^*}{\partial t^4} + \frac{\partial^3 B}{\partial t^3} \frac{\partial B^*}{\partial t} \right) + i \bar{\gamma} T_R |B|^2 \frac{\partial^2 |B|^2}{\partial t^2} \\ &\quad - i \bar{\gamma} |B|^2 \frac{\partial |B|^2}{\partial t} - \frac{\bar{\gamma}}{\omega_0} \left(B \frac{\partial^2}{\partial t^2} (|B|^2 B^*) + \frac{\partial}{\partial t} (|B|^2 B) \frac{\partial B^*}{\partial t} \right). \end{aligned} \quad (4.43)$$

Using Eqs. (4.42) and (4.43) in Eq. (4.37) we can find the evolution of frequency along the fiber to be

$$\begin{aligned} \frac{d\Omega}{dz} &= \frac{i}{2E} \int_{-\infty}^{\infty} i \frac{\beta_2}{2} \left[\left(\frac{\partial^2 B^*}{\partial t^2} \frac{\partial B}{\partial t} + \frac{\partial^2 B}{\partial t^2} \frac{\partial B^*}{\partial t} \right) - \left(B \frac{\partial^3 B^*}{\partial t^3} + B^* \frac{\partial^3 B}{\partial t^3} \right) \right] dt \\ &\quad + \frac{i}{2E} \int_{-\infty}^{\infty} \frac{\beta_3}{6} \left[\left(B^* \frac{\partial^4 B}{\partial t^4} - B \frac{\partial^4 B^*}{\partial t^4} \right) + \left(\frac{\partial^3 B^*}{\partial t^3} \frac{\partial B}{\partial t} - \frac{\partial^3 B}{\partial t^3} \frac{\partial B^*}{\partial t} \right) \right] dt \\ &\quad - \frac{i \bar{\gamma}}{2E\omega_0} \int_{-\infty}^{\infty} |B|^2 \left(B^* \frac{\partial^2 B}{\partial t^2} - B \frac{\partial^2 B^*}{\partial t^2} \right) dt - \frac{3i \bar{\gamma}}{2E\omega_0} \int_{-\infty}^{\infty} \frac{\partial |B|^2}{\partial t} \left(B^* \frac{\partial B}{\partial t} - B \frac{\partial B^*}{\partial t} \right) dt \\ &\quad + \frac{\bar{\gamma}}{E} T_R \int_{-\infty}^{\infty} |B|^2 \frac{\partial^2 |B|^2}{\partial t^2} dt - \frac{\bar{\gamma}}{E} \int_{-\infty}^{\infty} |B|^2 \frac{\partial |B|^2}{\partial t} dt. \end{aligned} \quad (4.44)$$

In order to calculate $d\Omega/dz$ we evaluate one by one the integrals on the right hand side of the Eq. (4.44). First consider the integration by parts of the first term in Eq. (4.44) given by

$$\begin{aligned} \int_{-\infty}^{\infty} \left(\frac{\partial^2 B^*}{\partial t^2} \frac{\partial B}{\partial t} + \frac{\partial^2 B}{\partial t^2} \frac{\partial B^*}{\partial t} \right) dt &= \left| \frac{\partial B}{\partial t} \right|^2 \Big|_{-\infty}^{\infty} - \int_{-\infty}^{\infty} \frac{\partial B^*}{\partial t} \frac{\partial^2 B}{\partial t^2} dt + \left| \frac{\partial B}{\partial t} \right|^2 \Big|_{-\infty}^{\infty} - \int_{-\infty}^{\infty} \frac{\partial B}{\partial t} \frac{\partial^2 B^*}{\partial t^2} dt. \\ &= - \int_{-\infty}^{\infty} \left(\frac{\partial^2 B^*}{\partial t^2} \frac{\partial B}{\partial t} + \frac{\partial^2 B}{\partial t^2} \frac{\partial B^*}{\partial t} \right) dt, \\ \int_{-\infty}^{\infty} \left(\frac{\partial^2 B^*}{\partial t^2} \frac{\partial B}{\partial t} + \frac{\partial^2 B}{\partial t^2} \frac{\partial B^*}{\partial t} \right) dt &= 0. \end{aligned} \quad (4.45)$$

From Eq. (4.18) we know that the second term in Eq. (4.44) vanishes. Now consider the third term in Eq. (4.44). Performing the integration by parts we get

$$\begin{aligned} \int_{-\infty}^{\infty} \left(B^* \frac{\partial^4 B}{\partial t^4} - B \frac{\partial^4 B^*}{\partial t^4} \right) dt &= B^* \frac{\partial^3 B}{\partial t^3} \Big|_{-\infty}^{\infty} - \int_{-\infty}^{\infty} \frac{\partial B^*}{\partial t} \frac{\partial^3 B}{\partial t^3} dt - B \frac{\partial^3 B^*}{\partial t^3} \Big|_{-\infty}^{\infty} + \int_{-\infty}^{\infty} \frac{\partial B}{\partial t} \frac{\partial^3 B^*}{\partial t^3} dt, \\ \int_{-\infty}^{\infty} \left(B^* \frac{\partial^4 B}{\partial t^4} - B \frac{\partial^4 B^*}{\partial t^4} \right) dt &= \int_{-\infty}^{\infty} \left(\frac{\partial^3 B^*}{\partial t^3} \frac{\partial B}{\partial t} - \frac{\partial^3 B}{\partial t^3} \frac{\partial B^*}{\partial t} \right) dt. \end{aligned} \quad (4.46)$$

Next consider

$$\begin{aligned} \int_{-\infty}^{\infty} \left(\frac{\partial^3 B^*}{\partial t^3} \frac{\partial B}{\partial t} - \frac{\partial^3 B}{\partial t^3} \frac{\partial B^*}{\partial t} \right) dt &= \frac{\partial^2 B^*}{\partial t^2} \frac{\partial B}{\partial t} \Big|_{-\infty}^{\infty} - \int_{-\infty}^{\infty} \frac{\partial^2 B^*}{\partial t^2} \frac{\partial^2 B}{\partial t^2} dt - \frac{\partial^2 B}{\partial t^2} \frac{\partial B^*}{\partial t} \Big|_{-\infty}^{\infty} + \int_{-\infty}^{\infty} \frac{\partial^2 B}{\partial t^2} \frac{\partial^2 B^*}{\partial t^2} dt, \\ \int_{-\infty}^{\infty} \left(\frac{\partial^3 B^*}{\partial t^3} \frac{\partial B}{\partial t} - \frac{\partial^3 B}{\partial t^3} \frac{\partial B^*}{\partial t} \right) dt &= 0. \end{aligned} \quad (4.47)$$

This means the third and fourth terms in Eq. (4.44) vanishes. Substituting Eqs. (4.45), (4.18), (4.46) and (4.47) into Eq. (4.44) we get

$$\begin{aligned} \frac{d\Omega}{dz} &= -\frac{\bar{\nu}\bar{\gamma}}{2E\omega_0} \int_{-\infty}^{\infty} |B|^2 \left(B^* \frac{\partial^2 B}{\partial t^2} - B \frac{\partial^2 B^*}{\partial t^2} \right) dt - \frac{3\bar{\nu}\bar{\gamma}}{2E\omega_0} \int_{-\infty}^{\infty} \frac{\partial |B|^2}{\partial t} \left(B^* \frac{\partial B}{\partial t} - B \frac{\partial B^*}{\partial t} \right) dt \\ &\quad + \frac{\bar{\gamma}}{E} T_R \int_{-\infty}^{\infty} |B|^2 \frac{\partial^2 |B|^2}{\partial t^2} dt - \frac{\bar{\gamma}}{E} \int_{-\infty}^{\infty} |B|^2 \frac{\partial |B|^2}{\partial t} dt. \end{aligned} \quad (4.48)$$

Now consider the first term in Eq. (4.48). Integrating by parts we get

$$\begin{aligned} \int_{-\infty}^{\infty} |B|^2 \left(B^* \frac{\partial^2 B}{\partial t^2} - B \frac{\partial^2 B^*}{\partial t^2} \right) dt &= B^* |B|^2 \frac{\partial B}{\partial t} \Big|_{-\infty}^{\infty} - \int_{-\infty}^{\infty} \frac{\partial B}{\partial t} \left(\frac{\partial B^*}{\partial t} |B|^2 + B^* \frac{\partial |B|^2}{\partial t} \right) dt \\ &\quad - B |B|^2 \frac{\partial B^*}{\partial t} \Big|_{-\infty}^{\infty} + \int_{-\infty}^{\infty} \frac{\partial B^*}{\partial t} \left(|B|^2 \frac{\partial B}{\partial t} + B \frac{\partial |B|^2}{\partial t} \right) dt, \\ &= - \int_{-\infty}^{\infty} \frac{\partial |B|^2}{\partial t} \left(B^* \frac{\partial B}{\partial t} - B \frac{\partial B^*}{\partial t} \right) dt. \end{aligned} \quad (4.49)$$

Expanding the next term in Eq. (4.48) by parts we get

$$\begin{aligned} \int_{-\infty}^{\infty} |B|^2 \frac{\partial^2 |B|^2}{\partial t^2} dt &= 2 \int_{-\infty}^{\infty} |B|^2 \left| \frac{\partial B}{\partial t} \right|^2 dt + \int_{-\infty}^{\infty} B |B|^2 \frac{\partial^2 B^*}{\partial t^2} dt + \int_{-\infty}^{\infty} |B|^2 B^* \frac{\partial^2 B}{\partial t^2} dt, \\ &= 2 \int_{-\infty}^{\infty} |B|^2 \left| \frac{\partial B}{\partial t} \right|^2 dt + B |B|^2 \frac{\partial B^*}{\partial t} \Big|_{-\infty}^{\infty} - \int_{-\infty}^{\infty} \frac{\partial B^*}{\partial t} \left[\frac{\partial B}{\partial t} |B|^2 + B \frac{\partial |B|^2}{\partial t} \right] dt \\ &\quad + B^* |B|^2 \frac{\partial B}{\partial t} \Big|_{-\infty}^{\infty} - \int_{-\infty}^{\infty} \frac{\partial B}{\partial t} \left[\frac{\partial B}{\partial t} |B|^2 + B \frac{\partial |B|^2}{\partial t} \right] dt, \\ \int_{-\infty}^{\infty} |B|^2 \frac{\partial^2 |B|^2}{\partial t^2} dt &= - \int_{-\infty}^{\infty} \left(\frac{\partial}{\partial t} |B|^2 \right)^2 dt, \end{aligned} \quad (4.50)$$

The last term in Eq. (4.48) can be evaluated as follows:

$$\begin{aligned} \int_{-\infty}^{\infty} |B|^2 \frac{\partial |B|^2}{\partial t} dt &= |B|^4 \Big|_{-\infty}^{\infty} - \int_{-\infty}^{\infty} |B|^2 \frac{\partial |B|^2}{\partial t} dt, \\ \int_{-\infty}^{\infty} |B|^2 \frac{\partial |B|^2}{\partial t} dt &= 0. \end{aligned} \quad (4.51)$$

Substituting Eqs. (4.49)–(4.51) in Eq. (4.48) we get the variation in the frequency of the optical pulse during propagation as

$$\frac{d\Omega}{dz} = -\frac{\bar{\nu}\bar{\gamma}}{E\omega_0} \int_{-\infty}^{\infty} \frac{\partial}{\partial t} |B|^2 \left(B^* \frac{\partial B}{\partial t} - B \frac{\partial B^*}{\partial t} \right) dt - \frac{\bar{\gamma}}{E} T_R \int_{-\infty}^{\infty} \left(\frac{\partial}{\partial t} |B|^2 \right)^2 dt. \quad (4.52)$$

This means both IRS and self-steepening leads to a shift in the pulse spectrum.

4.1.4 Evolution of chirp parameter

Next we find the evolution of the chirp parameter. Differentiating Eq. (4.4) with respect to z , we can write

$$\frac{d\tilde{C}}{dz} = \frac{i}{2E} \int_{-\infty}^{\infty} (t-T) \left[\frac{\partial}{\partial z} \left(B^* \frac{\partial B}{\partial t} \right) - \frac{\partial}{\partial z} \left(B \frac{\partial B^*}{\partial t} \right) \right] dt. \quad (4.53)$$

From Eqs. (4.42) and (4.43) we have

$$\begin{aligned} \frac{d\tilde{C}}{dz} = & \frac{-\beta_2}{4E} \int_{-\infty}^{\infty} (t-T) \left[\left(\frac{\partial^2 B^*}{\partial t^2} \frac{\partial B}{\partial t} + \frac{\partial^2 B}{\partial t^2} \frac{\partial B^*}{\partial t} \right) - \left(B \frac{\partial^3 B^*}{\partial t^3} + B^* \frac{\partial^3 B}{\partial t^3} \right) \right] dt \\ & + \frac{i\beta_3}{12E} \int_{-\infty}^{\infty} (t-T) \left[\left(B^* \frac{\partial^4 B}{\partial t^4} - B \frac{\partial^4 B^*}{\partial t^4} \right) + \left(\frac{\partial^3 B^*}{\partial t^3} \frac{\partial B}{\partial t} - \frac{\partial^3 B}{\partial t^3} \frac{\partial B^*}{\partial t} \right) \right] dt \\ & - \frac{\bar{\gamma}}{2E\omega_0} \int_{-\infty}^{\infty} (t-T) |B|^2 \left(B^* \frac{\partial^2 B}{\partial t^2} - B \frac{\partial^2 B^*}{\partial t^2} \right) dt - \frac{3\bar{\gamma}}{2E\omega_0} \int_{-\infty}^{\infty} (t-T) \frac{\partial |B|^2}{\partial t} \left(B^* \frac{\partial B}{\partial t} - B \frac{\partial B^*}{\partial t} \right) dt \\ & + \frac{\bar{\gamma}}{E} T_R \int_{-\infty}^{\infty} (t-T) |B|^2 \frac{\partial^2 |B|^2}{\partial t^2} dt - \frac{\bar{\gamma}}{E} \int_{-\infty}^{\infty} (t-T) |B|^2 \frac{\partial |B|^2}{\partial t} dt. \end{aligned} \quad (4.54)$$

In order to evaluate the first term in Eq. (4.54), consider the integral

$$\begin{aligned} \int_{-\infty}^{\infty} (t-T) \left(B \frac{\partial^3 B^*}{\partial t^3} + B^* \frac{\partial^3 B}{\partial t^3} \right) dt &= (t-T) B \frac{\partial^2 B^*}{\partial t^2} \Big|_{-\infty}^{\infty} - \int_{-\infty}^{\infty} \frac{\partial^2 B^*}{\partial t^2} \left(\frac{\partial B}{\partial t} (t-T) + B \right) dt \\ &+ (t-T) B^* \frac{\partial^2 B}{\partial t^2} \Big|_{-\infty}^{\infty} - \int_{-\infty}^{\infty} \frac{\partial^2 B}{\partial t^2} \left(\frac{\partial B^*}{\partial t} (t-T) + B^* \right) dt, \\ &= - \int_{-\infty}^{\infty} (t-T) \left(\frac{\partial B}{\partial t} \frac{\partial^2 B^*}{\partial t^2} + \frac{\partial B^*}{\partial t} \frac{\partial^2 B}{\partial t^2} \right) dt \\ &- \int_{-\infty}^{\infty} \left(B \frac{\partial^2 B^*}{\partial t^2} + B^* \frac{\partial^2 B}{\partial t^2} \right) dt. \end{aligned} \quad (4.55)$$

From Eq. (4.54) we can write the first term as

$$\begin{aligned} \int_{-\infty}^{\infty} (t-T) \left[\left(\frac{\partial^2 B^*}{\partial t^2} \frac{\partial B}{\partial t} + \frac{\partial^2 B}{\partial t^2} \frac{\partial B^*}{\partial t} \right) - \left(B \frac{\partial^3 B^*}{\partial t^3} + B^* \frac{\partial^3 B}{\partial t^3} \right) \right] dt \\ = 2 \int_{-\infty}^{\infty} (t-T) \left(\frac{\partial B}{\partial t} \frac{\partial^2 B^*}{\partial t^2} + \frac{\partial B^*}{\partial t} \frac{\partial^2 B}{\partial t^2} \right) dt + \int_{-\infty}^{\infty} \left(B \frac{\partial^2 B^*}{\partial t^2} + B^* \frac{\partial^2 B}{\partial t^2} \right) dt \end{aligned} \quad (4.56)$$

From Eq. (4.32) we can write Eq. (4.56) as

$$\begin{aligned} \int_{-\infty}^{\infty} (t-T) \left[\left(\frac{\partial^2 B^*}{\partial t^2} \frac{\partial B}{\partial t} + \frac{\partial^2 B}{\partial t^2} \frac{\partial B^*}{\partial t} \right) - \left(B \frac{\partial^3 B^*}{\partial t^3} + B^* \frac{\partial^3 B}{\partial t^3} \right) \right] dt \\ = 2 \int_{-\infty}^{\infty} (t-T) \left(\frac{\partial B}{\partial t} \frac{\partial^2 B^*}{\partial t^2} + \frac{\partial B^*}{\partial t} \frac{\partial^2 B}{\partial t^2} \right) dt - 2 \int_{-\infty}^{\infty} \left| \frac{\partial B}{\partial t} \right|^2 dt. \end{aligned} \quad (4.57)$$

Next integrating the first term in the above equation by parts we get

$$\begin{aligned} \int_{-\infty}^{\infty} (t-T) \left(\frac{\partial B}{\partial t} \frac{\partial^2 B^*}{\partial t^2} + \frac{\partial B^*}{\partial t} \frac{\partial^2 B}{\partial t^2} \right) dt &= (t-T) \left| \frac{\partial B}{\partial t} \right|^2 \Big|_{-\infty}^{\infty} - \int_{-\infty}^{\infty} \left((t-T) \frac{\partial B^*}{\partial t} \frac{\partial^2 B}{\partial t^2} - \left| \frac{\partial B}{\partial t} \right|^2 \right) dt \\ &\quad + (t-T) \left| \frac{\partial B^*}{\partial t} \right|^2 \Big|_{-\infty}^{\infty} - \int_{-\infty}^{\infty} \left((t-T) \frac{\partial B}{\partial t} \frac{\partial^2 B^*}{\partial t^2} - \left| \frac{\partial B^*}{\partial t} \right|^2 \right) dt, \\ \int_{-\infty}^{\infty} (t-T) \left(\frac{\partial B}{\partial t} \frac{\partial^2 B^*}{\partial t^2} + \frac{\partial B^*}{\partial t} \frac{\partial^2 B}{\partial t^2} \right) dt &= - \int_{-\infty}^{\infty} \left| \frac{\partial B}{\partial t} \right|^2 dt. \end{aligned} \quad (4.58)$$

Substituting Eq. (4.58) into Eq. (4.57) we get

$$\int_{-\infty}^{\infty} (t-T) \left[\left(\frac{\partial^2 B^*}{\partial t^2} \frac{\partial B}{\partial t} + \frac{\partial^2 B}{\partial t^2} \frac{\partial B^*}{\partial t} \right) - \left(B \frac{\partial^3 B^*}{\partial t^3} + B^* \frac{\partial^3 B}{\partial t^3} \right) \right] dt = -4 \int_{-\infty}^{\infty} \left| \frac{\partial B}{\partial t} \right|^2 dt. \quad (4.59)$$

Next to evaluate the terms in Eq. (4.54) with coefficient β_3 , consider the integral

$$\begin{aligned} \int_{-\infty}^{\infty} (t-T) \left(B^* \frac{\partial^4 B}{\partial t^4} - B \frac{\partial^4 B^*}{\partial t^4} \right) dt &= (t-T) B^* \frac{\partial^3 B}{\partial t^3} \Big|_{-\infty}^{\infty} - \int_{-\infty}^{\infty} \left((t-T) \frac{\partial B^*}{\partial t} \frac{\partial^3 B}{\partial t^3} + B^* \frac{\partial^3 B}{\partial t^3} \right) dt \\ &\quad - (t-T) B \frac{\partial^3 B^*}{\partial t^3} \Big|_{-\infty}^{\infty} + \int_{-\infty}^{\infty} \left((t-T) \frac{\partial B}{\partial t} \frac{\partial^3 B^*}{\partial t^3} + B \frac{\partial^3 B^*}{\partial t^3} \right) dt, \\ &= \int_{-\infty}^{\infty} (t-T) \left(\frac{\partial B}{\partial t} \frac{\partial^3 B^*}{\partial t^3} - \frac{\partial B^*}{\partial t} \frac{\partial^3 B}{\partial t^3} \right) dt \\ &\quad + \int_{-\infty}^{\infty} \left(B \frac{\partial^3 B^*}{\partial t^3} - B^* \frac{\partial^3 B}{\partial t^3} \right) dt. \end{aligned} \quad (4.60)$$

The first integral in Eq. (4.60) can be reduced to

$$\begin{aligned} \int_{-\infty}^{\infty} (t-T) \left(\frac{\partial B}{\partial t} \frac{\partial^3 B^*}{\partial t^3} - \frac{\partial B^*}{\partial t} \frac{\partial^3 B}{\partial t^3} \right) dt &= \frac{\partial B}{\partial t} \frac{\partial^2 B^*}{\partial t^2} (t-T) \Big|_{-\infty}^{\infty} - \int_{-\infty}^{\infty} \frac{\partial^2 B^*}{\partial t^2} \left(\frac{\partial^2 B}{\partial t^2} (t-T) + \frac{\partial B}{\partial t} \right) \\ &\quad - \frac{\partial B^*}{\partial t} \frac{\partial^2 B}{\partial t^2} (t-T) \Big|_{-\infty}^{\infty} + \int_{-\infty}^{\infty} \frac{\partial^2 B}{\partial t^2} \left(\frac{\partial^2 B^*}{\partial t^2} (t-T) + \frac{\partial B^*}{\partial t} \right), \\ &= \int_{-\infty}^{\infty} \left(\frac{\partial^2 B}{\partial t^2} \frac{\partial B^*}{\partial t} - \frac{\partial^2 B^*}{\partial t^2} \frac{\partial B}{\partial t} \right) dt. \end{aligned} \quad (4.61)$$

Now consider the next term in Eq. (4.60) given by

$$\begin{aligned} \int_{-\infty}^{\infty} \left(B \frac{\partial^3 B^*}{\partial t^3} - B^* \frac{\partial^3 B}{\partial t^3} \right) dt &= \frac{\partial^2 B^*}{\partial t^2} B \Big|_{-\infty}^{\infty} - \int_{-\infty}^{\infty} \frac{\partial^2 B^*}{\partial t^2} \frac{\partial B}{\partial t} dt - \frac{\partial^2 B}{\partial t^2} B^* \Big|_{-\infty}^{\infty} + \int_{-\infty}^{\infty} \frac{\partial^2 B}{\partial t^2} \frac{\partial B^*}{\partial t} dt, \\ &= \int_{-\infty}^{\infty} \left(\frac{\partial^2 B}{\partial t^2} \frac{\partial B^*}{\partial t} - \frac{\partial^2 B^*}{\partial t^2} \frac{\partial B}{\partial t} \right) dt. \end{aligned} \quad (4.62)$$

Using Eq. (4.60)–(4.62) we can write

$$\int_{-\infty}^{\infty} (t-T) \left[\left(B^* \frac{\partial^4 B}{\partial t^4} - B \frac{\partial^4 B^*}{\partial t^4} \right) + \left(\frac{\partial^3 B^*}{\partial t^3} \frac{\partial B}{\partial t} - \frac{\partial^3 B}{\partial t^3} \frac{\partial B^*}{\partial t} \right) \right] dt = 3 \int_{-\infty}^{\infty} \left(\frac{\partial^2 B}{\partial t^2} \frac{\partial B^*}{\partial t} - \frac{\partial^2 B^*}{\partial t^2} \frac{\partial B}{\partial t} \right) dt. \quad (4.63)$$

The next term in the evolution of chirp is governed by self steepening and is given by

$$\begin{aligned}
\int_{-\infty}^{\infty} (t-T)|B|^2 \left(B^* \frac{\partial^2 B}{\partial t^2} - B \frac{\partial^2 B^*}{\partial t^2} \right) dt &= (t-T)B^*|B|^2 \frac{\partial B}{\partial t} \Big|_{-\infty}^{\infty} - B|B|^2(t-T) \frac{\partial B^*}{\partial t} \Big|_{-\infty}^{\infty} \\
&\quad - \int_{-\infty}^{\infty} \frac{\partial B}{\partial t} \left(\frac{\partial B^*}{\partial t} |B|^2(t-T) + B^*(t-T) \frac{\partial |B|^2}{\partial t} + B^*|B|^2 \right) dt \\
&\quad + \int_{-\infty}^{\infty} \frac{\partial B^*}{\partial t} \left(|B|^2(t-T) \frac{\partial B}{\partial t} + B(t-T) \frac{\partial |B|^2}{\partial t} + B|B|^2 \right) dt \\
&= \int_{-\infty}^{\infty} |B|^2 \left(B \frac{\partial B^*}{\partial t} - B^* \frac{\partial B}{\partial t} \right) dt \\
&\quad - \int_{-\infty}^{\infty} (t-T) \frac{\partial |B|^2}{\partial t} \left(B^* \frac{\partial B}{\partial t} - B \frac{\partial B^*}{\partial t} \right) dt. \tag{4.64}
\end{aligned}$$

Next consider the integral

$$\begin{aligned}
\int_{-\infty}^{\infty} (t-T)|B|^2 \frac{\partial^2 |B|^2}{\partial t^2} dt &= 2 \int_{-\infty}^{\infty} |B|^2(t-T) \left| \frac{\partial B}{\partial t} \right|^2 dt + \int_{-\infty}^{\infty} B|B|^2(t-T) \frac{\partial^2 B^*}{\partial t^2} dt + \int_{-\infty}^{\infty} B^*|B|^2(t-T) \frac{\partial^2 B}{\partial t^2} dt \\
&= 2 \int_{-\infty}^{\infty} |B|^2(t-T) \left| \frac{\partial B}{\partial t} \right|^2 dt + B|B|^2(t-T) \frac{\partial B^*}{\partial t} \Big|_{-\infty}^{\infty} - \int_{-\infty}^{\infty} \frac{\partial B^*}{\partial t} |B|^2(t-T) \frac{\partial B}{\partial t} dt \\
&\quad - \int_{-\infty}^{\infty} \frac{\partial B^*}{\partial t} \left(B(t-T) \frac{\partial |B|^2}{\partial t} + B|B|^2 \right) dt + B^*|B|^2(t-T) \frac{\partial B}{\partial t} \Big|_{-\infty}^{\infty} \\
&\quad - \int_{-\infty}^{\infty} \frac{\partial B}{\partial t} |B|^2(t-T) \frac{\partial B^*}{\partial t} dt - \int_{-\infty}^{\infty} \frac{\partial B}{\partial t} \left(B^*(t-T) \frac{\partial |B|^2}{\partial t} + B^*|B|^2 \right) dt, \\
\int_{-\infty}^{\infty} (t-T)|B|^2 \frac{\partial^2 |B|^2}{\partial t^2} dt &= - \int_{-\infty}^{\infty} (t-T) \left(B \frac{\partial B^*}{\partial t} \frac{\partial |B|^2}{\partial t} + B^* \frac{\partial B}{\partial t} \frac{\partial |B|^2}{\partial t} \right) dt \\
&\quad - \int_{-\infty}^{\infty} |B|^2 \left(B \frac{\partial B^*}{\partial t} + B^* \frac{\partial B}{\partial t} \right) dt, \\
\int_{-\infty}^{\infty} (t-T)|B|^2 \frac{\partial^2 |B|^2}{\partial t^2} dt &= - \int_{-\infty}^{\infty} (t-T) \left(\frac{\partial |B|^2}{\partial t} \right)^2 dt - \int_{-\infty}^{\infty} |B|^2 \frac{\partial |B|^2}{\partial t} dt. \tag{4.65}
\end{aligned}$$

Using Eq. (4.51) we can write Eq. (4.65) as

$$\int_{-\infty}^{\infty} (t-T)|B|^2 \frac{\partial^2 |B|^2}{\partial t^2} dt = - \int_{-\infty}^{\infty} (t-T) \left(\frac{\partial |B|^2}{\partial t} \right)^2 dt. \tag{4.66}$$

The last term in Eq. (4.54) can be evaluated as follows:

$$\begin{aligned}
\int_{-\infty}^{\infty} (t-T)|B|^2 \frac{\partial |B|^2}{\partial t} dt &= (t-T)|B|^4 \Big|_{-\infty}^{\infty} - \int_{-\infty}^{\infty} |B|^2 \left(|B|^2 + (t-T) \frac{\partial |B|^2}{\partial t} \right) dt, \\
\int_{-\infty}^{\infty} (t-T)|B|^2 \frac{\partial |B|^2}{\partial t} dt &= -1/2 \int_{-\infty}^{\infty} |B|^4 dt. \tag{4.67}
\end{aligned}$$

Using the results in Eqs. (4.59), (4.63), (4.64), (4.66) and (4.67) in Eq. (4.54) we get the evolution of the chirp parameter along the fiber to be

$$\begin{aligned} \frac{d\tilde{C}}{dz} = & \frac{\beta_2}{E} \int_{-\infty}^{\infty} \left| \frac{\partial B}{\partial t} \right|^2 dt + \frac{i\beta_3}{4E} \int_{-\infty}^{\infty} \left(\frac{\partial^2 B}{\partial t^2} \frac{\partial B^*}{\partial t} - \frac{\partial^2 B^*}{\partial t^2} \frac{\partial B}{\partial t} \right) dt \\ & - \frac{i\bar{\gamma}}{E\omega_0} \int_{-\infty}^{\infty} (t-T) \frac{\partial |B|^2}{\partial t} \left(B^* \frac{\partial B}{\partial t} - B \frac{\partial B^*}{\partial t} \right) dt - \frac{i\bar{\gamma}}{2E\omega_0} \int_{-\infty}^{\infty} |B|^2 \left(B \frac{\partial B^*}{\partial t} - B^* \frac{\partial B}{\partial t} \right) dt \\ & - \frac{\bar{\gamma}}{E} T_R \int_{-\infty}^{\infty} (t-T) \left(\frac{\partial |B|^2}{\partial t} \right)^2 dt + \frac{\bar{\gamma}}{2E} \int_{-\infty}^{\infty} |B|^4 dt. \end{aligned} \quad (4.68)$$

For ultrashort pulses, the chirp is not only affected by GVD but also by TOD, self-steepening and IRS.

4.1.5 Evolution of the RMS width

Next we find the evolution of pulsewidth along the fiber length. For this we differentiate Eq. (4.5) with respect to z to obtain

$$2\sigma E \frac{d\sigma}{dz} = \int_{-\infty}^{\infty} (t-t)^2 \left[B^* \frac{\partial B}{\partial z} + B \frac{\partial B^*}{\partial z} \right] dt. \quad (4.69)$$

Using Eqs. (4.8) and (4.9) in Eq. (4.69) we can write

$$\begin{aligned} 2\sigma E \frac{d\sigma}{dz} = & i \frac{\beta_2}{2} \int_{-\infty}^{\infty} (t-T)^2 \left(B \frac{\partial^2 B^*}{\partial t^2} - B^* \frac{\partial^2 B}{\partial t^2} \right) dt + \frac{\beta_3}{6} \int_{-\infty}^{\infty} (t-T)^2 \left(B^* \frac{\partial^3 B}{\partial t^3} + B \frac{\partial^3 B^*}{\partial t^3} \right) dt \\ & - \frac{\bar{\gamma}}{\omega_0} \int_{-\infty}^{\infty} (t-T)^2 \left(B^* \frac{\partial}{\partial t} (|B|^2 B) + B \frac{\partial}{\partial t} (|B|^2 B^*) \right) dt. \end{aligned} \quad (4.70)$$

First we evaluate the terms whose coefficients depend on GVD parameter β_2 in Eq. (4.70) as follows:

$$\begin{aligned} \int_{-\infty}^{\infty} (t-T)^2 \left(B \frac{\partial^2 B^*}{\partial t^2} - B^* \frac{\partial^2 B}{\partial t^2} \right) dt = & (t-T)^2 B \frac{\partial B^*}{\partial t} \Big|_{-\infty}^{\infty} \\ & - \int_{-\infty}^{\infty} \frac{\partial B^*}{\partial t} \left(2(t-T)B + (t-T)^2 \frac{\partial B}{\partial t} \right) dt - (t-T)^2 B^* \frac{\partial B}{\partial t} \Big|_{-\infty}^{\infty} \\ & + \int_{-\infty}^{\infty} \frac{\partial B}{\partial t} \left(2(t-T)B^* + (t-T)^2 \frac{\partial B^*}{\partial t} \right) dt, \\ = & 2 \int_{-\infty}^{\infty} (t-T) \left(B^* \frac{\partial B}{\partial t} - B \frac{\partial B^*}{\partial t} \right) dt. \end{aligned} \quad (4.71)$$

From the definition of chirp parameter in Eq. (4.4) we can write Eq. (4.71) as

$$\int_{-\infty}^{\infty} (t-T)^2 \left(B \frac{\partial^2 B^*}{\partial t^2} - B^* \frac{\partial^2 B}{\partial t^2} \right) dt = -4i\tilde{C}E. \quad (4.72)$$

Next consider the terms in Eq. (4.70) whose coefficients depend on third order dispersion parameter β_3 given by

$$\begin{aligned}
\int_{-\infty}^{\infty} (t-T)^2 \left(B^* \frac{\partial^3 B}{\partial t^3} + B \frac{\partial^3 B^*}{\partial t^3} \right) dt &= (t-T)^2 B^* \frac{\partial^2 B}{\partial t^2} \Big|_{-\infty}^{\infty} \\
&\quad - \int_{-\infty}^{\infty} \frac{\partial^2 B}{\partial t^2} \left(2(t-T)B^* + (t-T)^2 \frac{\partial B^*}{\partial t} \right) dt + (t-T)^2 B \frac{\partial^2 B^*}{\partial t^2} \Big|_{-\infty}^{\infty} \\
&\quad - \int_{-\infty}^{\infty} \frac{\partial^2 B^*}{\partial t^2} \left(2(t-T)B + (t-T)^2 \frac{\partial B}{\partial t} \right) dt, \\
&= -2 \int_{-\infty}^{\infty} (t-T) \left(B^* \frac{\partial^2 B}{\partial t^2} + B \frac{\partial^2 B^*}{\partial t^2} \right) dt \\
&\quad - \int_{-\infty}^{\infty} (t-T)^2 \left(\frac{\partial B^*}{\partial t} \frac{\partial^2 B}{\partial t^2} + \frac{\partial B}{\partial t} \frac{\partial^2 B^*}{\partial t^2} \right) dt. \tag{4.73}
\end{aligned}$$

Next we evaluate the first term in Eq. (4.73) as follows:

$$\begin{aligned}
\int_{-\infty}^{\infty} (t-T) \left(B^* \frac{\partial^2 B}{\partial t^2} + B \frac{\partial^2 B^*}{\partial t^2} \right) dt &= (t-T) B^* \frac{\partial B}{\partial t} \Big|_{-\infty}^{\infty} - \int_{-\infty}^{\infty} \frac{\partial B}{\partial t} \left(\frac{\partial B^*}{\partial t} (t-T) + B^* \right) dt \\
&\quad + (t-T) B \frac{\partial B^*}{\partial t} \Big|_{-\infty}^{\infty} - \int_{-\infty}^{\infty} \frac{\partial B^*}{\partial t} \left(\frac{\partial B}{\partial t} (t-T) + B \right) dt, \\
&= -2 \int_{-\infty}^{\infty} (t-T) \left| \frac{\partial B}{\partial t} \right|^2 dt - \int_{-\infty}^{\infty} \left(B^* \frac{\partial B}{\partial t} + B \frac{\partial B^*}{\partial t} \right) dt \tag{4.74}
\end{aligned}$$

However the last term in Eq.(4.74) is given by

$$\begin{aligned}
\int_{-\infty}^{\infty} \left(B^* \frac{\partial B}{\partial t} + B \frac{\partial B^*}{\partial t} \right) dt &= |B|^2 \Big|_{-\infty}^{\infty} - \int_{-\infty}^{\infty} B \frac{\partial B^*}{\partial t} dt + |B|^2 \Big|_{-\infty}^{\infty} - \int_{-\infty}^{\infty} B^* \frac{\partial B}{\partial t} dt \\
&= - \int_{-\infty}^{\infty} \left(B^* \frac{\partial B}{\partial t} + B \frac{\partial B^*}{\partial t} \right) dt, \\
\int_{-\infty}^{\infty} \left(B^* \frac{\partial B}{\partial t} + B \frac{\partial B^*}{\partial t} \right) dt &= 0. \tag{4.75}
\end{aligned}$$

Substituting Eqs. (4.74) and (4.75) in (4.73) we have

$$\int_{-\infty}^{\infty} (t-T)^2 \left(B^* \frac{\partial^3 B}{\partial t^3} + B \frac{\partial^3 B^*}{\partial t^3} \right) dt = 4 \int_{-\infty}^{\infty} (t-T) \left| \frac{\partial B}{\partial t} \right|^2 dt - \int_{-\infty}^{\infty} (t-T)^2 \left(\frac{\partial B^*}{\partial t} \frac{\partial^2 B}{\partial t^2} + \frac{\partial B}{\partial t} \frac{\partial^2 B^*}{\partial t^2} \right) dt. \tag{4.76}$$

The last term in Eq. (4.76) can be written as

$$\int_{-\infty}^{\infty} (t-T)^2 \left(\frac{\partial B^*}{\partial t} \frac{\partial^2 B}{\partial t^2} + \frac{\partial B}{\partial t} \frac{\partial^2 B^*}{\partial t^2} \right) dt = (t-T)^2 \left| \frac{\partial B}{\partial t} \right|^2 \Big|_{-\infty}^{\infty} - \int_{-\infty}^{\infty} \frac{\partial B}{\partial t} \left((t-T)^2 \frac{\partial^2 B^*}{\partial t^2} + 2(t-T) \frac{\partial B^*}{\partial t} \right) dt$$

$$\begin{aligned}
& + (t-T)^2 \left| \frac{\partial B}{\partial t} \right|^2 \Big|_{-\infty}^{\infty} - \int_{-\infty}^{\infty} \frac{\partial B^*}{\partial t} \left((t-T)^2 \frac{\partial^2 B}{\partial t^2} + 2(t-T) \frac{\partial B}{\partial t} \right) dt \\
& = - \int_{-\infty}^{\infty} (t-T)^2 \left(\frac{\partial B^*}{\partial t} \frac{\partial^2 B}{\partial t^2} + \frac{\partial B}{\partial t} \frac{\partial^2 B^*}{\partial t^2} \right) dt - 4 \int_{-\infty}^{\infty} (t-T) \left| \frac{\partial B}{\partial t} \right|^2 dt \\
& \int_{-\infty}^{\infty} (t-T)^2 \left(\frac{\partial B^*}{\partial t} \frac{\partial^2 B}{\partial t^2} + \frac{\partial B}{\partial t} \frac{\partial^2 B^*}{\partial t^2} \right) dt = -2 \int_{-\infty}^{\infty} (t-T) \left| \frac{\partial B}{\partial t} \right|^2 dt. \tag{4.77}
\end{aligned}$$

Substituting Eq. (4.77) in Eq. (4.76) we have

$$\int_{-\infty}^{\infty} (t-T)^2 \left(B^* \frac{\partial^3 B}{\partial t^3} + B \frac{\partial^3 B^*}{\partial t^3} \right) dt = 6 \int_{-\infty}^{\infty} (t-T) \left| \frac{\partial B}{\partial t} \right|^2 dt. \tag{4.78}$$

The next step in finding the evolution of the pulse width along the fiber is to evaluate the term governed by self steepening in Eq. (4.70) as follows:

$$\int_{-\infty}^{\infty} (t-T)^2 \left(B^* \frac{\partial}{\partial t} (|B|^2 B) + B \frac{\partial}{\partial t} (|B|^2 B^*) \right) dt = 3 \int_{-\infty}^{\infty} (t-T)^2 |B|^2 \frac{\partial}{\partial t} |B|^2 dt. \tag{4.79}$$

Next consider the term on the right hand side of Eq. (4.79)

$$\begin{aligned}
& \int_{-\infty}^{\infty} (t-T)^2 |B|^2 \frac{\partial}{\partial t} |B|^2 dt = (t-T)^2 |B|^4 \Big|_{-\infty}^{\infty} - \int_{-\infty}^{\infty} |B|^2 \left(2|B|^2 (t-T) + (t-T)^2 \frac{\partial}{\partial t} |B|^2 \right) dt, \\
& \int_{-\infty}^{\infty} (t-T)^2 |B|^2 \frac{\partial}{\partial t} |B|^2 dt = - \int_{-\infty}^{\infty} (t-T) |B|^4 dt = 0. \tag{4.80}
\end{aligned}$$

Therefore Eq. (4.79) can be written as

$$\int_{-\infty}^{\infty} (t-T)^2 \left(B^* \frac{\partial}{\partial t} (|B|^2 B) + B \frac{\partial}{\partial t} (|B|^2 B^*) \right) dt = 0. \tag{4.81}$$

Substituting Eqs. (4.72), (4.78) and (4.81) into Eq. (4.70) we find the evolution of pulse width along the fiber to be

$$\frac{d\sigma}{dz} = \frac{\beta_2 C}{\sigma} + \frac{\beta_3}{2\sigma E} \int_{-\infty}^{\infty} (t-T) \left| \frac{\partial B}{\partial t} \right|^2 dt. \tag{4.82}$$

While the evolution of the width of ultra short pulses is unaffected by IRS and self-steepening, it depends on the TOD and GVD in the fiber. The above equations for the evolution of the pulse parameters reduce the complexity of the problem but they are still not in a useful form because they depend on the pulse shape $B(z, t)$, which is not known until Eq. (3.50) is solved. If one has some knowledge of the pulse shape and its dependence on the five moments, the problem can be solved approximately. As seen before in Chapter 2, there are several situations in which pulse shape is known a priori with a good degree of approximation. For example, in the case of standard

solitons, pulse shape can be assumed to maintain “sech” shape even if its width changes. As another example, pulse shape remain nearly Gaussian in a dispersion-managed fiber link [1]. In general, a Gaussian pulse can be assumed to maintain its shape during propagation inside optical fibers if the nonlinear length is much larger than the dispersion length [1]. We consider these two cases in the following two sections.

4.2 Fundamental Soliton

First let us consider the case of perturbed fundamental soliton. The pulse shape is then given by Eq. (3.7). The width parameter τ and the chirp parameter C appearing in this equation is related to the RMS width σ and the moment \tilde{C} respectively by a constant factor K such that $\tau^2 = K\sigma^2 = (12/\pi^2)\sigma^2$ and $C = K\tilde{C} = (12/\pi^2)\tilde{C}$. Substituting Eq. (3.7) for $B(z, t)$ in Eq. (4.22) we get

$$\frac{dE}{dz} = 0. \quad (4.83)$$

From Eq. (4.36) we have

$$\frac{dT}{dz} = \beta_2\Omega + \frac{\beta_3}{2E} \int_{-\infty}^{\infty} \left| \frac{\partial B}{\partial t} \right|^2 dt + \frac{3\bar{\gamma}}{2\omega_0 E} \int_{-\infty}^{\infty} |B|^4 dt. \quad (4.84)$$

Also from Eq. (3.11) we have

$$\frac{\partial B}{\partial t} = - \left[\frac{a}{\tau} \operatorname{sech} \left(\frac{t-T}{\tau} \right) \tanh \left(\frac{t-T}{\tau} \right) + a \operatorname{sech} \left(\frac{t-T}{\tau} \right) (-i\Omega - iC(t-T)/\tau^2) \right] \exp[i\phi - i\Omega(t-T) - iC(t-T)^2/2\tau^2]. \quad (4.85)$$

Hence

$$\left| \frac{\partial B}{\partial t} \right|^2 = \frac{a^2}{\tau^2} \operatorname{sech}^2 \left(\frac{t-T}{\tau} \right) \tanh^2 \left(\frac{t-T}{\tau} \right) + a^2 \operatorname{sech}^2 \left(\frac{t-T}{\tau} \right) [\Omega + C(t-T)/\tau^2]^2. \quad (4.86)$$

The integration of Eq. (4.86), can be performed analytically using Table 4.1 and the final result is

$$\int_{-\infty}^{\infty} \left| \frac{\partial B}{\partial t} \right|^2 dt = \Omega^2 E + \frac{E}{3\tau^2} \left(1 + \frac{\pi^2}{4} C^2 \right), \quad (4.87)$$

where $E = 2a\tau$. From Eq. (4.7) we can write

$$|B|^4 = a^4 \operatorname{sech}^4 \left(\frac{t-T}{\tau} \right). \quad (4.88)$$

$f(x)$	1	x^{2n+1}	x^2	x^{2n} $\tanh(x)$	$\tanh^2(x)$	$\operatorname{sech}^2(x)$	$\operatorname{sech}^2(x)$ $\tanh^2(x)$	$\operatorname{sech}^2(x)$ $x^{2n+1}\tanh^2(x)$	$x \operatorname{sech}^2(x)$ $\tanh(x)$
$\int_{-\infty}^{\infty} f(x) \operatorname{sech}^2(x) dx$	2	0	$\pi^2/6$	0	2/3	4/3	4/15	0	1/3

Table 4.1: Integration table to get the evolution of pulse parameters of fundamental soliton. Here n is an integer and takes values $0, 1, 2, \dots$

From Table 4.1 we have

$$\int_{-\infty}^{\infty} |B|^4 dt = \frac{E^2}{3\tau}. \quad (4.89)$$

Hence using Eqs. (4.84), (4.87) and (4.89), the evolution the pulse position can be written as

$$\frac{dT}{dz} = \beta_2 \Omega + \frac{\beta_3 \Omega^2}{2} + \frac{\beta_3}{6\tau^2} \left(1 + \frac{\pi^2}{4} C^2 \right) + \frac{\bar{\gamma} E}{2\omega_0 \tau}. \quad (4.90)$$

Next we use Eq.(3.7) in Eq. (4.52) to find the evolution of the frequency of the fundamental soliton as follows:

$$\frac{d\Omega}{dz} = -\frac{i\bar{\gamma}}{E\omega_0} \int_{-\infty}^{\infty} \frac{\partial}{\partial t} |B|^2 \left(B^* \frac{\partial B}{\partial t} - B \frac{\partial B^*}{\partial t} \right) dt - \frac{\bar{\gamma}}{E} T_R \int_{-\infty}^{\infty} \left(\frac{\partial}{\partial t} |B|^2 \right)^2 dt. \quad (4.91)$$

From Eqs. (3.7) and (4.85) we have

$$\left(B^* \frac{\partial B}{\partial t} - B \frac{\partial B^*}{\partial t} \right) = -2i \left[\Omega + C \frac{(t-T)}{\tau^2} \right] a^2 \operatorname{sech}^2 \left(\frac{t-T}{\tau} \right). \quad (4.92)$$

Also from Eq. (3.7) we can write

$$|B|^2 = a^2 \operatorname{sech}^2 \left(\frac{t-T}{\tau} \right). \quad (4.93)$$

Differentiating Eq. (4.93) with respect to t , we have

$$\frac{\partial |B|^2}{\partial t} = -\frac{2a^2}{\tau} \operatorname{sech}^2 \left(\frac{t-T}{\tau} \right) \tanh \left(\frac{t-T}{\tau} \right). \quad (4.94)$$

From Eqs. (4.92) and (4.94) we can write the first integral in Eq. (4.91) as

$$\int_{-\infty}^{\infty} \frac{\partial}{\partial t} |B|^2 \left(B^* \frac{\partial B}{\partial t} - B \frac{\partial B^*}{\partial t} \right) dt = \int_{-\infty}^{\infty} \frac{4ia^4}{\tau} \left[\Omega + C \frac{(t-T)}{\tau^2} \right] \operatorname{sech}^4 \left(\frac{t-T}{\tau} \right) \tanh \left(\frac{t-T}{\tau} \right) dt. \quad (4.95)$$

Using Table 4.1 we get

$$\int_{-\infty}^{\infty} \frac{\partial}{\partial t} |B|^2 \left(B^* \frac{\partial B}{\partial t} - B \frac{\partial B^*}{\partial t} \right) dt = \frac{iCE^2}{3\tau^3}. \quad (4.96)$$

Using Eq. (4.94) the second integral in Eq. (4.91) can be written as

$$\int_{-\infty}^{\infty} \left(\frac{\partial}{\partial t} |B|^2 \right)^2 dt = \frac{4a^4}{\tau^2} \int_{-\infty}^{\infty} \operatorname{sech}^4 \left(\frac{t-T}{\tau} \right) \tanh^2 \left(\frac{t-T}{\tau} \right) dt. \quad (4.97)$$

Again using Table 4.1 we get

$$\int_{-\infty}^{\infty} \left(\frac{\partial}{\partial t} |B|^2 \right)^2 dt = \frac{4E^2}{15\tau^3}. \quad (4.98)$$

Substituting Eqs. (4.95) and (4.98) into Eq. (4.91) we can write the evolution of the frequency of the fundamental soliton as

$$\frac{d\Omega}{dz} = \frac{\bar{\gamma}EC}{3\omega_0\tau^3} - \frac{4\bar{\gamma}T_R E}{15\tau^3}. \quad (4.99)$$

To find the evolution of the chirp next, we use Eq. (3.7) in Eq. (4.68). For a pulse of the form shown in Eq. (3.7), the constant K takes the value $12/\pi^2$. Hence Eq. (4.68) can be written as

$$\begin{aligned} \frac{dC}{dz} = & \frac{12\beta_2}{\pi^2 E} \int_{-\infty}^{\infty} \left| \frac{\partial B}{\partial t} \right|^2 dt + 3i \frac{\beta_3}{\pi^2 E} \int_{-\infty}^{\infty} \left(\frac{\partial^2 B}{\partial t^2} \frac{\partial B^*}{\partial t} - \frac{\partial^2 B^*}{\partial t^2} \frac{\partial B}{\partial t} \right) dt \\ & - \frac{12i\bar{\gamma}}{\pi^2 E \omega_0} \int_{-\infty}^{\infty} (t-T) \frac{\partial |B|^2}{\partial t} \left(B^* \frac{\partial B}{\partial t} - B \frac{\partial B^*}{\partial t} \right) dt - \frac{6i\bar{\gamma}}{\pi^2 E \omega_0} \int_{-\infty}^{\infty} |B|^2 \left(B \frac{\partial B^*}{\partial t} - B^* \frac{\partial B}{\partial t} \right) dt \\ & - 12 \frac{T_R \bar{\gamma}}{\pi^2 E} \int_{-\infty}^{\infty} (t-T) \left(\frac{\partial |B|^2}{\partial t} \right)^2 dt + \frac{6\bar{\gamma}}{\pi^2 E} \int_{-\infty}^{\infty} |B|^4 dt. \end{aligned} \quad (4.100)$$

Now we perform the integration of each term one by one. First we evaluate the term that depend on β_3 as follows:

From Eq. (4.85) we have

$$\begin{aligned} \frac{\partial^2 B}{\partial t^2} = & a \operatorname{sech} \left(\frac{t-T}{\tau} \right) \left[\frac{1}{\tau^2} \tanh^2 \left(\frac{t-T}{\tau} \right) - \frac{1}{\tau^2} \operatorname{sech}^2 \left(\frac{t-T}{\tau} \right) - \frac{i}{\tau} \tanh \left(\frac{t-T}{\tau} \right) \left(\Omega + C \frac{(t-T)}{\tau^2} \right) \right. \\ & \left. - \frac{iC}{\tau^2} - \frac{1}{\tau} \tanh \left(\frac{t-T}{\tau} \right) - i \left(\Omega + C \frac{(t-T)}{\tau^2} \right) \right] \times \exp[i\phi - i\Omega(t-T) - iC(t-T)^2/2\tau^2] \end{aligned} \quad (4.101)$$

Hence we find

$$\begin{aligned} \frac{\partial B^*}{\partial t} \frac{\partial^2 B}{\partial t^2} = & a^2 \operatorname{sech}^2 \left(\frac{t-T}{\tau} \right) \left[-\frac{1}{\tau^3} \tanh^3 \left(\frac{t-T}{\tau} \right) + \frac{1}{\tau^3} \operatorname{sech}^2 \left(\frac{t-T}{\tau} \right) \tanh \left(\frac{t-T}{\tau} \right) + \frac{iC}{\tau^3} \tanh \left(\frac{t-T}{\tau} \right) \right. \\ & + \frac{i}{\tau^2} \tanh^2 \left(\frac{t-T}{\tau} \right) \left(\Omega + C \frac{(t-T)}{\tau^2} \right) - \frac{i}{\tau^2} \operatorname{sech}^2 \left(\frac{t-T}{\tau} \right) \left(\Omega + C \frac{(t-T)}{\tau^2} \right) \\ & \left. + \frac{1}{\tau} \tanh \left(\frac{t-T}{\tau} \right) \left(\Omega + C \frac{(t-T)}{\tau^2} \right)^2 + \frac{C}{\tau^2} \left(\Omega + C \frac{(t-T)}{\tau^2} \right) - i \left(\Omega + C \frac{(t-T)}{\tau^2} \right)^3 \right]. \end{aligned} \quad (4.102)$$

Subtracting the complex conjugate of Eq. (4.102) from itself we get

$$\begin{aligned} \left(\frac{\partial^2 B}{\partial t^2} \frac{\partial B^*}{\partial t} - \frac{\partial^2 B^*}{\partial t^2} \frac{\partial B}{\partial t} \right) &= a^2 \operatorname{sech}^2 \left(\frac{t-T}{\tau} \right) \left[\frac{2iC}{\tau^3} \tanh \left(\frac{t-T}{\tau} \right) + \frac{2i}{\tau^2} \tanh^2 \left(\frac{t-T}{\tau} \right) \left(\Omega + C \frac{(t-T)}{\tau^2} \right) \right. \\ &\quad \left. - \frac{2i}{\tau^2} \operatorname{sech}^2 \left(\frac{t-T}{\tau} \right) \left(\Omega + C \frac{(t-T)}{\tau^2} \right) - 2i \left(\Omega + C \frac{(t-T)}{\tau^2} \right)^3 \right]. \end{aligned} \quad (4.103)$$

Using Table 4.1 and integrating Eq. (4.103) we get

$$\int_{-\infty}^{\infty} \left(\frac{\partial^2 B}{\partial t^2} \frac{\partial B^*}{\partial t} - \frac{\partial^2 B^*}{\partial t^2} \frac{\partial B}{\partial t} \right) dt = -\frac{2i}{\tau^2} E \Omega \left(\frac{1}{3} + \frac{\pi^2}{4} C^2 \right) - 2i \Omega^3 E. \quad (4.104)$$

Next we find the effect of self-steepening on the evolution of the chirp by evaluating the third and the fourth integrals in Eq. (4.100). From Eqs. (4.92) and (4.94) the third integral in Eq. (4.100) can be written as

$$\int_{-\infty}^{\infty} (t-T) \frac{\partial |B|^2}{\partial t} \left(B^* \frac{\partial B}{\partial t} - B \frac{\partial B^*}{\partial t} \right) dt = \frac{4a^4}{\tau} \int_{-\infty}^{\infty} (t-T) \operatorname{sech}^4 \left(\frac{t-T}{\tau} \right) \tanh \left(\frac{t-T}{\tau} \right) \left[\Omega + \frac{C}{\tau^2} (t-T) \right] dt. \quad (4.105)$$

From Table 4.1 Eq. (4.105) can be written as

$$\int_{-\infty}^{\infty} (t-T) \frac{\partial |B|^2}{\partial t} \left(B^* \frac{\partial B}{\partial t} - B \frac{\partial B^*}{\partial t} \right) dt = i \frac{\Omega E^2}{3\tau}. \quad (4.106)$$

The next integral in Eq. (4.100) can be written using Eqs. (4.92) and (4.93) as

$$\int_{-\infty}^{\infty} |B|^2 \left(B \frac{\partial B^*}{\partial t} - B^* \frac{\partial B}{\partial t} \right) dt = 2ia^4 \int_{-\infty}^{\infty} \left[\Omega + C \frac{(t-T)}{\tau^2} \right] \operatorname{sech}^4 \left(\frac{t-T}{\tau} \right) dt. \quad (4.107)$$

Using Table 4.1 to perform the integration we obtain

$$\int_{-\infty}^{\infty} |B|^2 \left(B \frac{\partial B^*}{\partial t} - B^* \frac{\partial B}{\partial t} \right) dt = 2i \frac{\Omega E^2}{3\tau}. \quad (4.108)$$

Next we evaluate the fifth integral in Eq. (4.100) using Eq. (4.94) and Table 4.1 as follows:

$$\begin{aligned} \int_{-\infty}^{\infty} (t-T) \left(\frac{\partial |B|^2}{\partial t} \right)^2 dt &= \frac{4a^4}{\tau^2} \int_{-\infty}^{\infty} (t-T) \operatorname{sech}^4 \left(\frac{t-T}{\tau} \right) \tanh^2 \left(\frac{t-T}{\tau} \right) dt, \\ \int_{-\infty}^{\infty} (t-T) \left(\frac{\partial |B|^2}{\partial t} \right)^2 dt &= 0. \end{aligned} \quad (4.109)$$

Using Eq. (4.89), the final integral in Eq. (4.100) is given by

$$\int_{-\infty}^{\infty} |B|^4 dt = \frac{E^2}{3\tau}. \quad (4.110)$$

Using Eqs. (4.87), (4.104), (4.106), (4.108), (4.109), (4.110), in Eq. (4.100), we write the evolution of chirp along the fiber as

$$\frac{dC}{dz} = \frac{12}{\pi^2}\beta_2\Omega^2 + \frac{\beta_2}{\tau^2}\left(\frac{4}{\pi^2} + C^2\right) + \frac{\beta_3\Omega}{2\tau^2}\left(\frac{4}{\pi^2} + 3C^2\right) + \frac{6}{\pi^2}\beta_3\Omega^3 + \frac{24\bar{\gamma}\Omega E}{\pi^2\omega_0\tau} + \frac{2\bar{\gamma}E}{\pi^2\tau}. \quad (4.111)$$

	$\beta_2 \times$	$\beta_3 \times$	$(\bar{\gamma}E/\omega_0) \times$	$\bar{\gamma}TRE \times$	$\bar{\gamma}E \times$
$\frac{dE}{dz}$	0	0	0	0	0
$\frac{dT}{dz}$	Ω	$\frac{\Omega^2}{2} + \frac{1}{6\tau^2}\left(1 + \frac{\pi^2}{4}C^2\right)$	$1/2\tau$	0	0
$\frac{d\Omega}{dz}$	0	0	$C/3\tau^3$	$-4/(15\tau^3)$	0
$\frac{dC}{dz}$	$\frac{12}{\pi^2}\Omega^2 + \frac{1}{\tau^2}\left(\frac{4}{\pi^2} + C^2\right)$	$\frac{\Omega}{2\tau^2}\left(\frac{4}{\pi^2} + 3C^2\right) + \frac{6}{\pi^2}\Omega^3$	$24\Omega/\pi^2\tau$	0	$2/(\pi^2\tau)$
$\frac{d\tau}{dz}$	C/τ	$\Omega C/\tau$	0	0	0

Table 4.2: Evolution of the pulse parameters for the Fundamental soliton obtained using the moment method

Next we find the evolution of the pulse width from Eq. (4.82). Substituting Eq. (3.7) into Eq. (4.82) and using $K = 12/\pi^2$, we get

$$\frac{d\tau}{dz} = \frac{\beta_2 C}{\tau} + \frac{6\beta_3}{\pi^2\tau E} \int_{-\infty}^{\infty} (t-T) \left| \frac{\partial B}{\partial t} \right|^2 dt. \quad (4.112)$$

From Eq. (4.86), the second integral in Eq. (4.112) can be evaluated using Table 4.1 as follows:

$$\begin{aligned} \int_{-\infty}^{\infty} (t-T) \left| \frac{\partial B}{\partial t} \right|^2 dt &= \frac{a^2}{\tau^2} \int_{-\infty}^{\infty} (t-T) \operatorname{sech}^2\left(\frac{t-T}{\tau}\right) \tanh^2\left(\frac{t-T}{\tau}\right) dt \\ &+ a^2 \int_{-\infty}^{\infty} (t-T) \operatorname{sech}^2\left(\frac{t-T}{\tau}\right) [\Omega + C(t-T)/\tau^2]^2 dt, \\ &= \frac{\pi^2}{6} \Omega C E. \end{aligned} \quad (4.113)$$

From Eqs. (4.112) and (4.113) we write the evolution of pulse width as

$$\frac{d\tau}{dz} = \frac{\beta_2 C}{\tau} + \beta_3 \Omega \frac{C}{\tau}. \quad (4.114)$$

The evolution of the pulse parameters found using the moment method for fundamental solitons are given by Table 4.2.

4.3 Gaussian Pulse

Next we consider the case of a DM soliton whose pulse shape is represented by a Gaussian profile as shown in Eq. (3.23). The width parameter, τ and the chirp parameter, C appearing in this equation are again related to the RMS width, σ and the moment \tilde{C} by a constant factor K such that $\tau^2 = K\sigma^2 = 2\sigma$ and $C = 2\tilde{C}$ respectively. In order to see how the evolution of the pulse parameters in such a case differ from that of the fundamental soliton, we use Eq. (3.23) for the pulse shape, $B(z, t)$ in the evolution equations obtained using the moment method. First the evolution of the pulse energy given by Eq. (4.22) remain unchanged. Hence

$$\frac{dE}{dz} = 0. \quad (4.115)$$

Next the evolution of the pulse position for the case of Gaussian pulses can be obtained by substituting Eq. (3.23) into Eq. (4.36). From Eq. (4.36) we have

$$\frac{dT}{dz} = \beta_2 \Omega + \frac{\beta_3}{2E} \int_{-\infty}^{\infty} \left| \frac{\partial B}{\partial t} \right|^2 dt + \frac{3\bar{\gamma}}{2\omega_0 E} \int_{-\infty}^{\infty} |B|^4 dt. \quad (4.116)$$

From Eq. (3.27) we have

$$\left| \frac{\partial B}{\partial t} \right|^2 = a^2 \left[\Omega^2 + (1 + C^2) \frac{(t - T)^2}{\tau^4} + 2\Omega C \frac{(t - T)}{\tau^2} \right]. \quad (4.117)$$

Integrating Eq. (4.117) with respect to t from $-\infty$ to ∞ using Table 4.3 we get

$$\begin{aligned} \int_{-\infty}^{\infty} \left| \frac{\partial B}{\partial t} \right|^2 dt &= a^2 \int_{-\infty}^{\infty} \left[\Omega^2 + (1 + C^2) \frac{(t - T)^2}{\tau^4} + 2\Omega C \frac{(t - T)}{\tau^2} \right] \exp[-(t - T)^2/\tau^2] dt, \\ \int_{-\infty}^{\infty} \left| \frac{\partial B}{\partial t} \right|^2 dt &= E\Omega^2 + E \frac{(1 + C^2)}{2\tau^2}, \end{aligned} \quad (4.118)$$

where $E = \sqrt{\pi} a^2 \tau$. Using Eq. (3.23) the final integral in Eq. (4.116) can be written as

$f(x)$	1	x	x^2	$\exp(-x^2)$	x^{2n+1}
$\int_{-\infty}^{\infty} f(x) \exp(-x^2) dx$	$\sqrt{\pi}$	0	$\sqrt{\pi}/2$	$\sqrt{\pi}/2$	0

Table 4.3: Integration table to get the evolution of pulse parameters of a Gaussian pulse

$$\int_{-\infty}^{\infty} |B|^4 dt = a^4 \int_{-\infty}^{\infty} \exp[-2(t - T)^2/\tau^2] dt \quad (4.119)$$

Using Table 4.3 we have

$$\int_{-\infty}^{\infty} |B|^4 dt = \frac{E^2}{\sqrt{2\pi\tau}}. \quad (4.120)$$

Hence the the evolution of the pulse position for Gaussian pulse is given by

$$\frac{dT}{dz} = \beta_2 \Omega + \frac{\beta_3}{2} \left[\Omega^2 + \frac{(1+C^2)}{2\tau^2} \right] + \frac{3\bar{\gamma}E}{\sqrt{8\pi\omega_0\tau}}. \quad (4.121)$$

Next we find the evolution of the frequency for the case of a DM soliton. For this we use Eq. (3.23) in Eq. (4.52) and find

$$\frac{d\Omega}{dz} = -\frac{\bar{\gamma}}{E\omega_0} \int_{-\infty}^{\infty} \frac{\partial}{\partial t} |B|^2 \left(B^* \frac{\partial B}{\partial t} - B \frac{\partial B^*}{\partial t} \right) dt - \frac{\bar{\gamma}}{E} T_R \int_{-\infty}^{\infty} \left(\frac{\partial}{\partial t} |B|^2 \right)^2 dt. \quad (4.122)$$

From Eqs. (3.23) and (3.27) we have

$$\left(B^* \frac{\partial B}{\partial t} - B \frac{\partial B^*}{\partial t} \right) = 2ia^2 [-\Omega - C(t-T)/\tau^2] \exp[-(t-T)^2/\tau^2], \quad (4.123)$$

and

$$\frac{\partial}{\partial t} |B|^2 = -2a^2 \frac{(t-T)}{\tau^2} \exp[-(t-T)^2/\tau^2]. \quad (4.124)$$

Hence the first integral in Eq. (4.122) can be written as

$$\int_{-\infty}^{\infty} \frac{\partial}{\partial t} |B|^2 \left(B^* \frac{\partial B}{\partial t} - B \frac{\partial B^*}{\partial t} \right) dt = -\frac{4ia^4}{\tau^2} \int_{-\infty}^{\infty} (t-T) [-\Omega - C(t-T)/\tau^2] \exp[-2(t-T)^2/\tau^2] dt \quad (4.125)$$

Using the Table 4.3 we perform the integration and obtain

$$\int_{-\infty}^{\infty} \frac{\partial}{\partial t} |B|^2 \left(B^* \frac{\partial B}{\partial t} - B \frac{\partial B^*}{\partial t} \right) dt = \frac{iCE^2}{\sqrt{2\pi\tau^3}}. \quad (4.126)$$

Next from Eq. (4.124) we can write the second integral in Eq.(4.122) as

$$\int_{-\infty}^{\infty} \left(\frac{\partial}{\partial t} |B|^2 \right)^2 dt = \frac{2a^4}{\tau^2} \int_{-\infty}^{\infty} 2 \frac{(t-T)^2}{\tau^2} \exp[-2(t-T)^2/\tau^2] dt. \quad (4.127)$$

Again using Table 4.3 we perform the integration to obtain

$$\int_{-\infty}^{\infty} \left(\frac{\partial}{\partial t} |B|^2 \right)^2 dt = \frac{E^2}{\sqrt{2\pi\tau^3}}. \quad (4.128)$$

Substituting Eqs. (4.126) and (4.128) into Eq. (4.122) we find the evolution of the frequency in the case of Gaussian pulses to be

$$\frac{d\Omega}{dz} = \frac{\bar{\gamma}EC}{\sqrt{2\pi\omega_0\tau^3}} - \frac{\bar{\gamma}T_RE}{\sqrt{2\pi\tau^3}}. \quad (4.129)$$

Next we find the evolution of the chirp for Gaussian pulses by using Eq. (3.23) along with $K = 2$, which is the value of the constant K in Eq. (4.54). From Eq. (4.54) we have

$$\begin{aligned} \frac{dC}{dz} &= \frac{2\beta_2}{E} \int_{-\infty}^{\infty} \left| \frac{\partial B}{\partial t} \right|^2 dt + i \frac{\beta_3}{2E} \int_{-\infty}^{\infty} \left(\frac{\partial^2 B}{\partial t^2} \frac{\partial B^*}{\partial t} - \frac{\partial^2 B^*}{\partial t^2} \frac{\partial B}{\partial t} \right) dt \\ &+ \frac{2i\bar{\gamma}}{E\omega_0} \int_{-\infty}^{\infty} (t-T) \frac{\partial |B|^2}{\partial t} \left(B^* \frac{\partial B}{\partial t} - B \frac{\partial B^*}{\partial t} \right) dt - \frac{3i\bar{\gamma}}{E\omega_0} \int_{-\infty}^{\infty} |B|^2 \left(B \frac{\partial B^*}{\partial t} - B^* \frac{\partial B}{\partial t} \right) dt \\ &- 2 \frac{T_R \bar{\gamma}}{E} \int_{-\infty}^{\infty} (t-T) \left(\frac{\partial |B|^2}{\partial t} \right)^2 dt + \frac{\bar{\gamma}}{E} \int_{-\infty}^{\infty} |B|^4 dt. \end{aligned} \quad (4.130)$$

Now we evaluate the integrals one by one. The result of the first integration is given in Eq. (4.117).

We now evaluate the second integral. From Eq. (3.27) we have

$$\frac{\partial^2 B}{\partial t^2} = a \left[\left(-i\Omega - (1+iC) \frac{(t-T)}{\tau^2} \right)^2 - \frac{(1+iC)}{\tau^2} \right] \exp \left[i\phi - i\Omega(t-T) - (1+iC) \frac{(t-T)^2}{2\tau^2} \right]. \quad (4.131)$$

Using Eqs. (3.27) and (4.131) the second integral can be written as

$$\begin{aligned} \int_{-\infty}^{\infty} \left(\frac{\partial^2 B}{\partial t^2} \frac{\partial B^*}{\partial t} - \frac{\partial^2 B^*}{\partial t^2} \frac{\partial B}{\partial t} \right) dt &= a^2 \int_{-\infty}^{\infty} \exp \left[-\frac{(t-T)}{\tau^2} \right] \left[-2i\Omega^3 + 2i\Omega(1-C^2) \frac{(t-T)^2}{\tau^4} - 4i\Omega^2 C \frac{(t-T)}{\tau^2} \right. \\ &\quad \left. - 2i\Omega^2 C \frac{(t-T)}{\tau^2} - 2iC(1+C^2) \frac{(t-T)^3}{\tau^6} - 4i(1+C^2) \frac{(t-T)^2}{\tau^4} - 2i \frac{\Omega}{\tau^2} \right] dt. \end{aligned} \quad (4.132)$$

Using Table 4.3 we perform the integration and obtain

$$\int_{-\infty}^{\infty} \left(\frac{\partial^2 B}{\partial t^2} \frac{\partial B^*}{\partial t} - \frac{\partial^2 B^*}{\partial t^2} \frac{\partial B}{\partial t} \right) dt = -2i\Omega^3 E - 3i\Omega(1+C^2)E/\tau^2. \quad (4.133)$$

From Eqs. (4.123) and (4.124) the third integral in Eq. (4.130) can be written as

$$\int_{-\infty}^{\infty} (t-T) \frac{\partial |B|^2}{\partial t} \left(B^* \frac{\partial B}{\partial t} - B \frac{\partial B^*}{\partial t} \right) dt = -4ia^4 \int_{-\infty}^{\infty} \frac{(t-T)^2}{\tau^2} \left[-\Omega - C \frac{(t-T)}{\tau^2} \right] \exp \left[-2 \frac{(t-T)^2}{\tau^2} \right] dt. \quad (4.134)$$

Using Table 4.3 and performing the integration we get

$$\int_{-\infty}^{\infty} (t-T) \frac{\partial |B|^2}{\partial t} \left(B^* \frac{\partial B}{\partial t} - B \frac{\partial B^*}{\partial t} \right) dt = i \frac{\Omega E^2}{\sqrt{2\pi\tau}}. \quad (4.135)$$

The next term in Eq. (4.130) can be written by using Eqs. (4.123) and (3.27) as

$$\int_{-\infty}^{\infty} |B|^2 \left(B \frac{\partial B^*}{\partial t} - B^* \frac{\partial B}{\partial t} \right) dt = 2ia^4 \int_{-\infty}^{\infty} \left[\Omega + C(t-T)/\tau^2 \right] \exp \left[-2(t-T)^2/\tau^2 \right] dt. \quad (4.136)$$

Using Table 4.3 Eq. (4.136) can be written as

$$\int_{-\infty}^{\infty} |B|^2 \left(B \frac{\partial B^*}{\partial t} - B^* \frac{\partial B}{\partial t} \right) dt = 2i \frac{\Omega E^2}{\sqrt{2\pi\tau}}. \quad (4.137)$$

The next integral in the evolution equation for chirp is evaluated using Eq. (4.124) in Eq. (4.130) as follows:

$$\int_{-\infty}^{\infty} (t-T) \left(\frac{\partial |B|^2}{\partial t} \right)^2 dt = 4a^4 \int_{-\infty}^{\infty} \frac{(t-T)^3}{\tau^6} \exp[-2(t-T)^2/\tau^2] dt. \quad (4.138)$$

From Table 4.3 we have

$$\int_{-\infty}^{\infty} (t-T) \left(\frac{\partial |B|^2}{\partial t} \right)^2 dt = 0. \quad (4.139)$$

Thus we can write the evolution of the chirp parameter for the case of Gaussian pulses using Eqs. (4.118), (4.120), (4.133), (4.135), (4.137) and (4.139) in Eq. (4.130) and the final result is given by

$$\frac{dC}{dz} = 2\beta_2\Omega^2 + \beta_2 \frac{(1+C^2)}{\tau^2} + \beta_3\Omega^3 + \beta_3 \frac{(1+C^2)}{\tau^2} + \frac{4\bar{\gamma}E\Omega}{\sqrt{2\pi\omega_0\tau}} + \frac{\bar{\gamma}E}{\sqrt{2\pi\tau}}. \quad (4.140)$$

Next we find the evolution of the pulse width for the case of Gaussian pulses. Substituting Eq. (3.23) in Eq. (4.82) and using that $K = 2$, we get

$$\frac{d\tau}{dz} = \frac{\beta_2 C}{\tau} + \frac{\beta_3}{\tau E} \int_{-\infty}^{\infty} (t-T) \left| \frac{\partial B}{\partial t} \right|^2 dt. \quad (4.141)$$

The integral on the right hand side of Eq. (4.141) can be evaluated analytically by using Eq. (4.117) and Table 4.3 as follows:

$$\begin{aligned} \int_{-\infty}^{\infty} (t-T) \left| \frac{\partial B}{\partial t} \right|^2 dt &= a^2 \int_{-\infty}^{\infty} (t-T) \left[\Omega^2 + (1+C^2) \frac{(t-T)^2}{\tau^4} + 2\Omega C \frac{(t-T)}{\tau^2} \right] \exp[-(t-T)^2/\tau^2] dt, \\ &= E\Omega C \end{aligned} \quad (4.142)$$

Substituting Eq. (4.142) into Eq. (4.141) we find the evolution equation for the pulse width for the case of Gaussian pulse to be

$$\frac{d\tau}{dz} = \frac{\beta_2 C}{\tau} + \frac{\beta_3 \Omega C}{\tau}. \quad (4.143)$$

To summarize, the evolution equations of the pulse parameters for the case of a Gaussian pulse using the moment method are summarized in Table 4.4.

Thus we see that the moment method is a simple analytical method that can give the evolution equations for the pulse parameters in the fiber thus enabling us to understand the propagation

	$\beta_2 \times$	$\beta_3 \times$	$(\bar{\gamma}E/\omega_0) \times$	$\bar{\gamma}T_R E \times$	$\bar{\gamma}E \times$
$\frac{dE}{dz}$	0	0	0	0	0
$\frac{dT}{dz}$	Ω	$\frac{\Omega^2}{2} + \frac{(1+C^2)}{4\tau^2}$	$3/\sqrt{8\pi\tau}$	0	0
$\frac{d\Omega}{dz}$	0	0	$C/\sqrt{2\pi\tau^3}$	$-1/\sqrt{2\pi\tau^3}$	0
$\frac{dC}{dz}$	$2\Omega^2 + \frac{(1+C^2)}{\tau^2}$	$\Omega^3 + \frac{(1+C^2)}{\tau^2}$	$4\Omega/\sqrt{2\pi\tau}$	0	$1/(\sqrt{2\pi\tau})$
$\frac{d\tau}{dz}$	C/τ	$\Omega C/\tau$	0	0	0

Table 4.4: Evolution of pulse parameters for Gaussian pulse obtained using the moment method

of optical pulses inside a fiber in both dissipative and non-dissipative limits. Also the results obtained using the variational method can be derived using the moment method. This can be seen immediately by setting β_3 , T_R and $1/\omega_0$ equal to 0 in the evolution equations obtained using the moment method. However, like the variational method, the moment method is also an approximate method. The main limitation of this analysis stems from the assumption that the pulse maintains its shape even though its width may change and it may become chirped.

4.4 Raman-induced Frequency shift

Since 1986, RIFS has been studied extensively for both constant dispersion and dispersion-managed fibers but mostly in the context of solitons [38]– [40]. However, as seen before in Chapter 3, RIFS is not necessarily a soliton effect. Now we apply the moment method to study the effect of IRS on fundamental soliton and Gaussian pulses in the case of both anomalous and normal dispersion regimes. We also keep the TOD and self-steepening terms since they become important for we consider pulses whose width is as small as 50 femtoseconds.

4.4.1 Fundamental Soliton

We first consider the propagation of standard solitons in a fiber with constant dispersion. Then from the previous sections we know that the five pulse parameters evolve as

$$\frac{dE}{dz} = 0 \quad (4.144)$$

$$\frac{dT}{dz} = \beta_2 \Omega + \frac{\beta_3}{2} \left[\Omega^2 + \frac{1}{3\tau^2} \left(1 + \frac{\pi^2}{4} C^2 \right) \right] + \frac{\bar{\gamma}E}{2\omega_0\tau}, \quad (4.145)$$

$$\frac{d\Omega}{dz} = -\frac{4T_R\bar{\gamma}E}{15\tau^3} + \frac{\bar{\gamma}CE}{3\omega_0\tau^3}, \quad (4.146)$$

$$\frac{d\tau}{dz} = \frac{\beta_2 C}{\tau} + \beta_3 \frac{C\Omega}{\tau}, \quad (4.147)$$

$$\frac{dC}{dz} = \left(\frac{4}{\pi^2} + C^2 \right) \frac{\beta_2}{\tau^2} + \frac{\beta_3 \Omega}{2\tau^2} \left(\frac{4}{\pi^2} + 3C^2 \right) + \frac{6}{\pi^2} \beta_3 \Omega^3 + \frac{2\bar{\gamma}E}{\pi^2 \tau} + \frac{12}{\pi^2} \beta_2 \Omega^2 + \frac{24\bar{\gamma}\Omega E}{\pi^2 \omega_0 \tau}. \quad (4.148)$$

Consider first the special case of chirp-free solitons launched in a fiber whose losses are exactly compensated through distributed amplification such that losses vanish effectively ($\alpha = 0$). The pulse energy E then remains constant and $\bar{\gamma} = \gamma$. If we ignore the higher-order effects except for IRS by setting $\omega_0 = 0$ and $\beta_3 = 0$ and use $C = 0$ in Eqs. (4.2)–(4.4), we find that τ remains constant along the fiber, as it should for solitons. Also, E and τ are not independent but related to each other by the soliton condition $L_D = L_{NL}$, which can be obtained from Eq. (4.4) by setting $dC/dz = 0$ if we neglect the Ω term and relate the peak power P_0 of the solitons to the soliton energy using $E = 2P_0\tau$. Using the condition $L_D = L_{NL}$, we find that $E = 2|\beta_2|/(\gamma\tau)$. If we substitute this relation in Eq. (4.146), the RIFS evolves as

$$\Omega(z) = -\frac{8T_R|\beta_2|z}{15\tau^4}. \quad (4.149)$$

Equation (4.149) is identical to the RIFS magnitude first estimated by Gordon using perturbation theory [36]. It shows that the RIFS increases linearly with distance but scales with pulse width as τ^{-4} , thereby becoming important only for pulses shorter than a few picoseconds. However, its derivation assumes that the soliton remains unchirped. From Eq. (4.148), C remains zero for solitons only if $\Omega = 0$. Equations (4.147) and (4.148) clearly show that C and τ both begin to change for standard solitons because of the RIFS. Thus, Eq. (4.149) is only valid in the limit in which the RIFS is small enough that it does not affect the soliton. We can find the validity condition for Eq. (4.149) in the absence of third-order dispersion and self-steepening, by requiring

in Eq. (4.148) that $|\beta_2|\Omega^2 \ll 2\gamma E/(\pi^2\tau)$. Using $E = 2|\beta_2|/(\gamma\tau)$, this condition is equivalent to requiring $\Omega\tau \ll 1$. Noting that the spectral width of a pulse scales inversely with the pulse width τ , we conclude that Eq. (4.149) is valid as long as the RIFS remains a small fraction of the pulse spectral width. In many practical situations, RIFS becomes large enough that it exceeds the spectral width of the pulse significantly.

We thus consider the more general case in which neither E nor τ remain constant along the fiber. The pulse energy E generally changes because of gain–loss variations introduced when losses are compensated periodically using optical amplifiers [1]. The soliton width τ begins to change as soon as the pulse becomes chirped ($C \neq 0$). Notice that the chirp parameter C does not appear directly in the Ω equation but it affects the RIFS through pulse-width changes. Using $\bar{\gamma} = \gamma e^{-\alpha z}$, the total frequency shift is found by integrating Eq. (4.146) and is given by

$$\Omega(z) = -\frac{4T_R\gamma E_0}{15} \int_0^z \frac{e^{-\alpha z}}{\tau^3} dz + \frac{\gamma E_0}{3\omega_0} \int_0^z C(z) \frac{e^{-\alpha z}}{\tau^3} dz \quad (4.150)$$

Note that the RIFS depends on the local pulse width as τ^{-3} and not as τ^{-4} , as suggested by Eq. (4.149). Of course, the z dependence of τ and C should be calculated by solving Eqs. (4.147) and (4.148), which in turn depends on Ω itself. It is this interdependence among τ , C and Ω that governs the eventual magnitude of the RIFS. Since these evolution equations are coupled they have to be solved numerically.

As a numerical example, consider the propagation of solitons with initial pulse width, $\tau_0 = 50$ fs (full width at half maximum about 88 fs) in a 10-m-long, dispersion-shifted fiber with the GVD of 4 ps/km/nm ($|\beta_2| = 5.1$ ps²/km). Figures 4.1 and 4.2 show the RIFS and pulse width τ as a function of distance z in the cases of anomalous and normal dispersion, respectively. The nonlinear parameter $\gamma = 1.994\text{W}^{-1}\text{km}^{-1}$ was calculated using an effective core area of $50\mu\text{m}^2$. Also $\alpha = 0.2$ dB/km and $\beta_3 = 0.1$ ps³/km. Consider the case of anomalous dispersion first as it corresponds to the propagation of solitons. The solid curve in Figure 4.1 shows the $C(0) = 0$ case that corresponds to standard solitons. The pulse width is indeed maintained in the beginning, as expected, but begins to increase after 2 m because of the RIFS and TOD effects. The magnitude of RIFS becomes comparable to the spectral width of the pulse (about 2 THz) at a distance of 2 m, and it begins to affect the soliton itself. Notice that Ω increases initially linearly up to a distance of 2 m but then begins to saturate as the pulse width increases. The use of Eq. (4.149) would be inappropriate under

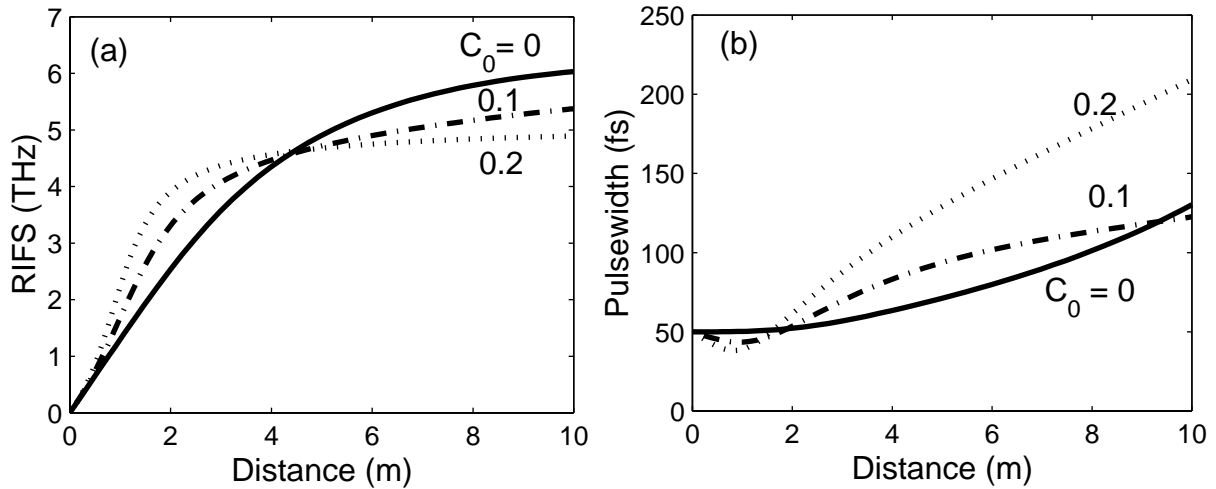


Figure 4.1: Evolution of Raman-Induced frequency shift (a) and pulse width (b) when sech-shaped pulses with $T_0 = 50$ fs propagate inside a 10-m-long fiber exhibiting anomalous dispersion ($D = 4$ ps/km-nm). The input chirp parameter C_0 varies in the range 0 to 0.2 for the three curves.

such conditions. The dashed and dash-dotted lines show that even a relatively small chirp affects the RIFS considerably. For positive values of C , the pulse is initially compressed, as expected for $\beta_2 C < 0$ [1], and then broadens after attaining its minimum width at a distance of about 1 m as explained in Chapter 2. For this reason Ω initially increases before saturating as the pulse broadens. The main point to note is that the chirp can increase the RIFS whenever $\beta_2 C < 0$ since the dispersion-induced chirp is in the opposite direction to that of the initial chirp and as a result the net chirp is reduced, leading to the initial pulse narrowing. The minimum pulse width occurs at the point at which the two chirps cancel each other. With a further increase in the propagation distance the dispersion-induced chirp starts to dominate over the initial chirp and the pulse begins to broaden. Hence the fiber length is not much longer than 10 m so that the dispersion induced chirp does not broaden the pulse. For $C < 0$, pulse begins to broaden immediately, and RIFS is reduced considerably.

Figure 4.2 shows the RIFS and pulse width as a function of distance in the case of normal dispersion. The solid line again shows the case $C(0) = 0$. Since the pulse begins to broaden right away, in contrast with the soliton case where the pulse width remained constant for up to 2 m, Ω quickly saturates and is thus considerably smaller in magnitude in the case of normal GVD. The dashed and dash-dotted lines show that it can be enhanced by chirping the input Gaussian pulse

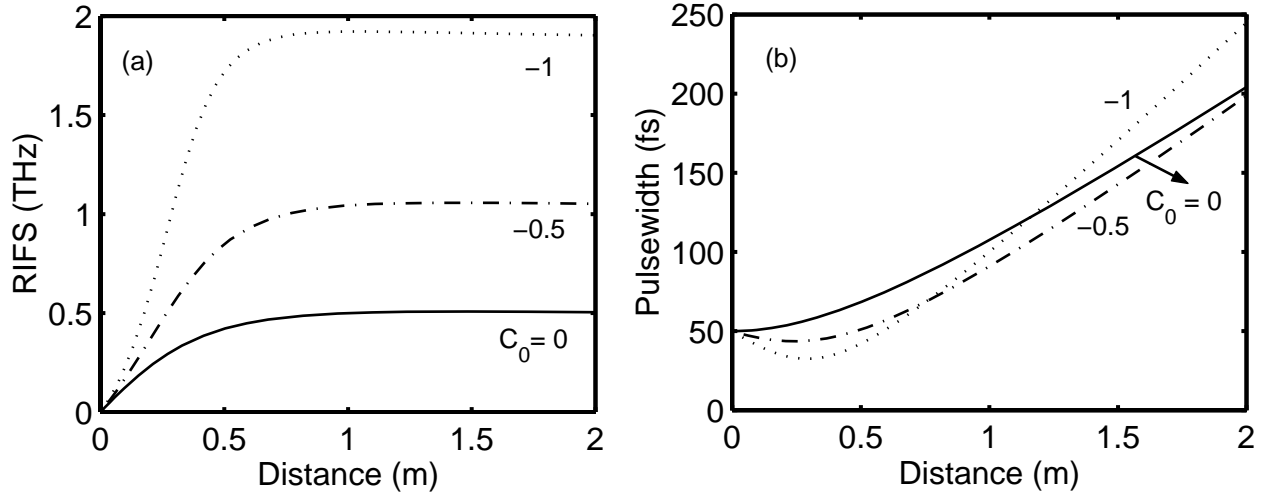


Figure 4.2: Evolution of Raman-Induced frequency shift (a) and pulse width (b) when sech-shaped pulses with $T_0 = 50$ fs propagate inside a 2-m-long fiber exhibiting normal dispersion ($D = -4$ ps/km-nm). The input chirp parameter C_0 varies in the range -1 to 0 for the three curves.

such that $\beta_2 C_0 < 0$. The reason is easily understood by noting that the pulse can be compressed by a factor of $\sqrt{2}$ for $|C_0| = 1$, and the compression factor can be increased even more for large values of the chirp. As seen in Fig. 4.2, almost the entire RIFS occurs within the first meter of the fiber, where pulse remains compressed and its magnitude is about three times larger for $|C_0| = 1$ compared with the $C_0 = 0$ case. With sufficiently large chirp, the RIFS can even become comparable to that obtained in the case of anomalous dispersion. We thus conclude that RIFS can be made large enough to be measurable even in the case of normal GVD through proper chirp control.

4.4.2 Chirped Gaussian Pulses

In this section we consider the case of a Gaussian pulse shape of the form

$$A(z, t) = \sqrt{\frac{E}{\pi\tau}} \exp[-(1 + iC)(t - T)^2 / 2\tau^2 + i\phi - i\Omega(t - T)]. \quad (4.151)$$

From the previous evaluations, the five pulse parameters then evolve as

$$\frac{dE}{dz} = 0, \quad (4.152)$$

$$\frac{dT}{dz} = \beta_2 \Omega + \frac{\beta_3}{2} \left[\Omega^2 + \frac{1 + C^2}{2\tau^2} \right] + \frac{3\gamma E}{\sqrt{8\pi\omega_0\tau}}, \quad (4.153)$$

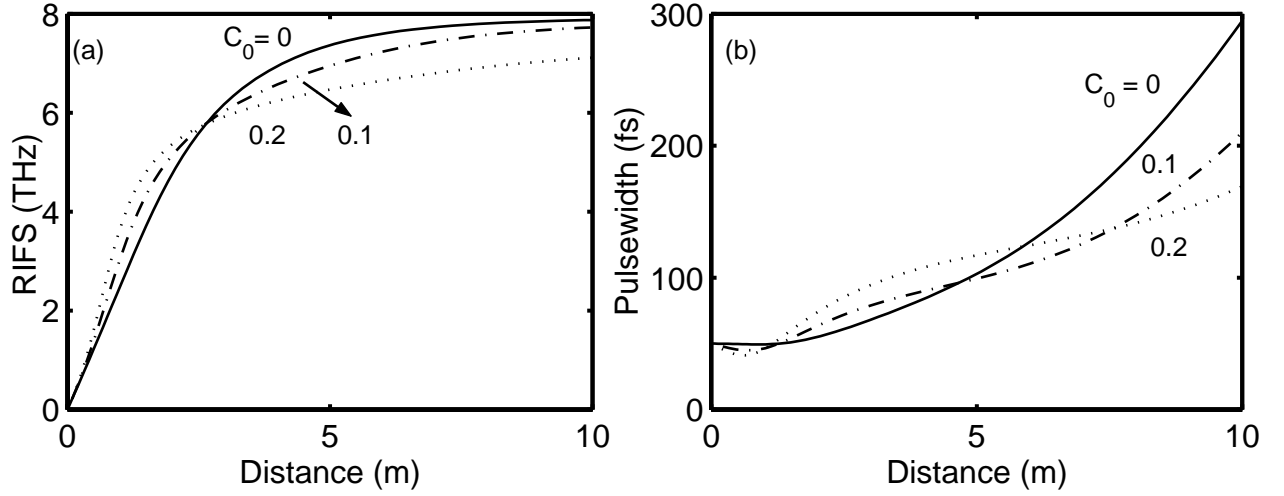


Figure 4.3: Evolution of Raman-Induced frequency shift (a) and pulse width (b) when Gaussian pulses with $T_0 = 50$ fs propagate inside a 10-m-long fiber exhibiting anomalous dispersion ($D = 4$ ps/km-nm). The input chirp parameter C_0 varies in the range 0 to 0.2 for the three curves.

$$\frac{d\Omega}{dz} = -\frac{T_R \bar{\gamma} E}{\sqrt{2\pi} \tau^3} + \frac{\bar{\gamma} C E}{\sqrt{2\pi} \omega_0 \tau^3}, \quad (4.154)$$

$$\frac{d\tau}{dz} = \frac{\beta_2 C}{\tau} + \frac{\beta_3 C \Omega}{\tau}, \quad (4.155)$$

$$\frac{dC}{dz} = \beta_2 \left(\frac{1+C^2}{\tau^2} \right) + \beta_3 \Omega^3 + \beta_3 \left(\frac{1+C^2}{\tau^2} \right) + \frac{\bar{\gamma} E}{\sqrt{2\pi} \tau} + 2\beta_2 \Omega^2 + \frac{4\bar{\gamma} \Omega E}{\sqrt{2\pi} \omega_0 \tau}. \quad (4.156)$$

Following the method discussed in the previous section for the case of ‘sech’ pulses, the RIFS in the Gaussian case is given by

$$\Omega(z) = -\frac{T_R \gamma E_0}{\sqrt{2\pi}} \int_0^z \frac{e^{-\alpha z}}{\tau^3} dz + \frac{\gamma E_0}{\sqrt{2\pi} \omega_0} \int_0^z C(z) \frac{e^{-\alpha z}}{\tau^3} dz. \quad (4.157)$$

where $C(z)$ and $\tau(z)$ should be found numerically by solving Eqs. (4.153)–(4.156). Equation (4.157) should be compared with Eq. (4.150) found in the “sech” case. It is evident that the exact shape of the pulse has a relatively minor effect on the magnitude of the RIFS. In particular, the functional dependence on the local pulse width and local magnitude of loss remains exactly the same. Even the numerical factor of $(2\pi)^{-1/2} \approx 0.4$ in the Gaussian case is only slightly larger than the factor of $4/15 \approx 0.267$ found in the “sech” case. This feature indicates that even if the pulse shape deviates somewhat from the shape assumed in applying the moment method, our analysis should still provide a good estimate of the RIFS in practice.

Figures 4.3 and 4.4 show the RIFS and pulse width of Gaussian pulses as a function of distance

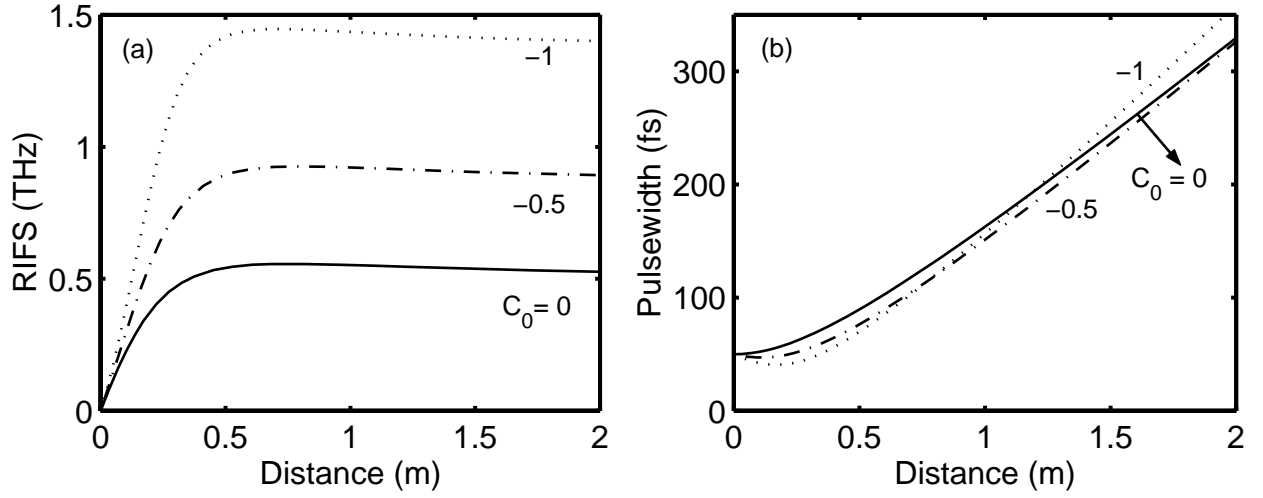


Figure 4.4: Evolution of Raman-Induced frequency shift (a) and pulse width (b) when Gaussian pulses with $T_0 = 50$ fs propagate inside a 2-m-long fiber exhibiting normal dispersion ($D = -4$ ps/km-nm). The input chirp parameter C_0 varies in the range -1 to 0 for the three curves.

in the cases of anomalous and normal dispersion, respectively, for the same 10-m long fiber and for the same set of parameters used for Figures 4.1 and 4.2. For a fair comparison with the soliton case, the initial pulse energy is chosen to be $E_0 = \sqrt{2\pi}|\beta_2|/(\gamma\tau)$ because $dC/dz = 0$ from Eq. (4.156) for this energy when $\Omega = 0$. In all cases, the solid line shows the case when $C_0 = 0$. In the case of anomalous dispersion (Fig. 4.3), the Gaussian pulse maintains its width up to 2 m, similar to the soliton case, and then broadens because of the RIFS and TOD effects. As expected, Ω increases linearly first and then saturates. Interestingly, the Gaussian pulses acquires a slightly larger RIFS compared with the ‘sech’ pulses as dispersion-induced broadening depends somewhat on the pulse shape. The dashed and dash-dotted lines show the effects of a positive initial chirp. Since $\beta_2 C_0 < 0$, the pulse undergoes an initial narrowing stage before broadening. A comparison of Figs. 4.1 and 4.3 shows that the pulses with nonzero initial chirp experience the compression stage twice. We attribute this to the imbalance between the dispersive and nonlinear effects in the case of initially chirped pulses. Other qualitative features are similar in the two cases. The case of normal dispersion shown in Figure 4.4 is quite similar to the results in Fig. 4.2 obtained for “sech” pulses. For chirp-free Gaussian pulses (solid line), RIFS saturates to a relatively small value of 0.5 THz. However, this value can be increased by applying a negative chirp so that $\beta_2 C_0 < 0$.

4.5 Chapter Summary

From the above results we conclude that the RIFS resulting from intrapulse Raman scattering is a general phenomenon that occurs for all pulses both in the normal and anomalous dispersion regimes of an optical fiber. The variational method cannot be used to calculate RIFS because of the dissipative nature of the Raman effect. However the moment method can be used to get the general evolution equations for the pulse parameters that can be applied to a given pulse shape. As an example we applied it to the cases of “sech” and Gaussian pulse shapes. The results also show that the RIFS depends not only on the width but also on the frequency chirp associated with the optical pulse. The RIFS becomes quite large in the case of ultrashort pulses because, as seen in Eqs. (4.150) and (4.157), it depends on the local pulse width as τ^{-3} and varies considerably with the history of pulse width changes. Whenever pulse width remains nearly constant along the fiber, RIFS can accumulate to relatively large values. This is the main reason why RIFS can be quite large for solitons. In the case of fundamental solitons, our expression for RIFS reduces to that of Gordon [36] as long as the RIFS is much smaller than the spectral width of the pulse. However, we show that even optical solitons do not maintain their width when RIFS becomes comparable to or larger than the spectral width of the pulse. Our analysis remains valid in this regime and shows how RIFS saturates to a constant value because of soliton broadening.

We also consider numerical examples in both the normal and anomalous dispersion regime using a 10-m long fiber in which femtosecond pulses are launched. Although RIFS is generally smaller for normal dispersion compared with the case of anomalous dispersion, it is large enough to be measurable experimentally. We also have included the effects of TOD and self-steepening in our analysis. We see that even though the TOD does not appear directly in our expression for RIFS, it does affect the RIFS through the frequency chirp. The main limitation of our analysis is that our results may not be valid if the pulse shape is known to change significantly during propagation.

Chapter 5

Amplifier Noise and Bit Error Rate

We now apply the moment method described in Chapter 4, to the problem of amplifier-induced noises as well as to find the degradation in system performance due to amplifier noise. In communication systems, the transmission is eventually limited by fiber losses. In order to overcome this limitation, optical amplifiers are used at regular intervals to compensate for fiber losses. Optical amplifiers amplify the optical signal through stimulated emission when the amplifier is pumped electrically or optically to achieve population inversion. Such amplifiers also degrade the amplified signal because of spontaneous emission that adds noise to the signal during its amplification. The system degradation is quantified through a parameter F_n , called the *amplifier noise figure* and defined as $F_n = 2n_{sp}$ where $n_{sp} = N_2/(N_2 - N_1)$ is the spontaneous emission factor related to the atomic populations N_1 and N_2 for the ground and excited states [1]. The noise added by these amplifiers to the signal is called the *Amplified Spontaneous Emission* (ASE) noise. The ASE noise accumulates over many amplifiers and degrades the optical signal as the number of amplifiers increases. As the ASE noise level increases, it begins to saturate optical amplifiers and reduces the gain of amplifiers located further down the fiber link. Hence the signal level drops further while ASE level increases. If the number of amplifiers is large, the signal will degrade so much that the system performance is largely reduced at the receiver.

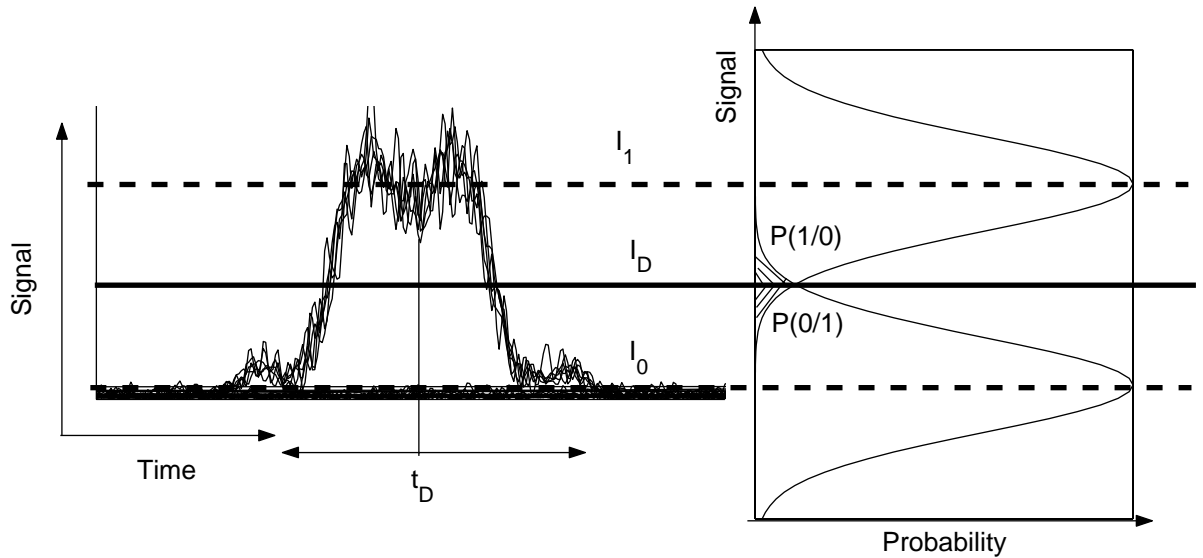


Figure 5.1: Bit Error probabilities.

5.1 Bit Error Rate

Optical receivers convert incident optical power into electric current through a photodiode. Among a group of optical receivers, a receiver is said to be more sensitive if it achieves the same performance with less optical power incident on it. The communications system performance is characterized by a quantity called the bit error rate (BER) which is defined as the average probability of incorrect bit identification of a bit by the decision circuit of the receiver [1]. For example, a BER of 2×10^{-6} would correspond to on average 2 errors per million bits. A commonly used criterion for digital optical receivers requires $\text{BER} \leq 1 \times 10^{-9}$. It is important for the signal to have minimum distortions in order to avoid a high BER at the receiver. This means that although the combined effects of GVD, SPM and IRS cannot be eliminated they need to be reduced so that the pulse can propagate with minimum distortions. Also the inevitable presence of amplifier noises can also cause pulse distortions and hence cause system degradation. In order to assess the system performance one needs to know how to calculate the BER of the system at the receiver end. In this chapter we calculate the BER of the system at the receiver in the presence of amplifier noises.

Figure 5.1 shows schematically the fluctuating signal received by the decision circuit, which samples it at the decision instant t_D determined through clock recovery. The sampled value I fluctuates from bit to bit around an average value I_1 or I_0 , depending on whether the bit corresponds

to 1 or 0 in the bit stream. The decision circuit compares the sampled value with the threshold value I_D and calls it bit 1 if $I > I_D$ or bit 0 if $I < I_D$. An error occurs if $I < I_D$ for bit 1 or if $I > I_D$ for bit 0 due to amplifier noises that add into the signal in the system. Both sources of errors can be included by defining the error probability as

$$\text{BER} = p(1)P(1/0) + p(0)P(0/1), \quad (5.1)$$

where $p(1)$ and $p(0)$ are the probabilities of receiving bits 1 and 0, respectively, $P(0/1)$ is the probability of deciding 0 when 1 is received, and $P(1/0)$ is the probability of deciding 1 when 0 is received. Since 1 and 0 bits are equally likely to occur, $p(1) = p(0) = 1/2$, and the BER becomes

$$\text{BER} = \frac{1}{2}[P(1/0) + P(0/1)]. \quad (5.2)$$

Figure 5.1 shows how $P(0/1)$ and $P(1/0)$ depend on the probability density function $p(I)$ of the sampled value I . The functional form of $p(I)$ depends on the statistics of noise sources responsible for current fluctuations. Assuming a Gaussian noise profile, one can write the functional form of $P(0/1)$ and $P(1/0)$ as

$$P(0/1) = \frac{1}{\sigma_1\sqrt{2\pi}} \int_{-\infty}^{I_D} \exp\left(-\frac{(I-I_1)^2}{2\sigma_1^2}\right) dI, \quad (5.3)$$

$$P(1/0) = \frac{1}{\sigma_0\sqrt{2\pi}} \int_{I_D}^{\infty} \exp\left(-\frac{(I-I_0)^2}{2\sigma_0^2}\right) dI, \quad (5.4)$$

where σ_1^2 and σ_0^2 are the corresponding variances. From the definition of the complimentary error function we have

$$\text{erfc}(x) = \frac{2}{\sqrt{\pi}} \int_x^{\infty} \exp(-x^2) dx. \quad (5.5)$$

Using Eq. (5.5) in Eqs. (5.3) and (5.4) we get

$$P(0/1) = \frac{1}{2} \text{erfc}\left(\frac{I_1 - I_D}{\sqrt{2}\sigma_1}\right), \quad (5.6)$$

$$P(1/0) = \frac{1}{2} \text{erfc}\left(\frac{I_D - I_0}{\sqrt{2}\sigma_0}\right). \quad (5.7)$$

Using Eqs.(5.6) and (5.7) in Eq. (5.2) we can write the BER as

$$\text{BER} = \frac{1}{4} \left[\text{erfc}\left(\frac{I_1 - I_D}{\sqrt{2}\sigma_1}\right) + \text{erfc}\left(\frac{I_D - I_0}{\sqrt{2}\sigma_0}\right) \right]. \quad (5.8)$$

Eq. (5.8) shows that the BER depends on the decision threshold I_D .

5.2 Q-factor

In practice, I_D is optimized to minimize the BER. Hence we minimize BER with respect to I_D using

$$\frac{d}{dx} \operatorname{erfc}[f(x)] = \frac{2}{\sqrt{\pi}} e^{-f^2} - \frac{df}{dx}, \quad (5.9)$$

and obtain

$$\frac{(I_1 - I_D)^2}{\sigma_1^2} = \frac{(I_D - I_0)^2}{\sigma_0^2} + \ln \left(\frac{\sigma_1}{\sigma_0} \right) \quad (5.10)$$

For most practical cases, the last term is negligible and hence we get

$$\frac{(I_1 - I_D)}{\sigma_1} = \frac{(I_D - I_0)}{\sigma_0}. \quad (5.11)$$

Hence we can find that the minimum occurs when

$$I_D = \frac{\sigma_0 I_1 + \sigma_1 I_0}{\sigma_0 + \sigma_1}. \quad (5.12)$$

When $\sigma_1 = \sigma_0$, $I_D = (I_1 + I_0)/2$, which corresponds to setting the decision threshold in the middle.

The BER is then given by

$$\text{BER} = \frac{1}{2} \operatorname{erfc} \left(\frac{Q}{\sqrt{2}} \right), \quad (5.13)$$

where the factor Q is given by

$$Q = \frac{I_1 - I_0}{\sigma_1 + \sigma_0}. \quad (5.14)$$

The Q factor is thus a dimensionless factor and is related to the BER as shown in Eq. (5.13). Figure 5.2 shows how BER varies with Q factor. The BER improves as Q increases and becomes lower than 10^{-12} for $Q = 7$. Now the expression for Q is in terms of the receiver current. Since the receiver current is directly a measure of optical power, P of the signal such that $I = RP$, where R is the responsivity of the photo detector, and the optical power is related to the energy of the signal pulse, we can write the Q factor in terms of the pulse energy as

$$Q = \frac{E^{(1)} - E^{(0)}}{\sigma_e^{(1)} + \sigma_e^{(0)}}, \quad (5.15)$$

where $E^{(1)}$, $(\sigma_e^2)^{(1)}$ are the energy and variance in energy of the 1 bits and $E^{(0)}$, $(\sigma_e^2)^{(0)}$ are the energy and variance in energy of the 0 bits. The variance in energy is defined as $\sigma_e^2 = \langle E^2 \rangle - \langle E \rangle^2$. Hence in order to evaluate the Q factor we need to calculate the variance in the energies of 1 and 0 bits at the receiver end.

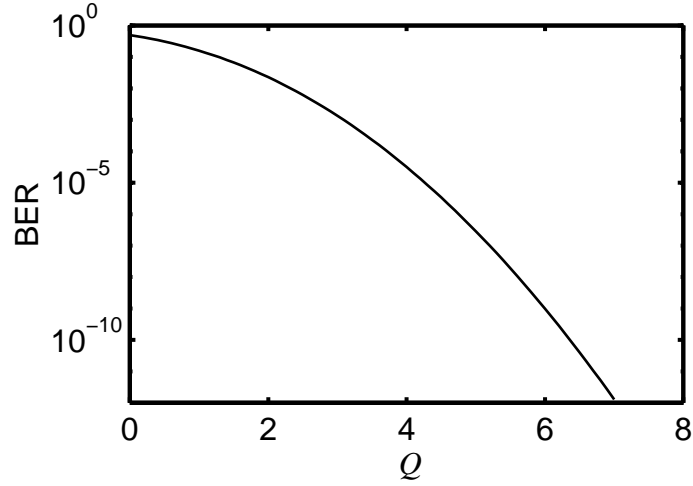


Figure 5.2: Bit Error rate versus Q factor.

5.2.1 Energy Fluctuations

In order to calculate the variance in the energies of 1 and 0 bits at the end of the system that use N amplifiers to compensate the fiber losses, we assume that all the amplifiers are spaced apart by the same length L_A and that the gain of the amplifiers $G = \exp(\alpha L_A)$ compensates the fiber losses in each section. Now using the moment method definition of energy and Eq. (4.22) we obtain the evolution of the pulse energy as

$$\frac{dE}{dz} = 0. \quad (5.16)$$

The use of amplifiers at regular intervals add fluctuations in energy due to the ASE of the amplifier. Thus including these effects of the amplifier the energy evolution is given by

$$\frac{dE}{dz} = \sum_{i=1}^N \delta E_i \delta(z - z_i), \quad (5.17)$$

where δE_i represents the noise added into the pulse energy by the i th amplifier located at z_i . Hence an ASE noise given by δE_i is added to the input energy. Integrating Eq. (5.17) over the length of one amplifier we find that the energy of the pulse after the i th amplifier is given by

$$E_i = E_{i-1} + \delta E_i. \quad (5.18)$$

This result is obtained by assuming that the amplifier gain has cancelled all the fiber losses in the previous section between $(i - 1)$ th amplifier and i th amplifier exactly.

Before we can calculate the variance in pulse energy, we have to calculate the first and second moments of the ASE noise δE_i . If the initial field before the i th amplifier is given by $A_{i-1}(z, t)$ then after the amplifier, we can write the effective field as $A_i(z, t) + \delta A_i$ where δA_i is the fluctuation in the field due to the ASE of the i th amplifier. From the definition of the pulse energy in Eq. (4.1) we can write the effective energy after the i th amplifier as

$$\begin{aligned} E_i + \delta E_i &= \int_{-\infty}^{\infty} (A_i + \delta A_i)(A_i^* + \delta A_i^*) dt, \\ &= \int_{-\infty}^{\infty} |A_i|^2 dt + \int_{-\infty}^{\infty} (A_i \delta A_i^* + A_i^* \delta A_i) dt + \int_{-\infty}^{\infty} |\delta A_i|^2 dt. \end{aligned} \quad (5.19)$$

From Eq. (4.1) we have

$$\delta E_i = \int_{-\infty}^{\infty} (A_i \delta A_i^* + A_i^* \delta A_i) dt + \int_{-\infty}^{\infty} |\delta A_i|^2 dt. \quad (5.20)$$

It is common to assume that $\delta A(t)$ is a Markoffian stochastic process such that

$$\langle \delta A_i(t) \delta A_j(t) \rangle = 0 \quad \langle \delta A_i^*(t) \delta A_j(t') \rangle = S \delta_{ij} \delta(t - t'), \quad (5.21)$$

where $S = n_{sp}(G - 1)h\nu$, h is Planck's constant and ν is the central frequency of the pulse spectrum [1]. Also on an average the noise field vanishes, i.e., $\langle \delta A_i \rangle = \langle \delta A_i^* \rangle = 0$. Using the above conditions we can easily calculate the first and second moments of δE_i .

First we calculate the first moment. From Eq. (5.20) we have

$$\langle \delta E_i \rangle = \left\langle \int_{-\infty}^{\infty} (A_i \delta A_i^* + A_i^* \delta A_i) dt + \int_{-\infty}^{\infty} |\delta A_i|^2 dt \right\rangle. \quad (5.22)$$

Using the condition that the noise field vanishes on average, the first integral vanishes. Using the correlation in Eq. (5.21) we get

$$\langle \delta E \rangle_i = \int_{-\infty}^{\infty} S \delta(t - t') dt = S. \quad (5.23)$$

The second moment of δE_i can be found as follows:

$$\begin{aligned} \langle \delta E_i(t) \delta E_j(t') \rangle &= \left\langle \int_{-\infty}^{\infty} dt' \int_{-\infty}^{\infty} dt A_i^*(t) \delta A_i(t) A_j^*(t') \delta A_j(t') \right\rangle + \left\langle \int_{-\infty}^{\infty} dt' \int_{-\infty}^{\infty} dt A_i^*(t) \delta A_i(t) A_j(t') \delta A_j^*(t') \right\rangle \\ &+ \left\langle \int_{-\infty}^{\infty} dt' \int_{-\infty}^{\infty} dt A_i^*(t) \delta A_i(t) \delta A_j(t') \delta A_j^*(t') \right\rangle + \left\langle \int_{-\infty}^{\infty} dt' \int_{-\infty}^{\infty} dt A_i(t) \delta A_i^*(t) A_j(t') \delta A_j^*(t') \right\rangle \\ &+ \left\langle \int_{-\infty}^{\infty} dt' \int_{-\infty}^{\infty} dt A_i(t) \delta A_i^*(t) A_j^*(t') \delta A_j(t') \right\rangle + \left\langle \int_{-\infty}^{\infty} dt' \int_{-\infty}^{\infty} dt A_i(t) \delta A_i^*(t) \delta A_j(t') \delta A_j^*(t') \right\rangle \\ &+ \left\langle \int_{-\infty}^{\infty} dt' \int_{-\infty}^{\infty} dt \delta A_i^*(t) \delta A_i(t) A_j^*(t') \delta A_j(t') \right\rangle + \left\langle \int_{-\infty}^{\infty} dt' \int_{-\infty}^{\infty} dt \delta A_i^*(t) \delta A_i(t) A_j(t') \delta A_j^*(t') \right\rangle \\ &+ \left\langle \int_{-\infty}^{\infty} dt' \int_{-\infty}^{\infty} dt \delta A_i^*(t) \delta A_i(t) \delta A_j^*(t') \delta A_j(t') \right\rangle. \end{aligned} \quad (5.24)$$

Using Eq. (5.21) we get

$$\langle \delta E^2 \rangle_i = 2S \int_{-\infty}^{\infty} dt |A|^2 + S^2 = 2SE_i + S^2. \quad (5.25)$$

Thus we have the first and second moments of δE_i . Since the amplifiers are equally spaced such that they exactly compensate for the fiber losses, the energy at the end of each amplifier is the same as the initial energy E_0 . Hence all $\langle \delta E \rangle_i$ and $\langle \delta E^2 \rangle_i$ are the same. Denoting the energy of 1 bits by superscript, 1, we can write the energy after i th amplifier for all 1 bits using Eq. (5.18) as

$$E_i^{(1)} = E_{i-1}^{(1)} + \delta E_i^{(1)}. \quad (5.26)$$

Taking the average of Eq. (5.26) and using Eq. (5.23) we get

$$\langle E \rangle_i^{(1)} = \langle E \rangle_{i-1}^{(1)} + S. \quad (5.27)$$

Thus we can find that at the end of N amplifiers

$$\langle E \rangle_N^{(1)} = \langle E \rangle_0^{(1)} + \sum_{i=1}^N S = \langle E \rangle_0^{(1)} + NS, \quad (5.28)$$

and since $\langle E \rangle_0^{(1)} = E_0$, the input pulse energy, Eq. (5.28) reduces to

$$\langle E \rangle_N^{(1)} = E_0 + NS, \quad (5.29)$$

Similarly using Eq. (5.26) we get

$$(E_i^2)^{(1)} = (E_{i-1}^2)^{(1)} + 2E_{i-1}^{(1)} \delta E_i^{(1)} + (\delta E_i^2)^{(1)}. \quad (5.30)$$

Taking the average of Eq. (5.30) and using Eqs. (5.23), (5.25) and (5.29) we get

$$\langle E^2 \rangle_i^{(1)} = \langle E^2 \rangle_{i-1}^{(1)} + 2S[E_0 + (i-1)S] + \langle \delta E^2 \rangle_i^{(1)}. \quad (5.31)$$

Thus after N amplifiers we get

$$\langle E^2 \rangle_N^{(1)} = \langle E^2 \rangle_0^{(1)} + 2 \sum_{i=1}^N S[E_0 + (i-1)S] + \sum_{i=1}^N \langle \delta E_i^2 \rangle^{(1)}. \quad (5.32)$$

Since for all 1 bits, $E_i \approx E_0$, $\langle \delta E \rangle_i^2 = 2SE_0 + S^2$ we perform the summation to get

$$\langle E^2 \rangle_N^{(1)} = \langle E^2 \rangle_0^{(1)} + 2NSE_0 + N(N-1)S^2 + N(2SE_0 + S^2) = \langle E^2 \rangle_0^{(1)} + 4NSE_0 + N^2S^2. \quad (5.33)$$

Using Eqs. (5.29) and (5.33) in the definition of the variance in the pulse energy we get

$$(\sigma_e^2)^{(1)} = (\sigma_E^2)^{(1)} + 2NSE_0, \quad (5.34)$$

where $(\sigma_E^2)^{(1)} = \langle E^2 \rangle_0^{(1)} - E_0^2$ is the initial variance in the pulse energy for 1 bits which is negligible compared to the fluctuations added by the ASE. Hence we can write

$$\sigma_e^{(1)} = \sqrt{2NSE_0}. \quad (5.35)$$

Performing a similar calculation for the 0 bits keeping in mind that the pulse energy $E_0 = 0$ for the 0 bits and hence for all 0 bits $\delta E_i^2 = S^2$ we find

$$\langle E \rangle_N^{(0)} = NS, \quad (5.36)$$

and

$$\langle E^2 \rangle_N^{(0)} = \langle E^2 \rangle_0^{(0)} + NS^2 + 2S^2 \sum_{i=1}^{N-1} i = \langle E^2 \rangle_0^{(0)} + N^2 S^2. \quad (5.37)$$

Hence the variance in pulse energy for the 0 bits is given by

$$(\sigma_e^2)^{(0)} = (\sigma_E^2)^{(0)}, \quad (5.38)$$

where $(\sigma_E^2)^{(0)} = \langle E^2 \rangle_0^{(0)}$ is the initial variance in the pulse energy for 0 bits which is negligible.

5.2.2 Q-factor Estimation

Using Eqs. (5.34) and (5.38) in Eq. (5.15) we can find the Q factor to be

$$Q = \sqrt{\frac{E_0}{2NS}}, \quad (5.39)$$

Eq. (5.39) shows that the Q factor is inversely proportional to the number of amplifiers. Thus having more amplifiers adds more noise into the system and hence reduces the Q factor leading to an increase in the BER.

The above calculations is based on the assumption that the receiver is noise free. However this is not the case even for a perfect receiver. Fundamental noise sources such as thermal noise and shot noise lead to current fluctuations in the receiver even when the optical power P is constant. As seen before P fluctuates due to amplifier noise. We have already evaluated the Q factor degradation due

to these fluctuations. Now we have to include the fluctuations caused by thermal and shot noise. Also while evaluating the Q factor we had neglected the initial fluctuations in energies, $(\sigma_E^2)^{(0)}$ and $(\sigma_E^2)^{(1)}$ at the transmitter. In order to evaluate the BER correctly, we have to take into account all the above noise sources. Since all these noise processes are independent random processes with approximately Gaussian statistics, the total variance of current fluctuations for 1 and 0 bits σ_1^2 and σ_0^2 respectively, can be obtained by simply adding individual variances.

Shot noise is a manifestation of the fact that the electric current consists of a stream of electrons that are generated at random times. It was first studied by Schottky in 1918 and has been investigated thoroughly since then [46], [47]–[49]. The variance in the noise current due to shot noise depends on the detector components in general [1]. Thermal noise manifests when random thermal motion of electrons in a resistor manifests as a fluctuating current even in the absence of an applied voltage [50], [51]. The variance in the noise current due to thermal noise does not depend on the current but depends on the absolute temperature [1]. Since 0 bits do not carry any optical power, the corresponding current, $I = 0$. Since shot noise fluctuations depend on the current, the 0 bits do not see any effects due to shot noise. Thus if we denote σ_s and σ_T as the current fluctuations due to shot and thermal noise respectively, and using $I = RP$ and $PT_0 = E_0$ where T_0 is a measure of pulse width, we can write the total variance in the current fluctuations for 1 and 0 bits as

$$\sigma_1^2 = \sigma_s^2 + \sigma_T^2 + \frac{R}{T_0^2}(\sigma_e^2)^{(1)}, \quad (5.40)$$

$$\sigma_0^2 = \sigma_T^2 + \frac{R}{T_0^2}(\sigma_e^2)^{(0)}. \quad (5.41)$$

Using Eqs. (5.34) and (5.38) in Eqs. (5.40) and (5.41) we get

$$\sigma_1^2 = \sigma_s^2 + \sigma_T^2 + \frac{R}{T_0^2}((\sigma_E^2)^{(1)} + 2NSE_0 - 2NS^2) \quad (5.42)$$

$$\sigma_0^2 = \sigma_T^2 + \frac{R}{T_0^2}(\sigma_E^2)^{(0)}. \quad (5.43)$$

We use Eqs. (5.42) and (5.43) along with $I_1 = \frac{R}{T_0}E_0$ and $I_0 = 0$ in Eq. (5.14) to get

$$Q = \frac{I_1}{\sigma_1 + \sigma_0},$$

$$Q = \frac{R}{T_0}E_0 \left([\sigma_s^2 + \sigma_T^2 + \frac{R}{T_0^2}((\sigma_E^2)^{(1)} + 2NSE_0 - 2NS^2)]^{1/2} + [\sigma_T^2 + \frac{R}{T_0^2}(\sigma_E^2)^{(0)}]^{1/2} \right)^{-1}. \quad (5.44)$$

Then the BER can be found using the Q factor obtained here in Eq. (5.13).

5.3 Chapter Summary

In this chapter we have shown how the amplifier noise can degrade the system performance by causing increased BER and thereby reducing the SNR of the system. We have derived an analytical expression for the Q factor and shown how the Q factor reduces as the number of amplifiers used in the system to compensate for fiber losses increases. In addition to these above mentioned noises, the BER is also affected by timing jitter. This is because the signal is sampled at the decision instant. If the pulse moves from its position randomly during propagation due to the presence of timing jitter, an 1 bit could be decided as 0 bit thus causing additional error. Thus when the ASE adds fluctuations into the pulse amplitude (energy), it affects the Q factor and hence the BER at the receiver while the timing jitter increases the BER by randomly moving the pulse from its original position. The following chapters are devoted to analytically calculating timing jitter using the moment method and to look for suitable methods capable of reducing the timing jitter.

Chapter 6

Timing Jitter in Lightwave Systems

Modern dispersion-managed lightwave systems are limited mainly by the nonlinear effects occurring inside optical fibers and by the amplified spontaneous emission (ASE) added at the amplifiers [52]. Optical solitons can solve the first problem to some extent since they use the self-phase modulation, a dominant nonlinear mechanism, to balance the residual dispersion [1]. However, the ASE noise remains a serious limitation of soliton systems; it manifests through a reduced signal-to-noise ratio and an increased timing jitter at the optical receiver [53]. Fluctuations in the arrival time of optical bits of information at the receiver is called *timing jitter*. The presence of timing jitter in the system can lead to increased BER at the receiver end. Figure 6.1 shows how timing jitter can lead to an incorrect bit identification thus leading to an increase in BER at the receiver end of the system. Curves (a) and (b) in Figure 6.1 show a single 1 bit that is shifted at the decision circuit of the receiver in the presence of the timing jitter. In the absence of timing jitter, the pulse is centered at the bit slot, and hence the corresponding signal is above the threshold value, I_D of the receiver. However, timing jitter can shift the pulse position randomly and cause the decision circuit to occasionally make a wrong identification of the bit. This degrades the system performance. If all pulses were to shift from their original position by the same amount, the problem can be overcome by changing the decision time t_D accordingly. However timing jitter shifts each pulse randomly and hence cannot be overcome by adjusting the decision time t_D .

The origin of timing jitter can be understood as follows. The ASE noise of the amplifiers used in the system adds random fluctuations in amplitude, frequency and temporal position of the

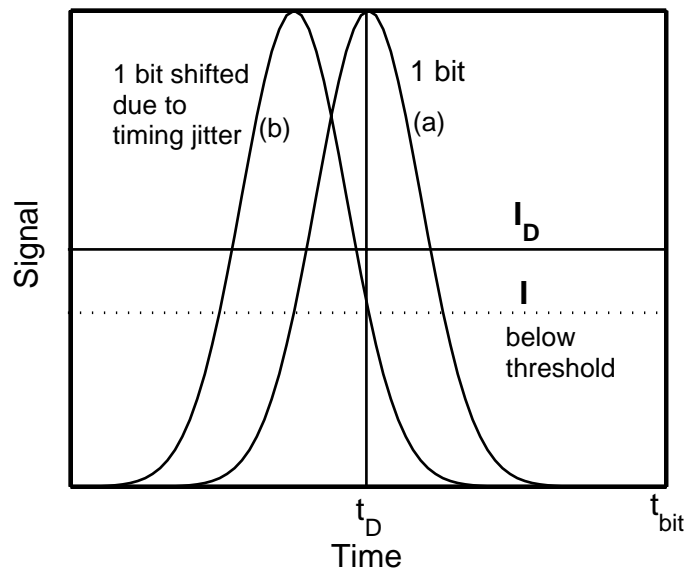


Figure 6.1: Increased BER due to timing jitter.

pulse. Temporal fluctuations directly lead to timing jitter [53]. Fluctuations in frequency affect the group velocity and hence the speed with which the pulse propagates through the fiber. Since the ASE induced fluctuation in the frequency is random, the transit time through the fiber link is also random. This is called the *Gordon-Haus timing jitter* [54]. For pulses whose pulse width are of the order of few picoseconds, we have seen in Chapter 4, that IRS and TOD becomes very important. Because of IRS, any fluctuation in the pulse amplitude is converted to frequency fluctuations and lead to *Raman jitter* [1]. TOD can also add additional timing jitter. Figure 6.2 shows a schematic of different origins of timing jitter.

It becomes essential to know how much timing jitter is accumulated at the end of the system so that one can estimate if the system will work within the allowed BER limit. The tolerable amount of jitter usually is given by 8% of the bit slot. Since bit slot is defined as $t_{bit} = B^{-1}$, where B is the bit rate, the allowed timing jitter in a system is inversely proportional to the bit rate of the system. In this Chapter we use the moment method to analytically calculate the Gordon-Haus timing jitter for systems using pulses whose pulse width are larger than 6 ps. For such systems the higher order terms are negligible and the main origin of timing jitter is due to fluctuations in the pulse frequency. In the first part of the Chapter we calculate the Gordon-Haus timing jitter for soliton and non-soliton systems. In the final part of the Chapter we calculate the Gordon-Haus timing

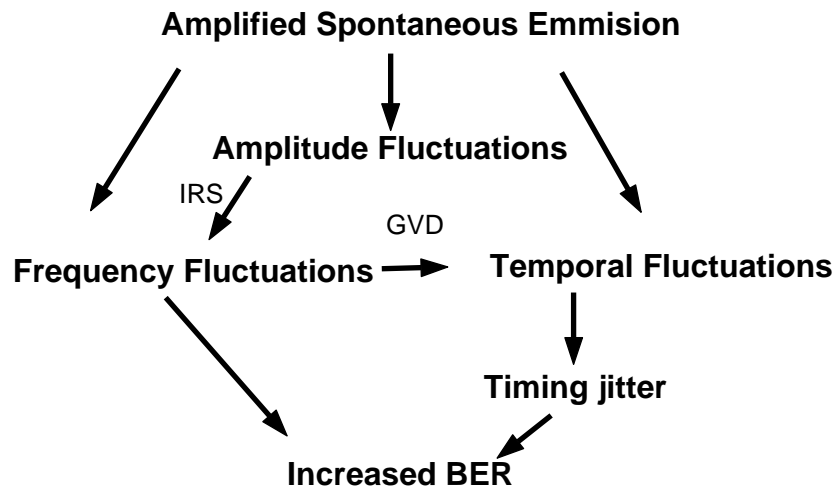


Figure 6.2: Origin of timing jitter.

jitter when more than one amplifiers are used within one map period.

6.1 Gordon-Haus Timing Jitter

The Gordon-Haus timing jitter was first studied for solitons in 1986 [54]. It was later recognized that timing jitter can occur with any transmission format and imposes a fundamental limitation on all long-haul systems designed with a cascaded chain of optical amplifiers [53]- [57]. Optical amplifiers affect both the amplitude and the phase of the amplified signal. Time dependent variations in the phase leads to fluctuations in the frequency of the pulse. Since GVD depends on the frequency because of dispersion, the speed at which a pulse propagates through the fiber is affected by each amplifier in a random fashion. Such random speed changes produce random shifts in the pulse position leading to Gordon-Haus timing jitter. We use the moment method to calculate the Gordon-Haus timing jitter at the end of a typical DM system consisting of periodic sequences of anomalous and normal dispersion fibers.

6.2 Single Amplifier per Map Period

As seen before in Chapter 1 the soliton systems are periodic after each map period and amplifiers are usually used after every 80 km and for a typical dispersion-managed system that uses bit rates

less than 40 Gb/s, the map period is usually around 80 km. In such systems at least one amplifier is used per map period to compensate for fiber losses. For this section we assume that one amplifier is placed at every 80 km, such that L_A is equal to map period, L_m . Since the higher-order terms are negligible, the propagation of an optical pulse in the fiber is governed by Eq. (3.3) and is given by

$$i \frac{\partial B}{\partial z} - \frac{\beta_2}{2} \frac{\partial^2 B}{\partial t^2} + \bar{\gamma} |B|^2 B = 0. \quad (6.1)$$

From the definition of the moment method in Chapter 4, we can write the energy, position and frequency of the optical pulse as

$$E = \int_{-\infty}^{\infty} |B|^2 dt, \quad (6.2)$$

$$T = \frac{1}{E} \int_{-\infty}^{\infty} t |B|^2 dt, \quad (6.3)$$

$$\Omega = \frac{i}{2E} \int_{-\infty}^{\infty} \left(B^* \frac{\partial B}{\partial t} - B \frac{\partial B^*}{\partial t} \right) dt, \quad (6.4)$$

respectively. We continue to find the evolution of these three parameters as shown in Chapter 4. Using Eqs. (6.1)–(6.4) we get the evolution of the three pulse parameters as

$$\frac{dE}{dz} = 0, \quad (6.5)$$

$$\frac{dT}{dz} = \beta_2 \Omega, \quad (6.6)$$

$$\frac{d\Omega}{dz} = 0. \quad (6.7)$$

The ASE of the amplifier affects all three parameters and hence change them in random fashion. Since in the absence of IRS, both position and the frequency are unaffected by the changes in the pulse energy, we can neglect the energy equation for now. However as we have seen in Chapter 5 the fluctuations in the pulse energy directly affect the BER of the system. Adding the amplifier-induced noise into the frequency and the position equations, we have

$$\frac{dT}{dz} = \beta_2 \Omega + \sum_{i=1}^N \delta T_i \delta(z - z_i), \quad (6.8)$$

$$\frac{d\Omega}{dz} = \sum_{i=1}^N \delta \Omega_i \delta(z - z_i), \quad (6.9)$$

where δT_i and $\delta \Omega_i$ are random fluctuations in the pulse position and frequency, respectively, introduced by the i th amplifier located at a distance z_i . Integrating Eqs. (6.8) and (6.9) over the length

of one amplifier we find that the position and frequency of the pulse after the i th amplifier are given by

$$T_i = T_{i-1} + b_2 \Omega_{i-1} + \delta T_i, \quad (6.10)$$

$$\Omega_i = \Omega_{i-1} + \delta \Omega_i, \quad (6.11)$$

where $b_2 = \int_0^{L_A} \beta_2(z) dz$.

The timing jitter in the system is defined as $\sigma_T^2 = \langle T^2 \rangle - \langle T \rangle^2$, where T is the pulse position at the receiver end and the angle brackets indicate averages over the ASE noise. In order to calculate the timing jitter, we need the second moments of $\delta \Omega_i$ and δT_i at every amplifier. To find these second moments, we use the moment method and note that the field after the i th amplifier is given by $A_i(z, t) + \delta A_i$ where δA_i is the fluctuation in the field due to the ASE of the i th amplifier. From the definition of frequency in Eq. (6.4), we have

$$\begin{aligned} E_i \Omega_i + \delta(E_i \Omega_i) &= \frac{i}{2} \int_{-\infty}^{\infty} \left((B_i^* + \delta B_i^*) \frac{\partial}{\partial t} (B_i + \delta B_i) - (B_i + \delta B_i) \frac{\partial}{\partial t} (B_i^* + \delta B_i^*) \right) dt \\ \delta(E_i \Omega_i) &= \frac{i}{2} \int_{-\infty}^{\infty} \left[B_i^* \delta \left(\frac{\partial B_i}{\partial t} \right) + \delta B_i^* \frac{\partial B_i}{\partial t} - B_i \delta \left(\frac{\partial B_i^*}{\partial t} \right) - \delta B_i \frac{\partial B_i^*}{\partial t} \right] dt. \end{aligned} \quad (6.12)$$

Integrating the first and the third terms in the above equation by parts we get

$$\int_{-\infty}^{\infty} B_i^* \delta \left(\frac{\partial B_i}{\partial t} \right) dt = B_i^* \delta B_i \Big|_{-\infty}^{\infty} - \int_{-\infty}^{\infty} \delta B_i \frac{\partial B_i^*}{\partial t} dt, \quad (6.13)$$

$$\int_{-\infty}^{\infty} B_i \delta \left(\frac{\partial B_i^*}{\partial t} \right) dt = B_i \delta B_i^* \Big|_{-\infty}^{\infty} - \int_{-\infty}^{\infty} \delta B_i^* \frac{\partial B_i}{\partial t} dt. \quad (6.14)$$

The first term in Eqs. (6.13) and (6.14) vanishes as the fields B^* and B vanish at the limits. Hence using Eqs. (6.13) and (6.14) in Eq. (6.12) we get

$$\delta(E_i \Omega_i) = -i \int_{-\infty}^{\infty} \left[\delta B_i \frac{\partial B_i^*}{\partial t} - \delta B_i^* \frac{\partial B_i}{\partial t} \right] dt. \quad (6.15)$$

We use the above equation to find $\delta \Omega_i$ as follows:

$$E_i \delta \Omega_i = \delta(E_i \Omega_i) - \Omega_i \delta E_i \quad (6.16)$$

From Eq. (5.20) we know δE_i . The last term in Eq. (5.20) which is due to noise beating with itself is small compared to the rest of the terms. Hence neglecting the last term and using Eqs. (5.20) and (6.15) in (6.16) we get

$$E_i \delta \Omega_i = -i \int_{-\infty}^{\infty} \left[\delta B_i \left(\frac{\partial B_i^*}{\partial t} - i \Omega_i B^* \right) - \delta B_i^* \left(\frac{\partial B_i}{\partial t} + i \Omega_i B \right) \right] dt. \quad (6.17)$$

Using the transformation

$$B_i = V_i e^{-i\Omega_i t}, \quad \frac{\partial B}{\partial t} + i\Omega_i B = \frac{\partial V}{\partial t} e^{-i\Omega_i t}, \quad (6.18)$$

in Eq. (6.17), we get

$$\delta\Omega_i = -\frac{i}{E_i} \int_{-\infty}^{\infty} \left[\delta V_i \frac{\partial V_i^*}{\partial t} - \delta V_i^* \frac{\partial V_i}{\partial t} \right] dt. \quad (6.19)$$

Next we find δT_i from the definition of position in Eq. (6.3).

$$E_i T_i + \delta(E_i T_i) = \int_{-\infty}^{\infty} t (B_i + \delta B_i) (B_i^* + \delta B_i^*) dt, \quad (6.20)$$

$$T_i \delta E_i + E_i \delta T_i = \int_{-\infty}^{\infty} t (B_i^* \delta B_i + B_i \delta B_i^*) dt, \quad (6.21)$$

Using the definition of δE_i from Eq. (5.20) in Eq. (6.21) we get

$$\delta T_i = \frac{1}{E_i} \int_{-\infty}^{\infty} (t - T) (B_i^* \delta B_i + B_i \delta B_i^*) dt. \quad (6.22)$$

Using the transformation in Eq. (6.18) we get

$$\delta T_i = \frac{1}{E_i} \int_{-\infty}^{\infty} (t - T) (V_i^* \delta V_i + V_i \delta V_i^*) dt. \quad (6.23)$$

From Eqs. (6.19) and (6.23) we can find the variances and cross correlation of $\delta\Omega_i$ and δT_i .

First from Eq. (6.19) we get

$$\delta\Omega_i^2 = -\frac{1}{E_i^2} \int_{-\infty}^{\infty} dt \int_{-\infty}^{\infty} dt' \left[\left(\delta V_i(t) \frac{\partial V_i^*(t)}{\partial t} - \delta V_i^*(t) \frac{\partial V_i(t)}{\partial t} \right) \left(\delta V_i(t') \frac{\partial V_i^*(t')}{\partial t'} - \delta V_i^*(t') \frac{\partial V_i(t')}{\partial t'} \right) \right] \quad (6.24)$$

From Eq. (5.21) we have

$$\langle \delta V_i(t) \delta V_j(t) \rangle = 0 \quad \langle \delta V_i^*(t) \delta V_j(t') \rangle = S \delta_{ij} \delta(t - t'), \quad (6.25)$$

where $S = n_{sp}(G - 1)h\nu$. Hence Eq. (6.24) becomes

$$\langle \delta\Omega^2 \rangle_i = \frac{2S}{E_i^2} \int_{-\infty}^{\infty} dt \left| \frac{\partial V_i}{\partial t} \right|^2 \quad (6.26)$$

Also using Eq. (6.25) in Eq. (6.19) we get

$$\langle \delta\Omega \rangle_i = 0. \quad (6.27)$$

Similarly squaring Eq. (6.23) we get

$$\delta T_i^2 = \frac{1}{E_i^2} \int_{-\infty}^{\infty} dt \int_{-\infty}^{\infty} dt' (t - T_i)(t' - T_i) [V_i^*(t)\delta V_i(t) + V_i(t)\delta V_i^*(t)][V_i^*(t')\delta V_i(t') + V_i(t')\delta V_i^*(t')]. \quad (6.28)$$

Using Eq. (6.25) in Eq. (6.28) we get

$$\langle \delta T^2 \rangle_i = \frac{2S}{E_i^2} \int_{-\infty}^{\infty} dt (t - T)^2 |V|^2. \quad (6.29)$$

Using Eq. (6.25) in Eq. (6.23) we get

$$\langle \delta T \rangle_i = 0. \quad (6.30)$$

Using Eq. (6.19) and (6.23) we have

$$\delta \Omega_i \delta T_i = -\frac{i}{E_i^2} \int_{-\infty}^{\infty} dt \int_{-\infty}^{\infty} dt' (t - T_i) \left[\delta V_i(t') \frac{\partial V_i^*(t')}{\partial t} - \delta V_i^*(t') \frac{\partial V_i(t')}{\partial t} \right] [V_i^*(t)\delta V_i(t) + V_i(t)\delta V_i^*(t)]. \quad (6.31)$$

Thus from Eq. (6.25) we get

$$\langle \delta \Omega \delta T \rangle_i = \frac{iS}{2E_i^2} \int_{-\infty}^{\infty} dt (t - T_i) \left[V_i \frac{\partial V_i^*}{\partial t} - V_i^* \frac{\partial V_i}{\partial t} \right]. \quad (6.32)$$

Now that we have found the second moments of $\delta \Omega_i$ and δT_i , we can write from Eqs. (6.10) and (6.11)

$$\Omega_i^2 = \Omega_{i-1}^2 + \delta \Omega_i^2 + 2\Omega_{i-1}\delta \Omega_i, \quad (6.33)$$

$$\Omega_i T_i = \Omega_{i-1} T_{i-1} + b_2 \Omega_{i-1}^2 + \Omega_{i-1} \delta T_i + \delta \Omega_i T_{i-1} + \beta_2 \delta \Omega_i + \delta \Omega_i \delta T_i, \quad (6.34)$$

$$T_i^2 = T_{i-1}^2 + b_2^2 \Omega_{i-1}^2 + 2b_2 \Omega_{i-1} T_{i-1} + \delta T_i^2 + 2T_{i-1} \delta T_i + 2b_2 \Omega_{i-1} \delta T_i. \quad (6.35)$$

Thus taking the average and using Eqs. (6.27) and (6.30) we get

$$\langle \Omega^2 \rangle_i = \langle \Omega^2 \rangle_{i-1} + \langle \delta \Omega^2 \rangle_i, \quad (6.36)$$

$$\langle \Omega T \rangle_i = \langle \Omega T \rangle_{i-1} + b_2 \langle \Omega^2 \rangle_{i-1} + \langle \delta \Omega \delta T \rangle_i, \quad (6.37)$$

$$\langle T^2 \rangle_i = \langle T^2 \rangle_{i-1} + b_2^2 \langle \Omega^2 \rangle_{i-1} + 2b_2 \langle \Omega T \rangle_{i-1} + \langle \delta T^2 \rangle_i. \quad (6.38)$$

Thus we know the variances and cross correlations of frequency and position at any i th amplifier and the noise added into them by the i th amplifier. These relations are valid for any pulse shape. To proceed further we need to assume a pulse shape. Previously we have seen two pulse shapes,

viz., the fundamental soliton and the Gaussian pulse shapes. As seen before, the fundamental soliton can maintain its shape and width in a constant anomalous dispersion fiber in the absence of fiber losses. However in the presence of fiber losses, the nonlinear effects cannot exactly cancel the dispersion effects because of the reduced power of the soliton and hence pulse broadens in the presence of dispersion. However, if one uses dispersion- decreasing fibers in the anomalous dispersion regime, the soliton can maintain its pulse width and shape. Another example of a soliton system is provided by dispersion-managed soliton systems. A dispersion managed soliton can be approximated by a chirped Gaussian pulse shape. Instead of using a DM soliton, one can also launch a low-power chirped Gaussian pulse through a fiber. In such a case, the pulse does not maintain its shape and width. However, by reducing the average dispersion to a value close to zero, we can reduce pulse broadening resulting from dispersion. Such systems are called chirped return-to-zero (CRZ) systems or non-soliton systems. We will use the results obtained in this section using the moment method for these three systems in the following sections.

6.2.1 Solitons Systems

As seen before, the existence of optical solitons in the fiber is the result of a balance between GVD and SPM. Such a soliton maintains its shape and width during propagation in an optical fiber. Fiber losses become the main limitation in such a soliton system. When amplifiers are used to overcome fiber losses, one would like to have minimum number of amplifiers, for both cost effectiveness and for minimizing the accumulated amplifier noises. We saw in Chapter 5 that when the number of amplifiers increases the Q factor decreases. In order to be able to achieve this, we saw that it was necessary to use dispersion management. We use the moment method to calculate timing jitter in such dispersion managed systems.

Fundamental soliton in Dispersion decreasing Fibers

The use of dispersion decreasing fibers (DDFs) for soliton communications was first proposed in 1987 which helped relax the restriction $L_A \ll L_D$ imposed normally on loss-managed solitons by decreasing the GVD along the fiber length [5]. The DDFs are designed such that the decreasing GVD counteracts the reduced SPM experienced by solitons weakened from fiber losses. Since

dispersion management is combined with loss management, the soliton evolution is governed by the NLS equation given by Eq. (6.1), except that β_2 is now a function of z such that $|\beta_2(z)| = |\beta_2(0)| \exp(-\alpha z)$. The result can be understood by noting that the soliton peak power and hence the nonlinearity parameter $\bar{\gamma}$ decreases exponentially in a lossy fiber in exactly the same fashion. So it is easy to deduce from Eq. (2.60) that $N = 1$ can be maintained, in spite of power losses.

In order to calculate the timing jitter at the end of such a system we use Eq. (6.36)–(6.38) with $|\beta_2(z)| = |\beta_2(0)| \exp(-\alpha z)$ to find that $b_2 = \beta_2(0)L_{\text{eff}}$ where $L_{\text{eff}} = [1 - \exp(-\alpha L_A)]/\alpha$. Also we know that unchirped fundamental solitons maintain their pulse shape of the form

$$B_i(z, t) = a_i \operatorname{sech} \left(\frac{t - T_i}{\tau_i} \right) \exp[i\phi_i - i\Omega_i(t - T_i)]. \quad (6.39)$$

where T_i , τ_i , ϕ_i and Ω_i are the position, pulse width, phase and frequency at the end of the i th amplifier. Hence from Eq. (6.18) we get

$$V_i(z, t) = a_i \operatorname{sech} \left(\frac{t - T_i}{\tau_i} \right) \exp(i\phi_i). \quad (6.40)$$

We find the ASE-induced fluctuations $\langle \delta\Omega^2 \rangle_i$ and $\langle \delta T^2 \rangle_i$ by using Eq. (6.40) in Eqs. (6.26) and (6.29). From Eq. (6.40) we have

$$\frac{\partial V_i}{\partial t} = - \left[\frac{a_i}{\tau_i} \operatorname{sech} \left(\frac{t - T_i}{\tau_i} \right) \tanh \left(\frac{t - T_i}{\tau_i} \right) \right] \exp(i\phi_i). \quad (6.41)$$

Multiplying Eq. (6.41) by its complex conjugate and substituting the result into Eq. (6.26) we get

$$\langle \delta\Omega^2 \rangle_i = \frac{2S}{E_i^2} \int_{-\infty}^{\infty} \frac{a_i^2}{\tau_i^2} \operatorname{sech}^2 \left(\frac{t - T_i}{\tau_i} \right) \tanh^2 \left(\frac{t - T_i}{\tau_i} \right) dt. \quad (6.42)$$

Using Table 3.1 we perform the integration to get

$$\langle \delta\Omega^2 \rangle_i = \frac{2S}{3E_i\tau_i^2}. \quad (6.43)$$

Similarly using Eq. (6.40) in Eq. (6.29) we get

$$\langle \delta T^2 \rangle_i = \frac{2S}{E_i^2} \int_{-\infty}^{\infty} (t - T_i)^2 \frac{a_i^2}{\tau_i^2} \operatorname{sech}^2 \left(\frac{t - T_i}{\tau_i} \right) dt. \quad (6.44)$$

Again using Table 3.1 we get

$$\langle \delta T^2 \rangle_i = \frac{\pi^2 S \tau_i^2}{6 E_i}. \quad (6.45)$$

Finally using Eqs. (6.40) and (6.41) in Eq. (6.32) we get

$$\langle \delta\Omega\delta T \rangle_i = 0. \quad (6.46)$$

Thus we have found the amplifier-induced fluctuations in frequency and position at each amplifier and their variances and correlation. Since the fundamental soliton maintains its shape and pulse width during propagation, the pulse width at the end of every amplifier is the same as the initial pulse width τ_0 . Also the energy of the pulse after every amplifier is restored to its initial value E_0 . Hence for the case of fundamental solitons the variances and cross correlations are the same at all the amplifiers. Hence dropping the subscript i , the variances and correlation at every amplifier are given by

$$\langle \delta\Omega^2 \rangle = \frac{2S}{3E_0\tau_0^2}, \quad \langle \delta T^2 \rangle = \frac{\pi^2 S\tau_0^2}{6 E_0}, \quad \langle \delta\Omega\delta T \rangle = 0. \quad (6.47)$$

Now using Eq. (6.47) in the recurrence relations in Eqs. (6.36)–(6.38), we can write after N amplifiers as

$$\langle \Omega^2 \rangle_N = \sum_{i=1}^N \langle \delta\Omega^2 \rangle, \quad (6.48)$$

$$\langle \Omega T \rangle_N = b_2 \sum_{i=1}^{N-1} \langle \Omega^2 \rangle, \quad (6.49)$$

$$\langle T^2 \rangle_N = b_2^2 \sum_{i=1}^{N-1} \langle \Omega^2 \rangle + 2b_2 \sum_{i=1}^{N-1} \langle \Omega T \rangle + \sum_{i=1}^N \langle \delta T^2 \rangle. \quad (6.50)$$

Performing the summation over n using the following results:

$$\sum_{i=1}^N 1 = N, \quad \sum_{i=1}^N i = N(N+1)/2, \quad \sum_{i=1}^N i^2 = N(N+1)(2N+1)/6, \quad (6.51)$$

we can rewrite the above equations to be

$$\langle \Omega^2 \rangle_N = N \langle \delta\Omega^2 \rangle, \quad (6.52)$$

$$\langle \Omega T \rangle_N = \frac{b_2}{2} N(N-1) \langle \delta\Omega^2 \rangle, \quad (6.53)$$

$$\langle T^2 \rangle_N = \frac{b_2^2}{6} N(N-1)(2N-1) \langle \delta\Omega^2 \rangle + N \langle \delta T^2 \rangle. \quad (6.54)$$

Also from Eqs. (6.27) and (6.30), we have $\langle T \rangle_N = 0$. Hence the timing jitter after N amplifiers is given by

$$\sigma_{GH}^2 = \frac{b_2^2}{6} N(N-1)(2N-1) \left(\frac{2S}{3E_0\tau_0^2} \right) + N \left(\frac{\pi^2 S\tau_0^2}{6 E_0} \right). \quad (6.55)$$

Noting that $N = L/L_A$, we see that for $N \gg 1$, the Gordon-Haus jitter increases with the total distance, L as L^3 . It also depends linearly on the accumulated dispersion b_2 and is inversely proportional to the pulse energy. A disadvantage of DDF is that the average dispersion along the link is often relatively large and since the Gordon-Haus jitter is larger for larger dispersion, it is better to use DM soliton systems since they have relatively smaller average dispersion.

Dispersion-Managed Solitons

We perform the same calculations that we did for fundamental solitons for DM solitons in this section. A typical DM system consists of a periodic sequence of anomalous- and normal-dispersion fibers. An optical amplifier is inserted for compensating fiber losses after one or several map periods. Each amplifier restores pulse energy to its original input value but, at the same time, adds spontaneous-emission noise. Although the DM soliton does not maintain its pulse width, it evolves periodically such that the pulse width and chirp are restored to its initial values after every map period L_m . Since the amplifier spacing is such that L_A is a multiple of L_m , the energy, width and chirp of the pulse are restored to their original values after every amplifier. Thus we see that the soliton systems are periodic after every amplifier. Assuming a Gaussian pulse shape of the form

$$B_i(z, t) = a_i \exp[i\phi_i - i\Omega_i(t - T_i) - (1 + iC_i)(t - T_i)^2/2\tau_i^2], \quad (6.56)$$

where T_i , τ_i , ϕ_i and Ω_i are the position, pulse width, phase and frequency at the end of the i th amplifier, we find that

$$V_i(z, t) = a_i \exp[i\phi_i - (1 + iC_i)(t - T_i)^2/2\tau_i^2]. \quad (6.57)$$

Using Eq. (6.57) in Eqs. (6.26), (6.29), (6.32), we obtain the variances and cross correlation of the ASE induced frequency and position fluctuations. Differentiating Eq. (6.57) with respect to t we get

$$\frac{\partial V_i}{\partial t} = a_i \exp[i\phi_i - (1 + iC_i)(t - T_i)^2/2\tau_i^2] [-(1 + iC_i)(t - T_i)/\tau_i^2], \quad (6.58)$$

Multiplying Eq. (6.58) by its complex conjugate and substituting the result into Eq. (6.26) we get

$$\langle \delta\Omega^2 \rangle_i = \frac{2S}{E_i^2} \int_{-\infty}^{\infty} \frac{a_i^2}{\tau_i^2} (1 + C_i^2) \frac{(t - T_i)}{\tau_i^2} \exp[-(t - T_i)^2/\tau_i^2] dt. \quad (6.59)$$

Using Table 3.2 we perform the integration to get

$$\langle \delta\Omega^2 \rangle_i = \frac{S}{E_i} \frac{(1 + C_i)}{\tau_i^2}, \quad (6.60)$$

Similarly using Eq. (6.57) in Eq. (6.29) we get

$$\langle \delta T^2 \rangle_i = \frac{2S}{E_i^2} \int_{-\infty}^{\infty} (t - T_i)^2 a_i^2 \exp[-(t - T_i)^2 / \tau_i^2] dt. \quad (6.61)$$

Again using Table 3.1 we get

$$\langle \delta T^2 \rangle_i = \frac{S\tau_i^2}{E_i}. \quad (6.62)$$

Finally using Eqs. (6.57) and (6.58) in Eq. (6.32) we get

$$\langle \delta\Omega\delta T \rangle_i = \frac{iS}{2E_i^2} \int_{-\infty}^{\infty} (t - T_i)^2 a_i^2 (-2iC_i) / \tau_i^2 \exp[-(t - T_i)^2 / 2\tau_i^2] dt. \quad (6.63)$$

Again using Table 3.2 we perform the integration and get

$$\langle \delta\Omega\delta T \rangle_i = \frac{SC_i}{E_i}. \quad (6.64)$$

Thus we have found the amplifier induced fluctuations in frequency and position at each amplifier and their variances and correlation. Since the DM soliton is periodic in evolution during propagation, its chirp, width and energy, at the end of every amplifier is the same as the initial chirp, C_0 , width, τ_0 and energy E_0 respectively. Hence for the case of DM solitons the variances and cross correlations are the same at all the amplifiers and so dropping the subscript i , the variances and correlation at every amplifier are given by

$$\langle \delta\Omega^2 \rangle = \frac{S}{E_0} \frac{(1 + C_0^2)}{\tau_0^2}, \quad \langle \delta T^2 \rangle = \frac{S\tau_0^2}{E_0}, \quad \langle \delta\Omega\delta T \rangle = \frac{SC_0}{E_0}. \quad (6.65)$$

Now using Eq. (6.65) in the recurrence relations in Eqs. (6.36)–(6.38), we can write after N amplifiers

$$\langle \Omega^2 \rangle_N = \sum_{i=1}^N \langle \delta\Omega^2 \rangle, \quad (6.66)$$

$$\langle \Omega T \rangle_N = b_2 \sum_{i=1}^{N-1} \langle \Omega^2 \rangle + \sum_{i=1}^N \langle \delta\Omega\delta T \rangle, \quad (6.67)$$

$$\langle T^2 \rangle_N = b_2^2 \sum_{i=1}^{N-1} \langle \Omega^2 \rangle + 2b_2 \sum_{i=1}^{N-1} \langle \Omega T \rangle + \sum_{i=1}^N \langle \delta T^2 \rangle, \quad (6.68)$$

Here b_2 can be written as $\beta_{av}L_A$, where $\beta_{av} = (\beta_a L_a + \beta_n L_n)/(L_a + L_n)$, L_a , β_a and L_n , β_n are the length and group velocity dispersion parameter of the anomalous and normal fiber sections. Performing the summation we get after N such amplifiers using Eq. (6.51)

$$\langle \Omega^2 \rangle_N = N \langle \delta \Omega^2 \rangle, \quad (6.69)$$

$$\langle \Omega T \rangle_N = \frac{b_2}{2} N(N-1) \langle \delta \Omega^2 \rangle + N \langle \delta \Omega \delta T \rangle, \quad (6.70)$$

$$\langle T^2 \rangle_N = \frac{b_2^2}{6} N(N-1)(2N-1) \langle \delta \Omega^2 \rangle + b_2 N(N-1) \langle \delta \Omega \delta T \rangle + N \langle \delta T^2 \rangle. \quad (6.71)$$

Also from Eqs. (6.27) and (6.30), we have $\langle T \rangle_N = 0$. Hence the timing jitter after N amplifiers is given by

$$\sigma_{GH}^2 = \frac{b_2^2}{6} N(N-1)(2N-1) \left(\frac{S}{E_0} \frac{(1+C_0^2)}{\tau_0^2} \right) + b_2 N(N-1) \left(\frac{SC_0}{E_0} \right) + N \left(\frac{S\tau_0^2}{E_0} \right). \quad (6.72)$$

From Eq. (6.72) we see that the leading term of Gordon-Haus jitter depends on the cubic power of distance similar to the case of fundamental solitons. However amplifier-induced fluctuations differ from the fundamental soliton case due to the difference in pulse shape. Also since the DM solitons are chirped initially, the timing jitter also depends on the initial chirp.

6.2.2 Non-soliton Systems

Even though solitons systems can help balance the GVD and nonlinear effects, many other nonlinear effects can seriously limit the system. Also even when using DM soliton systems, the GVD dispersion cannot be reduced too much because it is needed to compensate nonlinear effects. However non-soliton systems can have nearly zero average dispersion, since they have negligible nonlinear effects when operated at low powers. In a non-soliton system, input pulses are prechirped and then propagated along the DM link without requiring the periodicity condition, i.e., pulse width and chirp are not designed to recover their input values after each amplifier. Since the pulse peak power is low, the nonlinear effects are negligible but not absent. As seen before if the input pulse is initially chirped such that $\beta_2 C_0 < 0$, the pulse at the end of the fiber link may be shorter than the input pulse. If the dispersion map is made such that the pulse broadens in the first section and compresses in the second section, the impact of the nonlinear effects can be reduced significantly. This is because the pulse peak power is reduced considerably in the first section because of rapid

broadening of chirped pulses, while in the second section it is lower because of the accumulated fiber losses. Such dispersion-managed links are also referred to as quasi-linear transmission links and in such cases the average GVD can be reduced to a very low value.

We now calculate the timing jitter at the receiver end for such systems. The pulses in these systems can be approximated by Gaussian pulse shape of the form shown in Eq. (6.56). Hence the amplifier induced noises in frequency and position for such pulses are given by Eqs. (6.59), (6.62), (6.64). However the since non-soliton systems are not periodic, the noise variances and correlation are not the same at every amplifier. Their evolution hence depends on the evolution of the chirp and pulse width along the fiber. Using the moment method we have already derived the evolution of the chirp and pulse width and neglecting the higher order effects and the nonlinear term in Eqs. (4.155) and (4.156), they are given by

$$\frac{d\tau}{dz} = \frac{\beta_2 C}{\tau}, \quad (6.73)$$

$$\frac{dC}{dz} = \beta_2 \left(\frac{1+C^2}{\tau^2} \right). \quad (6.74)$$

Making a transformation $\tilde{z} = \beta_2 z$, we can write Eqs. (6.73) and (6.74) as

$$\frac{d\tau}{d\tilde{z}} = \frac{C}{\tau}, \quad (6.75)$$

$$\frac{dC}{d\tilde{z}} = \left(\frac{1+C^2}{\tau^2} \right). \quad (6.76)$$

From Eqs. (6.75) and (6.76) we find that

$$\begin{aligned} \frac{d}{d\tilde{z}} \left(\frac{1+C^2}{\tau^2} \right) &= \left(\frac{2C}{\tau^2} \right) \frac{1+C^2}{\tau^2} + (1+C^2) \left(-\frac{2}{\tau^3} \right) \frac{C}{\tau} \\ &= 0 \end{aligned} \quad (6.77)$$

Hence the quantity $(1+C^2)/\tau^2$ does not change during propagation. Physically this quantity is related to the spectral width of the pulse that remains a constant in a linear medium. Hence we can replace it by its initial value $(1+C_0^2)/\tau_0^2$. Eqs. (6.73) and (6.74) can be solved analytically and the solution is given by Eq. (3.39). Thus we can write the pulse width and chirp after the i th amplifier as

$$\tau_i = \tau_0 \left[\left(1 + iC_0 \frac{b_2}{\tau_0^2} \right)^2 + i^2 \frac{b_2^2}{\tau_0^4} \right]^{1/2}, \quad C_i = C_0 + i(1+C_0^2) \frac{b_2}{\tau_0^2}. \quad (6.78)$$

Thus using Eqs. (6.77) and (6.78) in Eqs. (6.60), (6.62) and (6.64) we can write the variances and cross correlation of amplifier induced fluctuations in frequency and position in the case of low power CRZ systems as

$$\langle \delta\Omega^2 \rangle_i = \frac{S}{E_0} \frac{(1+C_0^2)}{\tau_0^2}, \quad (6.79)$$

$$\langle \delta T^2 \rangle_i = \frac{S\tau_0^2}{E_0} \left[\left(1 + iC_0 \frac{b_2}{\tau_0^2} \right)^2 + i^2 \frac{b_2^2}{\tau_0^4} \right], \quad (6.80)$$

$$\langle \delta\Omega\delta T \rangle_i = \frac{S}{E_0} \left[C_0 + i(1+C_0^2) \frac{b_2}{\tau_0^2} \right]. \quad (6.81)$$

Initially at the transmitter the spectral width is given by $1/\tau_0^2$ since the pulses are unchirped and since the spectral width is unchanged in a linear medium, Eq. (6.79) can be replaced by

$$\langle \delta\Omega^2 \rangle_i = \frac{S}{E_0} \frac{1}{\tau_0^2}. \quad (6.82)$$

Now using Eqs. (6.79)–(6.81) in the recurrence relations in Eqs. (6.36)–(6.38), we can write after N amplifiers

$$\langle \Omega^2 \rangle_N = \frac{S}{E_0} \sum_{i=1}^N \frac{1}{\tau_0^2}, \quad (6.83)$$

$$\langle \Omega T \rangle_N = b_2 \sum_{i=1}^{N-1} \langle \Omega^2 \rangle + \frac{S}{E_0} \sum_{i=1}^N \left[C_0 + i(1+C_0^2) \frac{b_2}{\tau_0^2} \right], \quad (6.84)$$

$$\langle T^2 \rangle_N = b_2^2 \sum_{i=1}^{N-1} \langle \Omega^2 \rangle + 2b_2 \sum_{i=1}^{N-1} \langle \Omega T \rangle + \frac{S\tau_0^2}{E_0} \sum_{i=1}^N \left[\left(1 + iC_0 \frac{b_2}{\tau_0^2} \right)^2 + i^2 \frac{b_2^2}{\tau_0^4} \right]. \quad (6.85)$$

Performing the summation we get

$$\langle \Omega^2 \rangle_N = N \frac{S}{E_0} \frac{1}{\tau_0^2}, \quad (6.86)$$

$$\begin{aligned} \langle \Omega T \rangle_N &= \frac{b_2}{2} N(N-1) \frac{S}{E_0} \frac{1}{\tau_0^2} + \frac{b_2}{2} N(N+1) \frac{S}{E_0} \frac{(1+C_0^2)}{\tau_0^2} + N \frac{SC_0}{E_0}, \\ &= \frac{S}{E_0} N \left[N \frac{b_2}{\tau_0^2} + C_0 \right], \end{aligned} \quad (6.87)$$

$$\begin{aligned} \langle T^2 \rangle_N &= \frac{b_2^2}{6} N(N-1)(2N-1) \frac{S}{E_0} \frac{1}{\tau_0^2} + N \frac{S}{E_0} \frac{1+C_0^2}{\tau_0^2} + 2b_2 \frac{SC_0}{E_0} \left[\frac{N}{2}(N-1) \right. \\ &\quad \left. + \frac{N}{2}(N+1) \right] + \frac{S}{E_0} \frac{b_2^2}{\tau_0^2} \left[\frac{N}{6}(N+1)(2N+1) + \frac{N}{6}(N-1)(2N-1) + \frac{N}{2}(N-1) \right]. \end{aligned}$$

$$\langle T^2 \rangle_N = \frac{S}{E_0} \tau_0^2 N \left[1 + \left(C_0 + \frac{b_2 N}{\tau_0^2} \right)^2 \right]. \quad (6.88)$$

Thus using Eqs. (6.27), (6.30) and (6.88), we can find the timing jitter in the case of non-soliton systems after N amplifiers is given by

$$\sigma_{GH}^2 = \frac{S}{E_0} \tau_0^2 N \left[1 + \left(C_0 + \frac{b_2 N}{\tau_0^2} \right)^2 \right]. \quad (6.89)$$

From Eq. (6.89) we see that the Gordon-Haus jitter is cubic even in the case of non-soliton systems. Also similar to the case of DM solitons, the timing jitter in the case of the non-soliton system depends on the initial chirp. While in the DM soliton case, the sign and value of the initial chirp is fixed by the periodicity conditions, in the case of non-soliton systems, the value of the chirp and its sign can be used in a way to reduce the total jitter. This will be discussed in Chapter 8. So far in this chapter we have seen that in both soliton and non-soliton cases, the Gordon-Haus timing jitter is cubic in distance and is inversely proportional to the pulse energy. This result agrees with the results of Gordon and Haus, who first derived an expression for jitter in the case of fundamental solitons in a constant dispersion fiber and showed that the jitter is cubic in distance [54].

6.3 Multiple Amplifiers per Map Period

As seen in the previous section, the amplifier-induced noise depends on the amplifier gain. Hence larger the gain the greater the noise added to the system. One way to reduce the noise added by the ASE is by reducing the gain required by an amplifier. If more than one amplifiers with smaller gain are used such that the total gain of all the amplifiers compensate the total fiber losses, it can help reduce timing jitter, by reducing the ASE-induced noise of amplifiers. Thus distributed amplification can help reduce timing jitter [58]. In this section we calculate the timing jitter in systems when more than one amplifier is used within one map period.

Previously we found the amplifier-induced fluctuations in the frequency and position of the pulse. We also found the recurrence relations of variances and correlation of these fluctuations which show the growth of these ASE-induced noise between $i - 1$ and i th amplifiers. In order to extend these equations to the case of more than one amplifier in one map period, we assume that there are n_a amplifiers within one map period, each with gain G_i , and there are N such map periods in the entire fiber link. From Eqs. (6.36)–(6.38), we use the subscript i to denote an amplifier within a map period and subscript j to denote the map periods to write the recurrence relations for

the amplifier-induced noise between $i - 1$ and i th amplifiers in the j th map period as

$$\langle \Omega^2 \rangle_i = \langle \Omega^2 \rangle_{i-1} + \langle \delta \Omega^2 \rangle_i, \quad (6.90)$$

$$\langle \Omega T \rangle_i = \langle \Omega T \rangle_{i-1} + d_i \langle \Omega^2 \rangle_{i-1} + \langle \delta \Omega \delta T \rangle_i, \quad (6.91)$$

$$\langle T^2 \rangle_i = \langle T^2 \rangle_{i-1} + d_i^2 \langle \Omega^2 \rangle_{i-1} + 2d_i \langle \Omega T \rangle_{i-1} + \langle \delta T^2 \rangle_i. \quad (6.92)$$

where $d_i = \int_{z_{i-1}}^{z_i} \beta_2(z) dz$, is related to the net dispersion in the fiber section between the amplifiers $i - 1$ and i . Except d_i , all quantities in Eqs. (6.90)–(6.92) depend implicitly on the map period, j . Thus we can write the recurrence relations for the ASE-induced noise after the j th map period using Eqs. (6.90)–(6.92) repeatedly as

$$\langle \Omega^2 \rangle_j = \langle \Omega^2 \rangle_{j-1} + P_j, \quad (6.93)$$

$$\langle \Omega T \rangle_j = \langle \Omega T \rangle_{j-1} + b_2 \langle \Omega^2 \rangle_{j-1} + Q_j, \quad (6.94)$$

$$\langle T^2 \rangle_j = \langle T^2 \rangle_{j-1} + b_2^2 \langle \Omega^2 \rangle_{j-1} + 2b_2 \langle \Omega T \rangle_{j-1} + R_j. \quad (6.95)$$

where $b_2 = \sum_{i=1}^{n_a} d_i$ is the net dispersion of each map period and

$$P_j = \sum_{i=1}^{n_a} \langle \delta \Omega^2 \rangle_i, \quad (6.96)$$

$$Q_j = \sum_{i=1}^{n_a} \langle \delta \Omega \delta T \rangle_i + \sum_{i=1}^{n_a-1} \langle \delta \Omega^2 \rangle_i \left(\sum_{k=i+1}^{n_a} d_k \right), \quad (6.97)$$

$$R_j = \sum_{i=1}^{n_a} \langle \delta T^2 \rangle_i + \sum_{i=1}^{n_a-1} \langle \delta \Omega^2 \rangle_i \left(\sum_{k=i+1}^{n_a} d_k \right)^2 + 2 \sum_{i=1}^{n_a-1} \langle \delta \Omega \delta T \rangle_i \left(\sum_{k=i+1}^{n_a} d_k \right). \quad (6.98)$$

We can use Eqs. (6.90)–(6.92) to calculate the Gordon-Haus jitter by adding the contributions of N map periods. However, this step requires knowledge of the coefficients in Eqs. (6.96)–(6.98).

6.3.1 Soliton Systems

In order to evaluate the coefficients in Eqs. (6.96)–(6.98), first consider the case of a fundamental soliton system. The variances and cross correlations are then given by Eq. (6.47). Using Eq. (6.47) we see that for the case of the fundamental soliton the Eqs. (6.96)–(6.98) can be written as

$$P = \sum_{i=1}^{n_a} \langle \delta \Omega^2 \rangle, \quad (6.99)$$

$$Q = \sum_{i=1}^{n_a-1} \langle \delta\Omega^2 \rangle \left(\sum_{k=i+1}^{n_a} d_k \right), \quad (6.100)$$

$$R = \sum_{i=1}^{n_a} \langle \delta T^2 \rangle + \sum_{i=1}^{n_a-1} \langle \delta\Omega^2 \rangle \left(\sum_{k=i+1}^{n_a} d_k \right)^2. \quad (6.101)$$

The subscript j is dropped because the coefficients depend on the pulse parameters and hence remain the same after every map period for the soliton case. The variances of $\delta\Omega$ and δT are given by Eq. (6.47). Using Eqs. (6.99)–(6.101), in Eqs. (6.93)–(6.95) and also using the definition of $b_2 = \int_0^{L_m} \beta_2(z) dz = \sum_{i=1}^{n_a} d_i$, we get after N map periods

$$\langle \Omega^2 \rangle_N = NP, \quad (6.102)$$

$$\langle \Omega T \rangle_N = b_2 P(N-1)/2 + NQ, \quad (6.103)$$

$$\langle T^2 \rangle_N = P b_2^2 N(N-1)(2N-1)/6 + Q b_2 N(N-1) + NR. \quad (6.104)$$

Thus we can write the timing jitter after N map periods each using n_a amplifiers as

$$\sigma_{GH} = P b_2^2 N(N-1)(2N-1)/6 + Q b_2 N(N-1) + RN. \quad (6.105)$$

The coefficients P , Q and R are given by Eqs. (6.99)–(6.101). Equation (6.105) shows that our approach provides an analytic expression of the timing jitter that is valid even when multiple amplifiers are used within each map period. This equation also applies to the case of the DM soliton. However the coefficients P , Q and R in such a case are given by

$$P = \sum_{i=1}^{n_a} \langle \delta\Omega^2 \rangle, \quad (6.106)$$

$$Q = \sum_{i=1}^{n_a-1} \langle \delta\Omega^2 \rangle \left(\sum_{k=i+1}^{n_a} d_k \right) + \sum_{i=1}^{n_a} \langle \delta\Omega \delta T \rangle, \quad (6.107)$$

$$R = \sum_{i=1}^{n_a} \langle \delta T^2 \rangle + 2 \sum_{i=1}^{n_a-1} \langle \delta\Omega \delta T \rangle \left(\sum_{k=i+1}^{n_a} d_k \right) + \sum_{i=1}^{n_a-1} \langle \delta\Omega^2 \rangle \left(\sum_{k=i+1}^{n_a} d_k \right)^2. \quad (6.108)$$

The variances and cross correlation of $\delta\Omega$ and δT in the above equations are given by Eq. (6.65).

To demonstrate the most interesting features as simply as possible, we focus on a 10 Gbit/s DM soliton system, using two specific dispersion maps with a map period L_m of 80 km (typical value in practice) and consider how the jitter is affected when a second amplifier is placed within each map period. One map consists of a 76 km anomalous GVD section of dispersion shifted fiber

($D = 4$ ps/km-nm, $\alpha = 0.2$ dB/km, $A_{eff} = 55 \mu\text{m}^2$), followed by a 3.2 km section of dispersion-compensating fiber ($D = -80$ ps/km-nm, $\alpha = 0.4$ dB/km, $A_{eff} = 55 \mu\text{m}^2$), resulting in an average dispersion of about $D = 0.2$ ps/km-nm. For the 30-ps (full width at half maximum) unchirped pulses used for illustration, the map strength defined as

$$S_{\text{map}} = |D_a L_a - D_n L_n| / T_{\text{FWHM}}^2, \quad (6.109)$$

where D_a and D_n are the dispersion parameters of anomalous and normal sections of the fiber. The map strength given by Eq. (6.109) is a measure of how much the GVD varies between two sections in a map period. Thus we can see that the pulse width variations are much larger for maps with a larger map strength. Using the value of the parameters in Eq. (6.109) we find that the system has a relatively low value of $S_{\text{map}} = 0.62$ for this map. An amplifier is placed at the end of each DM stage of length $L_m = 79.2$ km. The spectral density of noise is calculated from $n_{sp} = 1.3$ (noise figure of about 4.1 dB for the lumped amplifier). The solid curve in Fig. 6.3 shows the timing jitter at the end of each amplifier as a function of transmission distance for $\tau_0 = 18.02$ ps (full width at half maximum, T_{FWHM} of 30 ps), $n_{sp} = 1.3$ and $h\nu = 0.8$ eV. The input chirp is $C_0 = 0.25$ and the input peak power is $P_0 = 3.04$ mW for solitons propagating in such a lightwave system.

To see how the jitter is affected by a second amplifier placed in each DM stage, we optimize the location of the second amplifier such that pulse breathing is minimized. For the map under consideration this occurs when the amplifier is placed at a transmission distance of 35 km in the dispersion shifted fiber section of the map. At this location of the amplifier, we can use the evolution equations of energy and chirp obtained using the moment method to get the initial power, $P_0 = 0.2051$ mW, initial chirp, $C_0 = 0.517$, and the chirp at the intermediate amplifier to be -0.01 . The dotted curve in Figure 6.3 shows that the GH jitter is reduced considerably when two amplifiers are used within each DM stage. We can understand this result by noting that the gain of each amplifier is lower, resulting in a lower value of spectral density of noise, S . In Fig. 6.3 the jitter is reduced by a factor of 2 when two amplifiers are used.

The second map is designed with a standard fiber and consists of a 66 km anomalous GVD section of a standard telecommunication fiber ($D = 16$ ps/km-nm, $\alpha = 0.2$ dB/km, $A_{eff} = 55 \mu\text{m}^2$), followed by a 13 km section of a dispersion-compensating fiber ($D = -80$ ps/km-nm, $\alpha = 0.4$ dB/km, $A_{eff} = 55 \mu\text{m}^2$), resulting in an average dispersion of about $D = 0.2$ ps/km-nm. From Eq. (5.108),

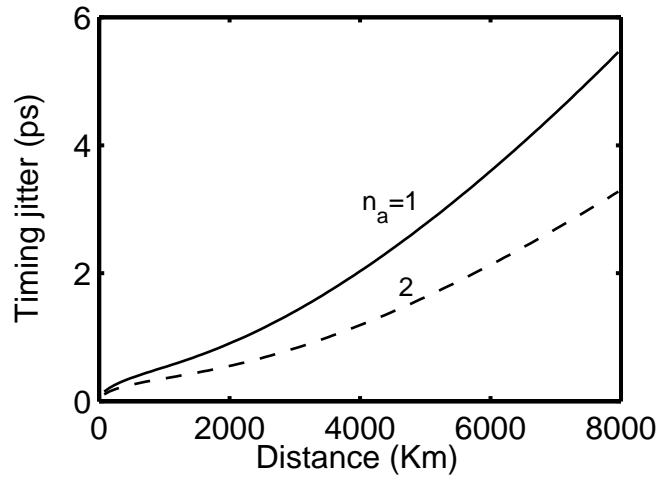


Figure 6.3: Timing jitter for a 10 Gb/s DM soliton system as a function of distance. A single amplifier is placed at the end of each map period at 79 km (solid line), where as a second amplifier is placed at a transmission distance of 35 km for the dashed curve. The map strength is 0.62 and the average dispersion is 0.2 ps/(km-nm).

the map strength with $T_{FWHM} = 30$ ps is given by $S_{map} = 2.33$, indicating a considerable change in pulse width in each map period. An amplifier is placed at the end of each DM stage of length $L_m = 79$ km. The solid curve in Fig. 6.4 shows the timing jitter at the end of each amplifier as a function of transmission distance for solitons of the same width used in Fig. 6.3 to ensure a fair comparison. The input chirp is $C_0 = 0.765$ and input peak power is $P_0 = 7.6$ mW for solitons propagating in such a lightwave system. The dashed curve in Fig. 6.4 shows how jitter is affected when a second amplifier is placed within each DM stage at a transmission distance of 24 km (location optimized to minimize pulse width changes). At this location of the amplifier, we can use the evolution equations of energy and chirp obtained using the moment method to get the initial power, $P_0 = 0.944$ mW, initial chirp, $C_0 = 2.05$, and the chirp at the intermediate amplifier to be 0.534.

A comparison of Figs. 6.3 and 6.4 shows several interesting features. Timing jitter is smaller for the map made with the standard fiber when one amplifier is used in each stage. This is a consequence of the higher pulse peak powers needed for a map with larger strengths and since Gordon-Haus timing jitter is inversely proportional to the energy, we can see reduced jitter when there is increase in energy. The second amplifier may increase or decrease the jitter, depending on transmission distance. For distances up to 2000 km the Gordon-Haus jitter is greater when

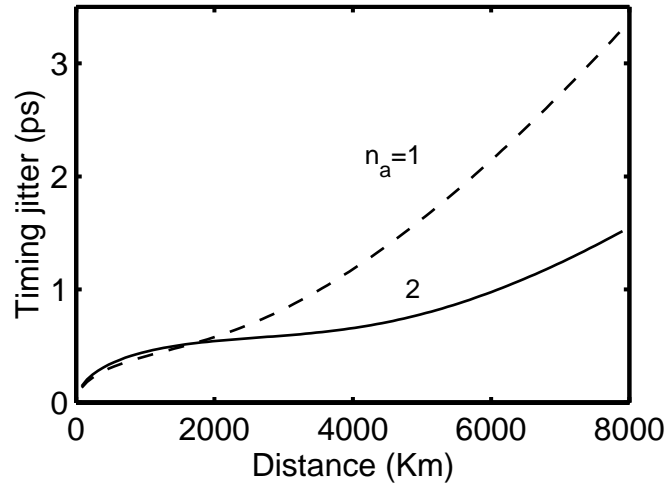


Figure 6.4: Same as Fig. 6.3 except here the map consists of 66km of standard fiber followed by 13 km of dispersion compensating fiber, resulting in a map strength of 2.33 and an average dispersion of 0.2 ps/(km-nm). The second amplifier is placed at a transmission distance of 24 km.

two amplifiers are used in each stage. For longer distances the second amplifier reduces timing jitter by a large amount (as much as a factor of 2 as shown in Figure 6.4). The reason behind this is related to the contribution of the Q term in Eq. (6.105). The expression for the Q term in Eq. (6.107) shows its dependence on the GVD accumulated up to the location of the amplifier. For an amplifier located at the end of a map period, $|d_k|$ in Eq. (6.107) is relatively small. But it can be quite large for the second amplifier located within the map period. As a result the Q term contribution becomes large at moderate distances even though this term grows as N^2 while P term grows as L^3 , thus reducing the timing jitter. This indicates that the use of multiple amplifiers in each map period can be beneficial for light-wave systems designed with standard fibers but that the amplifier locations should be chosen judiciously.

Next we consider a dispersion-managed system which uses a fundamental soliton of width, 18.02 ps in a DDF whose dispersion D decreases from 4 to 0.161 ps/(km-nm) over 80 km which will require an initial pulse power of 0.1 W, $\alpha = 0.2$ dB and $A_{eff} = 55 \mu\text{m}^2$, such that an amplifier is placed at every 80 km. Since the soliton pulse width remains the same, the location of the second amplifier is irrelevant. We place the second amplifier in the middle of the map period, at 40 km. The timing jitter in the presence of 1 and 2 amplifiers are shown in Figure 6.5. A comparison with the DM soliton system shows that the Gordon-Haus timing jitter in this system is smaller. This is

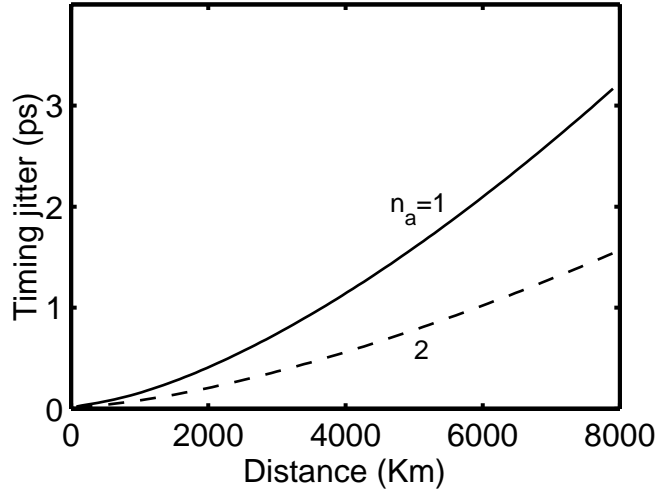


Figure 6.5: Same as Fig. 6.3 and 6.4 except here fundamental solitons are used in a DDF whose dispersion decreases from 4 to 0.161 ps/(km-nm) over 80 km. The second amplifier is placed at a transmission distance of 40 km.

due to the increased input power needed for such a system. Also the solid (1 amplifier) and dashed line (2 amplifiers) show that using 2 amplifiers can reduce Gordon-Haus jitter considerably.

To study the multi amplifier case analytically and find the extent of jitter reduction, we consider the Gordon-Haus jitter in long-haul lightwave systems for which N is so large that the dominant contribution to the timing jitter comes from the P term in Eq. (6.105), which exhibits a cubic dependence on N . This limit may require more than 100 amplifiers, depending on the map design. In the limit $N \gg 1$, the dominant term becomes

$$\sigma_{GH}^2 \approx P \frac{N}{3} (Nb_2)^2. \quad (6.110)$$

The A coefficient is obtained using Eqs. (6.96) and (6.65) for DM soliton systems. If we use the relation in Eq. (6.65) we can rewrite Eq. (6.110) as

$$\sigma_{GH}^2 \approx n_{sp} h \nu b_2^2 N^3 \frac{(1 + C_0^2)}{3\tau_0^2} \sum_{i=1}^{n_a} \frac{G_i - 1}{E_i}. \quad (6.111)$$

The quantities E_i and G_i represent the pulse energy at the end of the i th amplifier with gain G_i .

Equation (6.111) generalizes the previously derived expression for Gordon-Haus timing jitter to the case in which multiple amplifiers are used within each map period. Many lightwave systems are designed with only one amplifier per stage. In that case the last factor reduces to $[\exp(\alpha L_m) - 1]/E_0$, where E_0 is the energy of pulses launched at the input end. With several identical amplifiers per map period such that they have the same gain and are spaced apart by L_m/n_a ,

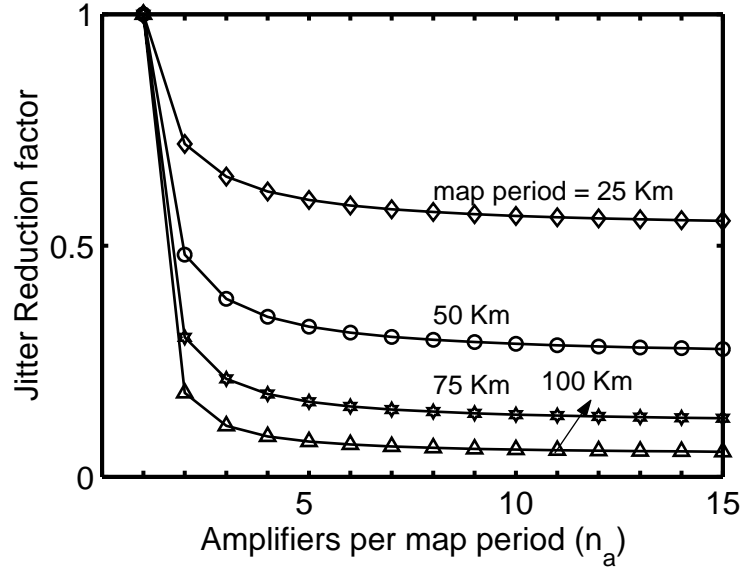


Figure 6.6: Reduction in timing jitter when several amplifiers are placed at equal distances in each map period.

$G_i = \exp(\alpha L_m/n_a) = G_t^{1/n_a}$, where $G_t = \exp(\alpha L_m)$ is the total gain of all the amplifiers in each map period of length L_m . The pulse energy at the output of each amplifier is also the same since each amplifier is designed to recover the input pulse energy. We can thus set $E_i = E_0$ in Eq. (6.111). The change in timing jitter with the use of multiple amplifiers is then given by a reduction factor defined as

$$f_r(n_a) = \frac{\sigma_{n_a}^2}{\sigma_{n_a=1}^2} = n_a \frac{G_t^{1/n_a} - 1}{G_t - 1}, \quad (6.112)$$

Figure 6.6 shows the reduction factor as a function of n_a for several values of the map period L_m . Although there is a practical limit to the number of amplifiers, the preceding results show that the use of several amplifiers reduces the timing jitter in the same way that it reduces amplifier noise [59].

The limit in which n_a tends to infinity corresponds to the case of distributed amplification. Our analysis shows that Gordon-Haus timing jitter is reduced when distributed amplification is used in place of one lumped amplifier per map period, and the reduction factor is given by

$$\frac{\sigma_{\text{distrib}}^2}{\sigma_{\text{lumped}}^2} = \frac{\alpha L_m}{\exp(\alpha L_m) - 1} = \frac{\ln G_t}{G_t - 1}, \quad (6.113)$$

where G_t is the total gain of the single lumped amplifier. As a simple example, consider a 50-km map period, $G_t = 10$ and assume total a loss of 10 dB over $L_m = 50$ km, then the Gordon-

Haus timing jitter is reduced by a factor of 3.9. It should be stressed that this result is based on the assumption that input pulse parameters remain unchanged in the two cases. In practice, the periodicity condition requires lower pulse energies in the case of distributed amplification. Since frequency noise variance scales inversely with E in Eq. (6.65), the reduction in timing jitter, in practice, is expected to be considerably smaller than that predicted by Eq. (6.113). The same reduction factor can be derived for the fundamental soliton in DDFs using Eq. (6.47).

6.3.2 Non-soliton Systems

In this section we focus on the non-soliton system in which the pulse parameters are not periodic. However the dependence of chirp and width of the pulse on distance is given by Eq. (6.78). We can rewrite Eq. (6.78) to find the chirp and pulse width at the i th amplifier in the j th map period when multiple amplifiers are used per map period to be

$$C_{ij} = C_0 + \left[(j-1)b_2 \frac{(1+C_0^2)}{\tau_0^2} + \frac{(1+C_0^2)}{\tau_0^2} \sum_{k=1}^i d_k \right], \quad (6.114)$$

$$\begin{aligned} \tau_{ij}^2 &= \frac{\tau_0^2}{(1+C_0^2)} [1+C_{ij}^2] \\ &= \tau_0^2 + (j-1)^2 \frac{(1+C_0^2)}{\tau_0^2} b_2^2 + \frac{(1+C_0^2)}{\tau_0^2} \left(\sum_{k=1}^i d_k \right)^2 + 2C_0(j-1)b_2 \\ &\quad + 2C_0 \sum_{k=1}^i d_k + 2(j-1) \frac{(1+C_0^2)}{\tau_0^2} b_2 \sum_{k=1}^i d_k, \end{aligned} \quad (6.115)$$

where C_0 is the initial chirp. Since in the case of a non-soliton system, the parameter $(1+C^2)/\tau^2$ remains unchanged, the variance in frequency fluctuations given by Eq. (5.78) remain the same for all the amplifiers. From Eq. (6.96) the coefficient P_i also remains the same for all the amplifiers and the coefficient P can be written as

$$P = \sum_{i=1}^{n_a} \frac{S_i}{E_i} \frac{(1+C_0^2)}{\tau_0^2}. \quad (6.116)$$

Using the Eqs. (6.114) and (6.115) in Eq. (6.97) and (6.98), we can find the coefficients Q_j and R_j as follows:

From Eq. (6.97) we know

$$Q_j = \sum_{i=1}^{n_a} \langle \delta\Omega \delta T \rangle_i + \sum_{i=1}^{n_a-1} \langle \delta\Omega^2 \rangle_i \left(\sum_{k=i+1}^{n_a} d_k \right),$$

$$\begin{aligned}
&= \sum_{i=1}^{n_a} \frac{S_i}{E_i} \left(C_0 + \left[(j-1)b_2 \frac{(1+C_0^2)}{\tau_0^2} + \frac{(1+C_0^2)}{\tau_0^2} \sum_{k=1}^i d_k \right] \right) \\
&+ \sum_{i=1}^{n_a-1} \frac{S_i}{E_i} \left(\frac{(1+C_0^2)}{\tau_0^2} \right) \sum_{k=i+1}^{n_a} d_k.
\end{aligned} \tag{6.117}$$

Using $b_2 = \sum_{k=1}^{n_a} d_k$, Eq. (6.117) reduces to

$$Q_j = \sum_{i=1}^{n_a} \frac{S_i}{E_i} C_0 + \sum_{i=1}^{n_a} j \left(\frac{(1+C_0^2)}{\tau_0^2} \right) b_2. \tag{6.118}$$

Similarly using Eq.(6.98) we have

$$\begin{aligned}
R_j &= \sum_{i=1}^{n_a} \langle \delta T^2 \rangle_i + \sum_{i=1}^{n_a-1} \langle \delta \Omega^2 \rangle_i \left(\sum_{k=i+1}^{n_a} d_k \right)^2 + 2 \sum_{i=1}^{n_a-1} \langle \delta \Omega \delta T \rangle_i \left(\sum_{k=i+1}^{n_a} d_k \right), \\
&= \sum_{i=1}^{n_a} \frac{S_i}{E_i} \left(\tau_0^2 + (j-1)^2 \frac{(1+C_0^2)}{\tau_0^2} b_2^2 + \frac{(1+C_0^2)}{\tau_0^2} \left(\sum_{k=1}^i d_k \right)^2 + 2C_0(j-1)b_2 \right. \\
&+ 2C_0 \sum_{k=1}^i d_k + 2(j-1) \frac{(1+C_0^2)}{\tau_0^2} b_2 \sum_{k=1}^i d_k \left. \right) + \sum_{i=1}^{n_a} \frac{S_i}{E_i} \frac{(1+C_0^2)}{\tau_0^2} \left(\sum_{k=i+1}^{n_a} d_k \right)^2 \\
&+ 2 \sum_{i=1}^{n_a} \frac{S_i}{E_i} \left(C_0 + \left[(j-1)b_2 \frac{(1+C_0^2)}{\tau_0^2} + \frac{(1+C_0^2)}{\tau_0^2} \sum_{k=1}^i d_k \right] \right) \left(\sum_{k=i+1}^{n_a} d_k \right).
\end{aligned} \tag{6.119}$$

Rearranging the terms in Eq. (6.119) and using $b_2 = \sum_{k=1}^{n_a} d_k$, we get

$$R_j = \sum_{i=1}^{n_a} \frac{S_i}{E_i} \tau_0^2 + \sum_{i=1}^{n_a} \frac{S_i}{E_i} \left[j^2 \left(\frac{(1+C_0^2)}{\tau_0^2} \right) b_2^2 \right] + 2 \sum_{i=1}^{n_a} \frac{S_i}{E_i} C_0 j b_2. \tag{6.120}$$

Using Eqs. (6.116), (6.118) and (6.120), in Eqs. (6.93)–(6.95), we get

$$\langle \Omega^2 \rangle_j = \langle \Omega^2 \rangle_{j-1} + \sum_{i=1}^{n_a} \frac{S_i}{E_i} \left(\frac{(1+C_0^2)}{\tau_0^2} \right), \tag{6.121}$$

$$\langle \Omega T \rangle_j = \langle \Omega T \rangle_{j-1} + b_2 \langle \Omega^2 \rangle_{j-1} + \sum_{i=1}^{n_a} \frac{S_i}{E_i} C_0 + \sum_{i=1}^{n_a} j \left(\frac{(1+C_0^2)}{\tau_0^2} \right) b_2, \tag{6.122}$$

$$\begin{aligned}
\langle T^2 \rangle_j &= \langle T^2 \rangle_{j-1} + b_2^2 \langle \Omega^2 \rangle_{j-1} + 2b_2 \langle \Omega T \rangle_{j-1} + \sum_{i=1}^{n_a} \frac{S_i}{E_i} \tau_0^2 \\
&+ \sum_{i=1}^{n_a} \frac{S_i}{E_i} \left[j^2 \left(\frac{(1+C_0^2)}{\tau_0^2} \right) b_2^2 \right] + 2 \sum_{i=1}^{n_a} \frac{S_i}{E_i} C_0 j b_2.
\end{aligned} \tag{6.123}$$

Comparing Eqs. (6.121)–(6.123) to Eqs. (6.83)–(6.85), we see that the multiple amplifier case is similar to the single amplifier except that there is an additional summation over the amplifiers

within the map period. Thus carrying out the summation first over the amplifiers and using $(1 + C^2)/\tau^2 = 1/\tau_0^2$, at the transmitter, and hence $P = \sum_{i=1}^{n_a} (S_i/E_0)1/\tau_0^2$, we get

$$\langle \Omega^2 \rangle_j = \langle \Omega^2 \rangle_{j-1} + \frac{S_t}{E_0} \left(\frac{1}{\tau_0^2} \right), \quad (6.124)$$

$$\langle \Omega T \rangle_j = \langle \Omega T \rangle_{j-1} + b_2 \langle \Omega^2 \rangle_{j-1} + \frac{S_t}{E_0} C_0 + j \frac{S_t}{E_0} \left(\frac{1 + C_0^2}{\tau_0^2} \right) b_2, \quad (6.125)$$

$$\begin{aligned} \langle T^2 \rangle_j &= \langle T^2 \rangle_{j-1} + b_2^2 \langle \Omega^2 \rangle_{j-1} + 2b_2 \langle \Omega T \rangle_{j-1} + \frac{S_t}{E_0} \tau_0^2 \\ &\quad + \frac{S_t}{E_0} \left[j^2 \left(\frac{1 + C_0^2}{\tau_0^2} \right) b_2^2 \right] + 2 \frac{S_t}{E_0} C_0 j b_2, \end{aligned} \quad (6.126)$$

where $S_t = \sum_{i=1}^{n_a} S_i$. Performing the summation over the map periods, we get

$$\langle \Omega^2 \rangle_N = N \frac{S_t}{E_0} \frac{1}{\tau_0^2}, \quad (6.127)$$

$$\langle \Omega T \rangle_N = \frac{b_2}{2} N(N-1) \frac{S_t}{E_0} \frac{1}{\tau_0^2} + \frac{b_2}{2} N(N+1) \frac{S_t}{E_0} \frac{(1 + C_0^2)}{\tau_0^2} + N \frac{S_t C_0}{E_0}, \quad (6.128)$$

$$\begin{aligned} \langle T^2 \rangle_N &= \frac{b_2^2}{6} N(N-1)(2N-1) \frac{S_t}{E_0} \frac{1}{\tau_0^2} + N \frac{S_t}{E_0} \frac{1 + C_0^2}{\tau_0^2} + 2b_2 \frac{S_t C_0}{E_0} \left[\frac{N}{2}(N-1) \right. \\ &\quad \left. + \frac{N}{2}(N+1) \right] + \frac{S_t}{E_0} \frac{b_2^2}{\tau_0^2} \left[\frac{N}{6}(N+1)(2N+1) + \frac{N}{6}(N-1)(2N-1) + \frac{N}{2}(N-1) \right]. \\ \langle T^2 \rangle_N &= \frac{S_t}{E_0} \tau_0^2 N \left[1 + \left(C_0 + \frac{b_2 N}{\tau_0^2} \right)^2 \right]. \end{aligned} \quad (6.129)$$

Hence from Eq. (6.129) we can write the Gordon-Haus jitter for the multiple amplifier case for non-soliton systems as

$$\sigma_{GH}^2 = \frac{S_t}{E_0} \tau_0^2 N \left[1 + \left(C_0 + \frac{b_2 N}{\tau_0^2} \right)^2 \right]. \quad (6.130)$$

We can see from Eq. (6.130) that the Gordon-Haus jitter is still cubic in distance and is similar to Eq. (6.89). The jitter is proportional to $S_t = \sum_{i=1}^{n_a} S_i$ for the multiple amplifier case. Comparing this with the one amplifier case we find that in the one amplifier case, the jitter is proportional to $S = n_{sp} h\nu (G - 1)$, where $G = \exp[-\alpha L_A]$ and in the multiple amplifier case, the jitter is proportional to $S_t = n_{sp} h\nu \sum_{i=1}^{n_a} (G_i - 1)$. Since the gain of each amplifier is such that $G_i = \exp[-\alpha z_i]$, we can see that using more than one amplifier can reduce timing jitter in non-soliton systems as well.

To show that using more than one amplifier can help reduce timing jitter even in non-soliton systems, we consider a non-soliton system using the same dispersion map as the one used for figure

6.4 except the pulse energy is reduced by a factor of 10 to minimize the nonlinear effects and the initial chirp is 0. Figure 6.7 shows the reduction in timing jitter when a second amplifier is placed at a distance of 24 km.

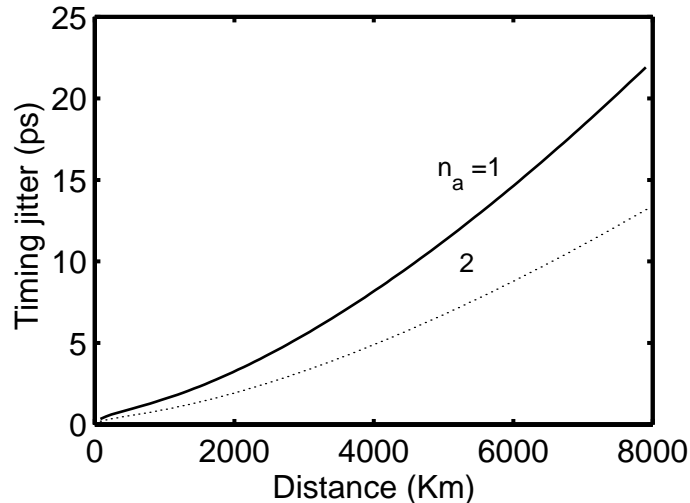


Figure 6.7: Same as Fig. 6.4 except this system uses one-tenth of the pulse energy used for Fig. 6.4 and the input pulses are unchirped. The second amplifier is placed at a transmission distance of 24 km.

6.4 Chapter Summary

In this Chapter we used the moment method to analytically derive the timing jitter at the end of a communication system employing amplifiers at regular intervals. We have extended the theory to systems using more than one amplifier per map period and shown that such systems can reduce timing jitter in both soliton and non-soliton systems. Even though using more than one amplifier per map period can help reduce timing jitter, there are few disadvantages to the idea. One of them is that it can cost more money to have more than one amplifier to amplify the signal within one map period. Also these amplifiers perturb the pulse and hence the soliton pulse may not be able to recover between the amplifiers if the amplifiers are placed very close to each other. In Chapter 4, we saw that the Q factor decreases when the number of amplifiers increases. Thus the BER of the system can be degraded. Thus when using more than one lumped amplifiers within a map period one must keep these things in mind. The above results also show that in the absence of GVD, the timing jitter will be due to amplifier fluctuations added into the position of the pulse and

grows linearly with distance. However in the presence of GVD the timing jitter is mainly due to fluctuations added into the frequency of the pulse and grows cubic in distance. Also the Gordon-Haus timing jitter is inversely proportional to the energy of the input pulse. Since generally soliton systems use higher input energy, they have lower timing jitter in the system compared to the non-soliton systems.

Chapter 7

Timing Jitter induced by Intrapulse Raman Scattering

In the previous Chapter we derived an analytical expression for the Gordon-Haus timing jitter for lightwave systems operating at bit rates less than 40 Gb/s. We saw that the Gordon-Haus timing jitter grows cubic with distance and can limit the system after several thousand kilometers. However, for systems operating at bit rates higher than 40 Gb/s, the higher-order effects such as IRS and TOD cannot be neglected. The TOD effects, can cause additional pulse broadening even in a soliton system leading to an increased timing jitter. The IRS effects, as seen before in Chapter 4, are responsible for frequency shifts that depend on the energy of the pulse. Any fluctuation in the pulse energy can be transferred to the frequency and hence to the position in the presence of GVD leading to another increase in timing jitter. This additional jitter due to the IRS is called *Raman Jitter*.

Since the allowed value of timing jitter is inversely proportional to the bit rate of the system, at high bit rates, the systems will be limited by timing jitter at shorter distances than the systems operating at lower bit rates. Hence, it becomes important to know the exact impact of the additional jitter induced by IRS and TOD in such systems. In this Chapter we use the moment method to get analytic expressions for timing jitter due to both the Raman and Gordon-Haus effects for high bit rate systems. Similar to the Gordon-Haus jitter, the Raman jitter occurs for both soliton and non-soliton systems. The Raman jitter has been studied in the context of constant-dispersion

fibers [60] and dispersion-decreasing fibers [55]. However, most lightwave systems make use of dispersion management. In this Chapter, we consider the impact of Raman-induced timing jitter on dispersion-managed (DM) systems and non-soliton systems to find how these systems are inherently limited by timing jitter at bit rates of 80 Gb/s or more.

Lightwave systems that operate at a bit rate of 80 Gb/s or more use very short pulses (≈ 1 ps). As an example, a 160 Gb/s may require a pulse width as short as 1 ps. For such systems, the pulse propagation in a fiber is governed by the NLS equation given in Eq. (3.51) and written again here as

$$\frac{\partial A}{\partial z} + \frac{\alpha}{2}A + \frac{i\beta_2}{2}\frac{\partial^2 A}{\partial t^2} - \frac{\beta_3}{6}\frac{\partial^3 A}{\partial t^3} = i\gamma|A|^2A - i\gamma T_R A \frac{\partial |A|^2}{\partial t}. \quad (7.1)$$

Here we have neglected the effect of self-steepening since they become important only for pulses shorter than 100 fs. Using the transformation given by Eq. (3.2) we can rewrite Eq. (7.1) as

$$\frac{\partial B}{\partial z} + \frac{i\beta_2}{2}\frac{\partial^2 B}{\partial t^2} - \frac{\beta_3}{6}\frac{\partial^3 B}{\partial t^3} = i\bar{\gamma}|B|^2B - i\bar{\gamma}T_R B \frac{\partial |B|^2}{\partial t}, \quad (7.2)$$

where $\bar{\gamma} = \gamma \exp[-\int_0^z \alpha(z)dz]$. Using Eq. (7.2) and the moment definitions of energy, frequency and position, we derive the evolution equations for the pulse parameters following the method of Chapter 4.

Using the results obtained in Chapter 4 and neglecting the effects of self-steepening in Eqs. (4.22), (4.36) and (4.52), we can write the evolution equations for the energy, frequency and position as

$$\frac{dE}{dz} = 0, \quad (7.3)$$

$$\frac{dT}{dz} = \beta_2\Omega + \frac{\beta_3}{2E} \int_{-\infty}^{\infty} \left| \frac{\partial B}{\partial t} \right|^2 dt, \quad (7.4)$$

$$\frac{d\Omega}{dz} = -\frac{\bar{\gamma}}{E} T_R \int_{-\infty}^{\infty} \left(\frac{\partial}{\partial t} |B|^2 \right)^2 dt. \quad (7.5)$$

The above equations simply describe the evolution of the three pulse parameters. However, we have to add the ASE-induced fluctuation into these equations in order to account for the effects of lumped amplifiers. Thus, Eqs. (7.3)–(7.5) should be modified as follows to include the amplifier noise:

$$\frac{dE}{dz} = \sum_i \delta E_i \delta(z - z_i), \quad (7.6)$$

$$\frac{dT}{dz} = \beta_2 \Omega + \frac{\beta_3}{2E} \int_{-\infty}^{\infty} \left| \frac{\partial B}{\partial t} \right|^2 dt + \sum_i \delta T_i \delta(z - z_i), \quad (7.7)$$

$$\frac{d\Omega}{dz} = -\frac{\bar{\gamma}}{E} T_R \int_{-\infty}^{\infty} \left(\frac{\partial}{\partial t} |B|^2 \right)^2 dt + \sum_i \delta \Omega_i \delta(z - z_i), \quad (7.8)$$

where δE_i , $\delta \Omega_i$, and δT_i are random fluctuations in the pulse energy, frequency, and position, respectively, introduced by the i th amplifier located at a distance z_i . We proceed to calculate timing jitter from the above equations using the same technique we used to calculate Gordon-Haus jitter in Chapter 6. However, because of the presence of energy, E in the equation for Ω due to IRS, we need to find the variances and correlations of the E , Ω and T . Also, the above equations show that the evolutions of these parameters are dependent on the pulse shape. Hence, to proceed further we need to assume a specific pulse shape. In the following sections we consider the cases of soliton and non-soliton systems one after the other.

7.1 Solitons Systems

As seen in the previous Chapter the soliton systems are periodic after every amplifier, and hence the evolution of the pulse parameters is also periodic in every fiber section before the amplifiers. We have also seen in Chapter 4 that this periodicity of the soliton system is valid in the presence of IRS only if the RIFS remains a small fraction of the pulse spectral width. For pulses whose width is larger than 100 fs the RIFS is small enough to satisfy the above condition and hence for systems under consideration the assumption that a soliton system is periodic remains valid. However when the pulse width is comparable to or less than 100 fs, one has to include the evolution equations for chirp and pulse width derived in Chapter 4 in the calculation of timing jitter.

7.1.1 Fundamental solitons in DDFs

We first consider the case of fundamental solitons propagating in DDFs. The pulse shape in such systems is given by Eq. (3.7). First let us consider the changes in the soliton position in such systems. Using Eq. (3.7) in Eq. (7.7) we find that the pulse position evolves from Eq. (4.90) as

$$\frac{dT}{dz} = \beta_2 \Omega + \frac{\beta_3 \Omega^2}{2} + \frac{\beta_3}{6\tau^2} + \sum_i \delta T_i \delta(z - z_i). \quad (7.9)$$

Next the evolution of the frequency can be found by using Eq. (3.7) in Eq. (7.8) and can be written using Eq. (4.99) as

$$\frac{d\Omega}{dz} = -\frac{4\bar{\gamma}T_R E}{15\tau^3} + \sum_i \delta\Omega_i \delta(z - z_i). \quad (7.10)$$

The evolution of the pulse energy is governed by Eq. (7.6). Now that we know how the energy, position and frequency of a fundamental soliton evolve, we can integrate Eqs. (7.6), (7.9) and (7.10) over one amplifier length to get

$$E(L_A) = E(0) + \delta E_1, \quad (7.11)$$

$$\Omega(L_A) = \Omega(0) + b_R E(0) + \delta\Omega_1, \quad (7.12)$$

$$\begin{aligned} T(L_A) = & T(0) + b_2 \Omega(0) + b_{2R} E(0) + b_3 + b_{3\Omega} \Omega^2(0) \\ & + b_{E\Omega} E(0) \Omega(0) + b_{3E} E^2(0) + \delta T_1, \end{aligned} \quad (7.13)$$

where the coefficients b_R , b_2 , b_{2R} , b_3 , b_{3E} , $b_{3\Omega}$ and $b_{E\Omega}$ are given by

$$b_2 = \beta_2(0)L_{\text{eff}}, \quad b_3 = \beta_3(0)L_{\text{eff}}/(6\tau^2), \quad (7.14)$$

$$b_R = -4\gamma T_R L_{\text{eff}}/(15\tau_0^3), \quad (7.15)$$

$$b_{2R} = -2\gamma T_R \beta_2(0)L_{\text{eff}}^2/(15\tau_0^3), \quad b_{3E} = \frac{\beta_3(0)}{2\alpha} \left(\frac{4\gamma T_R L_{\text{eff}}}{15\tau_0^3} \right)^2, \quad (7.16)$$

$$b_{3\Omega} = \frac{1}{2}L_{\text{eff}}\beta_3(0), \quad b_{E\Omega} = -\frac{4T_R\gamma\beta_3(0)}{15\tau_0^3}L_{\text{eff}}^2, \quad (7.17)$$

where L_{eff} is the effective length defined as

$$L_{\text{eff}} = [1 - \exp(-\alpha L_A)]/\alpha. \quad (7.18)$$

The expressions in Eqs. (7.14)–(7.17) were obtained by using $\bar{\gamma}(z) = \gamma(0)\exp(-\alpha z)$, $\beta_2(z) = \beta_2(0)\exp(-\alpha z)$ and $\beta_3(z) = \beta_3(0)\exp(-\alpha z)$ for fundamental solitons propagating in a DDF.

For simplicity, we neglect the contribution of higher-order terms containing $b_{3\Omega}$, b_{3E} and $b_{E\Omega}$. These terms involve the product of two small parameters, T_R and β_3 and can be neglected in most cases of practical interest. Hence we can write from Eqs. (7.11)–(7.13) the energy, frequency and position after any i th amplifier as

$$E_i = E_{i-1} + \delta E_i, \quad (7.19)$$

$$\Omega_i = \Omega_{i-1} + b_R E_{i-1} + \delta\Omega_i, \quad (7.20)$$

$$T_i = T_{i-1} + b_2 \Omega_{i-1} + b_{2R} E_{i-1} + b_3 + \delta T_i. \quad (7.21)$$

The timing jitter induced by the Raman and Gordon-Haus effects can be calculated using the definition of timing jitter, $\sigma_t^2 = \langle T^2 \rangle - \langle T \rangle^2$, where the angle brackets indicate average over the ASE noise. For this purpose, we need to find the variances and cross correlations of δE_i , $\delta \Omega_i$ and δT_i . In the calculation of timing jitter, we are interested in finding how much, on average, the pulse position has shifted at the end of the system. Since we are interested in finding the shift in 1 bits, we need δE_i , $\delta \Omega_i$ and δT_i for any given 1 bit. Using the moment method, we have calculated the variance and average of δE_i for 1 bits in Chapter 5. From Eqs. (5.23) and (5.25) we have

$$\langle \delta E \rangle_i = S, \quad \langle \delta E^2 \rangle_i \approx 2SE_i, \quad (7.22)$$

where we have neglected the last term, which is due to the beating of noise with itself, since it is small compared to the signal and noise beating with each other.

To find the cross correlations, we use the results obtained in the Chapters 5 and 6 using the moment method for δE_i and $\delta \Omega_i$ and δT_i . Neglecting any terms due to noise beating with itself and using Eqs. (5.22), (6.17) and (6.22) we obtain

$$\delta E_i = \int_{-\infty}^{\infty} (B_i \delta B_i^* + B_i^* \delta B_i) dt, \quad (7.23)$$

$$\delta \Omega_i = -\frac{i}{E_i} \int_{-\infty}^{\infty} \left[\delta B_i \left(\frac{\partial B_i^*}{\partial t} - i\Omega_i B^* \right) - \delta B_i^* \left(\frac{\partial B_i}{\partial t} + i\Omega_i B \right) \right] dt, \quad (7.24)$$

$$\delta T_i = \frac{1}{E_i} \int_{-\infty}^{\infty} (t - T) (B_i^* \delta B_i + B_i \delta B_i^*) dt. \quad (7.25)$$

Using the transformation in Eq. (6.18) we can write the above equations in terms of $V_i(z, t)$ as

$$\delta E_i = \int_{-\infty}^{\infty} (V_i \delta V_i^* + V_i^* \delta V_i) dt, \quad (7.26)$$

$$\delta \Omega_i = -\frac{i}{E_i} \int_{-\infty}^{\infty} \left[\delta V_i \frac{\partial V_i^*}{\partial t} - \delta V_i^* \frac{\partial V_i}{\partial t} \right] dt, \quad (7.27)$$

$$\delta T_i = \frac{1}{E_i} \int_{-\infty}^{\infty} (t - T) (V_i^* \delta V_i + V_i \delta V_i^*) dt. \quad (7.28)$$

From Eqs. (7.26)–(7.28) we obtain the correlations $\delta E_i \delta \Omega_i$ and $\delta E_i \delta T_i$ as

$$\delta E_i \delta \Omega_i = -\frac{i}{E_i} \int_{-\infty}^{\infty} dt \int_{-\infty}^{\infty} dt' \left[\delta V_i(t') \frac{\partial V_i^*(t')}{\partial t} - \delta V_i^*(t') \frac{\partial V_i(t')}{\partial t} \right] \times [V_i(t) \delta V_i^*(t) + V_i^*(t) \delta V_i(t)], \quad (7.29)$$

$$\delta E_i \delta T_i = \frac{1}{E_i} \int_{-\infty}^{\infty} dt \int_{-\infty}^{\infty} dt' (t - T_i) [V_i(t) \delta V_i^*(t) + V_i^*(t) \delta V_i(t)] \times [V_i(t') \delta V_i^*(t') + V_i^*(t') \delta V_i(t')]. \quad (7.30)$$

Taking the average of Eqs. (7.29) and (7.30) and using Eq.(6.25) we get

$$\langle \delta E \delta \Omega \rangle_i = \frac{iS}{E_i} \int_{-\infty}^{\infty} dt \left[V_i^* \frac{\partial V_i}{\partial t} - V_i \frac{\partial V_i^*}{\partial t} \right], \quad (7.31)$$

$$\langle \delta E \delta T \rangle_i = \frac{2S}{E_i} \int_{-\infty}^{\infty} dt (t - T_i) |V_i|^2. \quad (7.32)$$

For the fundamental soliton, the form of V_i is given in Eq. (6.40) as

$$V_i(z, t) = a_i \operatorname{sech} \left(\frac{t - T_i}{\tau_i} \right) \exp(i\phi_i). \quad (7.33)$$

From Eq. (7.33) the time derivative is given by

$$\frac{\partial V_i}{\partial t} = - \left[\frac{a_i}{\tau_i} \operatorname{sech} \left(\frac{t - T_i}{\tau_i} \right) \tanh \left(\frac{t - T_i}{\tau_i} \right) \right] \exp(i\phi_i). \quad (7.34)$$

Using Eqs. (7.33) and (7.34) in Eqs. (7.31) and (7.32) we finally obtain

$$\langle \delta E \delta \Omega \rangle_i = - \frac{2iS}{E_i} \int_{-\infty}^{\infty} \frac{a_i^2}{\tau_i} \operatorname{sech}^2 \left(\frac{t - T_i}{\tau_i} \right) \tanh \left(\frac{t - T_i}{\tau_i} \right) dt, \quad (7.35)$$

$$\langle \delta E \delta T \rangle_i = \frac{2S}{E_i} \int_{-\infty}^{\infty} dt (t - T_i) a_i^2 \operatorname{sech}^2 \left(\frac{t - T_i}{\tau_i} \right). \quad (7.36)$$

Using Table 4.1 and performing the integrations we get

$$\langle \delta E \delta \Omega \rangle_i = 0 \quad \langle \delta E \delta T \rangle_i = 0. \quad (7.37)$$

The variances of $\delta \Omega_i$ and δT_i and their correlation were found in Chapter 6 and are given by Eqs. (6.43), (6.45) and (6.46) for the case of the fundamental soliton. Since we know that soliton systems are periodic such that the pulse width and energy are recovered after every amplifier, the variances and cross correlations of δE , $\delta \Omega$ and δT in the case of fundamental solitons can be written, after dropping the subscript i , as

$$\langle \delta E^2 \rangle = 2SE_0, \quad \langle \delta \Omega \delta E \rangle = 0, \quad (7.38)$$

$$\langle \delta \Omega^2 \rangle = \frac{2S}{3E_0 \tau_0^2} \quad \langle \delta E \delta T \rangle = 0, \quad (7.39)$$

$$\langle \delta T^2 \rangle = \frac{\pi^2 S \tau_0^2}{6E_0} \quad \langle \delta \Omega \delta T \rangle = 0. \quad (7.40)$$

Now that we have found the second moments of δE , $\delta \Omega$ and δT , we can write the recurrence relations from Eqs. (7.19)–(7.21) as follows. The first moments are given by

$$\langle E \rangle_N = E_0 + \sum_{i=1}^N \langle \delta E \rangle, \quad (7.41)$$

$$\langle \Omega \rangle_N = b_R \sum_{i=1}^{N-1} \langle E \rangle_i + \sum_{i=1}^N \langle \delta \Omega \rangle, \quad (7.42)$$

$$\langle T \rangle_N = b_2 \sum_{i=1}^{N-1} \Omega_i + b_{2R} \sum_{i=1}^{N-1} E_i + \sum_{i=1}^N b_3 + \sum_{i=1}^N \langle \delta T \rangle. \quad (7.43)$$

Performing the summation using Eqs. (6.27), (6.30) and (7.22), we obtain

$$\langle E \rangle_N = E_0 + N S, \quad (7.44)$$

$$\langle \Omega \rangle_N = b_R N(N-1) S/2 + N b_R E_0, \quad (7.45)$$

$$\begin{aligned} \langle T \rangle_N &= b_2 b_R N(N-1)(2N-1) S/6 + b_2 b_R N(N-1) S/2 + b_{2R} N(N-1) S/2 + b_{2R} N E_0 \\ &\quad + N b_3. \end{aligned} \quad (7.46)$$

Next the second moments and correlations are found to be

$$\langle E^2 \rangle_i = \langle E^2 \rangle_{i-1} + \langle \delta E^2 \rangle_{i-1} + 2 \langle E \rangle_{i-1} \langle \delta E \rangle_i, \quad (7.47)$$

$$\langle E \Omega \rangle_i = \langle E \Omega \rangle_{i-1} + b_R \langle E^2 \rangle_{i-1} + \langle \delta E \delta \Omega \rangle_i, \quad (7.48)$$

$$\langle \Omega^2 \rangle_i = \langle \Omega^2 \rangle_{i-1} + b_R^2 \langle E^2 \rangle_{i-1} + 2 b_R \langle E \Omega \rangle_{i-1} + \langle \delta \Omega^2 \rangle_i, \quad (7.49)$$

$$\langle ET \rangle_i = \langle ET \rangle_{i-1} + b_2 \langle E \Omega \rangle_{i-1} + b_{2R} \langle E^2 \rangle_{i-1} + b_3 \langle E \rangle_{i-1} + \langle \delta E \delta T \rangle_i \quad (7.50)$$

$$\begin{aligned} \langle \Omega T \rangle_i &= \langle \Omega T \rangle_{i-1} + b_2 \langle \Omega^2 \rangle_{i-1} + b_{2R} \langle E \Omega \rangle_{i-1} + b_3 \langle \Omega \rangle_{i-1} + b_R \langle ET \rangle_{i-1} \\ &\quad + b_2 b_R \langle E \Omega \rangle_{i-1} + b_{2R} b_R \langle E^2 \rangle_{i-1} + b_3 b_R \langle E \rangle_{i-1} + \langle \delta \Omega \delta T \rangle_i \end{aligned} \quad (7.51)$$

$$\begin{aligned} \langle T \rangle_i &= \langle T \rangle_{i-1} + b_2^2 \langle \Omega^2 \rangle_{i-1} + b_{2R}^2 \langle E^2 \rangle_{i-1} + b_3^2 + \langle \delta T^2 \rangle_i + 2 b_2 \langle \Omega T \rangle_{i-1} + 2 b_{2R} \langle ET \rangle_{i-1} \\ &\quad + 2 b_3 \langle T \rangle_{i-1} + b_2 b_{2R} \langle E \Omega \rangle_{i-1} + 2 b_3 b_2 \langle \Omega \rangle_{i-1}. \end{aligned} \quad (7.52)$$

Summing up Eqs. (7.47)–(7.52) over N amplifiers, we get

$$\langle E^2 \rangle_N = \sum_{i=1}^N \langle \delta E^2 \rangle + 2 \sum_{i=1}^N \langle E \rangle_{i-1} \langle \delta E \rangle, \quad (7.53)$$

$$\langle E \Omega \rangle_N = b_R \sum_{i=1}^{N-1} \langle E^2 \rangle_i + \sum_{i=1}^N \langle \delta E \delta \Omega \rangle, \quad (7.54)$$

$$\langle \Omega^2 \rangle_N = b_R^2 \sum_{i=1}^{N-1} \langle E^2 \rangle_i + 2 b_R \sum_{i=1}^{N-1} \langle E \Omega \rangle_i + \sum_{i=1}^N \langle \delta \Omega^2 \rangle, \quad (7.55)$$

$$\langle ET \rangle_N = b_2 \sum_{i=1}^{N-1} \langle E \Omega \rangle_i + b_{2R} \sum_{i=1}^{N-1} \langle E^2 \rangle_i + b_3 \sum_{i=1}^{N-1} \langle E \rangle_i + \sum_{i=1}^N \langle \delta E \delta T \rangle \quad (7.56)$$

$$\langle \Omega T \rangle_N = b_2 \sum_{i=1}^{N-1} \langle \Omega^2 \rangle_i + b_{2R} \sum_{i=1}^{N-1} \langle E \Omega \rangle_i + b_3 \sum_{i=1}^{N-1} \langle \Omega \rangle_i + b_R \sum_{i=1}^{N-1} \langle ET \rangle_i$$

$$+ b_2 b_R \sum_{i=1}^{N-1} \langle E\Omega \rangle_i + b_{2R} b_R \sum_{i=1}^{N-1} \langle E^2 \rangle_i + \sum_{i=1}^N \langle \delta\Omega\delta T \rangle \quad (7.57)$$

$$\begin{aligned} \langle T^2 \rangle_N &= b_2^2 \sum_{i=1}^{N-1} \langle \Omega^2 \rangle_i + b_{2R}^2 \sum_{i=1}^{N-1} \langle E^2 \rangle_i + \sum_{i=1}^N b_3^2 + \sum_{i=1}^N \langle \delta T^2 \rangle \\ &+ 2b_2 \sum_{i=1}^{N-1} \langle \Omega T \rangle_i + 2b_{2R} \sum_{i=1}^{N-1} \langle E T \rangle_i + 2b_3 \sum_{i=1}^{N-1} \langle T \rangle_i \\ &+ b_2 b_{2R} \sum_{i=1}^{N-1} \langle E\Omega \rangle_i + 2b_3 b_2 \sum_{i=1}^{N-1} \langle \Omega \rangle_i. \end{aligned} \quad (7.58)$$

Performing the summation using Eqs. (6.51), (7.38)–(7.40), Eqs. (7.44)–(7.46) and

$$\sum_{i=1}^N i^3 = \left(\frac{N(N+1)}{2} \right)^2, \quad \sum_{i=1}^N i^4 = N(N+1)(2N+1)(3N^2+3N-1)/30, \quad (7.59)$$

we obtain the following analytical expressions:

$$\langle E^2 \rangle_N = N \langle \delta E^2 \rangle + 2NE_0 \langle \delta E \rangle, \quad (7.60)$$

$$\langle E\Omega \rangle_N = b_R N(N-1)/2 \langle \delta E^2 \rangle + b_R N(N-1)E_0 \langle \delta E \rangle + N \langle \delta E \delta \Omega \rangle, \quad (7.61)$$

$$\begin{aligned} \langle \Omega^2 \rangle_N &= b_R^2 \frac{N}{6} (N-1)(2N-1) \langle \delta E^2 \rangle + b_R^2 \frac{N}{3} (N-1)(2N-1)E_0 \langle \delta E \rangle \\ &+ b_R N(N-1) \langle \delta E \delta \Omega \rangle + N \langle \delta \Omega^2 \rangle, \end{aligned} \quad (7.62)$$

$$\begin{aligned} \langle ET \rangle_N &= b_2 \frac{N}{2} (N-1) \langle \delta E \delta \Omega \rangle + b_{2R} \frac{N}{2} (N-1) \langle \delta E^2 \rangle + b_R b_2 \frac{N}{12} (N-1)(2N-1) \langle \delta E^2 \rangle \\ &+ b_3 \frac{N}{2} (N-1)S + N \langle \delta E \delta T \rangle \\ &= \langle \delta E^2 \rangle \frac{N}{2} (N-1) \left(b_{2R} + b_R b_2 \frac{(2N-1)}{6} \right) + b_3 \frac{N}{2} (N-1)S, \end{aligned} \quad (7.63)$$

$$\begin{aligned} \langle \Omega T \rangle_N &= b_2 \frac{N}{2} (N-1) \langle \delta \Omega^2 \rangle + \langle \delta E \delta \Omega \rangle \left[b_{2R} \frac{N}{2} (N-1) + b_2 b_R \frac{N}{2} (N-1)^2 \right] \\ &+ \langle \delta E^2 \rangle \left[b_2 b_R^2 \frac{N}{24} (N-1)(N-2)(3N-1) + b_{2R} b_R \frac{N}{6} (N-1)(2N-1) \right] \\ &+ b_3 b_R \frac{N}{6} (N-1)(2N-1)S + b_R b_3 N(N-1)E_0 + N \langle \delta \Omega \delta T \rangle, \\ &= b_2 \frac{N}{2} (N-1) \langle \delta \Omega^2 \rangle + \langle \delta E^2 \rangle \left[b_2 b_R^2 \frac{N}{24} (N-1)(N-2)(3N-1) \right. \\ &\left. + b_{2R} b_R \frac{N}{6} (N-1)(2N-1) \right] + b_3 b_R \frac{N}{6} (N-1)(2N-1)S + b_R b_3 N(N-1)E_0, \end{aligned} \quad (7.64)$$

$$\begin{aligned} \langle T^2 \rangle_N &= b_2^2 \frac{N}{6} (N-1)(2N-1) \langle \delta \Omega^2 \rangle + N^2 b_3^2 + N \langle \delta T^2 \rangle + \langle \delta E^2 \rangle \left[b_{2R}^2 \frac{N}{6} (N-1)(2N-1) + b_2 b_{2R} b_R \right. \\ &\left. \frac{N}{4} (N-1)^2 (N-2) + b_R^2 b_2^2 \frac{N}{120} (N-1)(6N^3 - 20N^2 + 24N + 1) \right] + 2b_3 b_2 b_R \end{aligned}$$

$$\left[\frac{N}{3}(N-1)(N-2)S + \frac{N}{2}(N-1)^2(N-8)E_0 \right] + b_3 b_{2R} \left[\frac{N}{3}(N-1)(N-2)S + N(N-1)E_0 \right]. \quad (7.65)$$

Using Eqs. (7.46) and (7.65) in the definition of the timing jitter we obtain the timing jitter in the case of a fundamental soliton propagating in DDFs with periodic amplification to be

$$\sigma_t^2 = \sigma_{\text{GH}}^2 + R_1 \langle (\delta E)^2 \rangle + R_2, \quad (7.66)$$

where σ_{GH}^2 is the Gordon-Haus timing jitter evaluated in the previous Chapter and is given by

$$\sigma_{\text{GH}}^2 = \frac{b_2^2}{6} N(N-1)(2N-1) \langle \delta \Omega^2 \rangle + N \langle \delta T^2 \rangle, \quad (7.67)$$

and the coefficients R_1 and R_3 are given by

$$R_1 = N(N-1) [b_R^2 b_2^2 (N^3 - 10N^2 + 29N - 9)/120 + b_2 b_R b_{2R} (19N^2 - 65N + 48)/96 + b_{2R}^2 (2N-1)/6], \quad (7.68)$$

$$R_2 = N(N-1) b_3 [b_R (N-1)(N-2)/6 + b_{2R} (N-2)/3] S. \quad (7.69)$$

The R_1 term originates from the RIFS. For this reason, this contribution is referred to as the Raman jitter. The R_1 dominates for $N \gg 1$ because of its N^5 dependence. The R_2 term results from the combination of TOD and Raman effects and thus becomes important only for pulses much shorter than 1 ps. In the absence of the Raman and TOD effects, we recover the expression for the Gordon-Haus jitter obtained in Chapter 6. The leading term in the timing jitter given by Eq. (7.66) is due to RIFS and grows as N^5 whereas the Gordon-Haus term given by Eq. (7.67) grows as N^3 . Both of these contributions agree with the earlier results of Essiambre and Agrawal [55]. The same expression applies for constant-dispersion fibers with minor changes. The coefficients b_2 and b_3 require replacing L_{eff} with L_A because β_2 and β_3 are constant along the fiber and the coefficient b_{2R} changes to $4\gamma T_R (L_{\text{eff}} - L_A) / (15\alpha\tau_0^3)$ while b_R remains the same.

As a numerical example we consider a 160-Gb/s fundamental soliton in a 45-km-long DDF with $\beta_2(0) = 1.275$ ($D(0) = 1.0$ ps/(km-nm)). The fiber is assumed to have an effective area of $54 \mu\text{m}^2$, losses of 0.2 dB/km, $T_R = 3$ fs, and $\beta_3 = 0$. Optical amplifiers are spaced 45 km apart. The spectral noise density was calculated using $n_{sp} = 1.3$. The pulse width, $\tau_0 = 1.25$ ps, and hence the pulse energy, $E_0 = 0.9$ pJ so that it corresponds to a standard fundamental soliton. Figure 7.1

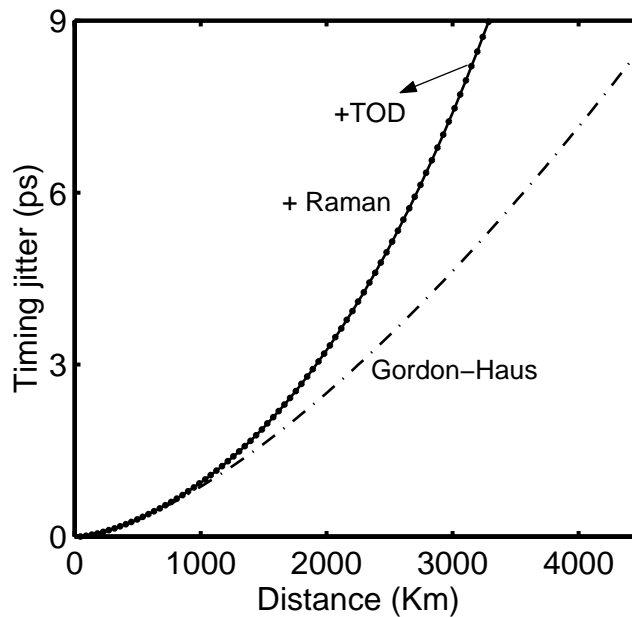


Figure 7.1: Timing jitter for a 160 Gb/s system using fundamental soliton in DDFs whose dispersion D decreases from 1 to 0.165 ps/(km-nm) over 45 km.

shows the dependence of timing jitter on distance for such a system. The dashed line shows the Gordon-Haus jitter obtained from Eq. (7.67), and the solid line shows the sum of Gordon-Haus and Raman jitter from Eq. (7.66). The effect of TOD is included in the dotted line. Since the Raman contributions from RIFS begins to dominate the jitter after 1000 km, it is evident that the system performance is mainly limited by the RIFS at high bit rates. Notice that the sum of Raman jitter and Gordon-Haus jitter is much larger in this case. This is due to the relatively large value of the average dispersion.

If we design the fundamental soliton system with the same average dispersion using a DDFs whose $|\beta_2|$ decreases from 0.24 to 0.04 ps²/km (D goes from 0.188 to 0.03 ps/(km-nm)) over 45 km, with a pulse energy of 0.17pJ, we obtain the results shown in Fig. 7.2. Timing jitter is now smaller than that of Fig. 7.1. This qualitative change is due to a reduced energy needed for fundamental solitons. The Raman jitter has its origin in energy fluctuations whose magnitude is proportional to the pulse energy. In contrast, the Gordon-Haus jitter is inversely proportional to the pulse energy. Thus, as the pulse energy decreases, the Gordon-Haus jitter increases but the Raman jitter decreases.

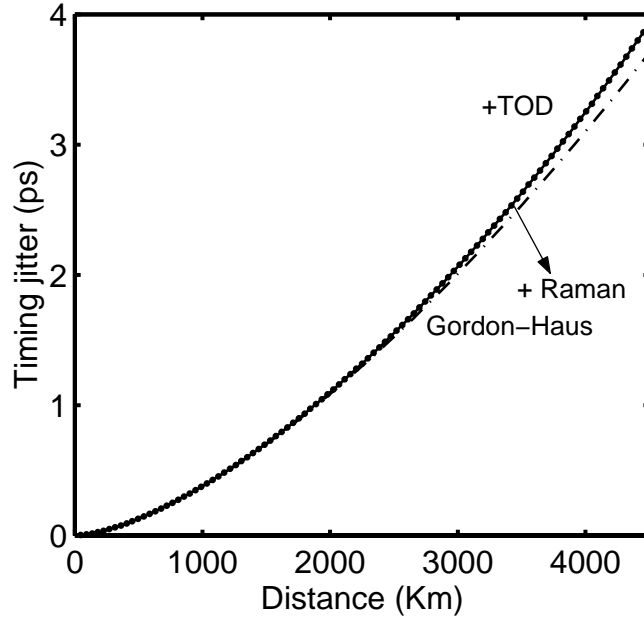


Figure 7.2: Timing jitter for a 160 Gb/s system using fundamental soliton in DDFs whose dispersion D decreases from 0.188 to 0.03 ps/(km-nm) over 45 km.

7.1.2 Dispersion-Managed Solitons

Next we consider the case of DM solitons. The pulse shape of such a soliton is then given by Eq. (6.56). Using Eq. (6.56) in Eqs. (7.6)–(7.8), we get

$$\frac{dE}{dz} = \sum_i \delta E_i \delta(z - z_i), \quad (7.70)$$

$$\frac{d\Omega}{dz} = -\frac{T_R \gamma E}{\sqrt{2\pi}\tau^3} + \sum_i \delta\Omega_i \delta(z - z_i), \quad (7.71)$$

$$\frac{dT}{dz} = \beta_2 \Omega + \frac{\beta_3(1+C^2)}{4\tau^2} + \beta_3 \frac{\Omega^2}{2} + \sum_i \delta T_i \delta(z - z_i), \quad (7.72)$$

Integrating Eqs. (7.70)–(7.72), over the length of one amplifier we get

$$E(L_A) = E(0) + \delta E_1, \quad (7.73)$$

$$\Omega(L_A) = \Omega(0) + b_R E(0) + \delta\Omega_1 \quad (7.74)$$

$$\begin{aligned} T(L_A) = T(0) + b_2 \Omega(0) + b_{2R} E(0) + b_3 + b_{3\Omega} \Omega^2(0) \\ + b_{E\Omega} E(0)\Omega(0) + b_{3E} E^2(0) + \delta T_1, \end{aligned} \quad (7.75)$$

where the coefficients $b_R, b_2, b_{2R}, b_3, b_{3E}, b_{3\Omega}$ and $b_{E\Omega}$ are given by

$$b_2 = \int_0^{L_A} \beta_2(z) dz, \quad b_3 = \int_0^{L_A} \frac{\beta_3(1+C^2)}{4\tau^2} dz, \quad (7.76)$$

$$b_R = - \int_0^{L_A} q(z) dz, \quad b_{2R} = - \int_0^{L_A} dz \beta_2(z) \int_0^z dz' q(z') \quad (7.77)$$

$$b_{3\Omega} = \frac{1}{2} \int_0^{L_A} \beta_3 dz, \quad b_{E\Omega} = - \frac{1}{2} \int_0^{L_A} dz \beta_3(z) \int_0^z q(z') dz', \quad (7.78)$$

$$b_{3E} = - \frac{1}{2} \int_0^{L_A} dz \beta_3(z) \left[\int_0^z q(z') dz' \right]^2, \quad q(z) = \frac{T_R \gamma \exp(-\alpha z)}{\sqrt{2\pi} \tau^3(z)}, \quad (7.79)$$

where we have used $\bar{\gamma}(z) = \gamma \exp(-\alpha z)$. Eqs. (7.73)–(7.75) look the same as Eqs. (7.11)–(7.13) except for the definitions of the coefficients, $b_R, b_2, b_{2R}, b_3, b_{3E}, b_{3\Omega}$ and $b_{E\Omega}$. However in the case of DM solitons, the situation is quite different. First, the pulse width τ is not constant but varies in a periodic fashion along the fiber link. It takes its minimum value in the middle of each fiber section forming the dispersion map. As a result, the maximum contribution to the frequency shift in Eq. (7.74) comes from this region. It is sometimes concluded that RIFS is smaller for DM solitons if we assume that τ in Eq. (7.77) corresponds to the minimum width of a DM soliton [61]. However, one should note that the pulse energy is enhanced considerably for DM solitons. Moreover, the contribution where the pulse width is minimum is reduced because of losses. For these reasons, the RIFS and hence the Raman jitter of DM solitons can exceed that of fundamental solitons.

For simplicity, we neglect the contribution of higher-order terms containing $b_{3\Omega}, b_{3E}$ and $b_{E\Omega}$ like we did for the fundamental soliton case and write the from Eqs. (7.73)–(7.75) the energy, frequency and position after any i th amplifier as

$$E_i = E_{i-1} + \delta E_i, \quad (7.80)$$

$$\Omega_i = \Omega_{i-1} + b_R E_{i-1} + \delta \Omega_i, \quad (7.81)$$

$$T_i = T_{i-1} + b_2 \Omega_{i-1} + b_{2R} E_{i-1} + b_3 + \delta T_i. \quad (7.82)$$

Next we find the variances and cross correlations of $\delta E_i, \delta \Omega_i$ and δT_i . From Eq. (6.57) and (6.58), we can write

$$V_i(z, t) = a_i \exp[i\phi_i - (1 + iC_i)(t - T_i)^2 / 2\tau_i^2], \quad (7.83)$$

$$\frac{\partial V_i}{\partial t} = a_i \exp[i\phi_i - (1 + iC_i)(t - T_i)^2 / 2\tau_i^2] [-(1 + iC_i)(t - T_i) / \tau_i^2]. \quad (7.84)$$

From Eqs. (5.23), (5.25), (6.60), (6.62) and (6.64), in chapters 5 and 6, we already know that for DM soliton the variances of δE , $\delta\Omega$ and δT and the cross correlation of $\delta\Omega$ and δT at the i th amplifier are given by

$$\langle \delta E^2 \rangle_i = 2SE_i, \quad \langle \delta E \rangle_i = S, \quad \langle \delta\Omega^2 \rangle_i = \frac{S(1+C_i^2)}{E_i \tau_i^2} \quad (7.85)$$

$$\langle \delta T^2 \rangle_i = \frac{S}{E_i} \tau_i^2, \quad \langle \delta\Omega \rangle_i = \langle \delta T \rangle_i = 0, \quad \langle \delta T \delta\Omega \rangle_i = \frac{S}{E_i} C_i. \quad (7.86)$$

From Eqs. (7.31) and (7.32) we have

$$\langle \delta E \delta\Omega \rangle_i = \frac{iS}{E_i} \int_{-\infty}^{\infty} dt \left[V_i^* \frac{\partial V_i}{\partial t} - V_i \frac{\partial V_i^*}{\partial t} \right], \quad (7.87)$$

$$\langle \delta E \delta T \rangle_i = \frac{2S}{E_i} \int_{-\infty}^{\infty} dt (t - T_i) |V_i|^2. \quad (7.88)$$

Using Eqs. (7.83) and (7.84) in Eqs (7.87) and (7.88), and using Table 4.3, we obtain

$$\langle \delta E \delta\Omega \rangle_i = \frac{S}{E_i} 2a_i^2 \frac{C_i}{\tau_i} \int_{-\infty}^{\infty} dt \frac{(t - T_i)}{\tau_i} \exp[-(t - T_i)^2 / \tau_i^2]$$

$$\langle \delta E \delta\Omega \rangle_i = 0 \quad (7.89)$$

$$\langle \delta E \delta T \rangle_i = \frac{2S}{E_i} a_i^2 \int_{-\infty}^{\infty} dt (t - T_i) \exp[-(t - T_i)^2 / \tau_i^2]$$

$$\langle \delta E \delta T \rangle_i = 0. \quad (7.90)$$

Dropping the subscript i due to periodicity of the DM soliton system we can write the variances and correlations of the fluctuation in energy, position and frequency added by every amplifier as

$$\langle \delta E^2 \rangle = 2SE_0, \quad \langle \delta\Omega \delta E \rangle = 0 \quad \langle \delta E \rangle = S, \quad (7.91)$$

$$\langle \delta\Omega^2 \rangle = \frac{S}{E_0} \frac{(1+C_0^2)}{\tau_0^2} \quad \langle \delta E \delta T \rangle = 0 \quad \langle \delta\Omega \rangle = 0, \quad (7.92)$$

$$\langle \delta T^2 \rangle = \frac{S}{E_0} \tau_0^2 \quad \langle \delta\Omega \delta T \rangle = \frac{S}{E} C_0 \quad \langle \delta T \rangle = 0. \quad (7.93)$$

Using the recurrence relations in Eqs. (7.80)–(7.82), the first moments of E , Ω and T after N such amplifiers are given by

$$\langle E \rangle_N = E_0 + \sum_{i=1}^N \langle \delta E \rangle, \quad (7.94)$$

$$\langle \Omega \rangle_N = b_R \sum_{i=1}^{N-1} \langle E \rangle_i + \sum_{i=1}^N \langle \delta\Omega \rangle, \quad (7.95)$$

$$\langle T \rangle_N = b_2 \sum_{i=1}^{N-1} \Omega_i + b_{2R} \sum_{i=1}^{N-1} E_i + \sum_{i=1}^N b_3 + \sum_{i=1}^N \langle \delta T \rangle. \quad (7.96)$$

Performing the summation using Eqs. (6.27), (6.30) and (7.22) we get

$$\langle E \rangle_N = E_0 + N S, \quad (7.97)$$

$$\langle \Omega \rangle_N = b_R N(N-1) S/2 + N b_R E_0, \quad (7.98)$$

$$\begin{aligned} \langle T \rangle_N &= b_2 b_R N(N-1)(2N-1) S/6 + b_2 b_R N(N-1) S/2 + b_{2R} N(N-1) S/2 + b_{2R} N E_0 \\ &\quad + N b_3. \end{aligned} \quad (7.99)$$

Next we consider the second moments of E , Ω , T and find that they evolve as

$$\langle E^2 \rangle_i = \langle E^2 \rangle_{i-1} + \langle \delta E^2 \rangle_{i-1} + 2 \langle E \rangle_{i-1} \langle \delta E \rangle_i, \quad (7.100)$$

$$\langle E\Omega \rangle_i = \langle E\Omega \rangle_{i-1} + b_R \langle E^2 \rangle_{i-1} + \langle \delta E \delta \Omega \rangle_i, \quad (7.101)$$

$$\langle \Omega^2 \rangle_i = \langle \Omega^2 \rangle_{i-1} + b_R^2 \langle E^2 \rangle_{i-1} + 2b_R \langle E\Omega \rangle_{i-1} + \langle \delta \Omega^2 \rangle_i, \quad (7.102)$$

$$\langle ET \rangle_i = \langle ET \rangle_{i-1} + b_2 \langle E\Omega \rangle_{i-1} + b_{2R} \langle E^2 \rangle_{i-1} + b_3 \langle E \rangle_{i-1} + \langle \delta E \delta T \rangle_i \quad (7.103)$$

$$\begin{aligned} \langle \Omega T \rangle_i &= \langle \Omega T \rangle_{i-1} + b_2 \langle \Omega^2 \rangle_{i-1} + b_{2R} \langle E\Omega \rangle_{i-1} + b_3 \langle \Omega \rangle_{i-1} + b_R \langle ET \rangle_{i-1} \\ &\quad + b_2 b_R \langle E\Omega \rangle_{i-1} + b_{2R} b_R \langle E^2 \rangle_{i-1} + b_3 b_R \langle E \rangle_{i-1} + \langle \delta \Omega \delta T \rangle_i \end{aligned} \quad (7.104)$$

$$\begin{aligned} \langle T^2 \rangle_i &= \langle T^2 \rangle_{i-1} + b_2^2 \langle \Omega^2 \rangle_{i-1} + b_{2R}^2 \langle E^2 \rangle_{i-1} + b_3^2 + \langle \delta T^2 \rangle_i + 2b_2 \langle \Omega T \rangle_{i-1} + 2b_{2R} \langle ET \rangle_{i-1} \\ &\quad + 2b_3 \langle T \rangle_{i-1} + b_2 b_{2R} \langle E\Omega \rangle_{i-1} + 2b_3 b_2 \langle \Omega \rangle_{i-1}. \end{aligned} \quad (7.105)$$

Summing up Eqs. (7.100)–(7.105) over N amplifiers, we get

$$\langle E^2 \rangle_N = \sum_{i=1}^N \langle \delta E^2 \rangle + 2 \sum_{i=1}^N \langle E \rangle_{i-1} \langle \delta E \rangle, \quad (7.106)$$

$$\langle E\Omega \rangle_N = b_R \sum_{i=1}^{N-1} \langle E^2 \rangle_i + \sum_{i=1}^N \langle \delta E \delta \Omega \rangle, \quad (7.107)$$

$$\langle \Omega^2 \rangle_N = b_R^2 \sum_{i=1}^{N-1} \langle E^2 \rangle_i + 2b_R \sum_{i=1}^{N-1} \langle E\Omega \rangle_i + \sum_{i=1}^N \langle \delta \Omega^2 \rangle, \quad (7.108)$$

$$\langle ET \rangle_N = b_2 \sum_{i=1}^{N-1} \langle E\Omega \rangle_i + b_{2R} \sum_{i=1}^{N-1} \langle E^2 \rangle_i + b_3 \sum_{i=1}^{N-1} \langle E \rangle_i + \sum_{i=1}^N \langle \delta E \delta T \rangle \quad (7.109)$$

$$\begin{aligned} \langle \Omega T \rangle_N &= b_2 \sum_{i=1}^{N-1} \langle \Omega^2 \rangle_i + b_{2R} \sum_{i=1}^{N-1} \langle E\Omega \rangle_i + b_3 \sum_{i=1}^{N-1} \langle \Omega \rangle_i + b_R \sum_{i=1}^{N-1} \langle ET \rangle_i \\ &\quad + b_2 b_R \sum_{i=1}^{N-1} \langle E\Omega \rangle_i + b_{2R} b_R \sum_{i=1}^{N-1} \langle E^2 \rangle_i + \sum_{i=1}^N \langle \delta \Omega \delta T \rangle \end{aligned} \quad (7.110)$$

$$\langle T^2 \rangle_N = b_2^2 \sum_{i=1}^{N-1} \langle \Omega^2 \rangle_i + b_{2R}^2 \sum_{i=1}^{N-1} \langle E^2 \rangle_i + \sum_{i=1}^N b_3^2 + \sum_{i=1}^N \langle \delta T^2 \rangle$$

$$\begin{aligned}
 & + 2b_2 \sum_{i=1}^{N-1} \langle \Omega T \rangle_i + 2b_{2R} \sum_{i=1}^{N-1} \langle ET \rangle_i + 2b_3 \sum_{i=1}^{N-1} \langle T \rangle_i \\
 & + b_2 b_{2R} \sum_{i=1}^{N-1} \langle E\Omega \rangle_i + 2b_3 b_2 \sum_{i=1}^{N-1} \langle \Omega \rangle_i.
 \end{aligned} \tag{7.111}$$

Performing the summation using Eqs. (6.51), (7.59), (7.91)–(7.93) and Eqs. (7.97)–(7.99), we finally obtain

$$\langle E^2 \rangle_N = N \langle \delta E^2 \rangle + 2NE_0 \langle \delta E \rangle, \tag{7.112}$$

$$\langle E\Omega \rangle_N = b_R N(N-1)/2 \langle \delta E^2 \rangle + b_R N(N-1)E_0 \langle \delta E \rangle + N \langle \delta E \delta \Omega \rangle, \tag{7.113}$$

$$\begin{aligned}
 \langle \Omega^2 \rangle_N &= b_R^2 \frac{N}{6} (N-1)(2N-1) \langle \delta E^2 \rangle + b_R^2 \frac{N}{3} (N-1)(2N-1)E_0 \langle \delta E \rangle \\
 &+ b_R N(N-1) \langle \delta E \delta \Omega \rangle + N \langle \delta \Omega^2 \rangle,
 \end{aligned} \tag{7.114}$$

$$\begin{aligned}
 \langle ET \rangle_N &= b_2 \frac{N}{2} (N-1) \langle \delta E \delta \Omega \rangle + b_{2R} \frac{N}{2} (N-1) \langle \delta E^2 \rangle + b_R b_2 \frac{N}{12} (N-1)(2N-1) \langle \delta E^2 \rangle \\
 &+ b_3 \frac{N}{2} (N-1)S + N \langle \delta E \delta T \rangle \\
 &= \langle \delta E^2 \rangle \frac{N}{2} (N-1) \left(b_{2R} + b_R b_2 \frac{(2N-1)}{6} \right) + b_3 \frac{N}{2} (N-1)S,
 \end{aligned} \tag{7.115}$$

$$\begin{aligned}
 \langle \Omega T \rangle_N &= b_2 \frac{N}{2} (N-1) \langle \delta \Omega^2 \rangle + \langle \delta E \delta \Omega \rangle \left[b_{2R} \frac{N}{2} (N-1) + b_2 b_R \frac{N}{2} (N-1)^2 \right] \\
 &+ \langle \delta E^2 \rangle \left[b_2 b_R^2 \frac{N}{24} (N-1)(N-2)(3N-1) + b_{2R} b_R \frac{N}{6} (N-1)(2N-1) \right] \\
 &+ b_3 b_R \frac{N}{6} (N-1)(2N-1)S + b_R b_3 N(N-1)E_0 + N \langle \delta \Omega \delta T \rangle, \\
 &= b_2 \frac{N}{2} (N-1) \langle \delta \Omega^2 \rangle + \langle \delta E^2 \rangle \left[b_2 b_R^2 \frac{N}{24} (N-1)(N-2)(3N-1) + b_{2R} b_R \frac{N}{6} (N-1)(2N-1) \right] \\
 &+ b_3 b_R \frac{N}{6} (N-1)(2N-1)S + b_R b_3 N(N-1)E_0 + N \langle \delta \Omega \delta T \rangle,
 \end{aligned} \tag{7.116}$$

$$\begin{aligned}
 \langle T^2 \rangle_N &= b_2^2 \frac{N}{6} (N-1)(2N-1) \langle \delta \Omega^2 \rangle + b_2 N(N-1) \langle \delta \Omega \delta T \rangle + N^2 b_3^2 + N \langle \delta T^2 \rangle \\
 &+ \langle \delta E^2 \rangle \left[b_{2R}^2 \frac{N}{6} (N-1)(2N-1) + b_2 b_{2R} b_R \frac{N}{4} (N-1)^2 (N-2) \right] \\
 &+ b_R^2 b_2^2 \frac{N}{120} (N-1)(6N^3 - 20N^2 + 24N + 1) \left] + 2b_3 b_2 b_R \left[\frac{N}{3} (N-1)(N-2)S \right. \right. \\
 &\left. \left. + \frac{N}{2} (N-1)^2 (N-8)E_0 \right] + b_3 b_{2R} \left[\frac{N}{3} (N-1)(N-2)S + N(N-1)E_0 \right].
 \end{aligned} \tag{7.117}$$

Using Eqs. (7.99) and (7.117) in the definition of the timing jitter we obtain the timing jitter in the case of DM soliton system with periodic amplification and is given by

$$\sigma_t^2 = \sigma_{\text{GH}}^2 + R_1 \langle (\delta E)^2 \rangle + R_2, \tag{7.118}$$

where σ_{GH}^2 is the Gordon-Haus timing jitter evaluated in the previous Chapter and is given by

$$\sigma_{\text{GH}}^2 = \frac{b_2^2}{6}N(N-1)(2N-1)\langle\delta\Omega^2\rangle + b_2N(N-1)\langle\delta\Omega\delta T\rangle + N\langle\delta T^2\rangle, \quad (7.119)$$

and the coefficients R_1 and R_3 are given by

$$R_1 = N(N-1)[b_R^2b_2^2(N^3 - 10N^2 + 29N - 9)/120 + b_2b_Rb_{2R}(19N^2 - 65N + 48)/96 + b_{2R}^2(2N-1)/6], \quad (7.120)$$

$$R_2 = N(N-1)b_3[b_R(N-1)(N-2)/6 + b_{2R}(N-2)/3]S. \quad (7.121)$$

As expected, the leading term in timing jitter is due to RIFS and grows as N^5 whereas the Gordon-Haus term grows as N^3 . The R_2 term gives the jitter due to TOD and Raman effects and becomes important only for pulses much shorter than 1 ps. Comparing Eq. (7.118) to Eq. (7.66), we see that the difference in the form of the expression for timing jitter between the DM and fundamental soliton cases is the presence of the N^2 term in the Gordon-Haus timing jitter in the case of DM soliton. This is because the input pulses are chirped in the case of DM solitons. Also the coefficients b_2 , b_3 , b_R and b_{2R} used in the timing jitter expressions depends on the evolution of the pulse width along the fiber and the local dispersion in the DM soliton case. Hence they will have to be calculated numerically using the moment equation for the pulse width for DM solitons.

To show the importance of the Raman jitter for lightwave systems, we consider a dispersion-managed system capable of operating at 160 Gb/s. The use of dense dispersion-management is essential at such high bit rates [62]. The dispersion map consists of 1.0 km of anomalous-GVD fiber with $D = 2.5$ ps/(km-nm) and 1.0 km of normal-GVD fiber with $D = -2.35$ ps/(km-nm). Each fiber section is assumed to have an effective area of $54 \mu\text{m}^2$, losses of 0.2 dB/km, $T_R = 3$ fs, and $\beta_3 = 0$. Optical amplifiers are spaced 40 km apart ($L_A = 40$ km, $L_m = 2$ km). The spectral noise density was calculated using $n_{sp} = 1.3$. The input Gaussian pulse parameters were found using the periodicity conditions for solitons on the moment equations for energy, pulse width and chirp, and have values $\tau_0 = 1.25$ ps, $C_0 = 1$ and $E_0 = 0.12$ pJ. Figure 7.3 shows the dependence of the timing jitter as a function of distance. The dashed line shows the contribution of Gordon-Haus jitter obtained from Eq. (7.119). The sum of the Raman and Gordon-Haus jitters is given by the solid line. The dots show the timing jitter including the effects of Raman jitter, Gordon-Haus jitter and TOD. Since the Raman contributions from RIFS begin to dominate the jitter after 500 km, it

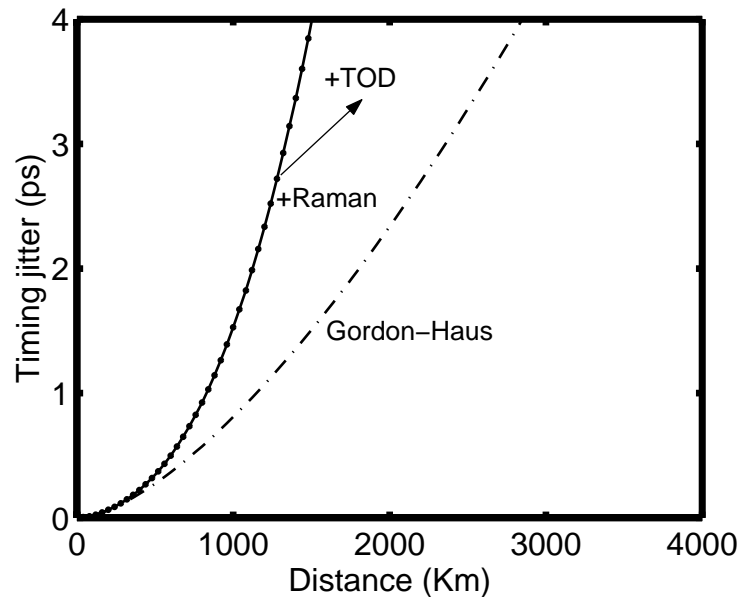


Figure 7.3: Timing jitter for a 160 Gb/s system using DM soliton with average dispersion $D_{av} = 0.1275$ ps/(km-nm).

is evident that the system performance is mainly limited by the Raman-induced frequency shift at high bit rates.

7.2 Non-soliton Systems

Next we consider the case of non-soliton systems. In non-soliton systems, input pulses are pre-chirped but they do not follow a periodic evolution pattern. In general, the chirp and the pulse width cannot be calculated analytically because of the nonlinear effects. However, in quasi-linear links in which the GVD of each fiber section is so large that the pulse spreads over several bit slots, the pulse evolution is nearly linear along the DM link. The chirp and the pulse width of the pulses as a function of distance can then be found analytically as shown in Chapter 6. Since the non-soliton system is not periodic, C and τ have different values at different amplifiers. This feature complicates the calculation somewhat but the procedure is straightforward. At the i th amplifier, the chirp and the pulse width can then be written from Eq. (6.78) as

$$C_i = C_0 + ib_2 \frac{(1 + C_0^2)}{\tau_0^2} \quad (7.122)$$

$$\tau_i^2 = \tau_0^2 \left[(1 + C_0^2) + 2iC_0 \frac{b_2}{\tau_0^2} + i^2 \frac{b_2^2}{\tau_0^4} \right]. \quad (7.123)$$

Also from Eq. (6.77) we know that the quantity $(1 + C^2)/\tau^2$ remains constant during propagation. Since at the transmitter end the pulse is unchirped, $(1 + C^2)/\tau^2 = (1 + C_0^2)/\tau_0^2 = 1/\tau_0^2$. At the end of each amplifier the energy of the pulse takes its initial value E_0 . Using all these in Eqs. (7.91)–(7.93) we can write the variances and correlations of the fluctuation in energy, position and frequency added by the i th amplifier as

$$\langle \delta E^2 \rangle_i = 2SE_0, \quad \langle \delta \Omega \delta E \rangle_i = 0 \quad \langle \delta E \rangle_i = S, \quad (7.124)$$

$$\langle \delta \Omega^2 \rangle_i = \frac{S}{E_0} \frac{1}{\tau_0^2} \quad \langle \delta E \delta T \rangle_i = 0 \quad \langle \delta \Omega \rangle_i = 0, \quad (7.125)$$

$$\langle \delta T^2 \rangle_i = \frac{S}{E_0} \tau_0^2 \left[(1 + C_0^2) + 2iC_0 \frac{b_2}{\tau_0^2} + i^2 \frac{b_2^2}{\tau_0^4} \right] \quad \langle \delta T \rangle_i = 0,$$

$$\langle \delta \Omega \delta T \rangle_i = \frac{S}{E} \left[C_0 + ib_2 \frac{(1 + C_0^2)}{\tau_0^2} \right]. \quad (7.126)$$

Using the recurrence relations in Eqs. (7.80)–(7.82), the first moments of E , Ω and T after N such amplifiers are given by

$$\langle E \rangle_N = E_0 + \sum_{i=1}^N \langle \delta E \rangle_i, \quad (7.127)$$

$$\langle \Omega \rangle_N = b_R \sum_{i=1}^{N-1} \langle E \rangle_i + \sum_{i=1}^N \langle \delta \Omega \rangle_i, \quad (7.128)$$

$$\langle T \rangle_N = b_2 \sum_{i=1}^{N-1} \Omega_i + b_{2R} \sum_{i=1}^{N-1} E_i + \sum_{i=1}^N b_3 + \sum_{i=1}^N \langle \delta T \rangle_i. \quad (7.129)$$

Performing the summation using Eqs. (6.27), (6.30) and (7.22) we get

$$\langle E \rangle_N = E_0 + N S, \quad (7.130)$$

$$\langle \Omega \rangle_N = b_R N(N-1) S/2 + N b_R E_0, \quad (7.131)$$

$$\langle T \rangle_N = b_2 b_R N(N-1)(2N-1) S/6 + b_2 b_R N(N-1) S/2 + b_{2R} N(N-1) S/2 + b_{2R} N E_0 + N b_3. \quad (7.132)$$

Next we consider the second moments and find that

$$\langle E^2 \rangle_i = \langle E^2 \rangle_{i-1} + \langle \delta E^2 \rangle_{i-1} + 2 \langle E \rangle_{i-1} \langle \delta E \rangle_i, \quad (7.133)$$

$$\langle E\Omega \rangle_i = \langle E\Omega \rangle_{i-1} + b_R \langle E^2 \rangle_{i-1} + \langle \delta E \delta \Omega \rangle_i, \quad (7.134)$$

$$\langle \Omega^2 \rangle_i = \langle \Omega^2 \rangle_{i-1} + b_R^2 \langle E^2 \rangle_{i-1} + 2b_R \langle E\Omega \rangle_{i-1} + \langle \delta \Omega^2 \rangle_i, \quad (7.135)$$

$$\langle ET \rangle_i = \langle ET \rangle_{i-1} + b_2 \langle E\Omega \rangle_{i-1} + b_{2R} \langle E^2 \rangle_{i-1} + b_3 \langle E \rangle_{i-1} + \langle \delta E \delta T \rangle_i \quad (7.136)$$

$$\begin{aligned} \langle \Omega T \rangle_i &= \langle \Omega T \rangle_{i-1} + b_2 \langle \Omega^2 \rangle_{i-1} + b_{2R} \langle E\Omega \rangle_{i-1} + b_3 \langle \Omega \rangle_{i-1} + b_R \langle ET \rangle_{i-1} \\ &\quad + b_2 b_R \langle E\Omega \rangle_{i-1} + b_{2R} b_R \langle E^2 \rangle_{i-1} + b_3 b_R \langle E \rangle_{i-1} + \langle \delta \Omega \delta T \rangle_i \end{aligned} \quad (7.137)$$

$$\begin{aligned} \langle T \rangle_i &= \langle T \rangle_{i-1} + b_2^2 \langle \Omega^2 \rangle_{i-1} + b_{2R}^2 \langle E^2 \rangle_{i-1} + b_3^2 + \langle \delta T^2 \rangle_i + 2b_2 \langle \Omega T \rangle_{i-1} + 2b_{2R} \langle ET \rangle_{i-1} \\ &\quad + 2b_3 \langle T \rangle_{i-1} + b_2 b_{2R} \langle E\Omega \rangle_{i-1} + 2b_3 b_2 \langle \Omega \rangle_{i-1}. \end{aligned} \quad (7.138)$$

Summing over N such amplifiers we get

$$\langle E^2 \rangle_N = \sum_{i=1}^N \langle \delta E^2 \rangle_i + 2 \sum_{i=1}^N \langle E \rangle_{i-1} \langle \delta E \rangle_i, \quad (7.139)$$

$$\langle E\Omega \rangle_N = b_R \sum_{i=1}^{N-1} \langle E^2 \rangle_i + \sum_{i=1}^N \langle \delta E \delta \Omega \rangle_i, \quad (7.140)$$

$$\langle \Omega^2 \rangle_N = b_R^2 \sum_{i=1}^{N-1} \langle E^2 \rangle_i + 2b_R \sum_{i=1}^{N-1} \langle E\Omega \rangle_i + \sum_{i=1}^N \langle \delta \Omega^2 \rangle_i, \quad (7.141)$$

$$\langle ET \rangle_N = b_2 \sum_{i=1}^{N-1} \langle E\Omega \rangle_i + b_{2R} \sum_{i=1}^{N-1} \langle E^2 \rangle_i + b_3 \sum_{i=1}^{N-1} \langle E \rangle_i + \sum_{i=1}^N \langle \delta E \delta T \rangle_i \quad (7.142)$$

$$\begin{aligned} \langle \Omega T \rangle_N &= b_2 \sum_{i=1}^{N-1} \langle \Omega^2 \rangle_i + b_{2R} \sum_{i=1}^{N-1} \langle E\Omega \rangle_i + b_3 \sum_{i=1}^{N-1} \langle \Omega \rangle_i + b_R \sum_{i=1}^{N-1} \langle ET \rangle_i \\ &\quad + b_2 b_R \sum_{i=1}^{N-1} \langle E\Omega \rangle_i + b_{2R} b_R \sum_{i=1}^{N-1} \langle E^2 \rangle_i + \sum_{i=1}^N \langle \delta \Omega \delta T \rangle_i \end{aligned} \quad (7.143)$$

$$\begin{aligned} \langle T^2 \rangle_N &= b_2^2 \sum_{i=1}^{N-1} \langle \Omega^2 \rangle_i + b_{2R}^2 \sum_{i=1}^{N-1} \langle E^2 \rangle_i + \sum_{i=1}^N b_3^2 + \sum_{i=1}^N \langle \delta T^2 \rangle_i \\ &\quad + 2b_2 \sum_{i=1}^{N-1} \langle \Omega T \rangle_i + 2b_{2R} \sum_{i=1}^{N-1} \langle ET \rangle_i + 2b_3 \sum_{i=1}^{N-1} \langle T \rangle_i \\ &\quad + b_2 b_{2R} \sum_{i=1}^{N-1} \langle E\Omega \rangle_i + 2b_3 b_2 \sum_{i=1}^{N-1} \langle \Omega \rangle_i. \end{aligned} \quad (7.144)$$

Performing the summation using Eqs. (6.51), (7.59), (7.130)–(7.132) and Eqs. (7.124)–(7.126)

we finally obtain

$$\langle E^2 \rangle_N = 4NSE_0 \quad (7.145)$$

$$\langle E\Omega \rangle_N = b_R N(N-1)(2SE_0), \quad (7.146)$$

$$\langle \Omega^2 \rangle_N = b_R^2 \frac{N}{3} (N-1)(2N-1)(2SE_0) + N \frac{S}{E_0} \frac{1}{\tau_0^2}, \quad (7.147)$$

$$\begin{aligned} \langle ET \rangle_N &= b_{2R} \frac{N}{2} (N-1)(2SE_0) + b_R b_2 \frac{N}{12} (N-1)(2N-1)(2SE_0) + b_3 \frac{N}{2} (N-1)S \\ &= (2SE_0) \frac{N}{2} (N-1) \left(b_{2R} + b_R b_2 \frac{(2N-1)}{6} \right) + b_3 \frac{N}{2} (N-1)S, \end{aligned} \quad (7.148)$$

$$\begin{aligned} \langle \Omega T \rangle_N &= b_2 \frac{N}{2} (N-1) \frac{S}{E_0} \frac{1}{\tau_0^2} + (2SE_0) \left[b_2 b_R^2 \frac{N}{24} (N-1)(N-2)(3N-1) + b_{2R} b_R \frac{N}{6} (N-1)(2N-1) \right] \\ &\quad + b_3 b_R \frac{N}{6} (N-1)(2N-1)S + b_R b_3 N(N-1)E_0 + \frac{b_2}{2} N(N+1) \frac{S}{E_0} \frac{(1+C_0^2)}{\tau_0^2} + N \frac{SC_0}{E_0}, \end{aligned} \quad (7.149)$$

$$\begin{aligned} \langle T^2 \rangle_N &= b_2^2 \frac{N}{6} (N-1)(2N-1) \frac{S}{E_0} \frac{1}{\tau_0^2} + N \frac{S}{E_0} \frac{1+C_0^2}{\tau_0^2} + 2b_2 \frac{SC_0}{E_0} \left[\frac{N}{2} (N-1) \right. \\ &\quad \left. + \frac{N}{2} (N+1) \right] + \frac{S}{E_0} \frac{b_2^2}{\tau_0^2} \left[\frac{N}{6} (N+1)(2N+1) + \frac{N}{6} (N-1)(2N-1) + \frac{N}{2} (N-1) \right] + N^2 b_3^2 \\ &\quad + (2SE_0) \left[b_{2R}^2 \frac{N}{6} (N-1)(2N-1) + b_2 b_{2R} b_R \frac{N}{4} (N-1)^2 (N-2) \right. \\ &\quad \left. + b_R^2 b_2^2 \frac{N}{120} (N-1)(6N^3 - 20N^2 + 24N + 1) \right] + 2b_3 b_2 b_R \left[\frac{N}{3} (N-1)(N-2)S \right. \\ &\quad \left. + \frac{N}{2} (N-1)^2 (N-8)E_0 \right] + b_3 b_{2R} \left[\frac{N}{3} (N-1)(N-2)S + N(N-1)E_0 \right]. \\ &= \frac{S}{E_0} \tau_0^2 N \left[1 + \left(C_0 + \frac{b_2 N}{\tau_0^2} \right)^2 \right] + (2SE_0) \left[b_{2R}^2 \frac{N}{6} (N-1)(2N-1) + b_2 b_{2R} b_R \frac{N}{4} (N-1)^2 (N-2) \right. \\ &\quad \left. + b_R^2 b_2^2 \frac{N}{120} (N-1)(6N^3 - 20N^2 + 24N + 1) \right] + N^2 b_3^2 + 2b_3 b_2 b_R \left[\frac{N}{3} (N-1)(N-2)S \right. \\ &\quad \left. + \frac{N}{2} (N-1)^2 (N-8)E_0 \right] + b_3 b_{2R} \left[\frac{N}{3} (N-1)(N-2)S + N(N-1)E_0 \right]. \end{aligned} \quad (7.150)$$

Using Eqs. (7.132) and (7.150) in the definition of the timing jitter we obtain the timing jitter in the case of the non-soliton system to be

$$\sigma_t^2 = \sigma_{\text{GH}}^2 + R_1(2SE_0) + R_2, \quad (7.151)$$

where σ_{GH}^2 is the Gordon-Haus timing jitter evaluated in the previous Chapter and is given by

$$\sigma_{\text{GH}}^2 = \frac{S}{E_0} \tau_0^2 N \left[1 + \left(C_0 + \frac{b_2 N}{\tau_0^2} \right)^2 \right], \quad (7.152)$$

and the coefficients R_1 and R_3 are given by

$$R_1 = N(N-1)[b_R^2 b_2^2 (N^3 - 10N^2 + 29N - 9)/120$$

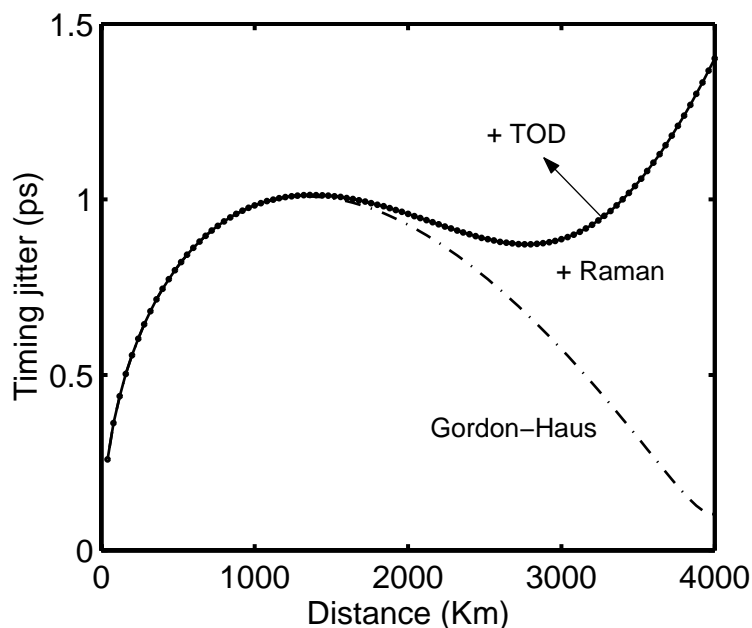


Figure 7.4: Timing jitter for a 160 Gb/s nonsoliton system with average dispersion $D_{av} = 0.04$ ps/(km-nm).

$$+b_2b_Rb_{2R}(19N^2 - 65N + 48)/96 + b_{2R}^2(2N - 1)/6], \quad (7.153)$$

$$R_2 = N(N - 1)b_3\left[b_R\frac{(N - 1)}{6}(N - 2) + b_{2R}\frac{(N - 2)}{3}\right]S. \quad (7.154)$$

Similar to the soliton case, the leading term in the timing jitter in non-soliton systems is due to RIFS and grows as N^5 while the Gordon-Haus term grows as N^3 . The TOD and Raman effects are given by the R_2 term. Eqs. (7.151) and (7.152) show that both Raman and Gordon-Haus jitter depends on the average dispersion of the system. Since non-soliton system can have nearly zero average dispersion, the timing jitter in the case of non-soliton systems can be reduced considerably compared to the soliton systems. Since in the case of non-soliton systems, the initial chirp of the pulse does not have to satisfy the periodicity condition, it can be chosen in such a way as to reduce the timing jitter of the system. This is called the pre-compensation technique. The next Chapter gives a detail account of different compensation techniques that can help reduce timing jitter. Even though this might help reduce Gordon-Haus jitter, this does not help reduce Raman jitter and the system is soon limited by Raman jitter.

As a numerical example we consider a non-soliton system capable of operating at 160 Gb/s using dense dispersion-management. The dispersion map is same as the one used for the DM system in Figure 7.3. The average dispersion of the system is reduced to $\beta_{av} = 0.05$ ps²/km by

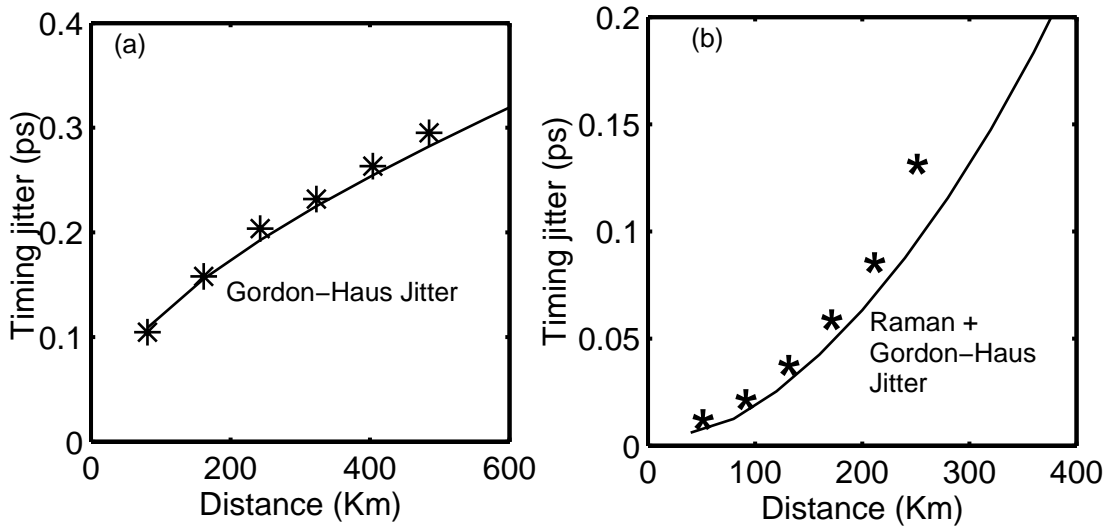


Figure 7.5: (a) Gordon-Haus timing jitter for a 10 Gb/s DM soliton system with average dispersion $D_{av} = 0.04$ ps/(km-nm). (b) Timing jitter for a 160 Gb/s DM system with average dispersion $D_{av} = 0.1275$ ps/(km-nm).

changing the dispersion of the normal-GVD fiber to be $D = -2.4$ ps/(km-nm). The parameters are also the same except that the initial chirp is chosen in such a way that it compensates the total accumulated dispersion along the fiber length, i.e., $C_0 = b_2 N / \tau_0^2$. This is called pre-compensation, which will be discussed in the next Chapter. Figure 7.4 shows the dependence of the timing jitter as a function of distance. The dashed line shows the contribution of Gordon-Haus jitter obtained from Eq. (7.152). The sum of Raman jitter and Gordon-Haus jitter is given by the solid line. The dotted line shows the timing jitter including the effects of Raman jitter, Gordon-Haus jitter and TOD. The Gordon-Haus timing jitter is reduced to a very low value due to the pre-compensation. However the Raman jitter still dominates the timing jitter thus limiting the non-soliton system.

7.3 Numerical Results

In this section we compare the results obtained in the previous sections with the results of numerical simulation obtained by solving the NLS equation Eq. (7.1) using the split-step fourier method. We first consider a 10-Gb/s dispersion-managed system with 10.5 km of anomalous-GVD fiber with $D = 4$ ps/(km-nm) and 9.7 km of normal-GVD fiber with $D = -4$ ps/(km-nm). Each fiber section has a loss of 0.2 dB/km, and effective area of $55 \mu\text{m}^2$. The amplifiers spacing is 80.8-km. The

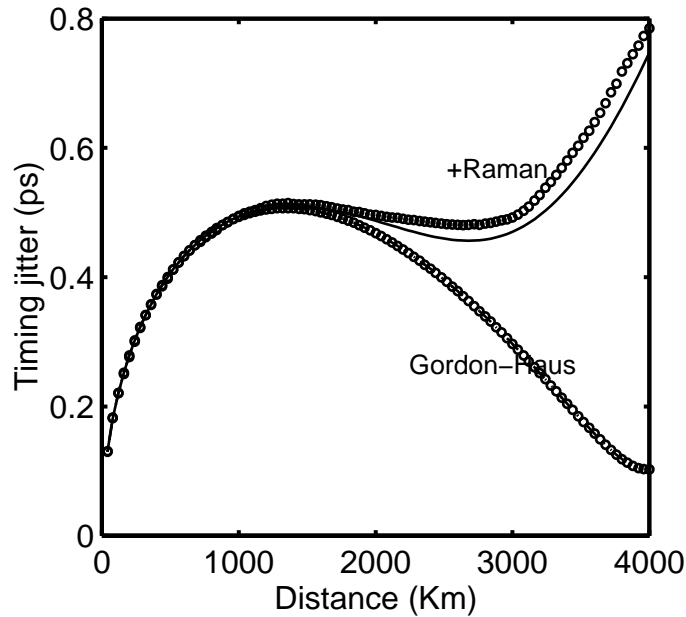


Figure 7.6: Timing jitter for a 160 Gb/s non-soliton system with average dispersion $D_{av} = 0.04$ ps/(km-nm).

spectral noise density was calculated using $n_{sp} = 1.3$. Since at this bit rate the effects of Raman jitter can be neglected, Figure 7.5(a) shows the timing jitter obtained by numerical simulation without the Raman contribution by asterisks and results for Gordon-Haus timing jitter from Eq. (7.119) by solid line. The timing jitter calculated from Eq. (7.119) closely agrees with those obtained by solving NLS using the split-step Fourier method.

Next, to verify the results obtained for Raman jitter, we consider the same DM system as the one used to obtain Figure 7.3. We compare the analytical results obtained in equation Eq. (7.118) to the results obtained through numerical simulations in Figure 7.5(b). The “stars” show the results of numerical simulation including the Raman term and the solid line represents the sum of Raman jitter and Gordon-Haus jitter obtained from the analytical results. The numerical simulation shows larger value of jitter than predicted by the above equations as the distance increases. This is due to the jitter induced by intra-channel cross phase modulation which is not considered in the above analysis.

We finally verify the results obtained for non-soliton systems in the previous section. Since the nonlinearity is negligible, the numerical analysis of these systems are fairly simple and we use ordinary differential equation (ODE) solvers to solve the moment equations Eqs. (7.70)–(7.72) to

calculate timing jitter directly. Figure 7.6 shows the results obtained through numerical simulation for the same non-soliton system as the one used for Figure 7.4 in dotted lines and the results of Eqs. (7.152) and (7.153) in solid and dashed line respectively. The figures shows that numerical simulation agrees perfectly with the theoretical result for Gordon-Haus jitter. However they show larger jitter than one predicted for Raman jitter. This discrepancy is due to the jitter induced by the higher order terms which are not considered in the above analysis.

7.4 Chapter Summary

In this Chapter we have derived an analytical expression for Raman-induced timing jitter in high-speed DM lightwave systems using the moment method. We have applied the general formalism to three types of lightwave systems corresponding to the use of DM solitons, fundamental solitons in DDFs, and CRZ pulses in a quasi-linear configuration. We were able to obtain simple analytic expressions for the timing jitter in each case. We compared the three configurations for a 160-Gb/s system and found that Raman jitter increases with the number, N of amplifiers as N^5 . Unlike Gordon-Haus jitter the Raman jitter is directly proportional to the pulse energy and hence increases with increased pulse energy.

The Raman jitter begins to dominate after 500 km in the case of DM solitons. In the case of fundamental solitons propagating inside DDFs, the Raman contribution can be made smaller by using a reduced pulse energy but the jitter is quite large. In the case of quasi-linear non-soliton systems, the Raman jitter dominates at large distance but can be reduced by reducing the average dispersion close to zero. In all cases, jitter can exceed the acceptable value (about 0.5 ps for 8% of the bit slot) after 1000 km or so, indicating that such systems cannot be operated over long distances unless a jitter-reduction scheme is implemented. Our expression of the timing jitter can be used in the case of dense dispersion management realized using multiple map periods between two neighboring amplifiers. We have included the effects of third-order dispersion as well in our analysis.

We have checked the accuracy of this calculation using numerical simulations. In the case of DM soliton systems, we verify our results by solving the NLS using split-step Fourier method and for non-soliton systems we use ODE solvers to verify our calculations. In both cases the

numerical simulations agree well with the analytical results. The minor discrepancies in the case of DM solitons is because of the additional timing jitter due to intra-channel interactions between the pulses. In the case of non-soliton systems the higher-order terms which were neglected during our analysis can cause additional jitter leading to increased jitter in the numerical simulations.

Chapter 8

Control of Timing Jitter

In previous chapters we have seen that the timing jitter ultimately limits the performance of all long-haul communications systems. It is essential to find a solution that can control the growth of timing-jitter in order to improve the system performance. The use of optical filters for controlling timing jitter of solitons was proposed as early as 1991 [63]–[65]. This approach makes use of the fact that ASE occurs over the entire bandwidth of the amplifier but the soliton spectrum occupies only a small fraction of it. The bandwidth of the filter is chosen such that the soliton bit stream passes through the filter but most of the ASE is blocked. If the optical filter is placed after each amplifier, it improves the SNR because of reduced ASE and also reduces timing jitter simultaneously. This was verified in an experiment in 1991 but the reduction was only 50% [64]. The moment method can be used to show that the use of filters after every amplifier can reduce timing jitter [66]. The filter technique can be improved dramatically by allowing the center frequency of the successive optical filters to slide slowly along the link. Such sliding-frequency filters avoid accumulation of ASE within the filter bandwidth and at the same time, reduce the growth of timing jitter [67]. As the filter passband shifts, solitons shift their spectrum as well to minimize filter induced losses while the spectrum of ASE cannot change. The net result is that the ASE noise that accumulated over a few amplifiers is filtered out when the soliton has shifted by more than its own bandwidth.

The filter technique improves the performance of the soliton systems. The two drawbacks of the filter technique are that it requires the input pulses to be solitons and that the optical filters have

to be placed after every amplifier and the filter introduces an additional loss for the soliton that should be compensated by increasing the gain of the amplifier. Hence, it becomes essential to find a simpler method which, can work for both soliton and non-soliton systems. In this Chapter we discuss two such methods. In the first section we discuss various dispersion compensation techniques in which timing jitter can be reduced by compensating for the total accumulated dispersion in the system [68]. We show that this technique works for both soliton and non-soliton systems. In the final section we show that using parametric amplifiers in place of erbium doped fiber amplifiers (EDFAs), can reduce not only Gordon-Haus timing jitter but also Raman jitter in both soliton and non-soliton systems.

8.1 Compensation Techniques

The dispersion compensation technique is a simple approach to reduce timing jitter in communication systems. From Chapter 6 we have seen that the Gordon-Haus jitter depends on the total accumulated GVD over the total length of the fiber. We can see from Eqs. (6.55), (6.72), (6.89), that for fundamental solitons in DDFs, DM solitons and non-solitons respectively, that the cubic term that dominates timing jitter at long distances depends on the accumulated GVD through the factor b_2 defined as $\int_0^{L_A} \beta_2 dz$. In the dispersion compensation technique, a fiber is added at the beginning of the system, or at the end of the system, or a combination of both, such that it reduces the accumulated GVD, thus reducing the timing jitter.

8.1.1 Soliton Systems

In soliton systems, a post-compensating fiber can be added at the end of the fiber link such that it reduces the accumulated GVD in the fiber link. Using the moment method we can find the contribution of the post-compensating fiber to the timing jitter. In order to do that, we assume that the post-compensation fiber is of length L_c and has a GVD coefficient β_{2c} . If before the post-compensation fiber, the frequency and the position of the pulse is given by Ω_N and T_N , from Eqs. (6.10) and (6.11), we can write the frequency and the position after the post-compensation

fiber as

$$\Omega_c = \Omega_N, \quad (8.1)$$

$$T_c = T_N + b_c \Omega_N, \quad (8.2)$$

where $b_c = \int_0^{L_c} \beta_{2c} dz$. The variances of Ω_c and T_c are given by

$$\langle \Omega_c^2 \rangle = \langle \Omega^2 \rangle_N, \quad (8.3)$$

$$\langle T_c^2 \rangle = \langle T^2 \rangle_N + b_c^2 \langle \Omega^2 \rangle_N + 2b_c \langle \Omega T \rangle_N. \quad (8.4)$$

Using the above equations and the results for $\langle \Omega^2 \rangle_N$, $\langle \Omega T \rangle_N$ and $\langle T^2 \rangle_N$ obtained in Chapter 6 we can find the timing jitter after the post compensation fiber for both fundamental solitons in DDF and DM solitons.

Fundamental solitons in DDF

For fundamental solitons in DDF we have found the timing jitter after N amplifiers in Chapter 6. Hence using Eqs. (6.52)–(6.54) in Eq. (8.4) we get the variance in position after the post-compensation fiber to be

$$\langle T_c^2 \rangle = N \langle \delta T^2 \rangle + N \langle \delta \Omega^2 \rangle \left[b_c^2 + \frac{b_2^2}{6} (N-1)(2N-1) + b_c b_2 (N-1) \right]. \quad (8.5)$$

Hence the timing jitter after the post compensation is given by

$$\sigma_c^2 = N \langle \delta T^2 \rangle + N \langle \delta \Omega^2 \rangle \left[b_c^2 + \frac{b_2^2}{6} (N-1)(2N-1) + b_c b_2 (N-1) \right]. \quad (8.6)$$

From Eq. (8.6) the leading term in timing jitter is still cubic. If the dispersion of the post-compensation fiber is such that $b_c = -y N b_2$, where y is the fraction of post-compensation, we can write the cubic term in Eq. (8.6) as

$$\sigma_c^2 \approx N^3 b_2^2 \langle \delta \Omega^2 \rangle [y^2 - y + 1/3]. \quad (8.7)$$

From Eq. (8.7) we find that the minimum value of σ_c^2 occurs when

$$\begin{aligned} \frac{d\sigma_c^2}{dy} &= 2y - 1 = 0 \\ y &= 1/2 \end{aligned} \quad (8.8)$$

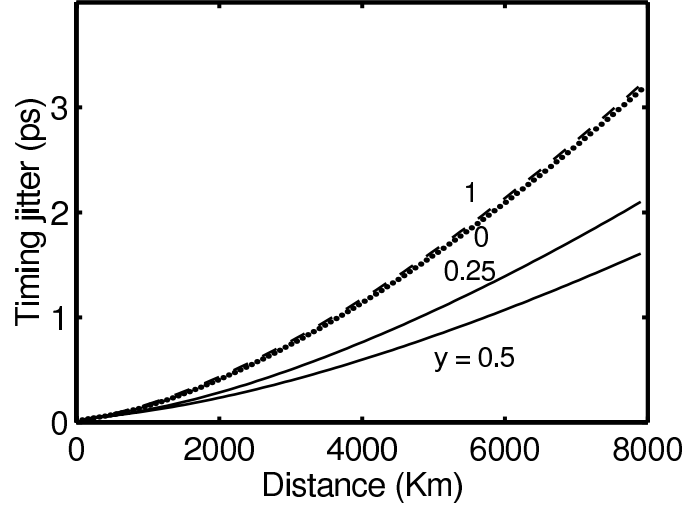


Figure 8.1: Effect of post-compensation on timing jitter of a 10-Gb/s fundamental solitons in DDF system for the same map as Fig. 6.5. Jitter is plotted as a function of transmission distance for 4 values of y representing the fraction of post-compensation.

Thus the minimum timing jitter occurs when one half of the accumulated GVD over the fiber link is compensated, and the minimized Gordon-Haus timing jitter is given by

$$\sigma_c^2 = \langle \delta\Omega^2 \rangle \frac{b_2^2}{6} N [1 + N^2/2] + N \langle \delta T^2 \rangle. \quad (8.9)$$

To study how post-compensation affects timing jitter, we consider the 10-Gb/s soliton systems with the dispersion map used for Fig. 6.5. Figure 8.1 shows changes in timing jitter for several values of y for the case of a single amplifier per map period. In the absence of post-compensation ($y = 0$), jitter becomes quite large with increasing distance (the dotted curve in Fig. 4). Even a small value of post-compensation ($y = 0.25$) reduces jitter considerably. The three most noteworthy features are that (i) jitter can be reduced but cannot be eliminated through post-compensation, (ii) jitter can be minimized with an optimum length of post-compensation fiber ($y = 0.5$), and (iii) 100% post-compensation makes the situation worse compared with no compensation.

An interesting question is whether post-compensation remains an effective technique for reducing the timing jitter even when more than one amplifiers are used in each map period. Figure 8.2 shows the jitter under conditions identical to those of Figure 8.1 except that a second amplifier is placed at a distance of 40 km. The post-compensation reduces the jitter for all values of $0 < y < 1$. Jitter is again minimum when $y = 0.5$. This result shows that post-compensation can reduce timing jitter even when more than one amplifier is used per map period.

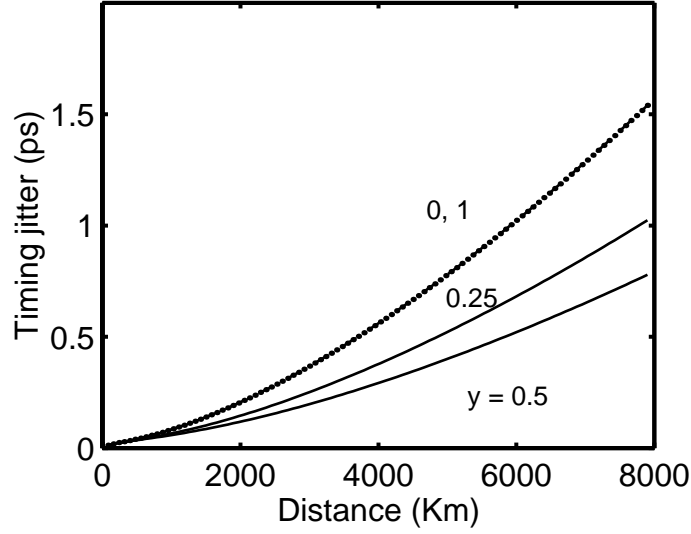


Figure 8.2: Same as Fig. 8.1, except a second amplifier is placed at 40 km.

Dispersion-managed solitons

In the case of DM solitons the timing jitter after N amplifiers can be written from Eq. (6.71) in Chapter 6. Hence using Eqs. (6.69)–(6.71) in Eq. (8.4) we get the timing jitter after the post-compensation fiber to be

$$\begin{aligned} \sigma_c^2 = & N\langle\delta T^2\rangle + N\langle\delta\Omega\delta T\rangle[b_2(N-1) + 2b_c] \\ & + N\langle\delta\Omega^2\rangle\left[\frac{b_2^2}{6}(N-1)(2N-1) + b_c^2 + b_cb_2(N-1)\right] \end{aligned} \quad (8.10)$$

From Eq. (8.10) the leading term in timing jitter is still cubic. If the dispersion of the post-compensation fiber is such that $b_c = -yNb_2$, where y is the fraction of post-compensation, we can write the cubic term in Eq. (8.10) as

$$\sigma_c^2 \approx N^3b_2^2\langle\delta\Omega^2\rangle[y^2 - y + 1/3]. \quad (8.11)$$

From Eq. (8.11) we find that the minimum value of σ_c^2 occurs when

$$\begin{aligned} \frac{d\sigma_c^2}{dy} = 2y - 1 = 0 \\ y = 1/2, \end{aligned} \quad (8.12)$$

and the minimized Gordon-Haus timing jitter can be written from Eq. (8.10) as

$$\sigma_c^2 = \langle\delta\Omega^2\rangle\frac{b_2^2}{6}N[1 + N^2/2] + N\langle\delta T^2\rangle - b_2N\langle\delta\Omega\delta T\rangle. \quad (8.13)$$

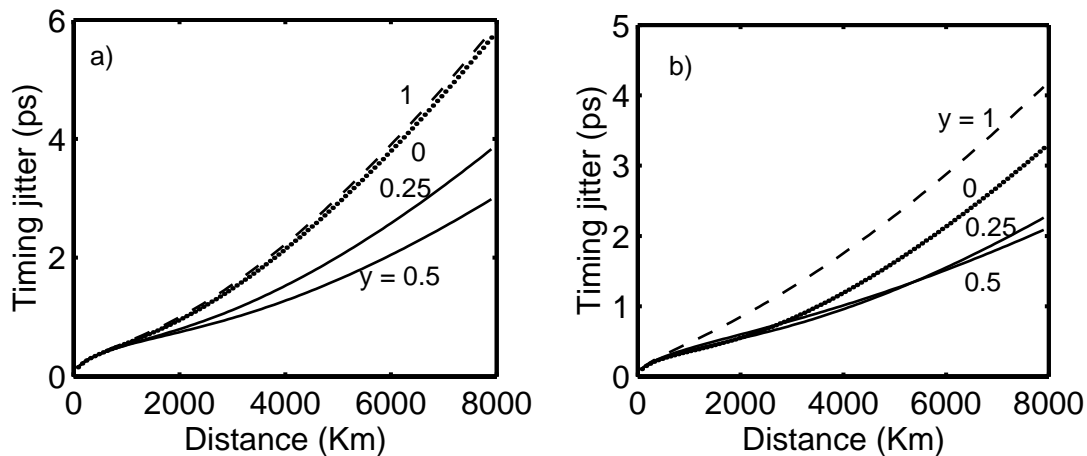


Figure 8.3: a) Effect of post-compensation on timing jitter of a 10-Gb/s DM soliton system for the same map as Fig. 6.3. Jitter is plotted as a function of transmission distance for 4 values of y representing the fraction of post-compensation. b) a second amplifier is placed at a distance of 35 km.

In order to show that post-compensation can reduce timing jitter for DM solitons, we consider the 10-Gb/s DM soliton systems with the dispersion map used for Fig. 6.3. Figure 8.3 shows changes in timing jitter for several values of y for the case of a) a single amplifier per map period and b) when a second amplifier is placed at 35 km. In the absence of post-compensation ($y = 0$), jitter becomes quite large with increasing distance (the dotted curve in Fig. 8.3). However post-compensation can help reduce the jitter. The jitter can be minimized with an optimum length of post-compensation fiber such that $y = 0.5$.

To see if these results hold even when the system has a larger map strength, we consider the DM system with the same dispersion map as the one used for Fig. 6.4. Figure 8.4 shows the jitter under conditions identical to those of Figure 8.3 for the same system as the one used for figure 6.4 except that a post-compensating fiber is added. For the case when there is one amplifier per map period the optimum compensation still remains 50%. When $y = -0.5$, the jitter is much worse than even when there is 100% post-compensation when the distances are more than 2500 km. This is because the term that depends on N^2 in Eq. (8.10) also contributes significantly to the timing jitter for moderate distances before the cubic term takes over, whereas the relation in Eq. (8.11) is based on the cubic term. This shows that one can reduce timing jitter whether the average dispersion in the system is positive or negative by choosing the dispersion of the post-compensation fiber accordingly.

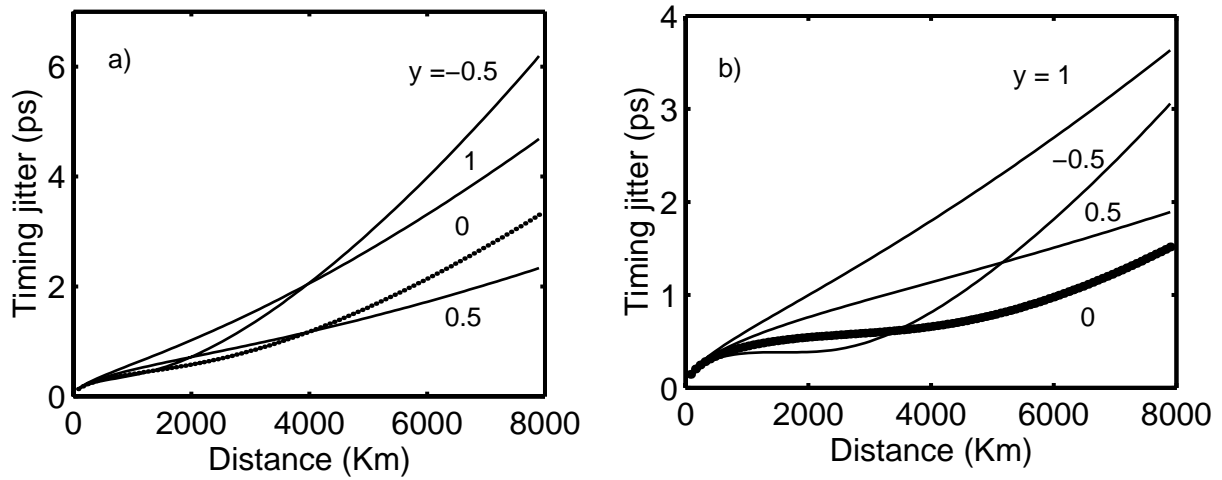


Figure 8.4: a) Effect of post-compensation on timing jitter of a 10-Gb/s DM soliton system for the same map as Fig. 6.4. Jitter is plotted as a function of transmission distance for 4 values of y representing the fraction of post-compensation. b) a second amplifier is placed at a distance of 24 km.

Next consider the situation shown in Figure 8.4(b) when a second amplifier is placed at 24 km. The jitter gets much worse for all positive values of y and for distances up to 5000 km. The lowest value of timing jitter is achieved for negative values of y . The reason for this is again related to the quadratic term in the timing jitter, which in the case of DM systems using multiple amplifiers per map period is given by the Q term from Eq. (6.105). Hence we conclude that the contribution of the Q term can be cancelled under some conditions by the use of negative values of the post-compensation parameter y . The optimum value of y is now given by $y = 0.5 + Q/(PNb_2)$. Thus we see that the optimum y in the case of multiple amplifiers depends on the ratio of the P and Q terms given by Eqs. (6.96) and (6.97). These results suggest that even though post-compensation helps reduce timing jitter, the role of post-compensation requires a careful analysis when multiple amplifiers are used in each map period.

8.1.2 Non-soliton Systems

Unlike soliton systems, the chirp of the non-soliton pulse does not satisfy any periodicity condition. Hence the chirp of these pulses can be chosen in such a way as to reduce timing jitter. Thus for non-soliton systems, the pre-chirp fiber can also act as the pre-compensation fiber. Such a non-soliton system consists of a pre-chirp (pre-compensation) fiber, the fiber link and a post-compensation

fiber. The effect of the post-compensation fiber can be found again using the moment method. Using Eqs. (6.86)–(6.88) in Eq. (8.4) we get the timing jitter after the post-compensation fiber to be

$$\begin{aligned}\sigma_c^2 &= \frac{S}{E_0} N \tau_0^2 \left[1 + \left(C_0 + \frac{b_2 N}{\tau_0^2} \right)^2 \right] + \frac{S}{E_0} N \frac{b_c^2}{\tau_0^2} + 2 \frac{S}{E_0} N b_c \left[N \frac{b_2}{\tau_0^2} + C_0 \right] \\ \sigma_c^2 &= \frac{S}{E_0} N \tau_0^2 \left[1 + \left(C_0 + \frac{b_c}{\tau_0^2} + \frac{b_2 N}{\tau_0^2} \right)^2 \right].\end{aligned}\quad (8.14)$$

From Eq. (8.14) we see that the cubic term in timing jitter can be completely cancelled if

$$C_0 + D + \frac{b_2 N}{\tau_0^2} = 0, \quad (8.15)$$

where $D = b_c/\tau_0^2$. This can be achieved by three ways we can make 1) $D = 0$ and $C_0 = b_2 N/\tau_0^2$ which is complete pre-compensation, 2) $C_0 = 0$ and $D = b_2 N/\tau_0^2$ which is complete post-compensation and 3) $D + C_0 = b_2 N/\tau_0^2$ which is a combination of both.

Any of these three compensation techniques will give minimum jitter at the receiver end which is linear in distance instead of cubic and is given by

$$\sigma_c^2 = \frac{S}{E_0} N \tau_0^2. \quad (8.16)$$

Although the final timing jitter does not depend on the fraction of pre- or post compensation, the timing jitter within the system does. At the receiver end of the non-soliton system, it does not matter how C_0 and D are chosen as long as $C_0 + D = -Nb_2/\tau_0^2$. However, in order to minimize the effects of interaction between neighbouring pulses within the channel during propagation, the timing jitter must be kept minimum not just at the receiver end but also within the fiber link. In order to find the optimum compensation technique, we need to find the fraction of pre- and post-compensation required so that the timing jitter both inside the fiber link and at the receiver end are minimum. If x is the fraction of pre-compensation, such that $x = -C_0\tau_0^2/Nb_2$ and y is the fraction of post-compensation such that $y = -D\tau_0^2/Nb_2$, we should find the values of x and y such that the maximum jitter within the fiber link will be equal to the final jitter at the end of the system thus keeping the jitter within small. The jitter within the fiber link after i th amplifier can be written using Eq. (6.89) to be

$$\sigma_i^2 = \frac{S}{E_0} i \tau_0^2 \left[1 + \left(C_0 + \frac{b_2 i}{\tau_0^2} \right)^2 \right]. \quad (8.17)$$

Multiplying and dividing the above equations on both sides by $N^2 b_2^2 / \tau_0^4$ and using the definition of the fraction of pre-compensation, x Eq. (8.17) can be written as

$$\sigma_i^2 = \frac{S}{E_0} N^3 \tau_0^2 \left(\frac{b_2^2}{\tau_0^4} \right) \frac{i}{N} \left[\frac{\tau_0^4}{N^2 b_2^2} + \left(\frac{i}{N} - x \right)^2 \right]. \quad (8.18)$$

Simplifying the above equation by defining $z = i/N$, where z is the fractional distance, $\varepsilon = \tau_0^4 / N^2 b_2^2$ and $K = N^3 \tau_0^2 S b_2^2 / (E_0 \tau_0^4)$, we have

$$\sigma_i^2 = Kz[\varepsilon + (z - x)^2]. \quad (8.19)$$

In most systems $\varepsilon \ll 1$ and is negligible for very long distances. The fractional distance z is assumed to be a continuous variable and when $x = 0$, the jitter is a monotonically increasing function of z . When $0 < x \leq 1$, the jitter has a local maximum within the system. The local extremes can be found by setting the first differential of Eq. (8.19) with respect to z to 0

$$\frac{d\sigma_i^2}{dz} = K[(z - x)^2 + 2z(z - x)] = 0, \quad (8.20)$$

and solving for z to get

$$z = x \text{ or } z = x/3. \quad (8.21)$$

From Eqs. (8.20) and (8.21) we can find that

$$\left. \frac{d^2\sigma_i^2}{dz^2} \right|_{z=x} = 2Kx > 0 \quad (8.22)$$

$$\left. \frac{d^2\sigma_i^2}{dz^2} \right|_{z=x/3} = -2Kx < 0 \quad (8.23)$$

Thus the local maximum in jitter occurs at $z = x/3$ and is given by

$$\sigma_{max}^2(x) = K \frac{4}{27} x^3. \quad (8.24)$$

The optimum fraction of pre-compensation can be found when the maximum jitter within the fiber link is equal to the maximum jitter at the receiver end when $z = 1$ and can be written as

$$K \frac{4}{27} x^3 = K(1 - x)^2. \quad (8.25)$$

Solving for x we get $x_{opt} = 3/4$. Thus we find that the optimum compensation is found to be 75% pre-compensation and 25% post-compensation.

When ϵ cannot be neglected, the optimum compensation can be found using the perturbation method as follows. The jitter within the fiber link is given by Eq. (8.19). We consider the linear term in z to be a small perturbation. Thus we can re-write Eq. (8.19) as

$$\sigma_i^2 = K(A + \epsilon B), \quad (8.26)$$

where $A = z(z-x)^2$ and $B = z$. Similarly z can be written as $z = z_0 + \epsilon z_1$. Differentiating Eq. (8.26) with respect to z to find the local maximum we get

$$\frac{d\sigma_i^2}{dz} = K \frac{dA}{dz} \Big|_{z=z_0+\epsilon z_1} + K\epsilon \frac{dB}{dz} \Big|_{z=z_0+\epsilon z_1} = 0. \quad (8.27)$$

Expanding A and B in a Taylor series up to the first order in ϵ we get

$$\begin{aligned} \frac{dA}{dz} \Big|_{z=z_0} + \epsilon \left[z_1 \frac{d^2A}{dz^2} \Big|_{z=z_0} + \frac{dB}{dz} \Big|_{z=z_0} \right] &= 0, \\ \frac{dA}{dz} \Big|_{z=z_0} = 0 \quad z_1 \frac{d^2A}{dz^2} \Big|_{z=z_0} + \frac{dB}{dz} \Big|_{z=z_0} &= 0. \end{aligned} \quad (8.28)$$

From the definitions of A and B we get

$$\begin{aligned} \frac{dA}{dz} \Big|_{z=z_0} &= 3z_0^2 - 4z_0x + x^2 = 0 \\ z_0 &= x, x/3 \end{aligned} \quad (8.29)$$

Taking the second differential of A with respect to z we find that

$$\begin{aligned} \frac{d^2A}{dz^2} \Big|_{z_0=x} &= 2x \\ \frac{d^2A}{dz^2} \Big|_{z_0=x/3} &= -2x \end{aligned} \quad (8.30)$$

Thus the local maximum in jitter occurs when $z_0 = x/3$.

Next to find z_1 , we use the second part of Eq. (8.28) to get

$$\begin{aligned} z_1 \frac{d^2A}{dz^2} \Big|_{z=z_0} + 1 &= 0 \\ z_1 &= \frac{1}{2x}. \end{aligned} \quad (8.31)$$

Using Eqs. (8.29) and (8.31) in the definition of A and B we can write

$$A(x) = \left(\frac{x}{3} + \frac{\epsilon}{2x} \right) \left[-\frac{2x}{3} + \frac{\epsilon}{2x} \right] \quad B(x) = \frac{x}{3} + \frac{\epsilon}{2x}. \quad (8.32)$$

Using Eq. (8.32) in Eq. (8.26) we find that the maximum jitter within the fiber link can be written to the first order in ϵ , as

$$\sigma_{max}^2 = K \left(\frac{4x^3}{27} + \frac{\epsilon x}{3} \right). \quad (8.33)$$

Equating the maximum jitter to the jitter at the receiver end we get

$$\begin{aligned} \frac{4x^3}{27} + \frac{\epsilon x}{3} &= (1-x)^2 + \epsilon, \\ \frac{4x^3}{27} - x^2 + 2x + \frac{\epsilon x}{3} - (\epsilon + 1) &= 0 = U(x). \end{aligned} \quad (8.34)$$

Now $U(x)$ can be written as $U(x) = U_0(x) + \epsilon U_1(x)$, where $U_0(x) = 4x^3/27 - x^2 + 2x$ and $U_1 = (x/3) - 1$ and the optimum fraction of pre-compensation, $x_{opt} = x_0 + \epsilon x_1$. Hence expanding $U_0(x)$ and $U_1(x)$ in Taylor's series we can write $U(x)$ to first order in ϵ from Eq. (8.34) as

$$\begin{aligned} U(x) &= U_0(x_0) + \epsilon \left(\frac{dU_0}{dx} \Big|_{x=x_0} x_1 + U_1(x_0) \right) = 0, \\ U_0(x_0) &= 0 \quad \frac{dU_0}{dx} \Big|_{x=x_0} x_1 + U_1(x_0) = 0 \end{aligned} \quad (8.35)$$

Using the definition of U_0 in Eq. (8.35) we get

$$\frac{4x_0^3}{27} - x_0^2 + 2x_0 = 0, \quad x_0 = 3/4. \quad (8.36)$$

Next to find x_1 , we use Eq. (8.35) to get

$$x_1 = -U_1(x_0) / \left(\frac{dU_0}{dx} \right)(x_0). \quad (8.37)$$

Using the definition of $U_0(x)$ in Eq. (8.37) we get

$$x_1 = -1. \quad (8.38)$$

Using Eqs. (8.38) and (8.36) we find that the optimum fraction of pre-compensation $x_{opt} = 3/4 + \epsilon$ which agrees with our previous result of $x_{opt} = 3/4$ when ϵ is negligible. Thus we see that the optimum compensation is still about 75% pre-compensation and 25% post-compensation.

To verify this prediction numerically, we plot in Fig. 8.5 the timing jitter as a function of distance for three different compensation techniques for a 40 Gb/s system using chirped Gaussian pulses of width 6.87 ps. The dispersion map consists of 10 km of anomalous dispersion fiber

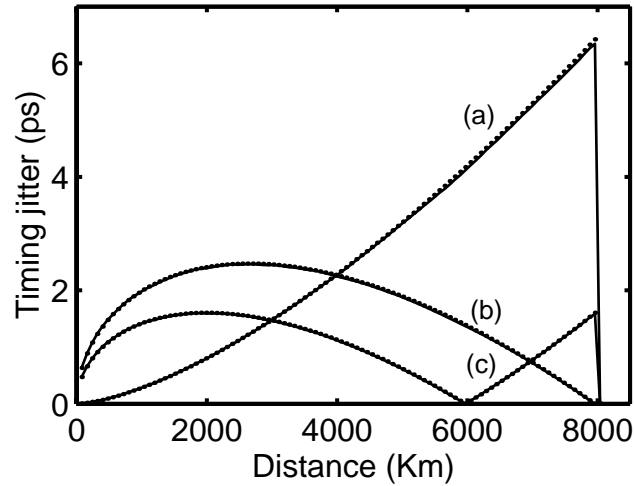


Figure 8.5: Effect of post-compensation on timing jitter of a 40-Gb/s non-soliton system with average dispersion 0.08 ps/km-nm. Jitter is plotted as a function of transmission distance for a) complete post-compensation, b) complete pre-compensation and c) optimum compensation. The dotted line show the result of numerical verification.

$D = 4\text{ps}/(\text{km}\cdot\text{nm})$ and 9.6 km of normal dispersion fiber of $D = -4\text{ ps}/\text{km}\cdot\text{nm}$. Each fiber section is assumed to have an effective area of $54\ \mu\text{m}^2$ and losses of 0.2 dB/km. Optical amplifiers are spaced 80 km apart. The spectral noise density was calculated using $n_{sp} = 1.3$. The average dispersion in this case is $0.1\text{ps}^2/\text{km}$. To ensure the quasi-linear nature of pulse propagation, the peak power of each pulse is taken to be 1 mW. The initial chirp is chosen so as to compensate for the accumulated dispersion according to the three different techniques. The curves (a), (b) and (c) show the cases of complete pre-compensation, complete post-compensation and optimum compensation techniques respectively. The solid lines represent the analytical result and the dots represent numerically averaged values over 10^4 realizations. Our analytical predictions are consistent with the numerical solutions of the moment equations, on which they are based. More importantly, Fig. 8.5 shows that when we choose 75% of pre-and 25% post-compensation, the jitter is indeed minimized along the entire fiber link.

8.2 Parametric amplifiers

At bit rates of up to 40 Gb/s, we have seen in Chapter 7 that the timing jitter is mainly due to the Gordon–Haus effect [52]. But at higher bit rates the pulse width becomes so short that timing

jitter is dominated by the Raman jitter caused by RIFS. We derived the analytic expressions for the timing jitter for systems using bit rates of more than 40 Gb/s in the cases of dispersion-managed (DM) solitons, fundamental solitons in dispersion-decreasing or constant-dispersion fibers, and non-soliton systems in Chapter 7, and showed that for a chain of N amplifiers, timing jitter resulting from the RIFS grows as N^5 while the Gordon-Haus jitter grows only as N^3 . The idea of using optical phase conjugation (OPC) for compensating the effects of GVD and self-phase modulation is well known and was pursued during the 1990s [69]. It has also been shown that OPC can be used to cancel the Raman-induced frequency shift [70] induced by the phenomenon of Raman scattering [1], and hence reduce timing jitter in lightwave systems designed using dispersion-decreasing fibers [71]. Parametric amplifiers can act as an optical phase conjugator, and the noise figure of such an amplifier is typically less than that of an EDFA. The basic idea behind the use of parametric amplifiers for jitter-compensation is to replace the erbium-doped fiber amplifiers (EDFAs) with the parametric amplifiers, which provide gain through four-wave mixing. In doing so both the Raman and Gordon-Haus contributions to the jitter can be reduced by a large amount. However the effects of third-order dispersion (TOD) cannot be compensated by using OPC.

Parametric amplifiers use a four-wave mixing process [1] in which the energy of one or more pumps is used to amplify a weak signal and to simultaneously generate one or more waves at the idler frequencies [72]–[74]. The most important feature of a parametric amplifier for our purpose is that the phase of the idler waves is related to the phase of the signal wave as $\phi_i = \phi_0 - \phi_s$ because of OPC, where ϕ_0 is a constant phase related to the pump phases. For a signal field with amplitude $B(z, t)$, the idler fields can be written as $B^*(z, t)$ within a constant phase factor. In practice, B and B^* have different wavelengths. In the case of two pumps, the three main idler frequencies are related to the signal frequency ω_s as $\omega_i = \omega_1 + \omega_2 - \omega_s$, $\omega'_i = 2\omega_1 - \omega_s$, $\omega''_i = 2\omega_2 - \omega_s$, where ω_1 and ω_2 are the pump frequencies [73]. In practice one should choose the idler whose frequency is close to the signal frequency so that all fiber parameters remain nearly the same for both fields. The proposed technique can tolerate a mismatch of 2 or 3 nm, especially if the dispersion slopes are matched along the DM fiber link but is likely to become unsuitable when the signal and idler wavelengths differ by more than 5 nm.

Consider a DM system in which parametric amplifiers are used periodically with a spacing L_A . The propagation of an optical pulse in the first fiber section before it is amplified by a paramet-

ric amplifier is governed by the generalized nonlinear Schrödinger (NLS) equation which can be written from Eq. (7.2) as

$$i\frac{\partial B}{\partial z} - \frac{\beta_2}{2}\frac{\partial^2 B}{\partial t^2} - i\frac{\beta_3}{6}\frac{\partial^3 B}{\partial t^3} + \bar{\gamma}|B|^2B = T_R\bar{\gamma}B\frac{\partial|B|^2}{\partial t}, \quad (8.39)$$

where $B(z, t)$ is the slowly varying amplitude of the pulse envelope, β_2 is the GVD coefficient, β_3 is the TOD parameter, $\bar{\gamma} = \gamma \exp[-\int_0^z \alpha(z)dz]$ is the nonlinear parameter responsible for self-phase modulation weakened by fiber losses, and the Raman parameter T_R accounts for the Raman-induced frequency shift. After the signal is amplified by the first parametric amplifier, the idler field is proportional to $B^*(z, t)$ if the pump has a narrow spectrum compared with the signal. If this field is used in the next fiber section, its evolution is governed by the following equation obtained by taking the complex conjugate of Eq. (8.39):

$$i\frac{\partial B^*}{\partial z} + \frac{\beta_2}{2}\frac{\partial^2 B^*}{\partial t^2} - i\frac{\beta_3}{6}\frac{\partial^3 B^*}{\partial t^3} - \gamma|B|^2B^* = T_R\gamma B^*\frac{\partial|B|^2}{\partial t}. \quad (8.40)$$

After the second amplifier, the signal goes back to $B(z, t)$ and hence would satisfy Eq. (8.39). It is thus evident that the evolution of each optical pulse is periodic with the period $2L_A$ rather than the amplifier spacing L_A . Within each period of length $2L_A$, we need to use Eqs. (8.39) and (8.40) in the two neighboring fiber spans of length L_A . A comparison of these two equations shows that the GVD parameter β_2 and the self-phase modulation parameter γ change sign after each amplifier. Since the Raman term is proportional to γ , it also changes its sign. The net result is that the GVD, self-phase modulation, and the Raman-induced frequency shift are compensated after every two amplifiers. This is the main advantage of using parametric amplifiers. Since TOD does not change sign, we can see that OPC does not help in reducing the TOD effects.

Using the results obtained in Chapter 7, in Eqs. (7.3)–(7.5) we can write the evolutions of energy, frequency and position of the pulse along the fiber section before an amplifier as

$$\frac{dE}{dz} = 0, \quad (8.41)$$

$$\frac{dT}{dz} = \beta_2\Omega + \frac{\beta_3}{2E} \int_{-\infty}^{\infty} \left| \frac{\partial B}{\partial t} \right|^2 dt, \quad (8.42)$$

$$\frac{d\Omega}{dz} = -\frac{\bar{\gamma}}{E} T_R \int_{-\infty}^{\infty} \left(\frac{\partial}{\partial t} |B|^2 \right)^2 dt. \quad (8.43)$$

The above equations can be modified as follows to include the amplifier noise:

$$\frac{dE}{dz} = \sum_i \delta E_i \delta(z - z_i), \quad (8.44)$$

$$\frac{dT}{dz} = \beta_2 \Omega + \frac{\beta_3}{2E} \int_{-\infty}^{\infty} \left| \frac{\partial B}{\partial t} \right|^2 dt + \sum_i \delta T_i \delta(z - z_i), \quad (8.45)$$

$$\frac{d\Omega}{dz} = -\frac{\bar{\gamma}}{E} T_R \int_{-\infty}^{\infty} \left(\frac{\partial}{\partial t} |B|^2 \right)^2 dt + \sum_i \delta \Omega_i \delta(z - z_i), \quad (8.46)$$

where δE_i , $\delta \Omega_i$, and δT_i are random fluctuations in the pulse energy, frequency, and position, respectively, introduced by the i th amplifier located at a distance z_i . We proceed to calculate timing jitter from these above equations like we did in Chapter 7.

8.2.1 Soliton Systems

Since parametric amplifiers can act as optical phase conjugators to restore the field to its original state after every two amplifiers, in the case of solitons, pulse parameters such as the chirp and the pulse width are restored to their input values after every two amplifiers. We first consider the case of systems using the fundamental soliton in DDFs that employ parametric amplifiers in place of EDFAs and in the following section we consider the case of DM soliton systems that use parametric amplifiers in place of EDFAs. In both cases we use the moment method to show that both Raman jitter and Gordon-Haus jitter can be reduced by the use of parametric amplifiers.

Fundamental solitons in DDFs

When fundamental solitons are launched inside a DDF, the soliton shape and width are preserved in spite of fiber losses. The GVD coefficient for DDFs in general decreases as $|\beta_2(z)| = |\beta_2(0)| \exp(-\alpha z)$ along the length of the fiber and reaches a value β_2^{\min} at the end of each fiber section of length L_A . The pulse shape in such a case is given by Eq. (6.39) to be

$$B_i(z, t) = a_i \operatorname{sech} \left(\frac{t - T_i}{\tau_i} \right) \exp[i\phi_i - i\Omega_i(t - T_i)]. \quad (8.47)$$

We used this form for the pulse shape in Chapter 7 to find the variances and cross-correlations in δE_i , $\delta \Omega_i$ and δT_i to be the same at every amplifier due to the periodicity of the soliton system.

From Eqs. (7.38)–(7.40) we can write the the variances and cross-correlations as

$$\langle \delta E^2 \rangle = 2SE_0, \quad \langle \delta \Omega \delta E \rangle = 0, \quad (8.48)$$

$$\langle \delta \Omega^2 \rangle = \frac{2S}{3E_0\tau_0^2} \quad \langle \delta E \delta T \rangle = 0, \quad (8.49)$$

$$\langle \delta T^2 \rangle = \frac{\pi^2 S \tau_0^2}{6E_0} \quad \langle \delta \Omega \delta T \rangle = 0. \quad (8.50)$$

As discussed before, the pulse evolution is periodic not after every amplifier but after every two amplifiers. We use this feature to calculate the impact of parametric amplification on the timing jitter. Consider a set of two amplifiers. Equations (8.44)–(8.46) show how E , Ω , and T evolve along the fiber link before the first amplifier. Integrating these equations over the amplifier spacing L_A and including the fluctuations induced by the first amplifier, we obtain from Eqs. (7.11)–(7.13) by neglecting the higher order terms

$$E(L_A) = E(0) + \delta E_1, \quad (8.51)$$

$$\Omega(L_A) = \Omega(0) + b_R E(0) + \delta \Omega_1 \quad (8.52)$$

$$T(L_A) = T(0) + b_2 \Omega(0) + b_{2R} E(0) + b_3 + \delta T_1. \quad (8.53)$$

The parameters b_2 , b_R , b_{2R} and b_3 are given by Eqs. (7.14)–(7.17).

We now consider changes in E , Ω and T after the first amplifier. Eqs. (8.44)–(8.46) can still be used if we change β_2 to $-\beta_2$ and $\bar{\gamma}$ to $-\bar{\gamma}$. Integrating these equations, E , Ω , and T after the second amplifier are given by

$$E(2L_A) = E(0) + \delta E_1 + \delta E_2, \quad (8.54)$$

$$\begin{aligned} \Omega(2L_A) &= \Omega(L_A) - b_R E(L_A) - \delta \Omega_2, \\ &= \Omega(0) - b_R \delta E_1 + \delta \Omega_1 - \delta \Omega_2, \end{aligned} \quad (8.55)$$

$$\begin{aligned} T(2L_A) &= T(L_A) - b_2 \Omega(L_A) + b_3 - b_{2R} E(L_A) + \delta T_2, \\ &= T(0) - b_2 b_R E(0) + 2b_3 - b_2 \delta \Omega_1 - b_{2R} \delta E_1 + \delta T_1 + \delta T_2, \end{aligned} \quad (8.56)$$

where the sign of Ω was reversed to account for the phase reversal at the parametric amplifier. These equations show that after every two amplifiers, the effects of Raman-induced frequency shift and GVD cancel precisely because of parametric amplification. We consider that the fundamental

soliton system uses N parametric amplifiers, grouped into M pairs so that $M = N/2$. Summing Eqs. (8.54)–(8.56) over M such pairs we get

$$\langle E \rangle_M = E_0 + 2MS, \quad (8.57)$$

$$\langle \Omega \rangle_M = -b_R MS, \quad (8.58)$$

$$\langle T \rangle_M = 2Mb_3 - b_2 b_R M E_0 - b_{2R} MS. \quad (8.59)$$

In order to find the timing jitter, we have to find the variance of T after N amplifiers. After any j th pair of amplifiers the variance of T can be written from Eq. (8.56) as

$$\begin{aligned} \langle T^2 \rangle_j = & \langle T^2 \rangle_{j-1} + 4b_3^2 + b_2^2 b_R^2 \langle E^2 \rangle_{j-1} + b_2^2 \langle \delta \Omega^2 \rangle_j + b_{2R}^2 \langle \delta E^2 \rangle_j + 2 \langle \delta T^2 \rangle_j + 4b_3 \langle T \rangle_{j-1} - \\ & 2b_2 b_R \langle ET \rangle_{j-1} + 2b_2 b_R b_{2R} \langle E \rangle_{j-1} \langle \delta E \rangle_j - 2b_{2R} \langle \delta E \rangle_j \langle T \rangle_{j-1} - 4b_2 b_R b_3 \langle E \rangle_{j-1}. \end{aligned} \quad (8.60)$$

In order to proceed further we need to find $\langle E^2 \rangle_M$ and $\langle ET \rangle_M$. Using Eqs. (8.54) and (8.56) we get

$$\langle E^2 \rangle_j = \langle E^2 \rangle_{j-1} + 2 \langle \delta E^2 \rangle_j, \quad (8.61)$$

$$\langle ET \rangle_j = \langle ET \rangle_{j-1} + 2b_3 \langle E \rangle_{j-1} - b_2 b_R \langle E^2 \rangle_{j-1} - b_{2R} \langle \delta E \rangle_j \langle E \rangle_{j-1} + 2 \langle \delta E \delta T \rangle. \quad (8.62)$$

Summing Eqs. (8.61) and (8.62) over M such pairs we get

$$\langle E^2 \rangle_M = 2M \langle \delta E^2 \rangle, \quad (8.63)$$

$$\langle ET \rangle_M = 2b_3 M (M_1) S - b_2 b_R M (M-1) \langle \delta E^2 \rangle - b_{2R} M (M-1) S^2. \quad (8.64)$$

Using Eqs. (8.63) and (8.64) in Eq. (8.60) we can find the variance in T after M pairs of amplifiers to be

$$\begin{aligned} \langle T^2 \rangle_M = & 4Mb_3^2 + b_2^2 b_R^2 M (M-1) \langle \delta E^2 \rangle + b_2^2 M \langle \delta \Omega^2 \rangle + b_{2R}^2 M \langle \delta E^2 \rangle + 2M \langle \delta T^2 \rangle + 4b_3^2 M (M-1) \\ & + \frac{2}{3} b_2^2 b_R^2 M (M-1) (M-2) \langle \delta E^2 \rangle + \frac{2}{3} b_2 b_R b_{2R} M (M-1) (M-2) S^2 \\ & + b_{2R} M (M-1) S^2 - \frac{8}{3} b_2 b_R b_3 M (M-1) (M-2) S. \end{aligned} \quad (8.65)$$

Using Eqs. (8.65) and (8.57) and substituting $M = N/2$ we can find the timing jitter when using parametric amplifiers in place of EDFAs to be

$$\sigma_{PA}^2 = \sigma_{GH}^2 + [b_2^2 b_R^2 (N^2 - 4)/12 + b_{2R}^2] N/2 \langle \delta E^2 \rangle + b_2 b_3 b_R S N (N-2) (N-4)/3, \quad (8.66)$$

$$\sigma_{GH}^2 = N (b_2^2/2) \langle \delta \Omega^2 \rangle + N \langle \delta T^2 \rangle. \quad (8.67)$$

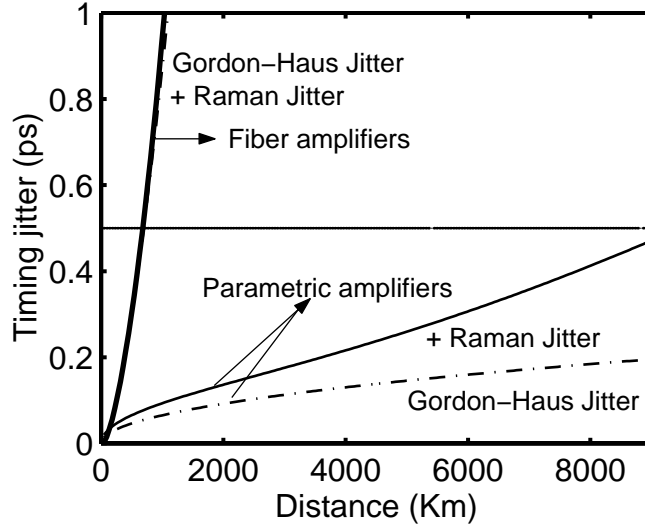


Figure 8.6: Timing jitter for a 160-Gb/s fundamental solitons in DDF system with 45-km amplifier spacing. The solid and dashed lines show respectively timing jitter with and without the Raman contribution for both EDFAs and parametric amplifiers. The map parameters are the same as Figure 7.1. The dotted line shows the acceptable value of timing jitter.

Eqs. (8.66) and (8.67) show Raman jitter and Gordon-Haus jitter grow cubic and linear in distance respectively when parametric amplifiers are used instead of EDFAs.

As a comparison we can write the Raman jitter and Gordon-Haus jitter when EDFAs are used from Eqs. (7.66) and (7.67) to be

$$\sigma_i^2 = \sigma_{\text{GH}}^2 + R_1 \langle (\delta E)^2 \rangle + R_2, \quad (8.68)$$

$$\sigma_{\text{GH}}^2 = \frac{b_2^2}{6} N(N-1)(2N-1) \langle \delta \Omega^2 \rangle + N \langle \delta T^2 \rangle, \quad (8.69)$$

and the coefficients R_1 and R_2 are given by

$$R_1 = N(N-1) [b_R^2 b_2^2 (N^3 - 10N^2 + 29N - 9)/120 + b_2 b_R b_{2R} (19N^2 - 65N + 48)/96 + b_{2R}^2 (2N-1)/6], \quad (8.70)$$

$$R_2 = N(N-1) b_3 [b_R (N-1)(N-2)/6 + b_{2R} (N-2)/3] S. \quad (8.71)$$

We see from Eqs. (8.66) - (8.71) that both the Raman jitter and the Gordon-Haus jitter are reduced considerably by using parametric amplifiers because they scale as N^3 and N , rather than N^5 and N^3 , respectively.

To illustrate the extent of timing jitter reduction offered by parametric amplifiers, we consider a dense dispersion-managed system capable of operating at 160 Gb/s using fundamental solitons in DDF system with a 45-km-long DDF with $D(0) = 1.0$ ps/(km-nm). The dispersion map is the same as the one used to study Raman jitter in Figure 7.1 in Chapter 7. Figure 8.6 shows the dependence of timing jitter on distance for such a system while using EDFAs and parametric amplifiers. The solid and dashed lines show respectively the total timing jitter with and without ($T_R = 0$) the Raman contribution. The dotted line shows the tolerable value of the jitter for a 160 Gb/s system (8% of the bit slot). The timing jitter limits the distance to below 500 km when using EDFAs. The use of parametric amplifiers reduces the jitter to within the tolerable value for distances as large as 8,000 km. Of course, other effects such as soliton collisions and Q -factor degradation may not allow transmission over 4000 km.

Dispersion-managed solitons

A DM system consists of a periodic sequence of anomalous- and normal-dispersion fiber sections. To compensate for fiber losses in such a system, an amplifier is placed after one or more map periods at L_A . The pulse shape in such a case is given by Eq. (6.56) to be

$$B_i(z, t) = a_i \exp[i\phi_i - i\Omega_i(t - T_i) - (1 + iC_i)(t - T_i)^2/2\tau_i^2], \quad (8.72)$$

Using this form of pulse shape we can write the variances and cross-correlations in δE_i , $\delta\Omega_i$ and δT_i from Eqs. (7.91)–(7.93) in Chapter 7 to be

$$\langle \delta E^2 \rangle = 2SE_0, \quad \langle \delta\Omega\delta E \rangle = 0 \quad \langle \delta E \rangle = S, \quad (8.73)$$

$$\langle \delta\Omega^2 \rangle = \frac{S}{E_0} \frac{(1 + C_0^2)}{\tau_0^2} \quad \langle \delta E\delta T \rangle = 0 \quad \langle \delta\Omega \rangle = 0, \quad (8.74)$$

$$\langle \delta T^2 \rangle = \frac{S}{E_0} \tau_0^2 \quad \langle \delta\Omega\delta T \rangle = \frac{S}{E} C_0 \quad \langle \delta T \rangle = 0. \quad (8.75)$$

The pulse evolution again is periodic not after every amplifier but after every two amplifiers. Using this feature for a set of two amplifiers, we calculate the impact of parametric amplification on the timing jitter. Integrating Eqs. (8.73)–(8.75) equations over the amplifier spacing L_A and including the fluctuations induced by the first amplifier, we obtain from Eqs. (7.80)–(7.82) by neglecting the higher order terms

$$E(L_A) = E(0) + \delta E_1, \quad (8.76)$$

$$\Omega(L_A) = \Omega(0) + b_R E(0) + \delta\Omega_1 \quad (8.77)$$

$$T(L_A) = T(0) + b_2 \Omega(0) + b_{2R} E(0) + b_3 + \delta T_1. \quad (8.78)$$

The parameters b_2 , b_R , b_{2R} and b_3 are given by Eqs. (7.76)–(7.79).

Integrating Eqs. (8.76)–(8.78) and changing β_2 to $-\beta_2$ and $\bar{\gamma}$ to $-\bar{\gamma}$ we find E , Ω and T after the second amplifier to be

$$E(2L_A) = E(0) + \delta E_1 + \delta E_2, \quad (8.79)$$

$$\Omega(2L_A) = \Omega(0) - b_R \delta E_1 + \delta\Omega_1 + \delta\Omega_2, \quad (8.80)$$

$$T(2L_A) = T(0) - b_2 b_R E(0) + 2b_3 - b_2 \delta\Omega_1 - b_{2R} \delta E_1 + \delta T_1 + \delta T_2. \quad (8.81)$$

The above equations show that after every two amplifiers, the effects of the Raman-induced frequency shift and GVD again cancel precisely because of parametric amplification. Next we consider that the DM soliton system also uses N parametric amplifiers, grouped into M pairs so that $M = N/2$. Summing Eqs. (8.79)–(8.81) over M such pairs we get

$$\langle E \rangle_M = E_0 + 2MS, \quad (8.82)$$

$$\langle \Omega \rangle_M = -b_R MS, \quad (8.83)$$

$$\langle T \rangle_M = 2Mb_3 - b_2 b_R M E_0 - b_{2R} MS. \quad (8.84)$$

In order to find the timing jitter, we have to find the variance of T after N amplifiers. After any j th pair of amplifiers the variance of T can be written from Eq. (8.78) as

$$\begin{aligned} \langle T^2 \rangle_j &= \langle T^2 \rangle_{j-1} + 4b_3^2 + b_2^2 b_R^2 \langle E^2 \rangle_{j-1} + b_2^2 \langle \delta\Omega^2 \rangle_j + b_{2R}^2 \langle \delta E^2 \rangle_j + 2\langle \delta T^2 \rangle_j \\ &\quad + 4b_3 \langle T \rangle_{j-1} - 2b_2 b_R \langle ET \rangle_{j-1} + 2b_2 b_R b_{2R} \langle E \rangle_{j-1} \langle \delta E \rangle_j - 2b_{2R} \langle \delta E \rangle_j \langle T \rangle_{j-1} \\ &\quad - 4b_2 b_R b_3 \langle E \rangle_{j-1} - 2b_2 \langle \delta\Omega \delta T \rangle_j. \end{aligned} \quad (8.85)$$

Using Eqs. (8.76) and (8.78) to find $\langle E^2 \rangle_M$ and $\langle ET \rangle_M$ we get

$$\langle E^2 \rangle_j = \langle E^2 \rangle_{j-1} + 2\langle \delta E^2 \rangle_j, \quad (8.86)$$

$$\langle ET \rangle_j = \langle ET \rangle_{j-1} + 2b_3 \langle E \rangle_{j-1} - b_2 b_R \langle E^2 \rangle_{j-1} - b_{2R} \langle \delta E \rangle_j \langle E \rangle_{j-1} + 2\langle \delta E \delta T \rangle. \quad (8.87)$$

Summing Eqs. (8.86) and (8.87) over M such pairs we get

$$\langle E^2 \rangle_M = 2M \langle \delta E^2 \rangle, \quad (8.88)$$

$$\langle ET \rangle_M = 2b_3 M(M_1)S - b_2 b_R M(M-1) \langle \delta E^2 \rangle - b_{2R} M(M-1)S^2. \quad (8.89)$$

Using Eqs. (8.88) and (8.89) in Eq. (8.85) we can find the variance in T after M pairs of amplifiers to be

$$\begin{aligned} \langle T^2 \rangle_M &= 4Mb_3^2 + b_2^2 b_R^2 M(M-1) \langle \delta E^2 \rangle + b_2^2 M \langle \delta \Omega^2 \rangle + b_{2R}^2 M \langle \delta E^2 \rangle + 2M \langle \delta T^2 \rangle + 4b_3^2 M(M-1) \\ &\quad + \frac{2}{3} b_2^2 b_R^2 M(M-1)(M-2) \langle \delta E^2 \rangle + \frac{2}{3} b_2 b_R b_{2R} M(M-1)(M-2) S^2 \\ &\quad + b_{2R} M(M-1) S^2 - \frac{8}{3} b_2 b_R b_3 M(M-1)(M-2) S - 2b_2 M \langle \delta \Omega \delta T \rangle. \end{aligned} \quad (8.90)$$

Using Eqs. (8.88) and (8.89) and substituting $M = N/2$ in Eq. (8.90), we find the timing jitter when using parametric amplifiers in place of EDFAs to be

$$\sigma_{PA}^2 = \sigma_{GH}^{\prime 2} + [b_2^2 b_R^2 (N^2 - 4)/12 + b_{2R}^2 N/2 \langle \delta E^2 \rangle + b_2 b_3 b_R S N(N-2)(N-4)/3], \quad (8.91)$$

$$\sigma_{GH}^{\prime 2} = N[(b_2^2/2) \langle \delta \Omega^2 \rangle - b_2 \langle \delta \Omega \delta T \rangle + \langle \delta T^2 \rangle]. \quad (8.92)$$

Eqs. (8.89) and (8.90) show that Raman jitter and Gordon-Haus jitter grow cubic and linear in distance respectively when parametric amplifiers are used instead of EDFAs. As a comparison we can write the Raman jitter and Gordon-Haus jitter when EDFAs are used from Eqs. (7.118) and (7.119) to be

$$\sigma_i^2 = \sigma_{GH}^2 + R_1 \langle (\delta E)^2 \rangle + R_2, \quad (8.93)$$

$$\sigma_{GH}^2 = \frac{b_2^2}{6} N(N-1)(2N-1) \langle \delta \Omega^2 \rangle + b_2 N(N-1) \langle \delta \Omega \delta T \rangle + N \langle \delta T^2 \rangle, \quad (8.94)$$

and the coefficients R_1 and R_2 are given by

$$\begin{aligned} R_1 &= N(N-1)[b_R^2 b_2^2 (N^3 - 10N^2 + 29N - 9)/120 \\ &\quad + b_2 b_R b_{2R} (19N^2 - 65N + 48)/96 + b_{2R}^2 (2N-1)/6], \end{aligned} \quad (8.95)$$

$$R_2 = N(N-1)b_3[b_R(N-1)(N-2)/6 + b_{2R}(N-2)/3]S. \quad (8.96)$$

We see from Eqs. (8.89) - (8.94) that both the Raman jitter and the Gordon-Haus jitter are reduced considerably by using parametric amplifiers because they scale as N^3 and N , rather than N^5 and N^3 , respectively. To illustrate the extent of timing jitter reduction offered by parametric amplifiers, we consider a dense dispersion-managed system capable of operating at 160 Gb/s. The map consists of 1-km section of anomalous-GVD fiber ($D = 2.5$ ps/km-nm) and another 1-km section of normal-GVD fiber ($D = -2.43$ ps/km-nm). In both fiber sections, $\alpha = 0.2$ dB/km, the nonlinear parameter

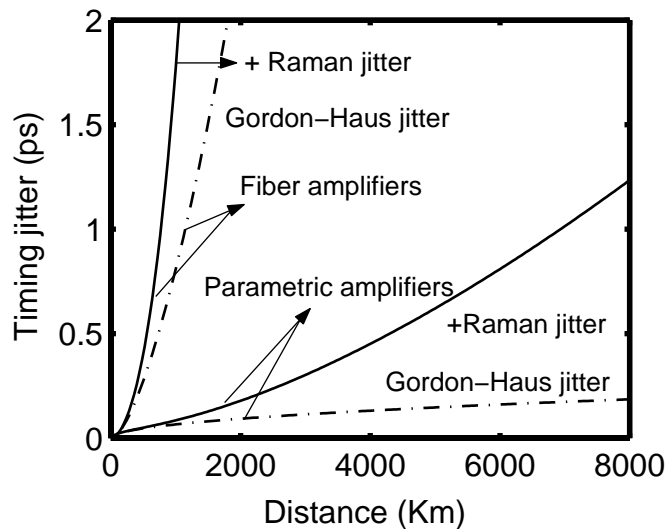


Figure 8.7: Timing jitter for a 160-Gb/s DM soliton system with 40-km amplifier spacing. The solid and dashed lines show respectively timing jitter with and without the Raman contribution for both EDFAs and parametric amplifiers. The dotted line shows the acceptable value of timing jitter.

$\gamma = 2.26 \text{ W}^{-1}/\text{km}$, the Raman parameter $T_R = 3 \text{ fs}$, and $\beta_3 = 0.1 \text{ ps}^3/\text{km}$. Amplifiers are placed 40 km apart. The noise figure for parametric amplifiers depends on the excess noise introduced by pump power fluctuations. We calculate the spectral noise density using $n_{sp} = 1.3$ for both parametric amplifiers and EDFAs (the worst-case scenario) which corresponds to a noise figure of 4.2 dB. The parameters for the input Gaussian pulse were found using the periodicity conditions for solitons and have values $\tau_0 = 1.25 \text{ ps}$, $C_0 = 1$ and $E_0 = 0.12 \text{ pJ}$ [7]. Figure 8.7 shows the increase in timing jitter as a function of distance in the cases of EDFAs and parametric amplifiers. The solid and dashed lines show respectively the total timing jitter with and without ($T_R = 0$) the Raman contribution. The dotted line shows the tolerable value of the jitter for a 160 Gb/s system (8% of the bit slot). In the absence of parametric amplifiers, the system performance is limited by the jitter to the extent that the soliton system cannot operate beyond 500 km. However when parametric amplifiers are used, the timing jitter is reduced so much that it limits the system performance only after 4000 km. (Of course, other effects such as soliton collisions and Q -factor degradation can limit the system before 4000 km.)

Next to verify that the use of parametric amplifiers in place of EDFAs can reduce both Gordon-Haus jitter and Raman jitter, we consider the same DM system as the one used to obtain Figure 8.7.

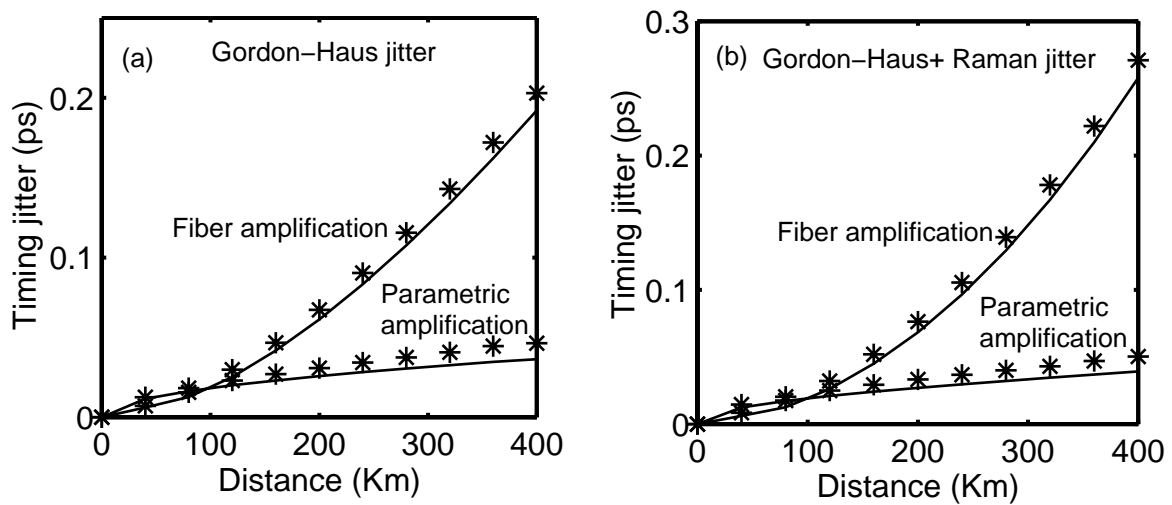


Figure 8.8: Gordon-Haus timing jitter for a 160 Gb/s DM soliton system when using parametric amplifiers and EDFAs. The 'stars' show numerical results and the solid line show the analytical results.

We compare the analytical results to the results obtained by numerical simulation in Figures 8.8 (a) and (b). The 'stars' show the results of the numerical simulation and the solid line show the analytical results. The numerical simulation shows a larger value of jitter than predicted by the above equations as the distance increases. This is due to the jitter induced by intra-channel cross phase modulation which is not considered in the above analysis. Figure 8.8 (a) and (b) shows Gordon-Haus jitter and Raman jitter as a function of distance respectively. The numerical simulations agree with the analytical predictions that the use of parametric amplifiers in place of EDFAs can reduce both Gordon-Haus jitter and Raman Jitter.

8.2.2 Non-soliton Systems

Non-soliton systems uses prechirped pulses of relatively low energy propagating along a DM link without enforcing a periodic evolution pattern. The chirp and the pulse width cannot be calculated at the location of each amplifier in the general case in which the nonlinear effects are included. However, in the case of quasi-linear propagation, the nonlinear term can be neglected, and the pulse evolution is nearly linear along the DM link. The chirp and the pulse width of the pulses can then be found analytically as shown in chapters 6 and 7. From chapters 6 and 7, since the noise variances and cross-correlations in the case of non-soliton systems depend on chirp and pulse width

at each amplifier, they are different at different amplifiers. After the first parametric amplifier, the chirp changes sign and from Eq. (7.122) can be written as

$$C_1 = -(C_0 + b_2/\tau_0^2), \quad (8.97)$$

After the second amplifier, the chirp C is restored to C_0 . Physically, the effect of dispersion is canceled for each pair of parametric amplifiers. Similarly, the pulse width after the first and second parametric amplifiers is given by

$$\tau_1 = \tau_0 \sqrt{1 + C_1^2}, \quad \tau_2 = \tau_0. \quad (8.98)$$

We note that from Eqs. (8.97) and (8.98) that both the chirp and pulse width are restored to their original values after every two amplifiers just like in the case of solitons. This feature is quite different compared with the case of EDFAs for which the width and chirp evolve in a non-periodic fashion. It results from the fact that even when the average dispersion is not zero, its effects are canceled for every pair of parametric amplifiers. Using this form of pulse shape we can write the variances and cross-correlations in δE_j , $\delta \Omega_j$ and δT_j after any j th pair of amplifiers from Eqs. (7.124)–(7.126) in Chapter 7 to be

$$\langle \delta E^2 \rangle_j = 2SE_0, \quad \langle \delta \Omega \delta E \rangle_j = 0 \quad \langle \delta E \rangle_j = S, \quad (8.99)$$

$$\langle \delta \Omega^2 \rangle_j = \frac{S}{E_0} \frac{(1 + C_0^2)}{\tau_0^2} \quad \langle \delta E \delta T \rangle_j = 0 \quad \langle \delta \Omega \rangle_j = 0, \quad (8.100)$$

$$\langle \delta T^2 \rangle_{j1} = \frac{S}{E_0} \tau_0^2 \sqrt{1 + C_1^2} \quad \langle \delta \Omega \delta T \rangle_{j1} = \frac{S}{E} C_1 \quad \langle \delta T \rangle_j = 0. \quad (8.101)$$

$$\langle \delta T^2 \rangle_{j2} = \frac{S}{E_0} \tau_0^2 \quad \langle \delta \Omega \delta T \rangle_{j2} = \frac{S}{E} C_0, \quad (8.102)$$

where $j1$ and $j2$ represent the first and the second amplifiers in the j th pair. Since only $\langle \delta T^2 \rangle_{j1}$ and $\langle \delta \Omega \delta T \rangle_{j1}$ depend on the chirp C_1 , we can use Eqs. (8.97) to rewrite them in terms of C_0 and τ_0 . We can then drop the subscript 1 and 2 for the rest of the variances and correlations which have the same value at all the amplifiers.

Using Eqs. (8.76)–(8.78) we find E , Ω and T after the second amplifier to be

$$E(2L_A) = E(0) + \delta E_1 + \delta E_2, \quad (8.103)$$

$$\Omega(2L_A) = \Omega(0) - b_R \delta E_1 + \delta \Omega_1 + \delta \Omega_2, \quad (8.104)$$

$$T(2L_A) = T(0) - b_2 b_R E(0) + 2b_3 - b_2 \delta \Omega_1 - b_{2R} \delta E_1 + \delta T_1 + \delta T_2. \quad (8.105)$$

Summing Eqs. (8.103)–(8.105) over M such pairs we get

$$\langle E \rangle_M = E_0 + 2MS, \quad (8.106)$$

$$\langle \Omega \rangle_M = -b_R MS, \quad (8.107)$$

$$\langle T \rangle_M = 2Mb_3 - b_2 b_R M E_0 - b_{2R} MS. \quad (8.108)$$

In order to find the timing jitter, we have to find the variance of T after N amplifiers. After any j th pair of amplifiers the variance of T can be written from Eq. (8.108) as

$$\begin{aligned} \langle T^2 \rangle_j &= \langle T^2 \rangle_{j-1} + 4b_3^2 + b_2^2 b_R^2 \langle E^2 \rangle_{j-1} + b_2^2 \langle \delta \Omega^2 \rangle_j + b_{2R}^2 \langle \delta E^2 \rangle_j \\ &\quad + 4b_3 \langle T \rangle_{j-1} - 2b_2 b_R \langle ET \rangle_{j-1} + 2b_2 b_R b_{2R} \langle E \rangle_{j-1} \langle \delta E \rangle_j - 2b_{2R} \langle \delta E \rangle_j \langle T \rangle_{j-1} \\ &\quad - 4b_2 b_R b_3 \langle E \rangle_{j-1} - 2b_2 \langle \delta \Omega \delta T \rangle_{j1} + \langle \delta T^2 \rangle_{j1} + \langle \delta T^2 \rangle_{j2}. \end{aligned} \quad (8.109)$$

Using Eqs. (8.103) and (8.105) to find $\langle E^2 \rangle_M$ and $\langle ET \rangle_M$ we get

$$\langle E^2 \rangle_j = \langle E^2 \rangle_{j-1} + 2\langle \delta E^2 \rangle_j, \quad (8.110)$$

$$\langle ET \rangle_j = \langle ET \rangle_{j-1} + 2b_3 \langle E \rangle_{j-1} - b_2 b_R \langle E^2 \rangle_{j-1} - b_{2R} \langle \delta E \rangle_j \langle E \rangle_{j-1} + 2\langle \delta E \delta T \rangle. \quad (8.111)$$

Summing Eqs. (8.110) and (8.111) over M such pairs we get

$$\langle E^2 \rangle_M = 2M \langle \delta E^2 \rangle, \quad (8.112)$$

$$\langle ET \rangle_M = 2b_3 M (M_1) S - b_2 b_R M (M - 1) \langle \delta E^2 \rangle - b_{2R} M (M - 1) S^2. \quad (8.113)$$

Using Eqs. (8.112) and (8.113) in Eq. (8.109) we can find the variance in T after M pairs of amplifiers to be

$$\begin{aligned} \langle T^2 \rangle_M &= 4Mb_3^2 + b_2^2 b_R^2 M (M - 1) (2SE_0) + b_2^2 M \frac{S}{E_0} \frac{1}{\tau_0^2} + b_{2R}^2 M (2SE_0) + 4b_3^2 M (M - 1) \\ &\quad + \frac{2}{3} b_2^2 b_R^2 M (M - 1) (M - 2) (2SE_0) + \frac{2}{3} b_2 b_R b_{2R} M (M - 1) (M - 2) S^2 \\ &\quad + b_{2R} M (M - 1) S^2 - \frac{8}{3} b_2 b_R b_3 M (M - 1) (M - 2) S + 2b_2 M \frac{S}{E_0} \left[C_0 + \frac{b_2}{\tau_0^2} \right] + 2 \frac{S}{E_0} \tau_0^2 \\ &\quad + \frac{S}{E_0} \tau_0^2 \left[C_0 + \frac{b_2}{\tau_0^2} \right]^2. \end{aligned} \quad (8.114)$$

Using Eqs. (8.112) and (8.113) and substituting $M = N/2$ in Eq. (8.114), we can find the timing jitter when using parametric amplifiers in place of EDFAs to be

$$\sigma_{PA}^2 = \sigma_{GH}^2 + [b_2^2 b_R^2 (N^2 - 4)/12 + b_{2R}^2] N/2 (2SE_0) + b_2 b_3 b_R S N (N - 2) (N - 4)/3, \quad (8.115)$$

$$\sigma_{\text{GH}}'^2 = N \frac{S}{E_0} \tau_0^2 \left[1 + \frac{1}{2} \left(C_0 + \frac{2b_2}{\tau_0^2} \right)^2 \right]. \quad (8.116)$$

Eqs. (8.115) and (8.116) show Raman jitter and Gordon-Haus jitter again grow cubic and linear in distance respectively when parametric amplifiers are used instead of EDFAs. When EDFAs are used the Raman jitter and Gordon-Haus jitter can be written from Eqs. (7.151) and (7.152) to be

$$\sigma_t^2 = \sigma_{\text{GH}}^2 + R_1(2SE_0) + R_3, \quad (8.117)$$

$$\sigma_{\text{GH}}^2 = \frac{S}{E_0} \tau_0^2 N \left[1 + \left(C_0 + \frac{b_2 N}{\tau_0^2} \right)^2 \right], \quad (8.118)$$

and the coefficients R_1 and R_3 are given by

$$R_1 = N(N-1)[b_R^2 b_2^2 (N^3 - 10N^2 + 29N - 9)/120 + b_2 b_R b_{2R} (19N^2 - 65N + 48)/96 + b_{2R}^2 (2N - 1)/6], \quad (8.119)$$

$$R_3 = N(N-1)b_3 \left[b_R \frac{(N-1)}{6} (N-2) + b_{2R} \frac{(N-2)}{3} \right] S. \quad (8.120)$$

We see from Eqs. (8.117) - (8.120) that both the Raman jitter and the Gordon-Haus jitter are reduced considerably by using parametric amplifiers in the case of non-soliton system because they scale as N^3 and N , rather than N^5 and N^3 , respectively. The Gordon-Haus timing jitter given by Eq. (8.116) when using parametric amplifiers can be further reduced by using pre-compensation discussed in the previous section. Since in this case the dispersion in one fiber section is cancelled in the next fiber section due to phase conjugation the accumulated dispersion can be seen from Eq. (8.116) to be $C_0 = -2b_2/\tau_0^2$ which is due to the noise variance in the frequency that has accumulated over the second fiber section. Thus the accumulated dispersion in this case is only over one amplifier length instead of the entire fiber link like in the case of EDFAs.

Similar to the case of DM solitons, the timing jitter can be reduced using parametric amplifiers in place of EDFAs. Figure 8.9 shows the impact of intrapulse Raman scattering on the performance of a 160-Gb/s non-soliton system using the same dispersion map used earlier for Figure 8.7. The pulse energy is reduced by a factor of 10 to reduce the nonlinear effects. The average dispersion is also reduced to $\beta_{\text{av}} = -0.005 \text{ ps}^2/\text{km}$ by changing the normal-GVD to $-2.492 \text{ ps}/(\text{km}\cdot\text{nm})$. In the case of EDFAs, the input chirp C_0 was chosen to be $|\beta_{\text{av}}|L/\tau_0^2$, where L is the total distance of propagation as is the condition for pre-compensation from the previous section. For systems

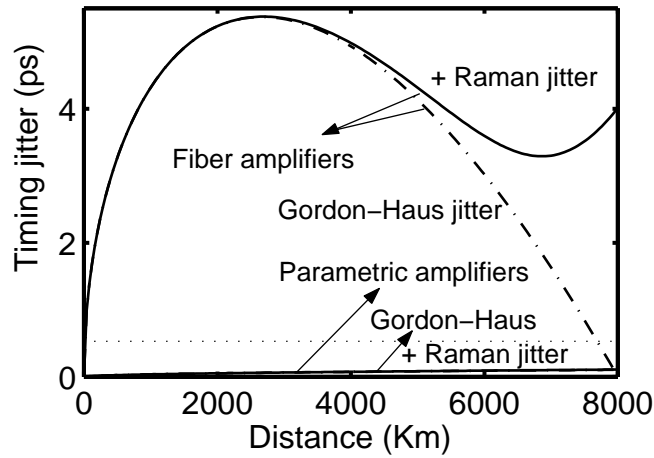


Figure 8.9: Timing jitter for a 160-Gb/s non-soliton system with 40-km amplifier spacing. The solid and dashed lines show respectively timing jitter with and without the Raman contribution for both EDFAs and parametric amplifiers. The map parameters are the same as the one used for Figure 8.7, except the average dispersion is reduced to $D_{av} = 0.004$ ps/km-nm. The dotted line shows the acceptable value of timing jitter.

with parametric amplifiers C_0 was chosen to be $2|\beta_{av}|L_A/\tau_0^2$. As expected, for lightwave systems designed using EDFAs, precompensation reduces the Gordon-Haus contribution but the Raman jitter increases with distance and ultimately limits the system after 3000 km. The use of parametric amplifiers reduces the Raman jitter considerably, and the system is not limited by jitter for distances as large as 10,000 km. Again other degradation factors not included here may limit the length to much smaller values even when parametric amplifiers are used.

8.3 Chapter Summary

In this Chapter we have studied two methods for controlling timing jitter in lightwave systems. First we saw that for systems that are limited mainly by Gordon-Haus jitter, dispersion compensation techniques can help reduce timing jitter. We used the moment method to show analytically that for soliton systems post-compensation can reduce timing jitter, provided that its magnitude is optimized properly. More specifically, post-compensation of residual dispersion by 50% reduces the jitter by a factor of 2 at long distances when a single amplifier is used for each map period. However, jitter actually increases if the residual dispersion is eliminated completely by use of a post-compensation fiber. When there are two or more amplifiers within each map pe-

riod the situation becomes complex to the extent that an increase in the average dispersion may reduce the jitter for moderate distances. We also showed that for non-soliton systems, both pre- and post-compensation can reduce timing jitter. In general, 100% compensation of the total dispersion in the case of non-soliton systems is essential for realizing jitter values comparable with those obtained for DM solitons. However we found that the optimum compensation in this case is 75% pre-compensation and 25% post-compensation. We used numerical simulations to verify this result.

Secondly, we used the moment method to show that both the Raman-induced and the ASE-induced timing jitter can be reduced considerably for lightwave systems using bit rates more than 40 Gb/s by replacing EDFAs with parametric amplifiers. Our expressions can be used even in the case of dense dispersion management, realized using multiple map periods between two neighboring amplifiers. We have included the effects of third-order dispersion as well. We have applied this general formalism to three types of lightwave systems corresponding to the use of DM solitons, fundamental solitons with DDFs, and chirped return-to-zero pulses in a quasi-linear configuration. We have obtained the analytic expressions for the timing jitter in each case. We compared the three configurations for a 160-Gb/s system and found that in all cases the timing jitter at the receiver end can be reduced by a large factor by replacing EDFAs with parametric amplifiers. Although parametric amplifiers have not yet been used for designing lightwave systems, the situation is likely to change in the near future in view of the recent advances in designing broadband parametric amplifiers [72]–[74].

Several assumptions made in our analysis must be satisfied before the jitter-reduction scheme using parametric amplifiers can be implemented successfully. First, the OPC process must create a phase-conjugated version of the signal. This is possible only if the pump phase does not fluctuate much. In practice, the line width of semiconductor lasers used for pumping is increased to ~ 1 GHz for suppressing the onset of stimulated Brillouin scattering. This is not of much concern for the following reason. At high bit rates, each optical pulse is so short (~ 1 ps) that the pump phase remains constant over its entire width. Thus, as long as the bit rate is much larger than the pump bandwidth, the OPC process is close to being ideal. The second issue is related to the mismatch between the signal and idler wavelengths. The main requirement here is that the dispersion parameter should be the same at both fields. This is possible only if they have the same wavelength. In

practice, the wavelength can differ by a few nanometers especially for fibers with low dispersion slopes, but larger differences are likely to become intolerable.

Chapter 9

Conclusions

In this thesis, we use the moment method to study the propagation of optical pulses in optical fibers. In particular we apply the moment method to study the effects of noise induced by the optical amplifiers on the input pulses and the effects of timing jitter on optical communications systems. The propagation of optical fields in fibers is governed by a nonlinear partial differential equation, called the nonlinear Schrödinger equation which can be derived from Maxwell's equations. Hence to understand the evolution of an optical pulse when it propagates through an optical fiber, it becomes necessary to solve the nonlinear Schrödinger equation. Since the equation is nonlinear we have to use approximate methods to solve this equation. We show that the variational method which is usually employed to study the propagation of optical pulse in fibers, cannot be used in the presence of intra-pulse Raman scattering, due to its dissipative nature. Hence it is necessary to find another method that will work even in the presence of dissipation in the system. The moment method which treats the optical pulse as a particle can be used for both dissipative and non dissipative systems.

First we use the moment method to study the effects of intrapulse Raman scattering on optical pulses propagating in fibers. Using the moment method we showed that the Raman-induced frequency shift resulting from intrapulse Raman scattering is a general phenomenon that occurs for all pulses both in the normal and anomalous dispersion regimes of an optical fiber. We apply the results to the cases of "sech" and Gaussian pulse shapes. The results show that the Raman-induced frequency shift depends not only on the width but also on the frequency chirp associated with

the optical pulse. The RIFS becomes quite large in the case of ultrashort pulses as it depends on the cubic inverse of the local pulse width and varies considerably with the history of pulse width changes. Whenever pulse width remains nearly constant along the fiber, Raman induced frequency shift can accumulate to relatively large values.

We show that even optical solitons do not maintain their width when Raman induced frequency shift becomes comparable to or larger than the spectral width of the pulse. Our analysis remains valid in this regime and shows how the Raman induced frequency shift saturates to a constant value because of soliton broadening. We give numerical examples of “sech” and Gaussian pulses in both the normal and anomalous dispersion regime using a 10-m long fiber in which femtosecond pulses are launched. Although Raman induced frequency shift is generally smaller for normal dispersion compared with the case of anomalous dispersion, it is large enough to be measurable experimentally. We include the effects of third-order dispersion and self-steepening in our analysis and show that it affects the frequency shift through the frequency chirp.

Next we used the moment method to study the effects of amplifier induced noise on communication system. We show that the amplifier induced noise can degrade the system by reducing the signal to noise ratio of the system and also can lead to timing jitter which can cause increased bit error rate there by reducing the signal to noise ratio. The amplifier induced noise affects the amplitude, the frequency, the position and the phase of the pulse. The fluctuations in pulse amplitude can reduce the signal to noise ratio of the system by reducing the Q factor of the system. We showed that for a system using N amplifiers periodically to compensate for fiber losses, we were able to find an analytic expression for the Q factor and show that it is inversely proportional to N . Thus the Q factor decreases as the number of amplifiers increases. We have included the effects of thermal and shot noise in our calculations to find the Q factor.

The fluctuations added by the amplifier to the frequency and the position of the pulse can cause timing jitter in the system leading to an increased bit error rate and thereby degrading the system. We use the moment method to analytically calculate timing jitter in communications systems using N amplifiers at regular intervals. We show that fluctuations in the frequency can affect the position of the pulse due to the presence of group velocity dispersion in system. The resulting timing jitter is called the Gordon-Haus timing jitter. Using the moment method we show that the Gordon-Haus timing jitter grows cubic with distance and is inversely proportional to the energy of the pulse.

For systems using bit rates up to 40 Gb/s, the timing jitter is mainly due to Gordon-Haus jitter. We apply this method to three types of systems, viz., i) systems using fundamental solitons in dispersion-decreasing fibers, ii) dispersion-managed soliton systems and iii) non-soliton systems. For all three cases we extend the theory to see the effects of using more than one amplifier within a map period. We found that using more than one amplifier within one map period can help reduce Gordon-Haus timing jitter in all three cases. However when using more than one amplifiers in the dispersion managed soliton systems to reduce Gordon-Haus timing jitter, the effectiveness of the technique seem to depend on the position of the second amplifier and on the dispersion map. We give numerical examples in all the three cases to show that using more than one amplifier within each map period can help reduce Gordon-Haus timing jitter. However, as the number of amplifiers increases, the Q factor decreases.

In the presence of intra-pulse Raman scattering, any fluctuations in the pulse amplitude affects the frequency of the pulse thus causing additional timing jitter. This jitter is called Raman jitter. For systems using bit rates more than 40 Gb/s, the intra-pulse Raman scattering and third-order dispersion effects cannot be neglected. We use the moment method to derive analytic expressions for Raman jitter for all three systems mentioned above. We show that Raman jitter dominates the timing jitter for these systems. The Raman jitter grows as fifth power of distance and can limit the system before the Gordon-Haus jitter limits the system. Since at such high bit rates the acceptable value of jitter is smaller, the results show that these systems are limited within 1000 km. Unlike Gordon-Haus jitter the Raman jitter is proportional to the pulse energy and since soliton systems require larger pulse energies, they have a larger value of timing jitter due to Raman jitter than non-soliton systems.

We have included the effects of third-order dispersion in our calculations. Our results can be used even in the case of dense dispersion management which is necessary to achieve such high bit rates. We have given numerical examples for all three systems to show our results. We have verified the accuracy of our analytical results using numerical simulations. In the case of soliton systems we verified our results using the split step Fourier method and for non-soliton systems we used ordinary differential equations solvers to verify our analytical results. The numerical simulations agrees well with our analytical results except for a minor discrepancy which is due to intra-pulse interactions in the case of solitons and due to higher order terms in the case of non-solitons.

Since timing jitter can limit the system considerably, it becomes essential to control timing jitter in communications systems. We propose a few different techniques for this purpose and show using the moment method that these techniques can reduce timing jitter in all the three systems considerably. For systems that are mainly limited by Gordon-Haus jitter we show that dispersion compensation techniques can help reduce timing jitter. In the case of soliton systems we show that post-compensation can help reduce Gordon-Haus jitter by half. When using one amplifier per map period, we see that even a small amount of post-compensation can help. However the optimum compensation turns out to be compensating for 50% of the total accumulated dispersion. However when using more than one amplifier per map period the optimum compensation seems to depend on the dispersion map of the system. We also show that both positive and negative average dispersion can be used to compensate for the accumulated dispersion in such a case.

For non-soliton systems both pre- and post-compensation techniques can be used to reduce timing jitter. In this case the timing jitter can be reduced to a linear function of distance rather than cubic thus reducing jitter by a large amount. There are three ways of accomplishing this, i) complete pre-compensation, ii) complete post-compensation and iii) a combination of both. We show that for all the three types of compensation, the jitter at the receiver end is the same. However in order to keep the jitter minimum both within the system and at the receiver end, the optimum compensation is 75% pre-compensation and 25% post-compensation. We verify this result using numerical simulations and show that the optimum compensation keeps the jitter minimum both within the system and at the receiver end. We give numerical examples of all three systems to show that dispersion compensation can reduce Gordon-Haus jitter considerably.

For systems using more than 40 Gb/s, we suggest using parametric amplifiers in place of erbium-doped fiber amplifiers. Since parametric amplifiers can act as phase conjugators and if we alternate between the signal and the idler pulses between amplifiers, we can compensate for group velocity dispersion, intra-pulse Raman scattering and self-phase modulation in the system. Such a technique can reduce both Raman jitter and Gordon-Haus jitter thus reducing timing jitter by considerable amounts for such high bit rate systems. We show using the moment method that using parametric amplifiers in place of fiber amplifiers can reduce Raman jitter to cubic dependence in distance instead of fifth power and Gordon-Haus jitter to linear in distance instead of cubic for all the three systems. Such systems are not jitter limited up to 5000 km. We give numer-

ical examples for each of the three systems to show our results. We have numerically verified our analytical results using numerical simulations and our numerical results agree with our analytical results.

Thus we conclude that the moment method is a simple method that can be used for studying the pulse propagation in optical fibers. This method works even when the system exhibits dissipation. The results we obtained using this method for Gordon-Haus jitter and Raman jitter in the case of fundamental solitons agrees with the previously obtained results of Gordon and Haus [54] and Essiambre [55] respectively. In the case of fundamental solitons, our expression for Raman induced frequency shift reduces to that of Gordon [36] so long as the shift is much smaller than the spectral width of the pulse. However to use the moment method we have to assume a pulse shape and that the pulse shape does not change during propagation. Hence results obtained using this method should be used with caution if the pulse shape changes significantly during propagations. In conclusion we feel that using the moment method we can learn a great deal more about the pulse evolution both in terms of uncovering new phenomena and better understanding similar systems.

Bibliography

- [1] G. P. Agrawal, *Fiber-Optic Communication Systems*, 3rd ed. (Wiley, New York, 2002).
- [2] J. I. Yamada, S. Machida and T. Kimura, “Ultimate low-loss single mode fiber”, *Electron. Lett.* **15**, 106-108 (1981).
- [3] V. E. Zakharov, A. B. Shabat, “Exact theory of two-dimensional self-focusing and one-dimensional self-modulation of waves in nonlinear media,” *Trans. Soveit Phys. JETP*, **34**, 62 (1972).
- [4] A. Hasegawa, *Optical Solitons in Fibers*, (Springer-Verlag, Berlin, 1989).
- [5] K. Tajima, “Compensation of soliton broadening in nonlinear optical fibers with loss”, *Opt. Lett.* **12**, 54–56 (1987).
- [6] C. S. Gardner, J. E. Greene, M. D. Kruskal and R. M. Miura, “Method for Solving the Korteweg-deVries Equation”, *Phys. Rev. Lett.* **19**, 1095–1097 (1967).
- [7] S. K. Turitsyn, I. Gabitov, E. W. Laedke, V. K. Mezentsev, S. L. Musher, E. G. Shapiro, T. Schafer, and K. H. Spatschek, “Variational approach to optical pulse propagation in dispersion compensated transmission systems”, *Opt. Commun.* **151**, 117–135 (1998).
- [8] J. N. Kutz, P. Holmes, S. G. Evangelides, and J. P. Gordon, “Hamiltonian dynamics of dispersion-managed breathers”, *J. Opt. Soc. Am. B*, **15**, 87–96 (1998).
- [9] A. Berntson, N. J. Doran, W. Forysiak, and J. H. B. Nijhof, “Power dependence of dispersion-managed solitons for anomalous, zero, and normal path-average dispersion, *Opt. Lett.* **23**, 900–902 (1998).

- [10] T. I. Lakoba, J. Yang, D. J. Kaup and B. A. Malomed, “Conditions for stationary pulse propagation in the strong dispersion management regime”, *Opt. Commun.* **149**, 366–375 (1998).
- [11] S. N. Vlasov, V. A. Petrishchev and V. I. Talanov, “Average description of wave beam in linear and nonlinear media (The method of moments)”, *Radiophys. Quantum Electron.* **14**, 1062–1070 (1971).
- [12] M. J. Ablowitz and P. A. Clarkson, *Solitons, Nonlinear Evolution Equations, and Inverse Scattering*, (Cambridge University Press, New York, 1991).
- [13] G. L. Lamb, Jr., *Elements of Soliton Theory*, (Dover, New York, 1994).
- [14] A. Hasegawa and Y. Kodama, *Solitons in Optical communications*, (Oxford University Press, New York, 1995).
- [15] T. Miwa, *Mathematics of Solitons*, (Cambridge University Press, New York, 1999).
- [16] T. I. Lakoba, D. J. Kaup, “Hermite-Gaussian expansion for pulse propagation in strongly dispersion managed fibers”, *Phys. Rev. E*, **58**, 6728–6741 (1998).
- [17] I. R. Gabitov, E. G. Shapiro, and S. K. Turistyn, “Asymptotic breathing pulse in optical transmission systems with dispersion compensation”, *Phys. Rev. E*, **55**, 3624–3633 (1997).
- [18] M. J. Ablowitz and G. Bioindini, “Multiscale pulse dynamics in communication systems with strong dispersion management”, *Opt. Lett.* **23**, 1668–1670 (1998).
- [19] C. Paré and P. A. Belangé, “Spectral domain analysis of dispersion management without averaging”, *Opt. Lett.* **25**, 881–883 (2000).
- [20] R. H. Hardin and F. D. Tappert, “ Applications of split-step fourier method to numerical solution of nonlinear and variable coefficient wave equations”, *SIAM Rev. Chronicle*, **15**, 423 (1973).
- [21] R. A. Fisher and W. K. Bischel, “Role of linear dispersion in plane wave self-phase modulation”, *Appl. Phys. Lett.* **23**, 661–663 (1973).

- [22] R. A. Fisher and W. K. Bischel, "Numerical studies of the interplay between self-phase modulation and dispersion for intense plane-wave laser pulses", *J. Appl. Phys.* **46**, 4921–4934 (1975).
- [23] G. P. Agrawal, *Nonlinear Fiber Optics*, 3rd ed. (Academic, San Diego, 2001).
- [24] K. S. Yee, "Numerical solution of initial boundary value problems involving Maxwell's equations in isotropic media", *IEEE Trans. Antennas Propag.* **14**, 302–307 (1966).
- [25] A. Taflove, "Review of the formulation and applications of the finite-difference time-domain method for numerical modeling of electromagnetic wave interactions with arbitrary structures", *Wave Motion*, **10**, 547–582 (1988).
- [26] C. F. Lee, R. T. Shin, and J. A. Kong, *Progress in Electromagnetic Research*, J. A. Kong, Ed. (Elsevier, New York, 1991).
- [27] S. Maeda, T. Kashiwa, and I. Fukai, "Full wave analysis of propagation characteristics of a through hole using the finite difference time domain method", *IEEE Trans. Microwave Theory Tech.* **39**, 2154–2159 (1991).
- [28] R. M. Joseph, S. C. Hagness, and A. Taflove, "Direct time integration of Maxwell's equations in linear dispersive media with absorption for scattering and propagation of femtosecond electromagnetic pulses", *Opt. Lett.* **16**, 1412–1414 (1991).
- [29] P. M. Goorjian and A. Taflove, "Direct time integration of Maxwell's equations in nonlinear dispersive media for propagation and scattering of femtosecond electromagnetic solitons", *Opt. Lett.* **17**, 180–182 (1992).
- [30] P. M. Goorjian and A. Taflove, R. M. Joseph and S. C. Hagness, "Computational modeling of femtosecond optical solitons from Maxwell's equations", *IEEE J. Quantum Electron.* **28**, 2416–2422 (1992).
- [31] R. M. Joseph, P. M. Goorjian, and A. Taflove, "Direct time integration of Maxwell's equations in two-dimensional dielectric waveguides for propagation and scattering of femtosecond electromagnetic solitons", *Opt. Lett.* **18**, 491–493 (1993).

- [32] R. W. Ziolkowski, and J. B. Judkins, "Full-wave vector Maxwell equation modeling of the self-focusing of ultrashort optical pulses in a nonlinear Kerr medium exhibiting a finite response time", *J. Opt. Soc. Am. B*, **10**, 186–198 (1993).
- [33] M. Zoboli, F. Di Pasquale, and S. Selleri, "Full-vectorial and scalar solutions of nonlinear optical fibers", *Opt. Commun.* **97**, 11–15 (1993).
- [34] E. A. Golovchenko, E. M. Dianov, A. M. Prokhorov, and V. N. Serkin, "Decay of optical solitons," *JETP Lett.* **42**, 87–91, (1985).
- [35] F. M. Mitschke and L. F. Mollenauer, "Discovery of the soliton self-frequency shift," *Opt. Lett.* **11**, 659–661, (1986).
- [36] J. P. Gordon, "Theory of the soliton self-frequency shift," *Opt. Lett.* **11**, 662–664, (1986).
- [37] Y. Kodama and A. Hasegawa, "Nonlinear pulse propagation in a monomode dielectric guide", *IEEE Journal of Quantum Electronics*, **23**, 510–524, (1987).
- [38] Yu. S. Kivshar, "Dark-soliton dynamics and shock waves induced by the stimulated Raman effect in optical fibers." *Phys. Rev. A*, **42**, 1757–1761, (1990).
- [39] G. P. Agrawal and G. Headley III, "Kink solitons and optical shocks in dispersive nonlinear media," *Phys. Rev. A*, **46**, 1573–1577 (1992).
- [40] Yu. S. Kivshar, B. A. Malomed, "Raman-induced optical shocks in nonlinear fibers," *Opt. Lett.* **18**, 485–487, (1993).
- [41] R. H. Stolen, J. P. Gordon, W. J. Tomlinson, and H. A. Haus, "Raman response function of silica-core fibers", *J. Opt. Soc. Am. B*, **6**, 1159–1166 (1989)
- [42] K. J. Blow and D. Wood, "Theoretical description of transient stimulated Raman scattering in optical fibers", *IEEE J. Quantum Electron.* **25**, 2665–2673 (1989).
- [43] P. V. Mamyshev and S. V. Chernikov, "Ultrashort-pulse propagation in optical fibers", *Opt. Lett.* **15**, 1076–1078 (1990).

- [44] S. V. Chernikov and P. V. Mamyshev, “Femtosecond soliton propagation in fibers with slowly decreasing dispersion”, *J. Opt. Soc. Am. B*, **8**, 1633–1641 (1991).
- [45] R. H. Stolen and W. J. Tomlinson, “Effect of the Raman part of the nonlinear refractive index on the propagation of ultrashort optical pulses in fibers”, *J. Opt. Soc. Am. B*, **9**, 565–573 (1992).
- [46] W. Schottky, “Small-Shot Effect and Flicker Effect”, *Phys. Rev.* **23**, 74–103 (1926).
- [47] W. R. Bennet, *Electrical Noise*, (McGraw-Hill, New York, 1960).
- [48] D. K. C. MacDonald, *Noise and Fluctuations: An Introduction*, (Wiley, New York, 1962).
- [49] F. N. H. Robinson, *Noise and Fluctuations in Electronic Devices and Circuits*, (Oxford University Press, Oxford, 1974).
- [50] J. B. Johnson, “Thermal Agitation of Electricity in Conductors”, *Phys. Rev.* **32**, 97–109 (1928).
- [51] H. Nyquist, “Thermal Agitation of Electric Charge in Conductors”, *Phys. Rev.* **32**, 110–113 (1928).
- [52] G. P. Agrawal, *Applications of Nonlinear Fiber Optics* (Academic, San Diego, 2001).
- [53] E. Iannone, F. Matera, A. Mecozzi, and M. Settembre, *Nonlinear Optical Communication Networks*, (Wiley, New York, 1998), Chap. 5.
- [54] J. P. Gordon and H. A. Haus, “Random walk of coherently amplified solitons in optical fiber transmission”, *Opt. Lett.* **11**, 665–667 (1986).
- [55] R. J. Essiambre and G. P. Agrawal, “Timing jitter of ultrashort solitons in high-speed communication systems. I. General formulation and application to dispersion-decreasing fibers”, *J. Opt. Soc. Am. B*, **14**, 314–322 (1997).
- [56] V. S. Grigoryan, C. R. Menyuk and R. M. Mu, “Calculation of timing and amplitude jitter in dispersion-managed optical fiber communications using linearization”, *J. Lightwave Technol.* **17**, 1347–1356 (1999).

- [57] J. Santhanam, C. J. McKinstrie, T. I. Lakoba and G. P. Agrawal, "Effects of precompensation and post-compensation on timing jitter in dispersion-managed systems", *Opt. Lett.* **26**, 1131–1133 (2001).
- [58] E. Poutrina and G. P. Agrawal, "Effect of distributed Raman amplification on timing jitter in dispersion-managed lightwave systems", *IEEE Photon. Technol. Lett.* **14**, 39–40 (2002).
- [59] A. Yariv, "Signal-to-noise considerations in fiber links with periodic or distributed optical amplification", *Opt. Lett.* **15**, 1064–1066 (1990).
- [60] D.-M. Baboiu, D. Mihalache and N. -C. Panoiu, "Combined influence of amplifier noise and intrapulse Raman scattering on the bit-rate limit of optical fiber communication systems", *Opt. Lett.* **20**, 1865–1867 (1995).
- [61] T. I. Lakoba and D. J. Kaup, "Influence of the Raman effect on dispersion-managed solitons and their interchannel collisions", *Opt. Lett.* **24**, 808–810 (1999).
- [62] A. H. Liang, H. Toda and A. Hasegawa, "High-speed soliton transmission in dense periodic fibers", *J. Opt. Soc. Am. B*, **24**, 798–801 (1999).
- [63] A. Mecozzi, J. D. Moores, H. A. Haus, and Y. Lai, "Soliton transmission control", *Opt. Lett.* **16**, 1841–1843 (1991).
- [64] L. F. Mollenauer, M. J. Neubelt, M. Haner, E. Litchman, S. G. Evangelides, B. M. Nyman, "Demonstration of error-free soliton transmission at 2.5 Gbit/s over more than 14000 km", *Electron. Lett.* **27**, 2055–2057 (1991).
- [65] Y. Kodama and A. Hasegawa, "Generation of asymptotically stable optical solitons and suppression of the Gordon-Haus effect", *Opt. Lett.* **17**, 31–33 (1992).
- [66] C. J. McKinstrie, "Effects of filtering on Gordon-Haus timing jitter in dispersion-managed systems", *J. Opt. Soc. Am. B*, **19**, 1275–1285 (2002).
- [67] L. F. Mollenauer, J. P. Gordon, S. G. Evangelides, "The sliding-frequency guiding filter: an improved form of soliton jitter control", *Opt. Lett.* **17**, 1575–1577 (1992).

- [68] W. Forysiak, K. J. Blow, and N. J. Doran, "Reduction of Gordon-Haus jitter by post-transmission dispersion compensation", *Electron. Lett.* **29**, 1225–1227 (1993).
- [69] S. Watanabe and M. Shirasaki, "Exact compensation for both chromatic dispersion and Kerr effect in a transmission fiber using optical phase conjugation", *J. Lightwave Tech.* **14**, 243–248 (1996).
- [70] S. Chi and S. Wen, "Recovery of the soliton self-frequency shift by optical phase conjugation", *Opt. Lett.* **19**, 1705–1707 (1994).
- [71] R. J. Essiambre and G. P. Agrawal, "Timing jitter of ultrashort solitons in high-speed communication systems. II. Control of jitter by periodic optical phase conjugation", *J. Opt. Soc. Am. B*, **14**, 323–330 (1997).
- [72] M. E. Marhic, F. S. Yang, M. C. Ho, and L. G. Kazovsky, "High-nonlinearity fiber parametric amplifiers with periodic dispersion compensation," *J. Lightwave Technol.* **17**, 210–215 (1999).
- [73] C. J. McKinstrie, S. Radic, and A. Chraplyvy, "Parametric amplifiers driven by two pump waves," *IEEE J. Sel. Topics Quant. Electron.* **8**, 538–547 (2002).
- [74] J. Hansryd, P. A. Andrekson, M. Westlund, J. Li, and P. O. Hedekvist, "Fiber-based optical parametric amplifiers and their applications", *IEEE J. Sel. Topics Quant. Electron.* **8**, 506–520 (2002).
- [75] A. Yariv, D. Fekete, D. M. Pepper, "Compensation for channel dispersion by nonlinear optical phase conjugation", *Opt. Lett.* **4**, 52–54 (1979).

Appendix A

Acronyms

ASE	amplified spontaneous emission
BER	bit error rate
CRZ	chirped return-to-zero
DDF	dispersion decreasing fiber
DM	dispersion managed
DMS	dispersion managed soliton
EDFA	erbium-doped fiber amplifier
fs	femto seconds
FWHM	full-width at half maximum
FWM	four wave mixing
GH	Gordon-Haus
GVD	group velocity dispersion
IRS	intra-pulse Raman scattering
NLS	non-linear Schrödinger equation
fs	femto seconds

ps	picoseconds
RIFS	Raman induced frequency shift
RMS	root mean square
SNR	signal to noise ratio
SPM	self phase modulation
SRS	stimulated Raman scattering
SSFS	soliton self frequency shift
TOD	third-order dispersion
WDM	wavelength division multiplexing